ABSTRACT

YAMAZAKI, MAI. The Chemical Modification of Chitosan Films for Improved Hemostatic and Bioadhesive Properties. (Under the direction of Dr. Samuel M. Hudson.)

Bioadhesives and hemostatic agents have been quite attractive as wound dressings. However, commercially available bioadhesives and hemostatic agents still have some limitations in terms of cytotoxicity, potential for bacterial infections, and cost performance. There is a need for developing bioresource-based adhesives that would overcome these limitations. The goal of this research is to fabricate novel bioadhesive and hemostatic agents with improved properties, provided by enhanced reactive bonding sites for bioadhesion, and enhanced blood clot forming ability for hemostatic agents.

To generate a novel bioadhesive, chitosan and silk fibroin (CS/SF) blend films with dangling aldehydes were prepared by a chemical reaction between amino groups of blend films and aldehyde groups of dialdehydes. The dangling free aldehyde groups can bond to the proteinatious amino groups of tissue, which improves the bioadhesiveness. Commercial glutaraldehyde (GA) and newly synthesized 1,10-didecanal were used for the chemical modification of blend films. A dialdehyde with a long carbon chain is considered to provide better accessibility of the aldehyde group, than a shorter one, to the amino groups. Currently, very few long-chain dialdehydes are commercially available due to the synthesis difficulties. The 1, 10-didecanal and modified CS/SF blend films were characterized and the quality of bioadhesion was evaluated by tissue peeling.

Novel chitosan and polyaspartic acid (CS/PAsp) polyelectrolyte complex films were successfully prepared as hemostatic agents by layer-by-layer assembly. CS is readily obtained from crustacean shell waste by a simple chemical process, whereas PAsp is easily

polymerized in one pot by thermal condensation of L-Asp and subsequent hydrolysis. CS and PAsp can form a polyelectrolyte complex, which is vital for various cell cycles. In addition to the reactive chemical functional groups of each polymer, CS and PAsp potentially provide a promising substrate for antibacterial action and blood coagulation, due to the nature of CS and PAsp. The chemical, physical, and biological properties of the layered films are described.

THE CHEMICAL MODIFICATION OF CHITOSAN FILMS FOR IMPROVED HEMOSTATIC AND BIOADHESIVE PROPERTIES

by

MAI YAMAZAKI

A dissertation submitted to the Graduate Faculty of

North Carolina State University

In partial fulfillment of the

Requirements for the degree of

Doctor of Philosophy

FIBER AND POLYMER SCIENCE

Raleigh, NC

2007

APPROVED BY:

_____	_____
Dr. Harold S. Freeman	Dr. Martin W. King
_____	_____
Dr. Bruce M. Novak	Dr. Samuel M. Hudson **Chair of Advisory Committee**

BIOGRAPHY

Mai Yamazaki was born in Chiba, Japan, 1980. She received B.S. and M.S. degrees in Polymer Science from Shinshu University, Japan, in 2002 and 2004, respectively. Her master's thesis work was elucidating the signal transduction pathway of osteoblastic cells cultured on the polyelectrolyte complex that facilitates the bone regeneration, using biological techniques. Subsequently, her interest was shifted to organic synthesis and chemical engineering from biochemistry to develop biomaterials for damaged tissue.

Currently, she is a Ph.D. student in the Fiber and Polymer Science Program, College of Textiles, North Carolina State University, Raleigh. Her research interests include designing biomaterials using degradable biopolymers, synthetic polypeptides, and peptides for tissue engineering, and evaluating their potential use in medical field. She has been studying under the direction of Dr. Samuel M. Hudson since 2004.

ACKNOWLEDGEMENTS

The author would like to express her most sincere appreciation to the Chairman of her Advisory Committee, Dr. Samuel Hudson, for all support, advice, encouragement, and guidance throughout the research. The author also would like to offer her deep gratitude to the other committee members, Dr. Harold Freeman, Dr. Bruce Novak, and Dr. Martin King for their support.

A great appreciation is extended to the research collaborator, Dr. Mike Danilich, from Luna Innovations Inc., for funds, advice, and discussion. Special thanks to Dr. Sabapathy Sankar, Dr. Yoko Aoyama, Dr. Keitaro Seto, and Mr. Matthew Lyndon from the Department of Chemistry, assistant with NMR, GC-MS, and synthetic work. Thanks to Dr. Richard Spontak from the Chemical and Biomolecular Engineering Department for the AFM discussion. Thanks to Mr. Chuck Mooney from the Analytical Instrumentation Facility for the SEM and AFM operation. Thanks to Dr. Nancy Monteiro-Riviere and Ms. Elisha Koivisto from the Veterinary School and Medicine for the blood supply. Thanks also are given to Dr. Keith Beck, Dr. Eun-Seok Gil, Dr. Sung-Won Ha, Ms. Birgit Anderson, Ms. Judy Elson and Mr. Philip Bradford from the Textile Engineering, Chemistry, and Science, for training in the use of laboratory facilities. The author thanks Dr. Renzo Shamey and Dr. Brent Smith from College of Textiles, for research discussions.

Finally, the author wishes to express her deepest appreciation to her family in Japan and all her friends at North Carolina State University.

TABLE OF CONTENTS

Page

LIST OF TABLES

Page

LIST OF FIGURES

Page

LIST OF SCHEMES

Page

CHAPTER 1

1. Background Review

1.1.1 Introduction

Natural, abundant polysaccharides are attractive agents for various biomedical applications, such as tissue engineering scaffolds, drug delivery vehicles, sealants, and permeable membranes, due to their biocompatibility, biodegradability, and nonimmunogenic properties. Bioadhesives have been intensively studied as alternative wound dressings [1-5] due to the toxicity and potential mutagenicity and carcinogenicity of synthetic dressings [6-8]. Commercially available protein-based adhesives overcome these problems, yet they still have some limitations in terms of high cost performance and potential bacterial infections [8, 9].

Another important attribute of a wound dressing is its hemostatic property, i.e. application to heavily bleeding wounds. Currently, only a few hemostatic agents approved by the FDA for acute hemorrhage are available [9, 10-14]. They are zeolite-based granules, protein-based glues, and chitosan-based sponges. However, all of them have some drawbacks, such as a lack of biodegradability, potential bacterial infection, high cost performance, and hardness of the material [3]. Therefore, developing a novel hemostatic agent has been a matter of continued interest.

Chitosan is a polysaccharide, which has potential utility for both wound dressing and hemostasis applications. Many studies of hemostatic agents made of chitosan derivatives have been done for hemorrhage control [15-21].

Chitosan, poly-β(1→4)-2-amino-deoxy-D-glucose, is a deacetylated form of chitin, which is the second most plentiful polysaccharide to be found in the cell walls of fungi and

skeletal composites of crustacea (Figure 1-2). It is a cationic polymer with high charge density in weakly acidic solution, which may lead to potential antibacterial and hemostatic properties, in addition to having good biocompatibility and biodegradability [3]. Highly deacetylated chitosan is considered to be an amorphous polymer with amino groups, which renders not only poly electrolytic effects, but also reactive sites for further chemical modifications. Nevertheless, not much research on highly deacetylated chitosan has involved investigating this substrate as a hemostatic agent.

Silk fibroin is a natural fibrous protein, mainly consisted of amino acids with small side groups, such as glycine, alanine and serine [22]. It has excellent mechanical strength and good biocompatibility, and oxygen and water permeability in the wet state, which suggests that it could be used as a wound dressing. However, the dried as-cast films are brittle due to the random coil conformation and difficult for practical use [23]. A composite structure of silk fibroin and chitosan may result in a reinforced structure, one which may biodegrade faster. Silk fibroin/chitosan blends have already been studied for various physical forms, such as films, fibers, and membranes [24-29].

Polyamino acids and polypeptides are also attractive materials, and good models for mimicking biomacromolecules. They have been studied not only for the general aspects of physical-chemical properties of proteins, but also for applications as biomaterials [30]. Among them, polyaspartic acid (PAsp) is useful because it is hydrophilic, soluble in water and degrades quickly under biological conditions [31]. In addition, PAsp is readily polymerized by heat, going through the polysuccinimide (PSI) intermediate without a metal catalyst, unlike

other polyamino acids [32-39]. Mostly, polyamino acids have been prepared by *N*-carboxyamino acid anhydride (NCA) polymerization [40].

Surface modification on biomaterials has also been extensively studied in order to improve the cell adhesion, which is one of the biggest problems on the biomaterial made of conventional synthetic polymers. Many cell types can be viable with the adhesion on the substrate. Therefore, developing biomaterials that provide the substrate for good cell attachment is the primary issue for tissue engineering. Many attempts have been made to improve cell adhesion and growth by coating or immobilizing the cell binding motif to the substrates, specially using peptides containing RGD sequence [41-51].

This thesis research consists of two major topics. One is fabricating a novel bioadhesive film with improved adhesion, by surface modification using dialdehydes. In Chapter 2, chitosan and silk fibroin (CS/SF) blend films containing dangling aldehyde groups were prepared by a chemical reaction between the amino groups of blend films and aldehyde groups of aliphatic dialdehydes. The remaining aldehyde groups can bond to the proteinatious amino groups of tissue, which improves the bioadhesion. Commercially available glutaraldehyde (GA) and newly synthesized 1,10-didecanal were used for the chemical modification of blend films. A dialdehyde with a long carbon chain is considered to provide better accessibility of the aldehyde group than a shorter one, to the amino groups. Currently, very few dialdehydes, especially long-chain dialdehydes, are commercially available due to the synthetic difficulties.

The second topic involves developing a novel biomaterial/hemostatic agent made of chitosan (CS) and polyaspartic acid (PAsp) polyelectrolyte complex. Polyelectrolyte complex

is usually considered as part of the components of extracellular matrix (ECM), which is vital for cell cycles. In Chapter 3, CS and PAsp bilayer (CS/PAspNa) and trilayer (CS/AspNa/CS) films are fabricated by solution casting. The layer-by-layer assembly of chitosan and PAsp potentially provides a substrate for antibacterial action and blood coagulation (hemostasis), as well as a good scaffold for cell growth and differentiation, due to the nature of CS and PAsp. The preliminary studies of chemical, physical, and biological properties of the layered films are described. Furthermore, chemical modification of the 3 layered film was carried out by grafting cell-binding peptide, RGD, synthesized by a conventional stepwise method. In Chapter 4, the peptide synthesis and the RGD-modified 3 layered film preparation are described along with results from preliminary biological tests to evaluate bioadhesive and hemostatic potential.

1.1.2 References

1. Lehr CM, Bouwstra JA, Schacht EH, Junginger HE. In vitro evaluation of mucoadhesive properties of chitosan and some other natural polymers. Intl J Pharm 1992; 78: 43-48.
2. Smart JD. The basics and underlying mechanisms of mucoadhesion. Adv Drug Deliv Rev 2005; 57: 1556-1568.
3. Hwang JJ, Stupp SI. Poly(amino acid) bioadhesives for tissue repair. J Biomater Sci Polymer Edn 2000; 11: 1023-1038.
4. Karikari AS, Edwards WF, Mecham JB, Long TE. Influence of peripheral hydrogen bonding on the mechanical properties of photo-cross-linked star-shaped poly(D,L-lactide) networks. Biomacromol 2005; 6: 2866-2874.
5. Matsuda S, Iwata H, Se N, IkadaY. Bioadhesion of gelatin films crosslinked with glutaraldehyde. J Biomed Mater Res 1999; 45: 20-27.
6. Park DH, Kim SB, Ahn KD, Kim EY, Kim YJ, Han DK. In vitro degradation and cytotoxicity of alkyl 2-cyanoacrylate polymers for application to tissue adhesives. J Appl Polym Sci 2003; 89: 3272-3278.
7. Tseng,YC, Tabata Y, Hyon SH, Ikada Y. In vitro toxicity test of 2-cyanoacrylate polymers by cell-culture method. J Biomed Mater Res 1990; 24: 1355-1367.
8. Ninan L, Monahan J, Stroshine RL, Wilker JJ, Shi RY. Adhesive strength of marine mussel extracts on porcine skin. Biomaterials 2003; 24: 4091-4099.
9. Whang HS, Kirsch W, Hudson SM. Hemostatic agents from chitin and chitosan J Macromol Sci Polym Rev 2005; 45: 309-323.
10. Pusateri AE, McCarthy SJ, Gregory KW, Harris RA, Cardenas L, McManus AT, Goodwin CW. Effect of a chitosan-based hemostatic dressing on blood loss and survival in a model of severe venous hemorrhage and hepatic injury in swine. J Trauma 2003; 54: 177-182.
11. Kheirabadi BS, Acheson EM, Deguzman R, Sondeen JL, Ryan KL, Delgado A, Dick EJ, Holcomb JB. Hemostatic efficacy of two advanced dressings in an aortic hemorrhage model in swine. J Trauma 2005; 59: 25-35.
12. Wedmore I, McManus JG, Pusateri AE, Holcomb JB. A special report on the chitosan-based hemostatic dressing: Experience in current combat operations. J Trauma

2006; 60: 655-658.

13. King K. Hemostatic dressings for the first responder: A review. Military Med 2004; 169: 716-720.
14. Alam HB, Burris D, DaCorta JA, Rhee P. Hemorrhage control in the battlefield: Role of new hemostatic agents. Military Med 2005; 170: 63-69.
15. Hirano S, Noishiki Y. The blood compatibility of chitosan and *N*-acylchitosans. J Biomed Mater Res. 1985; 19: 413-417.
16. Rao SB, Sharma CP. Use of chitosan as a biomaterial: Studies on its safety and hemostatic potential. J Biomed Mater Res 1997; 34: 21-28.
17. Klokkevold PR, Fukuyama H, Sung EC, Bertolami CN. The effect of chitosan (poly-*N*-acetyl glucosamine) on lingual hemostasis in heparinized rabbits. J Oral Maxillofac Surg 1999; 57: 49-52.
18. Chou TC, Fu E, Wu CJ, Yeh JH. Chitosan enhances platelet adhesion and aggregation. Biochem Biophys Res Com 2003; 302: 480-483.
19. Okamoto Y, Yano R, Miyatake K, Tomohiro I, Shigemasa Y, Minami S. Effects of chitin and chitosan on blood coagulation. Carbohydr Polym 2003; 53: 337-342.
20. Fischer TH, Connolly R, Thatte HS, Schwaitzberg SS. Comparison of structural and hemostatic properties of the poly-*N*-acetyl glucosamine Syvek Patch with products containing chitosan. Microsc Res Tech 2004; 63: 168-174.
21. Vournakis JN, Demcheva M, Whitson A, Guirca R, Pariser ER. Isolation, purification, and characterization of poly-*N*-acetyl glucosamine use as a hemostatic agent. J Trauma 2004; 57: S2-6.
22. Suzuki Y, Gage P, Brown DD. The genes for silk fibroin in *Bombyx mori*. J Mol Biol 1972; 70: 637-649.
23. Ha SW, Park YH, Hudson SM. Dissolution of *Bombyx mori* silk fibroin in the calcium nitrate tetrahydrate-methanol system and aspects of wet spinning of fibroin solution. Biomacromol 2003; 4: 488-496.
24. Kweon HY, Um IC, Park YH. Structural and thermal characteristics of *Antheraea pernyi* silk fibroin/chitosan blend film. Polymer 2001; 42: 6651-6656.
25. Gobin AS, Froude VE, Mathur AB. Structural and mechanical characteristics of silk

fibroin and chitosan blend scaffolds for tissue regeneration. J Biomed Mater Res 2005; 74A: 465-473.

26. Rujiravanit R, Kruaykitanon S, Jamieson AM, Tokura S. Preparation of crosslinked chitosan/silk fibroin blend films for drug selivery system. Macromol Biosci 2003; 3: 604-611.
27. Park WH, Jeong L, Yoo DI, Hudson S. Effect of chitosan on morphology and conformation of electrospun silk fibroin nanofibers. Polymer 2004; 45: 7151-7157.
28. Chen X, Li W, Shao Z, Zhong W, Yu T. Separation of alcohol–water mixture by pervaporation through a novel natural polymer blend membrane-chitosan/silk fibroin blend membrane. J Appl Polym Sci 1999; 73: 975-980.
29. Du CH, Zhu BK, Chen JY, Xu YY. Metal ion permeations of silk fibroin/chitosan blend membranes. Polym Int 2006; 55: 377-382.
30. Fasman GD. Poly-α-amino acids. Marcel Dekker, Inc., New York 1967; pp: v-viii.
31. Thombre SM, Sarwae BD. Synthesis and biodegradability of polyaspartic acid: A critical review. J Macromol Sci, Part A: Pure Appl Chem 2005; 42: 1299-1315.
32. Shinoda H, Asou Y, Suetsugu A, and Tanaka K. Synthesis and characterization of amphiphilic biodegradable copolymer, poly(aspartic acid-co-lactic acid). Macromol. Biosci. 2003; 3, 34-43.
33. Neri P, Antoni G, Benvenuti F, Cocola F, Gazzei G. Synthsis of α,β-poly[(2-hydroxyethyl)-DL-aspartamide], a new plasma expander. J Med Chem 1973; 16: 893-897.
34. Vlasák J, Rypáček F, Drobník J, Saudek V. Properties and reactivity of polysuccinimide. J Polym Sci: Polym Symposium 1979; 66: 59-64.
35. Tomida M, Nakato T, Kuramochi M, Shibata M, Matsunami S, Kakuchi T. Novel method of synthesizing poly(succinimide) and its copolymeric derivatives by acid-catalyzed polysondensation of L-aspartic acid. Polymer 1996; 37: 4435-4437.
36. Tomida M, Yabe M, Arakawa Y. Preparation conditions and properties of biodegradable hydrogels prepared by γ-irradiation ofpoly(aspartic acid)s synthesized by thermal polycondensation. Polymer 1997; 38: 2791-2795.
37. Nakato T, Kusuno A, Kakuchi T. Synthesis of poly(succinimide) by bulk

polycondensation of L-aspartic acid with an acid catalyst. J Polym Sci: Part A: Polym Chem 2000; 38: 117-122.

38. Doll KM, Shogren RL, Holser RA, Willett JL, Swift G. Polymerization of L-aspartic acid to polysuccinimide and copoly(succinimide-aspartate) in supercritical carbon dioxide. Letter Org Chem 2005; 2: 687-689.
39. Zhao Y, Su H, Fang L, Tan T. Superabsorbent hydrogels from poly(aspartic acid) with salt-, temperature- and pH-responsiveness properties. Polymer 2005; 46: 5368-5376.
40. Deming TJ. Polypeptide and polypeptide hybrid copolymer synthesis via NCA polymerization. Adv Polym Sci 2006; 202: 1-18.
41. Nakajima K, Hirano Y, Iida T, Nakajima A. Adsorption of plasma proteins on Arg-Gly-Asp-Ser peptide-immobilized poly(vinyl alcohol) and ethylene-acrylic acid copolymer films. Polym J 1990; 22: 985-990.
42. Lin HB, García-Echeverría C, Asakura S, Sun W, Mosher DF, Cooper SL. Endothelial cell adhesion on polyurethanes coating covalently attached RGD-peptides. Biomaterials 1992; 13: 905-914.
43. Quirk RA, Chan WC, Davies MC, Tendler SJB, Shakesheff KM. Poly(L-lysine)-GRGDS as a biomimetic surface modifier for poly(lactic acid). Biomaterials 2001; 22: 865-872.
44. Lin HB, Sun W, Mosher DF, García-Echeverría C, Schaufelberger K, Lelkes PI, Cooper SL. Synthesis, surface, and cell-adhesion properties of polyurethanes containing covalently grafted RGD-peptides. J Biomed Mater Res 1994; 28: 329-342.
45. Barrera D.A, Zylstra E, Lansbury P.T, and Langer R. Sysnthesis and RGD peptide modification of a new biodegradable copolymer: poly(lactic acid-*co*-lysin). J. Am. Chem. Soc. 1993; 115, 11010-11011.
46. Hu Y, Winn SR, Krajbich I, Hollinger JO. Porous polymer scaffolds surface-modified with arginine-glycine-aspartic acid enhance bone cell attachment and differentiation *in vitro*. J Biomed Mater Res. 2003; 64A, 583-590.
47. Cook AD, Hrkach JS, Gao NN, Johnson IM, PAjvani UB, Cannizzaro SM, Langer R. Characterization and development of RGD-peptide-modified poly(lactic acid-*co*-lysine) as an interactive, resorbable biomaterial. J Biomed Mater Res 1997; 35: 513-523.
48. Sugawara T, Matsuda T. Photochemical surface derivatization of a peptide containing

Arg-Gly-Asp (RGD). J Biomed Mater Res 1995; 29: 1047-1052.

49. Burdick JA, Anseth KS. Photoencapsulation of osteoblasts in injectable RGD-modified PEG hydrogels for bone tissue engineering. Biomaterials 2002; 23: 4315-4323.
50. Deng C, Tian H, Zhang P, Sun J, Chen X, Jing X. Synthesis and characterization of RGD peptide grafted poly(ethylene glycol)-*b*-poly(L-lactide)-*b*-poly(L-glutamic acid) triblock copolymer. Biomacromol 2006; 7: 590-596.
51. Knerr R, Weiser B, Drotleff S, Steinem C, Göpferich A. Measuring cell adhesion on RGD-modified, self-assembled PEG monolayers using the quartz crystal microbalance technique. Macromol Biosci 2006; 6: 827-838.

1.2 Literature Review

Chitosan Derivatives for Bioadhesive/Hemostatic Applications: Chemical and Biological Aspects

Abstract

Natural, abundant polysaccharides are attractive agents for various biomedical applications. Chitosan and its derivatives are known to have hemostatic and antibacterial potential. Although various types of hemostatic or antibacterial agents of chitosans have been suggested, the detailed mechanisms that effect immune response and hemostatic actions are still under investigation. The effects of chitosan and its derivatives used in several applications such as scaffolds, antibacterial agents, and hemostatic agents are described in this review.

1.2.1 Introduction

Recent advances in tissue engineering have been directed towards solving problems of patients who have suffered tissue/organ loss or skeletal defects [1,2]. Many natural, synthetic or their hybrid matrices have been developed to cover wound sites, replace lost tissue functions and support cell growth. For example, aliphatic polyesters such as poly(lactic acid) and poly(glycolic acid) are versatile biomaterials due to their biodegradability and biocompatibility [1-5]. Polyurethane is also a well-known biomaterial with biocompatibility, and the mechanical and physical properties necessary for a blood-contacting material [6-8].

Synthetic matrices have many advantages because their molecular design, mechanical/physical properties can be controlled and they can be manufactured on any scale.

However, the usage of synthetic scaffolds is still limited because of poor cell attachment/growth, adsorption of untargeted proteins and induction of thrombogenesis on the surface. Furthermore, some of the synthetic polymers, including polyesters, are difficult to modify due to the lack of sufficient reactive functional groups. On the other hand, natural substrates such as adhesive proteins have been extensively used because of excellent biocompatibility and bioactivity, however, they have batch-to-batch variations, and difficulties establishing large scale processes. Many attempts for establishing novel biomedical applications have been studied by modification or combination of natural polymers including proteins (e.g. collagen [9,10], silk fibroin [11]) and polysaccharides (e.g. cellulose [12], hyaluronan [13,14], alginate [15,16], chitin, and chitosan [17]).

As regard to polysaccharides, chitin and chitosan have been widely studied for use as biodegradable and biocompatible materials. Chitin is a poly-β(1→4)-N-acetyl-D-glucosamine which is known as a cell wall component of fungi and as a skeletal component of crustacea. The commercial source of chitin is mostly from crab, shrimp, and krill shells and fungi, of which large amounts are wasted in the food industry [18,19]. Several groups have studied how to extract chitin and produce chitosan from these resources [10,20]. A flow chart of chitin production is shown in Figure 1-1. Chitosan is a cationic poly-β(1→4)-2-amino-2-deoxy-D-glucose, obtained by deacetylation of chitin. When the degree of deacetylation of chitin is more than 50%, it is generally considered as chitosan. The chemical structure of chitosan is described in Figure 1-2. Although chitin and chitosan have potential as resources for commercial use, both chitin and chitosan are inherently insoluble in water, which makes these materials difficult to process. Only very strong acidic conditions, such as

with formic acid, di- or trichloroacetic acids, methansulfonic acid, and lithium chloride/amide, can solubilize chitin [21]. Chitosan is soluble in milder acids such as aqueous acetic acid. Their insolubility is usually attributed to intermolecular hydrogen bonding in the solid state [22].

There are many examples of chemical modification and salt formation to make chitosan soluble in water or organic solvent systems [23-29]. *N*- or *O*- substitutions by various moieties such as the carboxymethyl group, are typical chemical modifications. However, studies for unmodified chitosan dissolution, almost all have reported molecular weight lowering of chitosan [23-25]. As a result, chitosan has been developed for a wide range of applications such as water clarification, flocculants, cosmetic and pharmaceutical uses, and biomedical devices (Figure 1-3).

The biocompatibility, antigenecity and bioadhesiveness of chitosan has led to extensive studies of biomedical applications including antibacterial activities and hemostatic agents for wound dressings. It has been reported that chitosan has an antibacterial nature and greater advantages over the other commercially available hemostatics [22, 30, 31]. However, the biological effect of chitosan itself is still not fully understood in detail, because the chemical and physical properties of chitosan always depend on the molecular weight, degree of acetylation, degree of crystallinity, extent of ionization/free amino group, and so on [22]. The optimum conditions for chitosan processing are wide-ranging. Although various types of hemostatic agents of chitosan and its derivatives have been suggested, the evaluation method for hemostatic properties is varied with each research group and has not completely been standardized among researchers. Although various preparation conditions of chitosan (e.g.

molecular weight, pH, degree of deacetylation, viscosity and solubility) have been examined chemically and physically, their results are not always reflected on the hemostatic applications and few reports have been published about the relationship between chitosan characteristics and their effectiveness as biological agents.

In this review, some properties of chitosan will first be described such as biocompatibility and cytotoxicity that effect applications such as scaffolds and drug delivery systems. The use of chitosan and its derivatives for hemostatic applications and blood contacting test methods for clinical use will also be discussed.

Prompt control of wound hemorrhage remains a significant contemporary problem and an active search for effective, safe, and economical hemostatic agents warrants intensive research. Inadequate early response hemostasis is clearly identified as the major cause of excessive mortality whether associated with accident, trauma or surgical procedures. As a consequence of this recognized need, a need becoming more apparent with contemporary battlefield events, numerous research programs are in place to develop rapidly deployable hemostatic agents. Some are effective hemostats but have drawbacks. Hemostatic agents currently available commerically include the microcrystalline tectosilicates derived from aluminum and silicon oxides [32], poly-N-acetylglucosamine derived from marine algae [33], and the HemeCon bandage which is a lyophilized chitosan derivative[34]. Chitosan has been reluctantly accepted as a hemostatic agent because of uncertainty of its procoagulant effect, absence of patent protection, and the technical difficulties in both manufacture and application of chitosan as either a liquid, powder or flake. The procoagulant effect of chitosan appears to be a function of molecular weight - higher molecular weight polymers of

chitosan having greater procoagulant and antimicrobial effects. There is a paucity of characterizing chitosan preparations with regard to their degree of deacetylation (DD), molecular weight and other biochemical properties. A better understanding of mechanisms underlying chitosan mediated hemostasis is now emerging and these will be reviewed in the paper. For example, chitosan induces platelet adhesion aggregation with an evidence of calcium mobilization [35]. Chitosan as a cationic polymer acts on absorbent of negatively charged low molecular weight plasma proteins and red blood cell agglutinator [36]. Adhesion of the hemostatic agent to an injured vessel is an important component of the hemostatic process, but understanding of how and why chitosan attaches so firmly to the tissue mucosal surfaces remains uncertain.

1.2.2 Biocompatibility and cytotoxicity of chitosan-based matrices

One of the important aspects for a biocompatible material is the interaction between cells and material surfaces. The material surface is required to act as an artificial extracellular matrix (ECM) with a three-dimensional structure, which is vital for progression of the cell cycle [37,38]. Most cell types are not be viable without attachment to the scaffold since apoptosis (programmed cell death) is induced. Extracellular matrices are primarily *in vivo* proteoglycans. Artificial ECMs composed of these natural materials are reported to compensate for defects in tissue scaffolds, and thus prompt cell proliferation, differentiation and regeneration. For example, a highly porous scaffold made of chitosan derivative has been developed for a bioartificial liver device [37]. It is well known that polysaccharides termed glycosaminoglycans, control cell functions and are associated with bioadhesive proteins to

include collagen, fibronectin, and laminine. On the other hand, natural hydrophilic polymers have also been identified as drug delivery carriers because of the potentially safe, sustainable, and controllable release of drugs. To characterize and evaluate these man-made matrices from the viewpoint of biocompatibility and cytotoxicity, is the primary task necessary to apply these matrices for tissue engineering. Such chitosan-based scaffolds for tissue engineering and capsules for drug targeting applications in different cell types will be described in this section.

1.2.2.1 Scaffolds for tissue engineering

Any matrices used for tissue engineering are required to support the cells and restore and improve the cell function, including induction of the cell-specific cytokine and gene expressions. It is reported that a chitosan supplement to culture media accelerates the production of specific cytokines (IL-8) that are marker cytokines for angiogenesis in contrast to insignificant (L929) [39]. Other authors suggested that chitosan mediates rat peritoneal exudates macrophage (PEM) activation for immune stimulation confirmed by nitric oxide (NO) secretion [40]. Chitosan oligomers promote cell migration and proliferation of fibroblast (mouse fetal fibroblast; 3T6 cells) and vascular endothelium (HUVEC) (Figure 1-4, [41]).

Chitosan is a highly thrombogenic material, so it is suggested for use as wound dressings rather than supplements, because of the formation of granulation on the tissue [9,41,42]. Similarly, collagen, one of the structural proteins, is recognized as an appropriate tissue-culturing scaffold but is thrombogenic inducing platelet aggregation and blood

coagulation [9]. A crosslinked collagen/chitosan multi-layer matrix with few free carboxyl and amino groups resulted in decreased platelet adhesion but promoted hepatocyte adhesion due to the remaining free amino groups of chitosan. There is no quantitative information relating remaining amino groups or free carboxylate groups to an anticoagulant effect.

Although chitosan itself has an affinity for many types of cells, it is anticipated that cell proliferation, growth, and differentiation can be improved by chemically modifying the amino and hydroxyl groups of chitosan. Several peptide sequences that play important roles for cell behavior have been identified with RGD (Arg-Gly-Asp) and its analogs are the best recognized adhesive peptide sequences [43,44]. To enhance the rat osteosarcoma cell (ROC) adhesion the C-terminal of RGDS peptide was covalently bonded to the amino group of chitosan by a water-soluble carbodiimide [45]. No information is provided as to how the amino group on the N-terminal peptide was protected with immobilization. Chitosan modified film and porous scaffolds were prepared by casting (for film) and lyophilization (for sponge) and morphology observed by SEM (Figure 1-5). A peptide density of $1X10^{-12}$ mol/cm^2 on the scaffolds is sufficient to support the cell adhesion process and the RGDS-modified chitosan improved both cell attachment and mineralization, a typical differentiation phenomenon for osteoblasts.

The peptide GRGD was photochemically grafted to chitosan film using a photoreactive azide group spacer called SANPAH [46,47]. The film was further cross-linked with tripolyphosphate to enhance the adhesion and viability of human endothelial cells. The authors concluded that the peptide grafted chitosan and its cross-linked chitosan improved the endothelial cell growth. A photochemical reaction may have also occurred between the

azide group of the peptide-SANPAH fragment and hydroxyl group of chitosan as described in Figure 1-6. However, in general, the azide group was converted to a nitrene group. The nitrene reacts with the amino group, especially if the substrate contains a primary amine group. Furthermore, chitosan has two hydroxyl groups at the 3- and 6-positions in the structure (Figure 1-2) but no description was provided as to which hydroxyl group was most likely reacted with the crosslinker and to what extent the hydroxyl group was reacted. Generally, the primary alcohol at C-6 is considered more reactive in many cases. It is not clear whether the peptide or the amino groups of chitosan were photochemically immobilized resulting in ambiguous conclusions. Further work is needed to improve the scaffolds for tissue engineering because polystyrene culture plates, widely used for *in vitro* studies, showed better cell growth than these scaffolds.

Bioadhesive hydrogel also provides a suitable environment for tissue adhesion due to matrix softness [48]. Low molecular weight deacetylated and *O*-carboxymethylated chitin forms a polyampholytic hydrogel by mixing solutions in the presence of a cross-linking glutaraldehyde. An adhesion test was conducted to evaluate the interaction between the hydrogel and porcine dermis tissue *ex vivo*. A higher concentration (4wt%, deacetylated chitin:carboxymethylated chitin=95:5) of the hydrogel polymer with lower water content induced higher adhesion strength between tissue and hydrogel. The formation of ionic interactions between each polymer chain, contributed to the decreasing water content of the hydrogel. Hydrogel toughness improved with increasing polymer volume fraction enhancing tissue adhesion because of the high binding energy of the elastic hydrogel. In addition, the increased polymer volume fraction provided a higher surface density of the bioactive

polymer segment to interact and adhere to the tissue. It is anticipated that hydrogels made of chitosan and its derivatives represent another potential form of bioadhesive or hemostatic agents.

1.2.2.2 Microspheres and capsules as a drug carrier

Chitosan is widely used in pharmaceutical applications due to its versatility, biocompatibility, digestibility, and low-cost and is a valuable drug delivery vehicle. Drug delivery applications include oral, nasal, mucosal, and transdermal routes for drug targeting systems [49]. Chitosan is also used as a dietary supplement for controlling obesity because of its ability to bind with fat. Sustained drug release vehicles include microspheres, beads, compressed tablets, nanoparticles, gels, and films. Various kinds of drugs, proteins, and enzymes encapsuled in microspheres have been introduced as chitosan-based microparticular delivery systems [49,50].

Microsphere drug delivery is one model for the oral delivery of drugs [49-53]. An important element for a drug delivery system is to localize the drug at a particular part of the body for an effective clinical treatment. Oral administration of such a site-specific drug delivery system has become of recent interest. Controlling the release of peptides and low molecular weight drugs is one of the key issues to overcome problems including exposure of drugs to acid environments and prevention of degradation by enzymes in the gastrointestinal tract. Chitosan is a candidate drug control-release carrier due to its non-toxic and bioabsorbable nature.

Since chitosan salt is a cationic polysaccharide, the sustained-release of drugs can be controlled in the presence of various fatty acids such as stearic, palmitic, myristic, and lauric acid under different pH conditions [51]. One study, vancomycin hydrochloride, an antibiotic, was used as the drug. Chitosan salts were prepared by mixing chitosan with an aqueous solution of asparaginic acid and glutamic acid, or hydrochloric acid, and freeze-dried chitosan salts physically mixed with vancomycin hydrochloride. Finally, each chitosan salt-drug mixture was added to various fatty acid solutions containing nonionic surfactant Span60. Drug containing microspheres with 1-5μm diameters were obtained by a spray-drying method. The ability for sustained-release of drug was evaluated by the dialysis method. Solutions at pH 2.0 and 7.4, which assumed gastric and intestinal conditions, were used. At pH 2.0, the microspheres with longer alkyl chains (stearic and palmitic acid) suppressed the release of the drug significantly. On the other hand, at pH 7.4, overall drug release increased even in the drug coated with long alkyl chains. This might be caused by the increased solubility of the fatty acids at pH 7.4 compared to pH 2.0 due to the ionization of the carboxylic acid which promoted the release of free drug. As a consequence, it was concluded that fatty acids retarded the release of drug in acidic conditions.

Several chitosan derivatives of different molecular weight and deacetylation, such as *O*-hydroxyethyl chitosan, chitosan hydrochloride, chitosan lactate, chitosan glutamate, and crosslinked chitosan were evaluated in terms of cytotoxicity, blood cell lysis and horseradish peroxidase (HRP) release from the chitosan microspheres *in vitro* [52]. It is known that cationic polymers, such as poly-L-lysine, generally exhibit cytotoxicity towards cells in a concentration-dependent manner and cause blood cell lysis. The model drug, HRP, could be

entrapped and retained in chitosan microspheres crosslinked by glutaraldehyde although some active HRP was detected. All the soluble chitosan salts and *O*-hydroxyethyl chitosan exhibited cytotoxicity towards murine melanoma cells (B16F10), depending on their concentrations, even though they were less toxic than the positive control, poly-L-lysine. The counterion of chitosan affects the interaction between the protonated amine group and negatively charged cells, leading to the observed differences. SEM observation indicated that the plasma membrane was damaged by interaction with the microspheres. Polymer molecular weight is also an important factor for cytotoxity as higher molecular weight chitosan is significantly more toxic. Although glutaraldehyde is frequently used as a model crosslinking agent due to its low toxicity, the glutaraldehyde crosslinked chitosan microspheres were even more toxic. Some studies demonstrated that the immune response by glutaraldehyde crosslinked microspheres is due to the residual aldehyde, which could be removed by a bisulphite wash [53]. *In vitro* release of progesterone from the crosslinked chitosan microspheres is shown in Figure 1-7 [53]. Red blood cell lysis accompanied with hemoglobin release, occurred for all chitosan derivatives in a time and molecular weight dependent manner even at low chitosan concentration (1-100μg/ml) [52].

The chain flexibility of chitosan also plays an important role in determining the capsule characteristics including shape, break force, thermal properties, and drug-release ability of chitosan microspheres [54]. Microspheres were prepared with different deacetylation (DD=67.9-92.2%), molecular weight (Mw=$1.8X10^5$-$31.8X10^5$) with or without NaCl at various acidic conditions (pH=2-4). Highly deacetylated chitosan resulted in more molecular weight loss. The more deacetylated, the more flexible the chitosan chain becomes, thus the

chain tends to form a random coil, which has more intramolecular hydrogen bonds within the chain. This results in the chitosan chains being less entangled and more ellipsoid in shape. The enthalpy measured by DSC is higher due to the hydrogen bond formation in the capsules and therefore, their mechanical properties were generally weaker than those of less deacetylated microspheres. In contrast, the less deacetylated chitosan chain was more extended and had stronger intermolecular interactions, which made the chains more entangled contributing to reinforce the capsule structure with a more spherical shape. Molecular weight also influenced the number of the hydrogen bonds and entanglements and to the capacity for capsule formation. However, the molecular weight of the microspheres varies with the degree of deacetylation. Thus it seems to be difficult to conclude what parameters, either molecular weight or degree of acetylation, or both and to what extent both actually affected the chain flexibility and extent of entanglement [54].

1.2.3 Antibacterial activity of chitosan and its derivatives

It is important to clarify the antibacterial actions of scaffolds or wound dressings as well as biocompatibility and blood compatibility for hemostatic applications. When tissue is burned and damaged, the wound healing process is disrupted because of the surrounding normal tissue barrier system acts to prevent microbial infections [55]. Maintaining a moist wound not debilitated by microbes is a primary requirement for wound dressing materials. Microbes prefer to grow in necrotic, moist tissue leading to sepsis and mortality. Anti-microbial agents have been incorporated in the dressings but it is difficult to control the sustained-release of these materials. Wound dressings should also absorb the exudate or body

fluid produced from the wound area but not adhere to the wound surface too strongly, to avoid damaging newly formed tissues. Consequently, preventing wound invasion by microorganisms and removing excess exudate from the damaged tissue accelerates wound closure. Because of the antimicrobial and hemostatic effects of chitosan, wound dressings made of chitosan derivatives have been extensively studied to overcome those limitations [13,55-58].

1.2.3.1 Antibacterial actions

Chitosan and its derivatives are known as antimicrobial agents against a wide variety of bacteria and fungi [59,60]. Figure 1-8 shows culture media containing chitosan suppressing bacterial growth [61]. One hypothetical mechanism is that the chitosan polycation interacts with negatively charged bacterial surfaces to inhibit the bacterial growth [61]. Chitosan solutions at low concentrations induce wall permeability changes resulting in leakage of intracellular components of bacteria. At higher concentration, chitosan accumulated on the bacterial surface to disturb metabolite transport [59,61]. The antibacterial activity of chitosan itself, is exhibited only in acidic solutions due to the poor solubility above pH 6.5 and lack of cationic charges. Therefore, water-soluble chitosan derivatives including carboxymethylated chitosan and quaternary ammonium salts of chitosan are good candidates for anitibacterial applications [61-63]. *N*,*O*-carboxymethylated and *O*-carboxymethylated chitosan of different molecular weights and deacetylations have had antimicrobial activity tested against *E. coli* [61]. Antibacterial activity increases with increasing molecular weight of chitosan, though too high a molecular weight or concentration is counter productive. *N*-carboxymethylated chitosan does not inhibit bacterial

growth, attributed to the chemical modification of the amino group. They also postulated that too many amino groups on a single chain, might form a pseudo- crosslinked structure through intramolecular hydrogen bondings and the chitosan could not then interact with bacterial surfaces. The optimum molecular weight of chitosan for anti-microbial activity is about M_v=9.16X10^4. In similar experiments, however, the antibacterial activity increased with increasing deacetylation (M_v=12.7-27.4X10^4, DDA=74-96%) and concentration (M_w=5000, DDA=73%, C=0-0.50 w/v%) of chitosan. The highest deacetylated sample and the highest concentration of chitosan exhibited the best antibacterial activity. Unfortunately, there was no information about the theoretical amount of ammonium salt forming at the pH utilized, depending on the molecular weight of the chitosan. Further comparisons between ionized amino groups chitosan with high molecular weight and with higher concentration in the culture system are needed.

In another attempt to increase water solubility, the *N*-alkyl chitosan derivatives: *N*,*N*,*N*-trimethyl chitosan, *N*-*N*-propyl-*N*,*N*-dimethyl chitosan, *N*-furfuryl-*N*,*N*-dimethyl chitosan quaternary salts, were prepared through Schiff base intermediates with different molecular weights of chitosan [63]. *N*-furfuryl-*N*,*N*-dimethyl chitosan with low molecular weight (M_v=7.80X10^3) shows the highest water solubility, attributable to the quaternary salt formed and low molecular weight. The minimum inhibitory concentration (MIC) and minimum bacterial concentration (MBC) effects of quaternized chitosan against *E. coli* depend on molecular weight. Antibacterial activity increased while increasing the alkyl chain length and also increased in the presence of acetic acid. Quaternary chitosan ammonium salts exhibited a higher antibacterial effect than chitosan with particularly an acidic medium.

Studies of the biospecific fraction of chitosan have also been reported [64,66]. A small fraction of *N*-acetylated units (F_A) specifically bind to lysozymes and chitinases without cleavage of glycosidic linkages, whereas fully deacetylated chitosan does not [64]. The acetyl group is essential for binding with lysozymes with affinity strongly dependent on pH and ionic strength. The effect of chemical composition of chitosan (F_A) against *E. coli* was also examined in terms of various conditions such as molecular weight, pH, and ionic strength [65]. The chitosan adsorbed to *E. coli* strongly increased with pH. However, it decreased with increasing molecular weight, which was not consistent with other authors. Interestingly, chitosan with a highly acetylated fraction (F_A=0.49) flocculated *E. coli* most effectively, although the details of this mechanism are still in question. Nevertheless, an acetylated fraction of chitosan might interact with particular enzymes and cells biospecifically, whereas the amino group of chitosan might physically interact with them.

1.2.3.2 Bioadhesives for wound dressings

Several types of wound dressings are commercially available to support wound healing processes. Sponges, hydrogels, woven and non-woven dressings derived from natural, and abundant polymers have been developed for practical use. Since chitosan is acknowledged as a biodegradable, biocompatible, and bacteriostatic polysaccharide, many chitosan matrices for wound dressings with bioadhesiveness have been studied extensively [66,67].

A dual layer chitosan-based wound dressing was fabricated by combining carboxymethylated chitin hydrogel as an upper layer with chitosan acetate foam as a lower layer [55]. Although not specified, it is assumed that the foam is the acetate salt of chitosan.

The matrix was designed so that the upper hydrogel layer is able to absorb wound exudates and block microbial invasion and the lower foam layer serve as an antibacterial material. Indeed, the upper hydrogel was swollen and absorbed four times its own weight of water and its 50% vapor permeability was sufficient to prevent accumulation of exudates. The chitosan acetate foam incorporated chlorhexidine gluconate with an optimal loading concentration of 1% (w/v), releasing the antibiotic to inhibit bacterial growth of *Pseudomonas aeruginosa* and *Staphlycoccus aureus*.

An asymmetric chitosan membrane consisting of a top layer containing an interconnected microporous skin surface and sponge-like macroporous sublayer has been prepared by an immersion-precipitation phase inversion (IPPI) method [56]. The advantage of this assembly is to achieve both prevention of bacterial invasion and regulation of evaporative water loss. Thickness and density of the membrane can be varied, depending on the per-evaporation conditions. The membrane exhibits moderate water evaporation, oxygen permeability and fluid drainage ability due to the dense skin surface, and the thick and porous sublayer of chitosan membrane. It inhibits bacterial invasion and penetration into the membrane because of the dense surface and antibacterial nature of chitosan. A rat skin wound area covered with chitosan membrane stopped bleeding since chitosan is a hemostatic agent and rapid epithelialization was facilitated.

Hydrogels are considered as a substitute for fibrin glue. Fibrin glue has been widely applied for medical purposes such as wound sealant. The preparation contains fibrinogen, thrombin, factor III, and protease inhibitor, all necessary for hemostasis and blood coagulation. Due to difficulty of its mass production and contaminant suppression, a novel

biological adhesive with better properties has been desired [57]. Although crosslinked gelatin and cyanoacrylate polymers have been developed, they are not suitable for biomedical applications because of their high toxicity. In contrast, polysaccharides and their derivatives including chitin, chitosan and hyarulonan are known as biocompatible materials and have been used for healing processes and supporting tissue defects. Since chitosan has antibacterial and hemostatic effects, a chitosan derivative with both azide and lactose moieties were photochemically crosslinked to prepare a hydrogel adhesive [57,58]. Lactobionic acid and 4-azidobenzoic acid were introduced to chitosan by stepwise condensation reactions with TEMED (N,N,N',N'-tetramethylethylenediamine) and EDC (1-ethyl-3-(3-dimethylaminopropyl) carbodiimide). The reactive azido group was converted to nitrene by UV irradiation which reacted with the remaining amino groups of chitosan, causing hydrogel formation. There was no information about the degree of modified functional groups and the remaining amino groups in the chitosan. Water solubility (around neutral pH) of modified chitosan increased with increasing lactose concentration and low concentrations of azide did not alter water solubility. The time required for UV irradiation to form a hydrogel is 30 sec and it is faster than fibrin glue. Binding and sealing strength of Az-CH-LA increased with increasing concentration. Even though cultured cells (human skin fibroblast, coronary smooth muscle cells, and endothelial cells) did not adhere onto the chitosan surface very well, cell viability was retained without toxicity. The authors also demonstrated with *in vivo* experiments, that advanced granulation tissue formed and epithelialization occurred, when treated with chitosan hydrogel, which facilitated rapid wound occlusion [58].

1.2.4. Hemostatic potential of chitosan and its derivatives

Hemostatic materials have different surface properties from blood contacting materials that are non-thrombogenic. The development of artificial biomaterials that contact blood (e.g. prosthetic vascular grafts) have a primary consideration for being anti-thrombogenic. Thrombosis on the material surface remains a serious bioengineering problem despite demonstrated good blood compatibility. As an example of thrombosis, small caliber prosthetic vascular grafts (O.D. < 3 mm) invariably resulting in thrombus formation in the short term and intimal hyperplasia occurs in the long term [68]. Thrombosis is assumed to be caused by plasma protein adhesion, platelet activation and clot formation. For example, polyurethane (PU) is a well-known biomaterial with good biocompatibility and mechanical properties for biomedical applications. However, the usage of PU is still limited because of the poor cell attachement/growth or the induction of thrombinogenesis on the surface. Many attempts have been made, such as chemically or photochemically modifying the PU surface to overcome these problems [68,69]. Bioactive molecules such as prostaglandine E_1, albumin, and heparin or its derivatives with sulfate groups have also been used to modify the material surface in order to decrease the thrombogenicity [70-73]. They have an anticoagulation property, however, which also induces haemorrhage of the tissue. When chitosan is applied as a blood contacting material, such anticoagulant modifications are usually applied [70,72]. The effect of chemical structure modifications and physical form of the chitosan upon hemostasis was recently reviewed [22]. In addition, several commercially available hemostatic agents including a chitosan derivative approved by Food and Drug

Administration have been used in recent combat operations and their effectiveness has been reported [74,75]. Chitosan, itself, is not suitable for a blood contacting material in spite of its biocompatibility.

Due to this blood coagulating nature, chitosan has been a desirable material as a hemostatic agent in addition to its biocompatible and antibacterial characteristics. This hemostatic activity of chitosan is important for understanding the mechanism of action as a coagulant and developing medical bandages which control bleeding during surgery. Several studies report that the hemostatic mechanism induced from chitosan is independent of the classical blood coagulation cascade [22,76-78]. However, because of the complexity of the blood coagulation mechanism itself, it is still difficult to clarify how chitosan effects this mechanism. A wide variety of evaluation methods have been adopted to examine the hemostatic properties, and will be introduced in a later section. Nevertheless, it is important to understand what factors in blood influence the hemostatic mechanism, especially for the potential clotting cascade induced by chitosan.

1.2.4.1 Factors involving the blood coagulation mechanism

The blood coagulation mechanism is still under investigation because of the complexity of the hemostatic-thrombotic system. Hemker et al introduced the first law of hemostasis and thrombosis: increasing thrombin formation causes more thrombosis but less bleeding, and decreasing thrombin formation causes more bleeding but less thrombosis [79]. Recent studies allowed monitoring the thrombin generation in platelet poor plasma (PPP) and platelet rich plasma (PRP) by using fluorogenic thrombin substrates [79]. However, it is still

challenging to evaluate blood coagulation as close as possible *in vivo,* because the actual blood circulation time is shorter than that time required for whole blood clotting.

Currently, two major pathways are believed to trigger blood coagulation (Figure 1-9, [80, 81]). One is the adsorption of plasma proteins such as albumin, γ-globulin, fibrinogen, and prothrombin onto the material surfaces. Factor XII, an intermediate of the intrinsic coagulation pathways is activated following the protein adsorption to initiate the clotting cascade. The other pathway is cell-bound thrombin generation involving tissue factor cells called monocytes and perivascular cells and platelets. It is pointed out that the activated platelets induce the interaction between platelet membrane glycoprotein (e.g. GPIIb/IIIa complex, von Willebrand factor) and sub-endothelial matrix [80]. Thrombin and collagen play an important role for platelet activation to produce procoagulant phospholipids [79]. Several biomaterials such as polyethylene and polyurethane that induce thrombosis on surfaces have been used in conjunction with several plasma factors including prothrombin, fibrinopeptide, blood coagulation inhibitor called protein kinase C, and thrombin-antithrombin III complex [81-83]. A platelet reaction at artificial surfaces triggers thrombosis (Figure 1-10).

In the case of chitosan, several hemostasis evaluations have been reported [83-91]. However, many test methods have been applied to different types of tissue in different articles. Chitosan's hemostasis might be caused by the non-classic coagulation pathway, whose mechanism and detailed phenomena are still unclear. Nevertheless, these studies mainly focus on the blood coagulation time and platelet adhesion and aggregation induced by

chitosan. The effect of chiotosan and its derivatives on hemostasis potential and the hemostasis tests suggested in several studies is introduced in the following section.

1.2.4.2 Hemostasis evaluations for chitosan and its derivatives

When examining normal baseline blood parameters *in vitro*, hematocrit, hemoglobin concentration, platelet count, prothrombin time, activated partial thromboplastin time and plasma fibrinogen concentration are evaluated [83]. There are no standardized or universally accepted methods for evaluating chitosan mediated hemostasis. The chitosan hemostasis pathway appears to be fundamentally different from "classic" coagulation pathways. Since it is already known that platelet aggregation was observed on chitosan materials microscopically, the morphology of platelets was considered to affect the blood coagulation system. Platelet-related cytokines and proteins have been examined in addition to general coagulation tests [83].

In vitro examination of blood clotting ability is widely used for diagnosing clotting disorders in the medical field and, is assessed in regard to several coagulation factors. Accepted blood coagulation tests are prothrombin time (PT), partial thromboplastin time (PTT), thrombin time (TT), activated partial thromboplastin time (APTT), clot retraction time (CRT), plasma recalcification time (PRT) [76], and whole blood clotting time (WBCT) [21,76,84]. Similar coagulation tests, such as blood coagulation time (BCT) [85], fibrin clot formation time [86], R_{APTT}, R_{TT}, R_{PT} values (ratio of APTT, TT or PT to those of the control assays) [87], have been reported. Test methods and results vary on collection of the blood specimen. Platelet aggregation (PA) is one of the key phenomena in blood coagulation

induced by chitosan derivatives. PA was monitored by a light penetration [85] or turbidimetric device [21,35], and scanning electron microscopy (SEM) [76,84,85,87,88]. The platelet activation was assessed by counting the number of Coomassie brilliant blue-stained platelets [88]. Some studies also focused on red blood cell morphology by SEM (Figure 1-11, [77]) and cell aggregation measured spectrophotometrically (OD_{528}) [86]. Some cytokines released from platelets have been considered as important factors to enhance early wound healing processes. Thus, platelet derived growth factor (PDGF-AB) and transforming growth factor β1 (TGF-β1) release has been measured by enzyme immunoassay [85]. Platelet activation, intracellular calcium level in platelets and glycoprotein IIb/IIIa complex on platelet surface have been examined to elucidate details of the chitosan-induced blood coagulation mechanism [35].

Laboratory animals with different wound models have been treated with chitosan derivatives for *in vivo* testing. Sutures coated with chitosan, *N*-acyl-chitosans, chitosan-tropocollagen fibers and their *N*-modified fibers were introduced into the lumen of dog's jugular and femoral veins [90,91]. The blood clot formed around the fibers was observed macroscopically. In other studies, lingual bleeding time, systematic bleeding time, and systematic coagulation time was measured when chitosan solution was introduced onto lacerated rabbit tongue [77]. Severe swine liver injury due to the lacerated major vessels was treated with a chitosan acetate salt dressing and the effect of the dressing was studied by monitoring blood loss, fluid use, hemostasis time and survival (Figure 1-12, [83]). Furthermore, hemostasis performance of poly-*N*-acetyl Glucosamine (p-GlcNac) fiber was

observed until bleeding was stopped by continuous compression at the wound area in swine spleen [86].

1.2.4.3 Effects of chitosan and its derivatives on blood coagulation

Various chitosan-based hemostatic agents have been developed and tested for their potential usability *in vitro* or *vivo* [22]. An early study incorporated a silk polyfilament coated with chitosan and *N*-acetyl and *N*-hexanoyl chitosans [90]. A thick coagulum formed on the chitosan suture inserted to the lumen of a dog's peripheral veins due to the rough fibril surface with less on the smooth surface of *N*-modified chitosan. Hirano et al [91] pointed out that blood components tended to adsorb physically onto rough surfaces. Chitosan-tropocollagen, *N*-acetyl chitosan, and *N*-acetyl chitosan-tropocollagen fibers were inserted into the lumen of a dog's jugular and femoral veins in a similar manner [91]. Chitosan-tropocollagen and *N*-acetylated chitosan fibers caused weak blood clots to form but almost no blood clots formed on *N*-acetyl chitosan-tropocollagen and tropocollagen fibers. Introducing carboxy groups into the *N*- and *O*- positions increased activated partial thromboplastine time (ATPP) and thrombin time (TT) more than that just due to the amino groups [87]. Thus, carboxylation of *N*- and *O*- positions tends to prolong the blood coagulation time.

The effect of chitosan on hemostasis has been investigated for several chitosan physical forms. It was found that chitosan solution in 2% aqueous acetic acid caused hemagglutination even at low concentration and the whole blood clotting time (WBCT) is reduced by 40% [76]. Chitosan did not induce red blood cell lysis. Chitosan interacted with the red blood cell

membrane and led to the erythrocyte aggregation as seen by SEM observation (Figure 1-11). The hemostatic property was attributed to electrostatic interaction by the cationic nature of chitosan at pH's below 6.4. The authors concluded that chitosan hemostasis is obtained by a process independent of the normal blood clotting cascade but dependent on red blood cell agglutination. Similar conclusions were derived from other studies. For example, topical administration of chitosan dissolved in 0.2% glacial acetic acid solution shortened the lingual bleeding time of rabbit to 43% of the control [77]. SEM observation demonstrated that the red blood cells treated with chitosan solution lost their typical biconcave morphology and coalesced into a clot. It has been hypothesized that chitosan promotes hemostasis by linking erythrocytes together to form a lattice to entrap the cells.

Platelet activation has been another line of study for understanding chitosan-mediated hemostasis. Chitosan coated microtiter plates enhanced platelet adhesion and aggregation concentration and time dependency [35]. Significantly, chitosan influenced the intracellular calcium level known as the second messenger in platelets and GPIIb/IIIa expression on platelets. Since platelets don't adhere to endothelial cells under normal conditions, this feature would implicates platelet activation for initiating hemostasis. It is known that fibrinogen-GPIIb/IIIa binding could be observed in the final common pathway of blood coagulation. Therefore, chitosan might account for the interaction between activated platelets and damaged tissue to promote the wound healing process.

Chitin also seems to have hemostatic potential. Chitin and chitosan suspension in phosphate buffered saline (PBS) reduced blood coagulation time (BCT) in a dose-dependent manner [85]. They shortened the BCT to 30-40% of the control, even at a low concentration

(0.1 mg/ml). Chitin and chitosan have a hemostatic effect due to a physical binding effect and the amino group in their chemical structure. Chitosan is more effective than chitin for hemostasis, whereas chitin induces more platelet aggregation than chitosan. Cytokine (PDGF-AB and TGF-β1) release considered important in the wound healing process is greater for chitosan than chitin, and far less for latex and other controls. Chitosan forms stronger platelet aggregates by interacting with platelets on membranes. Porous sponges of chitosan acetate salt also significantly reduced blood and other fluid loss for a swine liver injury, compared to the swine treated with control gauze sponge [83]. The authors indicated that a fully *N*-acetylated chitin sheet (p-GlcNAc) reduced hemostasis time compared to the control. Fully *N*-acetylated chitin is found in some algal sources and is termed "chitan" [92,93].

Dependency of chitosan's hemostatic effect on molecular weight has been demonstrated with water-soluble chito-oligosaccharide (COS) and highly deacetylated chito-oligosaccharide (HDCOS) [21]. Both 10% of COS and HDCOS prolonged the WBCT compared to the PBS control. There was no significant difference between COS and HDCOS in WBCT. Furthermore, these polymers did not have a significant effect on the platelet aggregation compared to the control. These results indicated that low molecular weight chitosans did not have a hemostatic effect and that only chitosan polymers of a minimum critical molecular weight have hemostatic potential.

In contrast, chitosan-based hemostatic agents did not always manifest improved hemostasis than Syvek p-GlcNAc [86]. The p-GlcNAc is a fiber with a crystalline beta-form three-dimensional structure [86,94] derived from micro-algae [95]. It is distinguished from other

N-acetyl glucosamine based polymers such as chitin, chitosan, and hyaluronan. Chitin and chitosan are the copolymers of *N*-acetylglucosamine and *N*-glucosamine, and have been poorly defined in published hemostasis studies in terms of degree of deacetylation and the polymer chain structure [95].

A commercially available chitosan-based hemostatic agent, Clo-Sur® PAD is entirely composed of chitosan. Chitoseal® consists of a thin layer of chitosan coated onto PET filament, and hemostatic properties have been compared to other chitosan derivatives [86]. Red blood cell aggregation was observed with p-GlcNAc in a concentration-dependent manner but not for the other two chitosan-based materials. Platelets absorbed onto p-GlcNAc are inferred to be in an activated state, similar to fibrin-platelet interactions, whereas no platelet activation was noted in other chitosan controls. Furthermore, p-GlcNAc appeared to be more effective in controlling bleeding in swine splenic trauma compared to two other chitosan derivatives. These different behaviors between p-GlcNAc and other chitosan materials are assured to result from structural differences. Although the aligned beta three-dimensional structure of p-GlcNAc is rare in nature, its fibril strand size was similar to that of fibrin. It was concluded that the unique, large surface area structure of p-GlcNAc might be one of the reasons why it is effective in its interaction with blood proteins and cells for promoting hemostasis. However, it is still a question why the chitosan-based hemostatic agents were not effective in this study. Though the effectiveness of chitosan derivatives as hemostatic agents has been demonstrated in numerous studies, the hemostatic mechanism mediated by chitosan derivatives is still unknown.

1.2.5 Conclusions

Chitosan and its derivatives have been found to have hemostatic potential as well as anti-microbial activity and biocompatibility. Chitosan is easily obtained from chitin by a relatively simple chemical reaction. Since chitin and chitosan derivatives are relatively inexpensive hemostatic agents and available fibrinogen-based hemostatic agents are potentially infectious and expensive, further studies are clearly warranted. In most studies, chitosan and its derivatives enhanced platelet and erythrocyte aggregation, a feature necessary to initiate blood coagulation. It has been clarified that not only the physical form of chitosans, along with molecular weight, degree of deacetylation, surface characteristics, but also their chemical structures affect hemostatic and antibacterial actions. However, various chitosan compositions with different molecular weight, deacetylation, counter ions, and solvents have been used in different antibacterial or blood coagulation tests, which makes it difficult to compare all results. More details of the blood coagulation cascade and its mechanism induced by chitosans are also expected to clarify and distinguish the action of chitosan on the classic cascade. In addition, fully chemically and physically characterized chitosan and its derivatives are needed in order to elucidate the effects on antibacterial and hemostatic actions. Standardized test methods are needed to compare the results in a more meaningful way.

1.2.6 References

1. Barrera DA, Zylstra E, Lansbury PT, Langer R. Sysnthesis and RGD peptide modification of a new biodegradable copolymer: poly(lactic acid-*co*-lysin). J Am Chem Soc 1993; 115: 11010-11011.
2. Hu Y, Winn SR, Krajbich I, Hollinger JO. Porous polymer scaffolds surface-modified with arginine-glycine-aspartic acid enhance bone cell attachment and differentiation *in vitro*. J Biomed Mater Res 2003; 64A: 583-590.
3. Moon SI, Lee CW, Miyamoto M, Kimura Y. Melt polycondensation of L-lactic acid with Sn(II) catalysts activated by various proton acids: a direct manufacturing route to high molecular weight poly(L-lactic acid). J Polym Sci Part A 2000; 38: 1673-1679.
4. Moon SI, Lee CW, Miyamoto M, Kimura Y. Melt/solid polycondensation of L-lactic acid: an alternative route to poly(L-lactic acid) with high molecular weight. Polymer 2001; 42: 5059-5062.
5. Shinoda H, Asou Y, Suetsugu A, Tanaka K. Synthesis and characterization of amphiphilic biodegradable copolymer, poly(aspartic acid-co-lactic acid). Macromol Biosci 2003; 3: 34-43.
6. Hsu SH, Chen WC. Improved cell adhesion by plasma-induced grafting of L-lactide onto polyurethane surface. Biomaterials 2000; 21: 359-367.
7. Lin HB, Garcia-Echeverria C, Asakura S, Sun W, Mosher DF, Cooper SL. Endothelial cell adhesion on polyurethanes containing covalently attached RGD-peptides. Biomaterials 1992; 13: 905-914.
8. Takahashi A, Kita R, Kaibara M. Effects of thermal annealing of segmentated-polyurethane on surface properties, structure and antithrombogenecity. J mater med 2002; 13: 259-264.
9. Wang XH, Li DP, Wang WJ, Feng QL, Cui FZ, Xu YX, Song XH, Werf M. Crosslinked collagen/chitosan matrix for artificial livers. Biomaterials 2003; 24: 3213-3220.
10. Wang X, Yan Y, Zhang R. A comparison of chitosan and collagen sponges as hemostatic dressings. J Bioact Compat Polym 2006; 21: 39-53.
11. Hirano S, Nakahira T, Nakagawa M, Kim SK. The preparation and applications of

functional fibres from crab shell chitin. J Biotech 1999; 70: 373-377.

12. Ishihara K, Takayama R, Nakabayashi N, Fukumoto K, Aoki J. Improvement of blood compatibility on cellulose dialysis membrane. Biomaterials 1992; 13: 235-239.
13. Yamane S, Iwasaki N, Majima T, Funakoshi T, Masuko T, Harada K, Minami A, Monde K, Nishimura S. Feasibility of chitosan-based hyaluronic acid hybrid biomaterial for a novel scaffold in cartilage tissue engineering. Biomaterials 2005; 26: 611-619.
14. Kukolikova L, Bakos D, Alexy P, Hanzelova S, Zhong W. Optimization of the properties of chitosan lactate/hyaluronan film. J Appl Polym Sci 2006; 100: 1413-1419.
15. Knill CJ, Kennedy JF, Mistry J, Smart G, Groocock MR, Williams HJ. Alginate fibres modified with unhydrolyzed and hydrolyzed chitosans for wound dressings. Carbohydr Polym 2004; 55: 65-76.
16. Remuñán-López C, Bodmeier R. Mechanical, water uptake and permeability properties of crosslinked chitosan glutamate and alginate films. J Control Release 1997; 44: 215-225.
17. Mori T, Okumura M, Matsuura M, Ueno K, Tokura S, Okamoto Y, Minami S, Fujinaga T. Effects of chitin and its derivatives on the proliferation and cytokine production of fibroblasts *in vitro*. Biomaterials 1997; 18: 947-951.
18. Kumar MNVR, Hudson SM. Encyclopedia of Biomaterials and Biomedical Engineering., New York: Dekker Pub, 2004. p. 310-323.
19. Meanwell JLR, Shama G. Chitin in a dual role as substrate for *Streptomyces griseus* and as adsorbent for streptomycin produced during fermentation. Enzyme Microb Tech 2006; 38: 657-664.
20. Teng WL, Khor E, Tan TK, Lim LY, Tan SC. Concurrent production of chitin from shrimp shells and fungi. Carbohydr Res 2001; 332: 305-316.
21. Lin CW, Lin JC. Characterization and blood coagulation evaluation of the water-soluble chitooligosaccharides prepared by a facile fractionation method. Biomacromol 2003; 4: 1691-1697.
22. Whang HS, Kirsch W, Hudson SM. Hemostatic agents from chitin and chitosan J Macromol Sci Polym Rev 2005; 45: 309-323.
23. Muzzarelli RAA, Ilari P. Solubility and structure of *N*-carboxymethlchitosan. Int J Biol

Macromol 1994; 16: 177-180.

24. Signini R, Campana Filho SP. On the preparation and characterization of chitosan hydrochloride. Polym Bull 1999; 42: 159-166.
25. Kubota N, Tastumoto N, Sano T, Toya K. A simple preparation of half *N*-acetylated chitosan highly soluble in water and aqueous organic solvents. Carbohydr Res 2000; 324: 268-274.
26. Chen XG, Park HJ. Chemical characteristics of *O*-carboxymethyl chitosans related to the preparation conditions. Cabohydr polym 2003; 53: 355-359.
27. Ramos VM, Rodríguez NM, Díaz MF, Rodríguez MS, Heras A, Agulló E. *N*-methylene phosphonic chitosan. Effect of preparation methods on its properties. Carbohydr Res 2003; 52: 39-46.
28. Baumann H, Faust V. Concepts for improved regioselective placement of *O*-sulfo, *N*-sulfo, N-acetyl, and N-carboxymethyl groups in chitosan derivatives. Carbohydr Res 2001; 331: 43-57.
29. Kurita K, Ikeda H, Yoshida Y, Shimojoh M, Harata M. Chemoselective protection of the amino groups of chitosan by controlled phthaloylation: Facile preparation of a precursor useful for chemical modifications. Biomacromol 2002; 3: 1-4.
30. Neuffer MC. Hemostatic dressings for the first responder: A review. Military Med 2004; 169: 716-720.
31. Alam HB, Burris D, DaCorta JA, Rhee P. Hemorrhage control in the battlefield: Role of new hemostatic agents. Military Med 2005; 170: 63-69.
32. Alam HB, Uy GB, Miller D, Koustova E, Hancock T, Inocencio R, Anderson BS, Llorente O, Rhee P. Comparative analysis of hemostatic agents in a swine model of lethal groin injury. J Trauma 2003; 54:1077-1082.
33. Chan MW, Schwaitzberg SD, Demcheva M, Vournakis J, Finkielsztein S, Connolly RJ. Comparison of poly-*N*-acetyl glucosamine (P-GlcNAc) with absorbable collagen (Actifoam), and fibrin sealant (Bolheal) for achieving hemostasis in a swine model of splenic hemorrhage. J Trauma 2000; 48: 454-458.
34. Yackel EL Kenyon WO. The oxidation of cellulose by nitrous dioxide. J Am Chem Soc 1942; 64: 124-127.

35. Chou TC, Fu E, Wu CJ, Yeh JH. Chitosan enhances platelet adhesion and aggregation. Biochem Biophys Res Com 2003; 302: 480-483.
36. Evans, EE Kent SP. The use of basic polysaccharides in histochemistry and cytochemistry: IV-precipitation and agglutination of biological materials by aspergillus polysaccharide and deacetylated chitin. J Histochem Cytochem 1962; 10: 24-28.
37. Seo SJ, Choi YJ, Akaike T, Higuchi A Cho CS. Alginate/galactosylated chitosan/heparin scaffold as a new synthetic extracellular matrix for hepatocytes. Tissue Eng 2006; 12: 33-44.
38. Peng CK, Yu SH, Mi FL, Shyu SS. Polysaccharide-based artificial extracellular matrix: Preparation and characterization of three-dimensional, macroporous chitosan and chondroitin sulfate composite scaffolds. J Appl Polym Sci 2006; 99: 2091-2100.
39. Mori T, Okumura M, Matsuura M, Ueno K, Tokura S, Okamoto Y, Minami S, Fujinaga T. Effects of chitin and its derivatives on the proliferation and cytokine production of fibroblasts *in vitro*. Biomaterials 1997; 18: 947-951.
40. Peluso G, Petillo O, Ranieri M, Santin M, Ambrosio L, Calabró D, Avallone B, Balsamo G. Chitosan-mediated stimulation of macrophage function. Biomaterials 1994; 15: 1215-1220.
41. Okamoto Y, Watanabe M, Miyatake K, Morimoto M, Shigemasa Y, Minami S. Effects of chitin/chitosan and their oligomers/monomers on migrations of fibroblasts and vascular endothelium. Biomaterials 2002; 23: 1975-1979.
42. Wang XH, Li DP, Wang WJ, Feng QL, Cui FZ, Xu YX, Song XH. Covalent immobilization of chitosan and heparin on PLGA surface. Int J Biol Macromol 2003; 33: 95-100.
43. Lin HB, Sun W, Mosher DF, Carcia-Echeverria C, Schaufelberger K,Lelkes PI, Cooper SL. Synthesis, surface, and cell-adhesion properties of polyurethanes containing covalently grafted RGD-peptides. J Biomed Mater Res 1994; 28: 329-342.
44. Li J, Yun H, Gong Y, Zhao N, Zhang X. Investigation of MC3T3-E1 cell behavior on the surface of GRGDS-coupled chitosan. Biomacromol 2006; 7: 1112-1123.

45. Ho MH, Wang DM, Hsieh HJ, Liu HC, Hsien TY, Lai JY, Hou LT. Preparation and characterization of RGD-immobilized chitosan scaffolds. Biomaterials 2005; 26: 3197-3206.
46. Chung TW, Lu YF, Wang SS, Lin YS, Chu SH. Growth of human endothelial cells on photochemically grafted Gly-Arg-Gly-Asp (GRGD) chitosans. Biomaterials 2002; 23: 4803-4809.
47. Chung TW, Lu YF, Wang HY, Chen WP, Wang SS, Lin YS, Chu SH. Growth of human endothelial cells on different concentration of Gly-Arg-Gly-Asp (GRGD) grafted chitosan surface. Artificial Organ 2003; 27: 155-161.
48. Zhao X, Kato K, Fukumoto Y, Nakamae K. Synthesis of bioadhesive hydrogels from chitin derivatives. Int J Adhesion Adhesive 2001; 21: 227-232.
49. Paul W, Sharma CP. Chitosan, a drug carrier for the 21st century: a review. S T P Pharma Sciences. 2000; 10: 5-22.
50. Lameiro MH, Lopes A, Martins LO, Alves PM, Melo E. Incorporation of a model protein into chitosan-bile salt microparticles. Intl J Pharm 2006; 312: 119-130.
51. Cerchiara T, Luppi B, Bigucci F, Petrachi M, Orienti I, Zecchi V. Controlled release of vancomycin from freeze-dried chitosan salts coated with different fatty acids by spray-drying. J Microencapsulation 2003; 20: 473-478.
52. Carreno-Gomez B, Duncan R. Evaluation of the properties of soluble chitosan and chitosan microspheres. Int J Pherm 1997; 148: 231-240.
53. Jameela SR, Kumary TV, Lal AV, Jayakrishnan A. Progesterone-loaded chitosan microspheres: a long acting biodegradable controlled delivery system. J Control Release 1998; 52: 17-24.
54. Chen RH, Tsaih ML, Lin WC. Effects of chain flexibility of chitosan molecules on the preparation, physical, and release characteristics of the prepared capsule. Carbohydr Polym 1996; 31: 141-148.
55. Loke WK, Lau SK, Yong LL, Khor E, Sum CK. Wound dressing with sustained anti-microbial capability. J Biomed Mater Res 2000; 53: 8-17.

56. Mi FL, Shyu SS, Wu YB, Lee ST, Shyoug JY, Huang RN. Fabrication and characterization of a sponge-like asymmetric chitosan membrane as a wound dressing. Biomaterials 2001; 22: 165-173.
57. Ono K, Saito Y, Yura H, Ishikawa K, Kurita A, Akaike T, Ishihara M. Photocrosslinkable chitosan as a biological adhesive. J Biomed Mater Res 2000; 49: 289-295.
58. Ishihara M, Nakanishi K, Ono K, Sato M, Kikuchi M, Yura H, Matsui T, Hattori H, Uenoyama M, Kurita A. Photocrosslinkable chitosan as a dressing for wound occlusion and accelerator in healing process. Biomaterials 2002; 23: 833-840.
59. Rabea EI, Badawy MET, Stevens CV, Smagghe G, Steurbaut W. Chitosan as antimicrobial agent: Applications and mode of action. Biomacromol. 2003; 4: 1457-1465.
60. Sarasam A, Krishnaswamy RK, Madihally SV. Blending chitosan with polycaprolactone: Effects on physicochemical and antibacterial properties. Biomacromol 2006; 7: 1131-1138.
61. Liu XF, Guan YL, Yang DZ, Li Z, Yao KD. Antibacterial action of chitosan and carboxymethylated chitosan. J Appl Polym Sci 2001; 79: 1324-1335.
62. Zhao L, Mitomo H, Zhai M, Yoshii F, Nagasawa N, Kume T. Synthesis of antibacterial PVA/CM-chitosan blend hydrogels with electron beam irradiation. Carbohydr Polym 2003; 53: 439-446.
63. Jia Z, Shen D, Xu W. Synthesis and antibacterial activities of quaternary ammonium salt of chitosan. Carbohydr Res 2001; 333: 1-6.
64. Sasaki C, Kristiansen A, Fukamizo T, Vårum KM. Biospecific fractionation of chitosan. Biomacromol 2003; 4: 1686-1690.
65. Strand SP, Vårum KM, Østgaard K. Interactions between chitosans and bacterial suspensions: adsorption and flocculation. Colloids Surf B 2003; 27: 71-81.
66. Venter JP, Kotzé AF, Auzély-Velty R, Rinaudo M. Synthesis and evaluation of the mucoadhesivity of a CD-chitosan derivative. Intl J Pharm 2006; 313: 36-42.
67. Wittaya-areekul S, Prahsarn C. Development and in vitro evaluation of chitosan-polysaccharides composite wound dressings. Intl J Pharm 2006; 313: 123-128.

68. Takahashi A, Kita R, Kaibara M. Effects of thermal annealing of segmented-polyurethane on surface properties, structure and antithrombogenicity. J Mater Sci: Mater Med 2002; 13: 259-264.
69. Hsu SH, Chen WC. Improved cell adhesion by plasma-induced grafting of L-lactide onto polyurethane surface. Biomaterials 2000; 21: 359-367.
70. Chandy T, Sharma CP. Prostaglandin E1-immobilized poly(vinyl alcohol)-blended chitosan membranes: Blood compatibility and permeability properties. J Appl Polym Sci 1992; 44: 2145-2156.
71. Kottke-Marchant K, Anderson JM, Uemura Y, Marchant RE. Effect of albumin coating on the *in vitro* blood compatibility of Dacron® arterial prostheses. Biomaterials 1989; 10: 147-155.
72. Beena MS, Chandy T, Sharma CP. Heparin immobilized chitosan-poly ethylene glycol interpenetrating network: antithrombogenicity. Art Cells Blood Subs Immob Biotech 1995; 23: 175-192.
73. Ko TM, Lin JC, Cooper SL. Surface characterization and platelet adhesion studies of plasma-sulphonated polyethylene. Biomaterials 1993; 14: 657-664.
74. Wedmore I, McManus JG, Pusateri AE, Holcomb JB. A special report on the chitosan-based hemostatic dressing: Experience in current combat operations. J Trauma 2006; 60: 655-658.
75. Pusateri AE, Holcomb JB, Kheirabadi BS, Alam HB, Wade CE, Ryan KL. Making sense of the preclinical literature on advanced hemostatic products. J Trauma 2006; 60: 674-682.
76. Rao SB, Sharma CP. Use of chitosan as a biomaterial: Studies on its safety and hemostatic potential. J Biomed Mater Res 1997; 34: 21-28.
77. Klokkevold PR, Fukuyama H, Sung EC, Bertolami CN. The effect of chitosan (poly-*N*-acetyl glucosamine) on lingual hemostasis in heparinized rabbits. J Oral Maxillofac Surg 1999; 57: 49-52.
78. Hemker HC, Dieri RA, Béguin S. Thrombin generation assays: accruting clinical relevance. Curr Opin Hematol 2004; 11: 170-175.

79. Mao C, Qiu Y, Sang H, Mei H, Zhu A, Shen J, Lin S. Various approaches to modify biomaterial surfaces for improving hemocompatibility. Adv Colloid Interface Sci 2004; 110: 5-17.
80. Hanson SR. Encyclopedia of Biomaterials and Biomedical Engineering. New York: Dekker Pub, 2004. p. 144-154.
81. Cenni E, Ciapetti G, Cervellati M, Cavedagna D, Falsone G, Gamberini S, Pizzoferrato A. Activation of the plasma coagulation system induced by some biomaterials. J Biomed Mater Res 1996; 31: 145-148.
82. Bordenave L, Lbaquey C, Bareille R, Lefebvre F, Lauroua C, Guerin V, Rouais F, More N, Vergnes C, Anderson JM. Endothelial-cell compatibility testing of 3 different pelletanes. J Biomed Mater Res 1993; 27: 1367-1381.
83. Pusateri AE, McCarthy SJ, Gregory KW, Harris RA, Cardenas L, McManus AT, Goodwin CW. Effect of a chitosan-based hemostatic dressing on blood loss and survival in a model of severe venous hemorrhage and hepatic injury in swine. J Trauma 2003; 54: 177-182.
84. Queiroz AAA, Ferraz HG, Abraham GA, Fernandez M, Bravo AL, Roman JS. Development of new hydroactive dressings based on chitosan membranes: Characterization and *in vivo* behavior. J Biomed Mater Res 2003; 64A: 147-154.
85. Okamoto Y, Yano R, Miyatake K, Tomohiro I, Shigemasa Y, Minami S. Effects of chitin and chitosan on blood coagulaiton. Carbohydr Polym 2003; 53: 337-342.
86. Fischer TH, Connolly R, Thatte HS, Schwaitzberg SS. Comparison of structural and hemostatic properties of the poly-*N*-acetyl glucosamine Syvek Patch with products containing chitosan. Microsc Res Tech 2004; 63: 168-174.
87. Ronghua H, Yumin D, Jianhong Y. Preparation and anticoagulant activity of carboxybutyrylated hydroxyethyl chitosan sulfates. Carbohydr Polym. 2003; 51: 431-438.
88. Zhu A, Zhang M, Wu J, Shen J. Covalent immobilization of chitosan/heparin complex with a photosensitive hetero-bifunctional crosslinking reagent on PLA surface. Biomaterials 2002; 23: 4657-4665.

89. Amiji MM. Permeability and blood compatibility properties of chitosan-poly(ethylene oxide) blend membranes for haemodialysis. Biomaterials 1995; 16: 593-599.
90. Hirano S, Noishiki Y. The blood compatibility of chitosan and *N*-acylchitosans. J Biomed Mater Res. 1985; 19: 413-417.
91. Hirano S, Zhang M, Nakagawa M, Miyata T. Wet spun chitosan-collagen fibers, their chemical *N*-modifications, and blood compatibility. Biomaterials 2000; 21: 997-1003.
92. Mclachlan J, Mcinnes AG, Falk M. Studies on chitan (chitin-poly-N-acetylglucosamine) fibers of diatom thalassiosira fluviatilis hustedt. 1. Production and isolationof chitan fibers. Canadian J botany 1965; 43: 707.
93. Smucker RA. Chitin primary production. Biochem System Ecol 1991; 19: 357-369.
94. Vournakis JN, Demcheva M, Whitson A, Guirca R, Pariser ER. Isolation, purification, and characterization of poly-*N*-acetyl glucosamine use as a hemostatic agent. J Trauma 2004; 57: S2-6.
95. Vournakis J, Pariser ER, Finkielszlein S, Helton M. Poly-N-acetyl glucosamine. US patent No. 5623064, 1997.

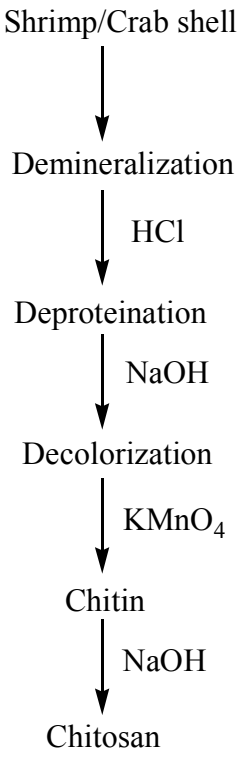

Figure 1-1 A flow chart of chitin and chitosan production.

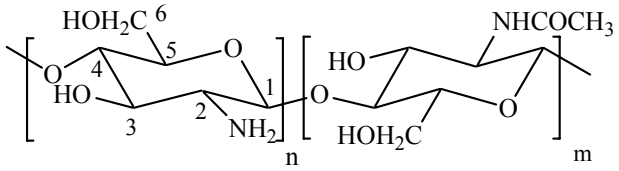

Figure 1-2 The Chemical structure of chitosan. Chitosan is the copolymer with n>0.5.

Field	Application
Health care	Contact lens/eye bandages Wound-healing ointments and dressings Orthopaedics Anticholesterol and fat-binding Surgical sutures Drug delivery Ophthalmology Dentistry Transportation of cells
Food and beverages	Anticholesterol and fat-binding Food stabilizer Flavour and tastes Food packaging Nutritional additives Preservation
Agriculture	Seed treatments (coating) Feed ingredients (animal feed) Nematocides and insecticides
Cosmetics and toiletries (personal care)	Hair treatment Skin care Oral care
Waste and water treatment (clarification)	Sewage effluents Drinking water Recovering metals Pools and spas Treating food wastes
Product separation and recovery (bioapplications)	Membrane separation Chromatographic matrix Immobilization of enzymes/cells Recover valuable bioproducts

Figure 1-3 Various applications of chitosan [49].

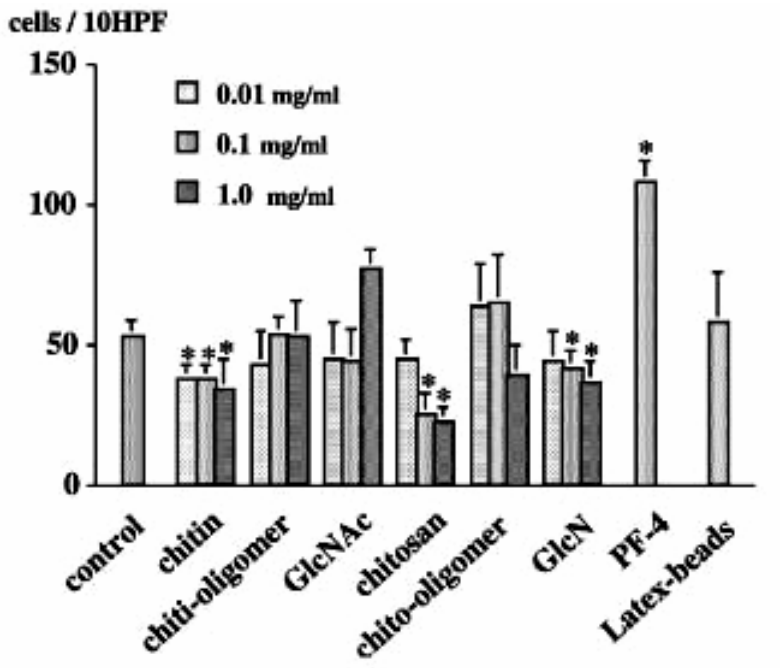

Figure 1-4 Direct affects of chitin, chitosan and their derivatives on migration activity of 3T6 cells [41]. Control: culture medium, GluNAc: N-acetyl-D-glucosamine, GlcN: D-glucosamine, chiti-oligomer: a mixture of GlcNAc1 and GlcNAc6, chito-oligomer: a mixture of GlcN1 and GlcN6, PF-4: human recombinant platelet factor-4. Data displays means±SD for at least three replicates. *p<0.05 from control.

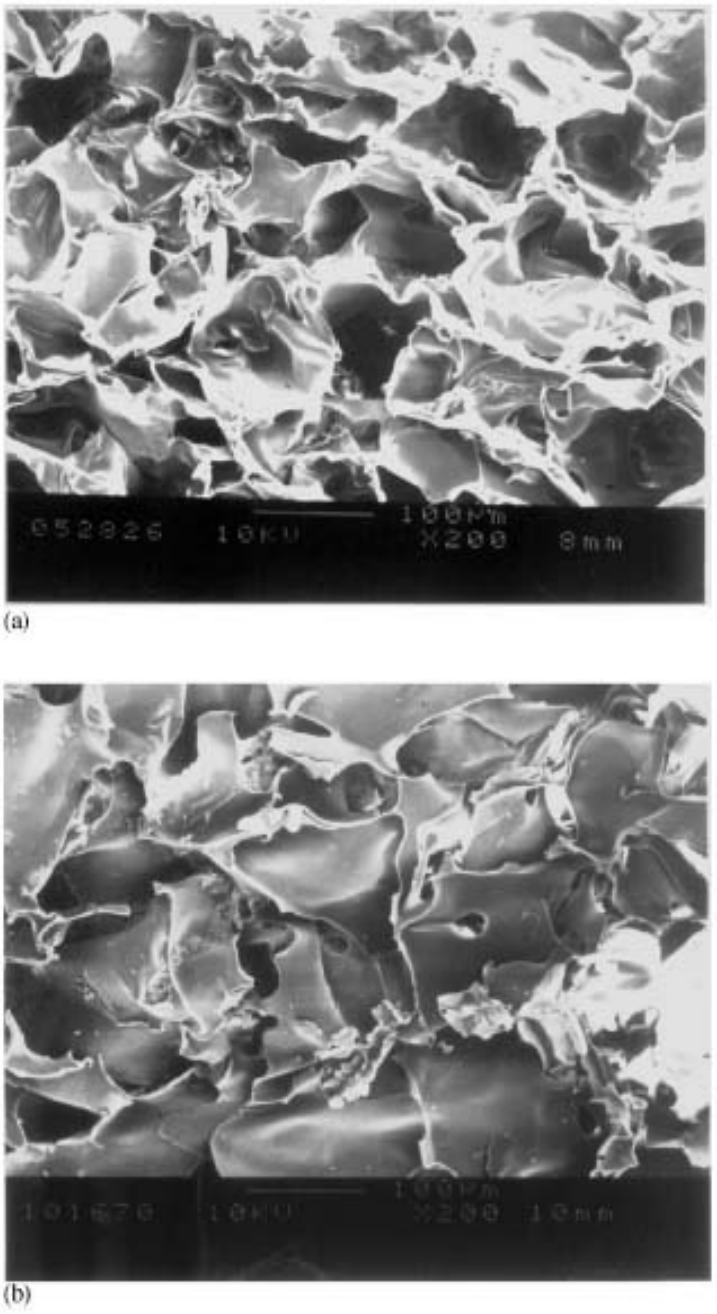

Figure 1-5 Morphology of the chitosan scaffold prepared by lyophilization (SEM, x 200) [45]. (a) Before RGDS immobilization, (b) After RGDS immobilization.

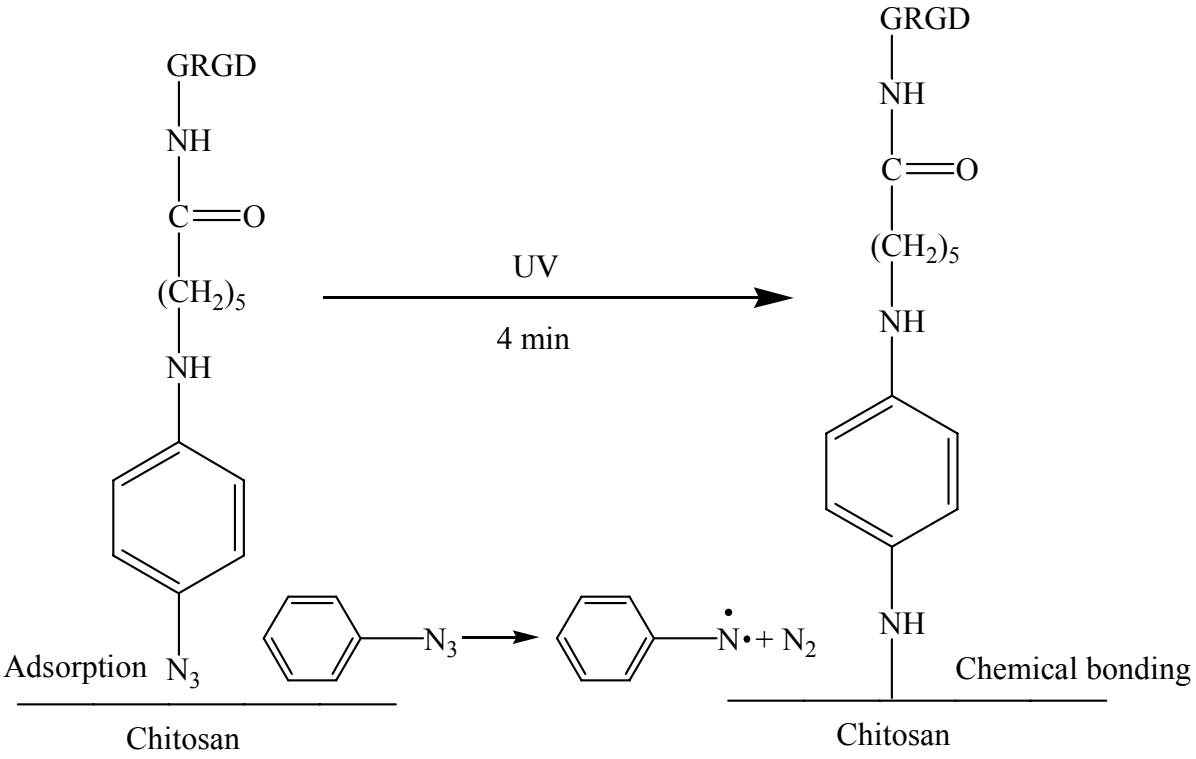

Figure 1-6 A synthetic scheme of photochemical immobilization of GRGD to chitosan [47].

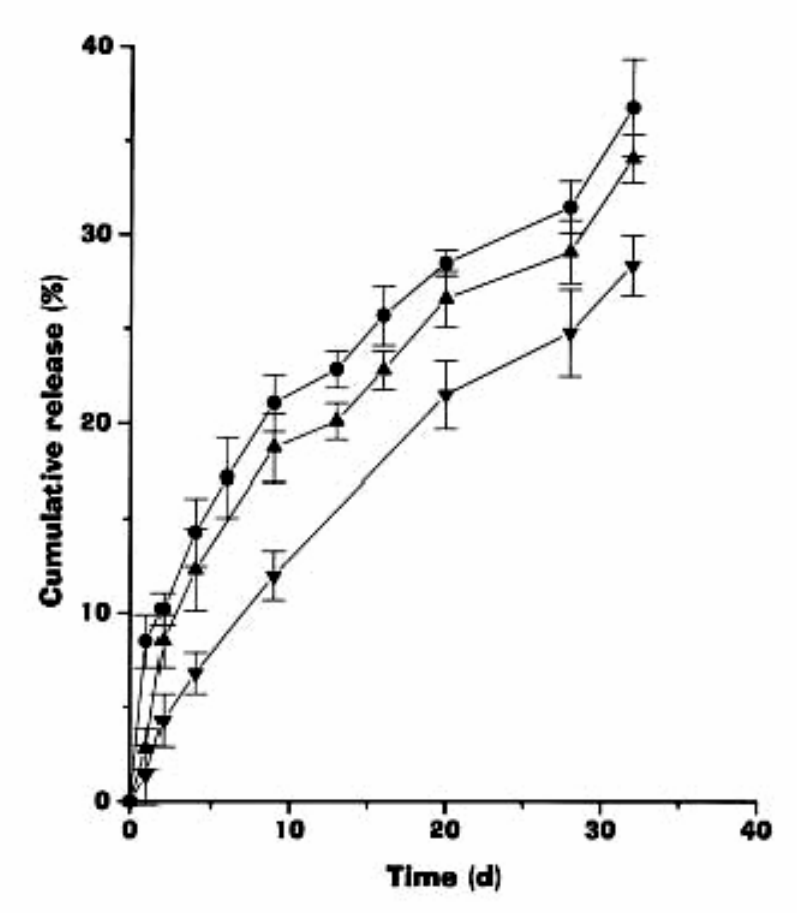

Figure 1-7 *In vitro* release of progesterone from chitosan microsphere crosslinked 10mL of glutaraldehyde saturated toluene into phosphate buffer at 37□ as a function of particle size [53]; 45-90μm (●), 90-150μm (▲), 150-300μm(▼).

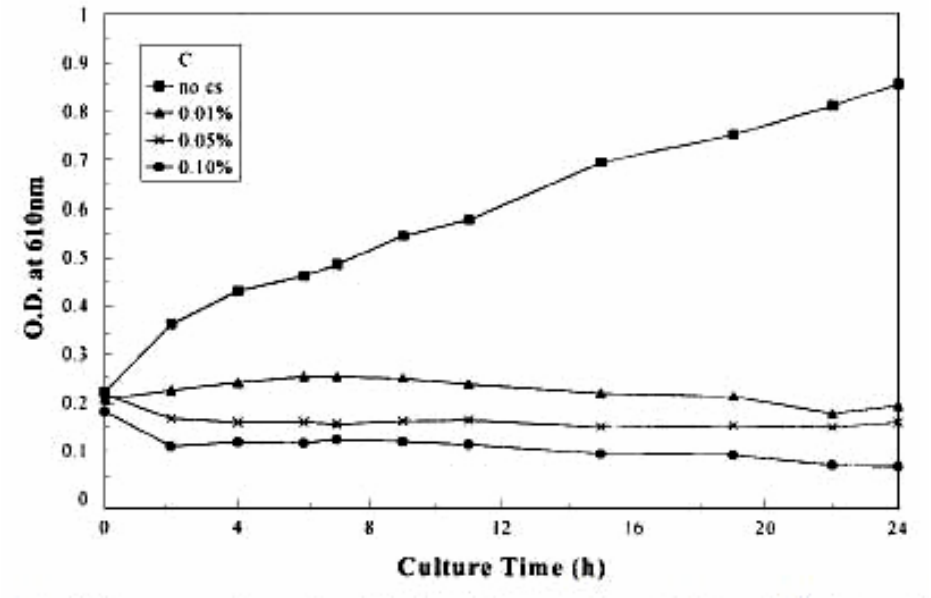

Figure 1-8 OD versus culture time for the chitosan (M_v=5.11 x 10^4) whose C in the medium at 0.01, 0.05, and 0.10% against *E. coli* [61].

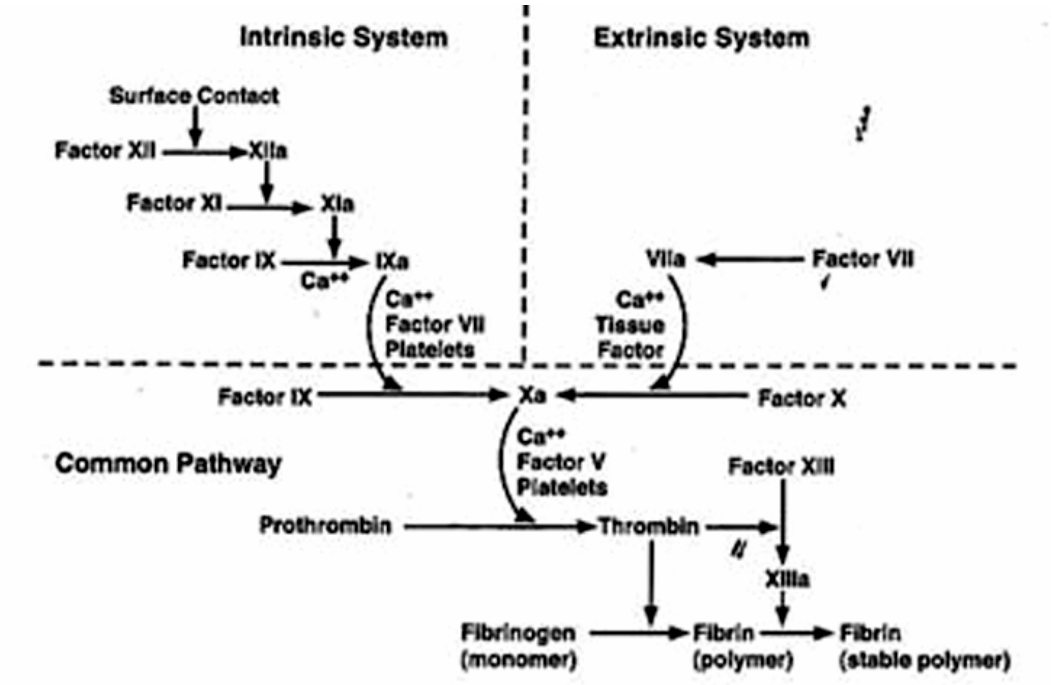

Figure 1-9 Blood coagulation pathways [80]. Clotting factors (proenzymes), identified by Roman numerals, interact in a sequential series of enzymatic activation reactions (coagulation cascade) leading to the amplified production of the enzyme thrombin, which in turn activates fibrinogen to form a fibrin polymer that stabilizes a clot or thrombus.

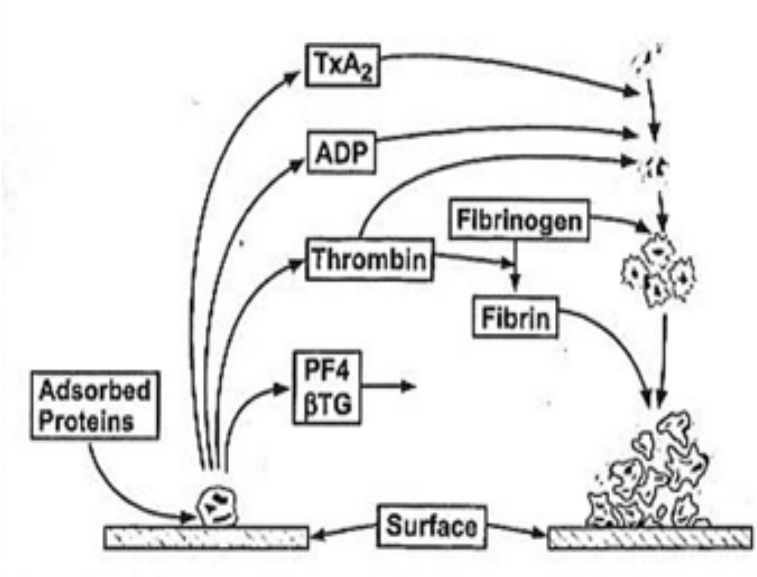

Figure 1-10 Platelet reaction at material surfaces [80]. Following protein adsorption, platelets adhere and release their α-granule contents, including ADP. Thrombin production is catalyzed locally by platelet membrane phospholipids. Thranbaxane A_2 (TxA_2) is synthesized. ADP, TxA_2, and thrombin then recruit additional circulating platelets into an enlarging platelet mass that is stabilized by fibrin.

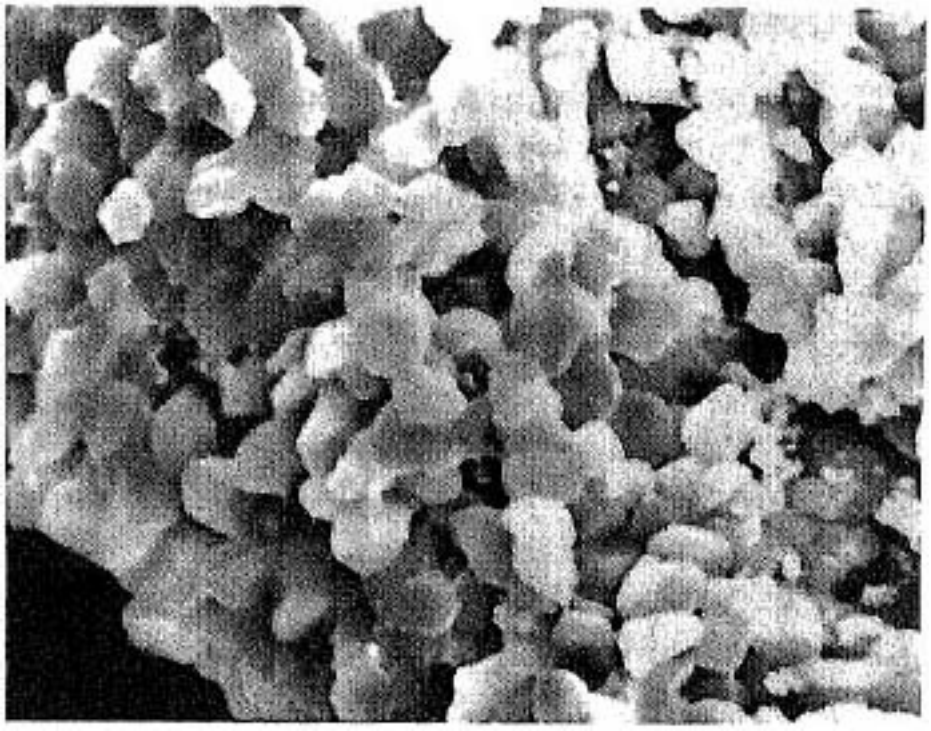

Figure 1-11 SEM of a blood clot formation from chitosan-treated lingual incision [77]. Red blood cells have lost their typical biconcave morphology and they appear to have an unusual affinity toward one another (original magnification x 2000).

Variable	Gauze Sponge Control Group	Chitosan Group	*p* Value of Difference
Posttreatment blood loss (mL)	2,879 (95% CI, 788–10,513)	264 (95% CI, 82–852)	<0.01
Posttreatment blood loss (mL/kg body weight)	102.4 (95% CI, 28.2–371.8)	9.4 (95% CI, 2.9–30.3)	<0.01
Fluid use (mL)	6614 (95% CI, 2,519–17,363)	1793 (95% CI, 749–4,291)	0.03
Survival (%)	2/7 (28.6)	7/8 (87.5)	0.04
Survival time (min: nonsurvivors only)	38.4 ± 5.8 (n = 5)	10.0 (n = 1)	N/A
Hemostasis at 1 minute (%)	0	50	0.08
Hemostasis at 2 minutes (%)	0	50	0.08
Hemostasis at 3 minutes (%)	0	62	0.03
Hemostasis at 4 minutes (%)	0	62	0.03

CI, confidence interval.

Figure 1-12 Effect of a chitosan-based hemostatic dressing on blood loss and survival in swine [83]. Posttreatment blood loss, fluid use, time for hemostasis, and survival are tabulated.

CHAPTER 2

2. Novel Dialdehyde-Modified Chitosan/Silk Fibroin Blend Films for Improved Bioadhesive Properties

Abstract

Bioadhesives have been quite attractive as wound dressings. However, commercially available bioadhesives still have some limitations in terms of cytotoxicity, potential bacterial infections, and cost performance. There is a need for developing bioresource-based bioadhesives that would overcome these limitations.

In this study, chitosan and silk fibroin (CS/SF) blend films with dangling aldehydes were prepared by a chemical reaction between amino groups of blend films and aldehyde groups of alkyl dialdehydes. Commercially available glutaraldehyde (GA) and newly synthesized 1,10-didecanal were used for the chemical modification of CS/SF blend films. The presence of a free aldehyde group in the film was qualitatively determined by colorimetric tests and Fourier Transformed Infrared (FTIR) spectra. In bioadhesion tests, the modified blend films exhibited improved peeling strength compared to controls. Further improvement of the quantitative method will be needed to determine the absolute amount of free aldehyde groups modified on films.

2.1 Introduction

Natural, abundant polysaccharides, including chitosan, are attractive agents for various biomedical applications for tissue engineering and tissue regeneration, due to their biocompatibility, biodegradability, and nonimmunogenic properties, as well as protein-based

biomaterials. As described in the previous chapter, chitosan and its derivatives are promising biomaterials.

Bioadhesives have been widely studied as alternative wound dressings [1-5] due to the toxicity and potential mutagenicity and carcinogenicity of synthetic ones [6-8]. Commercially available protein-based adhesives overcome these problems, yet they still have some limitations in terms of high cost and potential bacterial infections [8, 9].

Silk fibroin is a natural fibrous protein, and has excellent mechanical strength and good biocompatibility, and oxygen and water permeability in the wet state, which suggests that it could be used as a wound dressing. Silk fibroin/chitosan blends have already been studied in various physical forms, such as films, fibers, and membranes [10-15], for various purposes.

Commercially available dialdehydes, such as glutaraldehyde and glyoxal are often used for crosslinking of chitosan and other polymers with amino groups in their backbone to improve the mechanical and structural properties for the blends. However, the dialdehydes can also provide free aldehyde groups in a variety of substrates (e.g. films, sponges, and fibers). The bonding strength between gelatin and porcine skin increased due to the Schiff base formed between free aldehyde groups dangled from gelatin and the amino groups in the tissue [5]. The dialdehydes may provide a different bonding strength against the tissue, depending on the carbon chain length. Shorter chain length may limit accessibility of the aldehyde groups to the proteinatious amino groups. Since commercially available dialdehydes have relatively shorter carbon chains, it will be necessary to synthesize a dialdehyde with a longer linear carbon chain. Currently, very few dialdehydes, specially a long-chain dialdehyde, are commercially available due to the synthesis difficulties.

In this study, chitosan and silk fibroin were blended at different ratios, and their as-cast films were prepared at room temperature. The blend films were treated with glutaraldehyde and 1,10-didecanal, to improve the adhesiveness onto tissue. The dialdehyde and treated blend films were then characterized by FTIR spectroscopy. Finally, a tissue adhesion test was conducted *ex vivo* by peeling apart the samples on a tensile test device.

2.2 Experimental

2.2.1 Materials

Grade 5A raw *Bombyx mori* silk was obtained from Fiaçào de Seda Bratac S.S. (Brazil). Chitosan was acquired from Natural Biopolymer, Inc. (Raymond, WA). All other chemicals used in this study were purchased from Fisher Scientific or Aldrich Chemicals and used without further purification.

2.2.2 Silk Fibroin (SF) solution preparation

SF solution was prepared according to the method previously described by Ha et al [16, 17]. The dried *Bombyx mori* raw silk was degummed with 0.25% w/v sodium lauryl sulfate and 0.25% w/v sodium carbonate in boiling water for 1 h in order to remove sericin. The bath ratio was 1:10 w/v. The remaining silk fibroin was carefully washed with a large amount of deionized water and dried in a vacuum oven at room temperature. Dried bulk silk fibroin was mixed with calcium nitrate solution ($Ca(NO_3)_2 \cdot 4H_2O$:MeOH = 3/1 w/w) to prepare 10 % (w/w) SF solution. The mixture was stirred with a mechanical stirrer for 6 h at 65ºC until the silk fibroin fibers were completely dissolved. The SF solution was diluted to a final

concentration of 1 % (w/w) after dialysis of the SF solution with cellulose membrane in deionized water for 4 days (molecular weight cut off: 6,000-8,000Da).

2.2.3 Chitosan (CS) solution preparation

As-received chitosan was further deacetylated according to the modified method published by Lim et al [18]. This involved heating chitosan powder in 50% NaOH aqueous solution at 120ºC with reflux for 2.5 h under nitrogen purge. The resulting product was washed by soxhlet extraction with methanol for 1 day, and subsequent washing with deionized water in a beaker. The dried chitosan powder with M_v=1.71x10^5, DD=98.3% was dissolved into 0.2M acetic acid (HOAc) solution by stirring to prepare 1 w/w% chitosan solution (CS).

2.2.4 Chitosan/Silk Fibroin (CS/SF) blend film fabrication

The solutions of SF and CS were mixed by hand in a plastic bottle with a cap and cast into 100 or 150 mm diameter petri dishes at different compositions (CS:SF=1/1, 2/1, and 1/2). Pure CS or SF films were also included in this study. The total amount of solution was 20.0g for the 100 mm dish and 45.0g for the 150 mm dish. The solutions were allowed to evaporate at room temperature over 2 days. In the case of pure SF formation, the solution was placed in the refrigerator during the drying period to minimize recrystallization of fibroin, which leads to brittle films. All of the films were easy to peel and remove from the dishes.

2.2.5 Preparation of 2,4-dinitrophenyl hydrazone of heptanal

The 2,4-DNPH method is widely used for the determination of aldehyde groups in

materials by UV-visible spectroscopy and HPLC analysis [19-21]. 2,4-Dinitrophenyl hydrazone of heptanal was prepared from 2,4-dinitrophenylhydrazine (2,4-DNPH) in order to make a standard curve. The reaction sequence is described in Scheme 2-1. The 2,4-DNPH solution was prepared by a method described previously [19]. 2,4-DNPH (5.0g) containing ca. 50% water was dissolved in 25mL of concentrated H_2SO_4 and then added to 35mL of water and 125mL of 99% EtOH. A solution of heptanal (1.14g, 0.01mol) in 40mL of EtOH was added to 150mL of the 2,4-DNPH stock solution. A vivid yellow precipitate was immediately formed and the reaction was kept for 1 h. The crude product was collected by filtration and washed twice with 50mL of 5% $NaHCO_3$ solution and twice with 50mL of water. The product was recrystallized from 99% EtOH and collected by filtration (Yield: 2.553g, 86.7%).

2.2.6 Standard curve of 2,4-DNPH-heptanal

The obtained 2,4-DNPH-heptanal powder (14.7mg, 5mmol) was dissolved in 10mL of acetonitrile in a volumetric flask. Other solutions at different concentrations were prepared by diluting this stock solution. The standard curve was created from the absorbance value of each solution detected by UV-Vis spectroscopy (λ_{max}=361nm, ε=2.2x10^4). The molar absorptivity constant was calculated by the following Lambert-Beer's equation:

$$A=\varepsilon cl$$

This calibration curve is shown in Figure 2-1.

2.2.7 Synthesis of 1,10-didecanal

A method for the oxidation of primary and secondary alcohols to carbonyl compounds with high conversions was reported by Corey et al [22]. The 1,10-didecanal synthesis using a modified Corey method, is shown in Scheme 2-2. A normal diol, 1,10-decandiol, was oxidized using the modified method. Stirred dimethyl sulfide (3.105g, 50mmol) was prepared at 0 ºC under argon atmosphere in a 200mL three necked flask. A suspension of N-chlorosuccinimide (5.3mg, 40mmol) in 100mL of methylene chloride was stirred and added to the flask. The complex was then cooled to –25 ºC in CCl_4-dry ice bath with stirring. Solid 1,10-decanediol (1.75g, 10mmol) in 5mL of toluene was added and then stirred for 2.5 h. A solution of triethylamine (3.03g, 30mmol) was added, and the cooling bath was then removed. Diethyl ether (100mL) was added and the solution was washed twice with 1% HCl solution (30mL). The organic layer was washed twice with water and dried using $MgSO_4$ overnight. The dried solution was concentrated, and a yellowish liquid (1.21g, 70%) was obtained and diluted with $CHCl_3$ to a desired concentration.

2.2.8 Glutaraldehyde treated CS/SF blend film preparation

All films, except for pure SF film, were treated with two kinds of glutaraldehyde (GA) solution. The concentration of GA was 0.01 and 0.05M, respectively. Films were soaked with the solution for 10 seconds and washed with deionized water for 10 min then air-dried for 1 day. Only chitosan film was neutralized with 1N NaOH for 10 min before GA treatment. This procedure prevented swelling of the film. On the other hand, blend films were treated with 0.05M NaOMe/MeOH solution for 10 min before GA treatment, to induce β-sheet

conformation of SF and to obtaine the free amine form of chitosan. All GA treated films were stored in a desiccator over $CaSO_4$ until they were used.

2.2.9 Didecanal treated CS/SF blend film preparation

All films were treated with 0.053M 1,10-didecanal in $CHCl_3$. Films were soaked with the solution for 10 sec and washed with deionized water for 10 min then air-dried for 1 day. All didecanal treated films were stored in a desiccator for later use.

2.2.10 Fourier Transform Infrared (FTIR) and FT-Attenuated Total Reflectance (FTIR-ATR) Spectroscopy

The reaction products of the didecanal synthesis, dissolved in chloroform were analyzed using NaCl as a window material. The CS/SF blend films and the didecanal treated films were placed on a Ge crystal and the data were collected. All spectra were obtained using a Thermo Nicolet 510P FT-IR Spectrometer with OMNIC software. The scans were performed with an average of 32 repeated scans at 4 cm^{-1} scan resolution.

2.2.11 Gas Chromatography-Mass spectrometry

Gas chromatography with mass spectrometry (GC/MS) was used for the identification of didecanal, utilizing a Hewlett Packard G1800A GCD system equipped with DB-5MS capillary column (30m x 0.25mm, 0.25μm film thickness) and an electron multiplier detector. The reaction product, diluted with $CHCl_3$, was automatically injected by the splitless mode, at the flow rate of 1mL/min. The temperature was programmed as a ramp of 10 ºC /min, from 60

to 300 ºC, and the inlet and flame ionization detector temperature was set to 280 ºC. The chromatogram and spectrum were obtained using Chem Station B.02.04.

2.2.12 UV-Visible spectroscopy

All UV/visible absorption measurements were performed and the spectra were analyzed by using a Varian Cary 3E spectrophotometer with Cary 300 software.

2.2.13 Thermogravimetric analysis

Thermal degradation measurements were performed and the thermograms were obtained using the Perkin Elmer TGA Pyris 1^{TM}. Pure CS, SF, and the blend films, with or without dialdehyde treatment of ca. 5-6mg, were mounted onto a Pt pan sample holder. All samples were heated under N_2 purging until the absorbed solvent and water were almost completely evaporated. Each analysis was run from 25 to 900ºC at the rate of 50ºC/min. The thermograms indicating the weight loss of the sample were obtained as a function of time.

2.2.14 Dissolving test of CS/SF blend films

CS/SF films (raw films, GA treated films, and didecanal treated films) were cut into 1cm x 1cm size, for the determination of crosslinking. They were soaked in 2mL of $Ca(NO_3)_2 \cdot 4H_2O$/MeOH solution and 96% HCO_2H, with and without heat, for 2 days. The 2,4-DNPH treated CS/SF films (raw films and GA treated films) were also prepared in the same manner and soaked in 2mL of 96% HCO_2H with and without heat for 2 days. The absorbance of a solution of each sample was measured at 361 nm using an absorption spectrophotometer.

2.2.15 Bioadhesion/peeling tests

Porcine intestines were used as the biological testing substrate. The tissue samples were obtained from the Nahunta Pork Center, Nahunta, NC. They were immediately excised after slaughter and stored at –5 ºC in isotonic buffered saline at pH 7.4 (2.38 g of Na_2HPO_4, 0.19g of KH_2PO_4, and 8.0g of NaCl in 1000 mL deionized water). The intestine tissue was carefully washed the next day, the loose surface membranes were removed, and the tissue was cut into 1cm x 3cm sections. Each chitosan/silk fibroin blend film was cut into 1cm x 1cm squares, and each was sandwiched between the two tissue samples and covered by two glass plates. A 50g weight was placed onto the 1cm x 1cm bonding area under the glass for 10 min. Both ends of the tissue samples were clamped at a gauge length of 1cm, and the peeling test was immediately conducted at the rate of 6 mm/min (Instron Model 5544 with a 5N load cell). The load to the tissue for peeling was plotted as a function of extension of the clamps. Polyethylene film, chitosan, and blend films, without GA or didecanal treatment, were used as controls. Five to six replicates were obtained for each sample.

2.3 Results and Discussions

2.3.1 Synthesis of 1,10-didecanal

Figure 2-2 provides the FTIR spectra of the 1,10-decanediol (starting material) and didecanal synthesized by oxidation. Evidence of the oxidation was demonstrated from absorptions at 2717, 1777, 1708, and 679 cm^{-1}. The absorption at 2717 cm^{-1} was assigned to the overtone of C-H bending in aldehydes. Absorptions at 1777 and 1708 cm^{-1} were assigned

as the C=O stretch in carbonyls and aldehydes. The absorption at 679 cm^{-1} was assigned to C-C-CHO bending. Since the peaks corresponding to –OH stretch at 3406 and 3342 cm^{-1} in 1,10-decanediol greatly decreased and peaks of C=O stretch appeared, it was concluded that the alcohol was oxidized to the aldehyde during the reaction. However, the product might contain residual alcohol or monoaldehyde, because absorptions around 1000 cm^{-1} were still observed.

Figure 2-3 and 2-4 show the GC-MS chromatogram and spectra of the resulting oxidation product. A clear peak for 1,10-decanediol was observed at a retention time at 15.34 min, which indicates the presence of unreacted starting material. The peak at retention time 13.75 min was assigned as the corresponding 1,10-didecanal. Even though 1,10-didecanal is not commercially available, the retention time should be close to those two peaks because of the chemical structural similarities between them. Therefore, the peak of retention time at 14.54 min was assigned to corresponding mono-aldehyde. The product mixture was found to be 1,10-decanediol, 1,10-didecanal, and mono-aldehyde substituted decanol in ratio about 3:2:1.

In order to obtain stronger evidence of the presence of 1,10-didecanal, the colorimetric 2,4-DNPH method was also conducted. Figure 2-5 is a digital image of the didecanal treated CS/SF films. The vivid yellow colored films clearly indicated the presence of free aldehyde groups. Since one aldehyde in the molecule was reacted with amino groups in CS or SF, there must be a free aldehyde group available for reacting with 2,4-DNPH solution. The yellow color indicating the hydrazone formed between aldehyde groups in didecanal and hydrazine

groups in 2,4-DNPH was not diminished by washing with H_2O. Therefore, evidence of the presence of 1,10-didecanal in the final product was supported qualitatively.

Few studies about successful dialdehydes synthesis methods have been reported. Reductive oxidation with borane and pyridinium chlorochromate (PCC) was performed to convert various carboxylic acid salts to corresponding aldehydes [23]. The yield of dialdehydes from dicarboxylic acid salts was quite low, whereas the conversion of carboxylic acids, such as hexanoic and decanoic acid salts to the corresponding aldehydes, was successful. However, the presence of chromium results in producing toxic waste. Catalytic hydrogenation of carboxylic acids via acyl(carboxylato)palladium complexes can provide various aldehydes, including dialdehydes, effectively [24]. However, certain dicarboxylic acids yield small amounts of the corresponding dialdehydes, when the diacid was easily converted to the anhydride. A high pressure reactor is required for the hydrogenation process. The modified Corey method used in this study still had a selectivity problem during the oxidation process. Nevertheless, this method is useful due to the simple equipment and mild condition if further improvement in a proper reaction condition is made. However, the amphiphilic nature of the didecanal and higher carbon dialdehydes limits their solubility.

2.3.2 Characterization of CS/SF blend films

The FTIR-ATR spectra of CS/SF blend films are shown in Figure 2-6. There was evidence of high degree of deacetylation of pure chitosan film due to the absence of the characteristic bands of C=O stretch at 1650 cm^{-1} and N-H deformation at 1540 cm^{-1} for the secondary amides. Evidence of the CS was demonstrated by absorptions at 1555, 1075, and

1031 cm^{-1}. The absorptions at 1555 and 1075 cm^{-1} were assigned to the $R\text{-}NH_3^+$ deformation and C-N stretch in primary amines. The latter peak had a shoulder which also indicated the presence of C-O-C antisym stretch of ether bonds. The absorption at 1032 cm^{-1} was assigned to the C-O stretch of primary alcohols in the sugar ring. On the other hand, SF showed characteristic peaks at 1645 and 1540 cm^{-1}, which were assigned to C=O stretch and N-H deformation in secondary amides of SF. As the composition of the CS decreased with increasing SF in order of CS, CS/SF=2/1, 1/1, 1/2, and SF, the characteristic peaks of CS decreased and those of SF increased. Since all blend films have relatively few free aldehyde groups, their spectra did not exhibit the presence of 2,4-DNPH and the change of the shape in spectra, as seen in Figure 2-7. Figure 2-8 shows digital images of CS, blend, and SF films treated only with 2,4-DNPH. All films had only a faint yellow color, which indicated little chemical reaction happened between films and 2,4-DNPH, and it was mostly washed out. The control film of low density polyethylene (LDPE) film, shown in Figure 2-9, did not exhibit any yellow color, as expected. Though this colorimetric test using 2,4-DNPH was frequently used for monitoring the presence of aldehydes in gas and liquid phases [19-21], few papers have reported detection of aldehydes on films. Shannon et al reported the colorimetric monitoring on resin-bonded aldehydes [25].

TGA thermograms of as-cast CS, SF, and CS/SF blend films are shown in Figure 2-10 and the corresponding data summary are listed in Table 2-1. Three decomposition steps could be observed in the thermogram. The first weight loss occurred in the range of 100-200 ºC, which is attributed to water and HOAc evaporation [26]. The second step, the main decomposition for both CS and SF components, which occurred in the range of 300-400 ºC

should be due to the degradation of the polysaccharide chains and degradation of deacetylated units of chitosan [27] and to the decomposition of side chain groups of SF. The degradation temperature of pure chitosan film was lower than those of pure SF and blend films. In addition, the degradation rate of chitosan was higher than the others.

Since the chitosan used through the entire experiments was highly deacetylated, compared to as-received chitosans, the films had lower thermal stability than chitin, as-received chitosan, and SF due to the less *N*-acetyl groups. Surprisingly, high deacetylated CS is less stable than the partially deacetylated one, because chitin is more stable due to the hydrogen bond of the amide group. The strong thermal decomposition of SF around this temperature range should be related to the disintegration of intermolecular interaction and the partial scissions of the molecular structure [15,17,27,28]. On the other hand, pure SF and blend films had a similar trend, which would indicate the influence of intermolecular interactions between the CS and SF, once they were mixed [15]. These interactions would include hydrogen bondings and Van der Waals force. The third decomposition step in the range of 400-900 ºC would be governed by the further decomposition of chitosan and the main protein backbone of SF [17]. Whereas the amount of pure chitosan film residue at 340 ºC was much less than the other films, due to the lower thermal stability of CS, the residue differences at 550 ºC were not as significant. Therefore, incorporating SF moieties surely affected the thermal stability of the blend films.

2.3.3 Characterization of GA treated CS/SF blend films

The FTIR-ATR spectra of GA treated CS/SF blend films are shown in Figure 2-11. Since SF solution was water-soluble, water-diluted GA treatment was not suitable for SF film. After the reaction between CS/SF blend films and GA, free dangling aldehyde groups were found at the chitosan C-2 position. Particularly, the characteristic C=O stretch peak of aldehyde groups was shown at 1735 cm^{-1} as a shoulder in the GA treated CS film. Comparing with other blend films, the aldehyde peak appeared at a higher wavenumber as a shoulder of the peak, corresponding to the C=O stretch in amides of around 1630 cm^{-1}. They were not observed in non-GA treated films, as shown in Figure 2-6. The newly formed imine peak (C=N stretch, 1690-1640 cm^{-1}) between amino and aldehyde groups was not detected as a single peak due to the many other overlapping peaks. The FTIR-ATR spectra of GA and 2,4-DNPH treated CS/SF blend films are shown in Figure 2-12. All aldehyde groups were converted to imines by reaction with 2,4-DNPH. The peak and shoulder, indicating the aldehyde group in Figure 2-11, were diminished in the spectra in Figure 2-12. The result also indicated the presence of free aldehyde groups in GA treated films. Figure 2-13 shows digital images of CS, blend, and SF films treated with GA and 2,4-DNPH. All films had a vivid yellow color, which indicated a chemical reaction occurred between dangling aldehydes of CS/SF blend films and 2,4-DNPH. The result also supported the conclusion that GA cross-linked amino groups in chitosan, to some extent.

TGA thermograms of as-cast CS, SF, and CS/SF blend films treated with 0.01M glutaraldehyde are shown in Figure 2-14, and the corresponding data summary are listed in Table 2-2. Three decomposition steps could be observed in the thermogram, the same as for

non-glutaraldehyde treated films. The first weight loss occurred in the range of 100-200 ºC, which is attributed to water and acetic acid evaporation. The second step, the main decomposition for both CS and SF components, occurring in the range of 300-400 ºC, should be due to the degradation of the polysaccharide chains and dehydration of deacetylated units of chitosan and to the decomposition of side chain groups of SF. The degradation temperature of pure chitosan film was shifted higher by 30 ºC, compared to non-GA treated CS and closer to those of pure SF and blend films. In addition, the degradation rate was lower than that of non-GA treated CS. When GA was used as a crosslinking agent for poly(vinyl alcohol), the thermal stability of the polymer was improved [29].

These results indicate that chitosan with dangling aldehyde groups might be crosslinked to some extent which increases the thermal stability, in addition to the intermolecular interactions in pure SF and blend films. Nevertheless, CS and CS/SF blended films must have some dangling free aldehyde groups on the surface, according to the colorimetric test results (See section 2.3.6). Since SF is mainly composed of amino acids with relatively small side groups, such as glycine and alanine [30], which have no way to make bonds with GA, SF itself would have very few dangling aldehyde groups. Overall, the third decomposition step in the range of 400-900 ºC exhibited similar trends as non-GA treated films. While the amount of GA treated chitosan film residue at 340 ºC was more than that of non-GA treated chitosan, due to the improved thermal stability, the residue differences among the films at 550 ºC were not significant. Therefore, GA treatment on the CS and blend films mainly affects the second degradation step.

2.3.4 Characterization of didecanal treated CS/SF blend films

The FTIR-ATR spectra of didecanal treated CS/SF blend films are shown in Figure 2-15. After the reaction between CS/SF blend films and didecanal, free dangling aldehyde groups with a longer alkyl chain than GA were found at the chitosan C-2 position. The characteristic C=O stretch peak of aldehyde groups was found at 1720 cm^{-1} in all didecanal treated films, except for CS/SF=1/2. The aldehyde peak appeared at a higher wavenumber as a shoulder of the peak corresponding to the C=O stretch in amides around 1650 cm^{-1}. Very sharp peaks at 2925 and 2855 cm^{-1} were assigned to CH antisym and sym stretches due to the long alkyl chain of didecanal. The newly formed imine peak (C=N stretch, 1690-1640 cm^{-1}) between amino and aldehyde groups was not detected as a single peak due to the many other overlapping peaks.

The FTIR-ATR spectra of didecanal and 2,4-DNPH treated CS/SF blend films are shown in Figure 2-16. At this stage, all aldehyde groups must be converted to the corresponding imine by reaction with 2,4-DNPH. The peak in Figure 2-15, for aldehyde group at 1720 cm^{-1}, was diminished in the spectra in Figure 2-16. The result also indicated the presence of free aldehyde groups in didecanal treated films. Figure 2-5 shows digital images of CS, blend, and SF films treated with didecanal and 2,4-DNPH. All films had a vivid yellow color, which indicated a chemical reaction occurred between dangling aldehydes of CS/SF blend films and 2,4-DNPH. The result also supported the evidence that didecanal reacted with amino groups in chitosan to some extent. Over all, this colorimetric test was found to be a useful qualitative characterization method for surface modifications needed to detect free aldehyde groups in the material.

TGA thermograms of as-cast CS, SF, and CS/SF blend films treated with 0.05M didecanal are shown in Figure 2-17, and the corresponding data summary are listed in Table 2-3. Three decomposition steps could be observed in the thermogram, the same as for non-glutaraldehyde and GA treated films. The first weight loss occurred in the range of 100-200 ºC, which is attributed to water and acetic acid evaporation. The second step, the main decomposition for both CS and SF components, which occurred in the range of 300-400 ºC, should be due to the degradation of the polysaccharide chains and dangling aldehyde chains, dehydration of deacetylated units of chitosan, and the decomposition of side chain groups of SF. The degradation temperature of films with higher chitosan content (CS, CS/SF 2/1, and CS/SF 1/1) was shifted higher by 10-15 ºC than that of GA treated films, which maybe due to the chemically bonded aldehyde chains. Higher SF content films, such as CS/SF 1/2 and SF did not exhibit such an apparent temperature shifting because SF does not have many reactive sites towards aldehyde groups, which was confirmed by the colorimetric test. These results indicate that dangling long alkyl dialdehyde chains might have contributed to the thermal stability to some extent, even though the amount of aldehyde bonded to chitosan amino groups was not high (See section 2.3.6). Overall, the third decomposition step in the range of 400-900 ºC exhibited similar trends as non-GA and GA treated films. While the amount of residue from didecanal treated chitosan-containing film at 340 ºC was more than that of non-GA or GA treated ones, due to the improved thermal stability, the residue differences at 550 ºC were not as significant among the films. Therefore, didecanal treatment on the CS and blend films mainly affects the second degradation step.

2.3.5 Dissolution tests of CS/SF blend films

Dissolution tests were conducted in order to evaluate the extent of cross-linking of the CS/SF blend films as represented in Table 2-4. Initial tests used a $Ca(NO_3)_2 \cdot 4H_2O$ solution, known as a good solvent for SF. Only the untreated pure SF film dissolved and all other films, including dialdehyde treated films (0.01M and 0.05M GA, and 0.05M didecanal), were not dissolved due to the incorporation of CS. A subsequent test was conducted using 96% HCO_2H, known as a common solvent for both CS and SF. Untreated pure CS and SF dissolved within ten minutes at room temperature. All untreated CS/SF blend films were completely dissolved after 1 day at room temperature. All films treated with 0.01M GA were completely dissolved within 2 days under heat, whereas those films treated with 0.05M GA, except for pure SF film, retained their integrity after 2 days, even with the addition of heat. When 0.01M GA treated films were placed in the solution at room temperature, a large portion of all films remained even after 4 days. Since the dialdehyde treated films potentially contained a mixture of crosslinks and dangling free aldehyde groups, films treated with a high concentration of GA tended to be retained in the solvent. The shrinkage of films after treatment of GA also indicated the presence of crosslinks. Films treated with 0.05M GA were not used in other experiments because the films were brown colored, probably due to the oxidation of the film in the reactive free aldehyde groups.

All films treated with 0.05M didecanal were dissolved after 6 h at room temperature. Even though the weight percent of didecanal was 0.05M, the actual concentration of didecanal was assumed to be lower than 0.05M, because the solution was the mixture of the reaction products. Therefore, the dialdehyde concentration of 0.01M was not tried throughout the

experiments. Indeed, the film was not brown colored after the treatment. Little shrinkage was observed in didecanal treated films, and this phenomenon indicated that fewer crosslinks were present.

Overall, crosslinks in films are expected to contribute to the wet strength, while dangling free aldehyde groups may improve the bonding strength to tissue. An ability to control the degree of crosslinks and free aldehydes will likely influence the degradation rate and bioadhesiveness of the film.

2.3.6 Determination of the amount of reacted dialdehydes to CS/SF blend films

Figure 2-18 shows the hydrazone UV-visible absorption at 361nm for the 0.01M GA treated CS/SF blend films dissolved in 96% HCO_2H. The absorbance increased with increasing CS composition because of the larger amount of amino group at higher CS incorporation, which could react with GA than in film of lower CS composition. The quantitative measurement may not be accurate, because the standard curve Figure 2-1 was made in acetonitrile, which is a common solvent for 2,4-DNPH, not in 96% HCO_2H. Nevertheless, the absorbance can be comparable for relative amounts of the free aldehyde groups.

Since all films were not completely dissolved at room temperature, the absorbance of film was directly measured as an alternative method. A similar trend was observed when the absorbance of films was measured by UV-visible spectroscopy, as shown in Figure 2-19. Theoretically, the amount of free amino group that can react with dialdehydes is larger in the CS film than in the other blend films. Therefore, the chances of forming crosslinks in CS film

are likely better than in other blend films. Since the standard curve seen in Figure 2-1 was obtained in solution, the concentration of free dangling aldehyde group determined by this method may not be accurate for the film. The absorbance value would vary, depending on the film thickness and uniformity of reacted dialdehydes and 2,4-DNPH, and the degree of dissolution of the film. Therefore, other testing methods will be required to determine the exact amount of dangling aldehyde group in the film for future work, such as the LC (Liquid Chromatography) method, which allows calculation of the amount of unreacted 2,4-DNPH with aldehyde in the film, by extraction. Nevertheless, the colorimetric measurement seems to have revealed the presence of the relative free aldehyde group.

Figure 2-20 shows the hydrazone absorbance at 361nm of 0.05M didecanal treated CS/SF blend films dissolved in 96% HCO_2H. The absorbance increased with increasing CS composition, possibly due to the larger amount of amino group which could form crosslinks, rather than due to the film with lower CS composition. This trend also corresponded to the results found in the case of 0.01M GA treated films. It indicated that SF incorporated film could effectively generate dangling free aldehyde groups rather than crosslinks between the molecules. As mentioned above, these results are not exact since 96% HCO_2H was used instead of acetonitrile, and the standard curve was used as a reference to compare the relative difference in amount of the free aldehyde groups in films.

2.3.7 Bioadhesion/peeling tests of CS/SF blend films

Intestinal tissue is often used for bioadhesion tests due to the stronger adhesiveness among mucosal tissues [31,32]. The mean load-extension curve of each layered film is

described in Figures 2-21 and 2-22. The peeling load was monitored while the film sample (1 x 1 cm) was peeled. The control of tissue-tissue peeling curve indicates the force is attributed to the surface tension between two slices of tissue, and low-density polyethylene (LDPE) exhibits almost no adhesion (Figure 2-21). Untreated films with dialdehydes clearly showed the trend in higher peeling strength than that of tissue-tissue control. The CS (DD=98.3) exhibited slightly low peeling strength among the untreated films, due to the absence of protein moieties (Figure 2-21).

On the other hand, the GA treated CS/SF blend films, except for GA treated CS, generally exhibited much higher peeling load than that of control, and also higher than untreated films (Figure 2-22, above). In the previous section, the conclusion was made that crosslinking occurred in GA treated CS film, which reduced the reactive aldehyde groups. Therefore, the effect of GA treatment on bioadhesiveness was not significant, compared to the other GA treated blend films. However, all didecanal treated films did not improve the bioadhesivenes as much as GA did (Figure 2-22, below). Therefore, the general trend was that the peeling load of them was slightly lower than that of untreated films, due to the low concentration of didecanal present on the films and the hydrophobicity of the film by didecanal treatment in $CHCl_3$. These load-extension curves indicate that the force applied to films during tissue peeling was almost constant to the end of testing.

The mean load at 5 and 7mm extension by peeling, a relatively plateau region, were depicted to compare the peeling load among controls and samples in Figure 2-23. Figure 2-23 (a) shows the load required at 5mm to peel two slices of porcine tissue holding various films. The control, porcine tissue without films, exhibited low peeling load values compared to

untreated CS/SF films, because CS/SF films can form physical bonds between amino acid residues and CS functional groups. For example, the CS/SF=2/1 film exhibited 1.8 times higher strength than that of the tissue control. Untreated CS/SF blend films (2/1, 1/1, 1/2) showed almost the same peeling load, about 6mN. Overall, the CS/SF blend films had approximately 1.8 fold of peeling strength on average, whereas the untreated CS film exhibited 1.5 fold of bioadhesion, compare to the control. The CS/SF films without treatment tended to show lower load values than those of GA treated CS/SF films, except for the GA treated CS film. The GA treated CS/SF=1/1 exhibited the highest peeling load among all samples, and 3.7 and 2.5 times higher than those of LDPE and the tissue control, respectively. Also, the GA CS/SF=1/1 was 1.7 times that of the untreated CS and 2.5 times the GA treated CS film. However, the GA treated CS film had almost the same peeling strength as the tissue control and even lower than that of CS without GA treatment. Didecanal treated CS/SF blend films exhibited slightly improved peeling strength, compared to the tissue control, but the peeling load was almost the same as the untreated CS film.

According to the colorimetric tests described in the former section, the GA treated CS film presumably contained crosslinks. The crosslink may reduce the number of free amino groups and aldehyde groups in the chemical structure, which disturbs the ionic/physical interactions between the tissue and film. On the other hand, blend films possess more dangling free aldehydes, which facilitate the formation of stronger chemical bonds between amino groups in tissue and aldehyde groups in films, in addition to physical bonds. The didecanal treated CS film slightly improved the peeling strength, whereas the didecanal treated CS/SF=1/1 film did not. The concentration of didecanal should be lower than that of GA

because the didecanal contained impurities. The total free aldehyde groups in didecanal treated films, 1 x 1 cm in size, may be lower than those of GA treated films. However, in the case of didecanal treated CS film, the concentration seems to be low enough to prevent crosslink formation. As a result, the didecanal treated CS film might exhibit an improved peeling strength. Another possible reason for the lower peeling load of didecanal treated CS/SF blend films, is the wettability after the didecanal treatment. Unlike GA, the didecanal was dissolved in $CHCl_3$ and thus the film hydrohobicity became higher after treatment by didecanal. This assumption will be confirmed by the contact angle measurement of the film surface.

Figure 2-23 (b) shows the load required at 7mm extension to peel two slices of porcine tissue holding various films. A similar trend was observed in the case of extension at 7mm. The GA treated CS/SF blend film group exhibited the highest peeling strength among all samples. The GA treated CS/SF=1/1 film had 2.3 and 1.7 times higher peeling strength than those of the tissue control and untreated CS film, respectively. The CS/SF blend films without GA treatment exhibited 1.6 times higher than the tissue control on average, and had better bioadhesiveness, than didecanal treated CS/SF blend films, probably because of the same reason described above.

2.4 Conclusions and Suggestions for Future Work

The CS/SF blend films with dangling aldehydes have been prepared by the chemical reaction between amino groups of blend films and aldehyde groups of dialdehydes. Colorimetric tests confirmed the presence of free aldehyde groups by forming hydrazones, though the absolute amount of aldehyde groups was still difficult to determine. In order to

devise a better quantitative measurement of dangling aldehydes, unreacted dialdehyde amount can be detected by High Performance Liquid Chromatography (HPLC), if a known concentration of dialdehyde solution is used when treating blend films with it.

Synthesizing dialdehydes is generally difficult and thus commercially available dialdehydes have limited availability [23,24]. Even though the modified Corey method required a simple and mild reaction condition, the reaction resulted in producing undesirable by-products probably because of the stoichimometric amount of oxidizing agent. Some dialdehydes have been effectively obtained by direct hydrogenation in the presence of palladium catalysts [24]. This method will be useful for producing 1,10-didecanal if pressurized hydrogenation equipment is available.

Bioadhesion tests demonstrated the dialdehyde (GA) treated films improved bonding strength of porcine tissue as much as 2.5 and 1.7 times of the tissue control and untreated CS film at most. However, didecanal treated CS and CS/SF blend films exhibited about the same or slightly low bioadhesiveness, compared to untreated CS film, probably due to the increasing hydrophobicity of the films after didecanal treatment. Further improvement in bioadhesiveness can be expected by treating the blend film with higher concentrations of dialdehydes.

2.5 References

1. Lehr CM, Bouwstra JA, Schacht EH, Junginger HE. In vitro evaluation of mucoadhesive properties of chitosan and some other natural polymers. Intl J Pharm 1992; 78: 43-48.
2. Smart JD. The basics and underlying mechanisms of mucoadhesion. Adv Drug Deliv Rev 2005; 57: 1556-1568.
3. Hwang JJ, Stupp SI. Poly(amino acid) bioadhesives for tissue repair. J Biomater Sci Polymer Edn 2000; 11: 1023-1038.
4. Karikari AS, Edwards WF, Mecham JB, Long TE. Influence of peripheral hydrogen bonding on the mechanical properties of photo-cross-linked star-shaped poly(D,L-lactide) networks. Biomacromol 2005; 6: 2866-2874.
5. Matsuda S, Iwata H, Se N, IkadaY. Bioadhesion of gelatin films crosslinked with glutaraldehyde. J Biomed Mater Res 1999; 45: 20-27.
6. Park DH, Kim SB, Ahn KD, Kim EY, Kim YJ, Han DK. In vitro degradation and cytotoxicity of alkyl 2-cyanoacrylate polymers for application to tissue adhesives. J Appl Polym Sci 2003; 89: 3272-3278.
7. Tseng,YC, Tabata Y, Hyon SH, Ikada Y. In vitro toxicity test of 2-cyanoacrylate polymers by cell-culture method. J Biomed Mater Res 1990; 24: 1355-1367.
8. Ninan L, Monahan J, Stroshine RL, Wilker JJ, Shi RY. Adhesive strength of marine mussel extracts on porcine skin. Biomaterials 2003; 24: 4091-4099.
9. Whang HS, Kirsch W, Hudson SM. Hemostatic agents from chitin and chitosan. J Macromol Sci Polym Rev 2005; 45: 309-323.
10. Kweon HY, Um IC, Park YH. Structural and thermal characteristics of Antheraea pernyi silk fibroin/chitosan blend film. Polymer 2001; 42: 6651-6656.
11. Gobin AS, Froude VE, Mathur AB. Structural and mechanical characteristics of silk fibroin and chitosan blend scaffolds for tissue regeneration. J Biomed Mater Res 2005; 74A: 465-473.
12. Rujiravanit R, Kruaykitanon S, Jamieson AM, Tokura S. Preparation of crosslinked chitosan/silk fibroin blend films for drug selivery system. Macromol Biosci 2003; 3: 604-611.

13. Park WH, Jeong L, Yoo DI, Hudson S. Effect of chitosan on morphology and conformation of electrospun silk fibroin nanofibers. Polymer 2004; 45: 7151-7157.
14. Chen X, Li W, Shao Z, Zhong W, Yu T. Separation of alcohol–water mixture by pervaporation through a novel natural polymer blend membrane-chitosan/silk fibroin blend membrane. J Appl Polym Sci 1999; 73: 975-980.
15. Du CH, Zhu BK, Chen JY, Xu YY. Metal ion permeations of silk fibroin/chitosan blend membranes. Polym Int 2006; 55: 377-382.
16. Ha SW, Park YH, Hudson SM. Dissolution of *Bombyx mori* silk fibroin in the calcium nitrate tetrahydrate-methanol system and aspects of wet spinning of fibroin solution. Biomacromol 2003; 4: 488-496.
17. Gil ES, Spontak RJ, Hudson SM. Effect of β-Sheet crystals on the thermal and rheological behavior of protein-based hydrogels derived from gelatin and silk fibroin. Macromol Biosci 2005; 5: 702-709.
18. Lim SH, Hudson SM. Synthesis and antimicrobial activity of a water-soluble chitosan derivative with a fiber-reactive group. Carbohydr Res 2004; 339: 313-319.
19. Behforouz M, Bolan JL, Flynt MS. 2,4-Dinitrophenylhydrazones: A modified method for the preparation of these derivatives and an explanation of previous conflicting results. J Org Chem 1985; 50: 1186-1189.
20. Pötter W, Karst U. Identification of chemical interferences in aldehyde and ketone determination using dual-wavelength detection. Anal Chem 1996; 68: 3354-3358.
21. Van Leeuwen SM, Hendriksen L, Karst U. Determination of aldehydes and ketones using derivatization with 2,4-dinitrophenylhydrazine and liquid chromatography-atmospheric pressure photoionization-mass spectrometry. J Chrom A 2004; 1058: 107-112.
22. Corey EJ, Kim CU. A new and highly effective method for the oxidation of primary and secondary alcohols to carbonyl compounds. J Am Chem Soc 1972; 94: 7586-7587.
23. Cha JS, Park JH, Lee DY. Exceptionally facile conversion of carboxylic acid salts to aldehydes by reductive oxidation with borane and pyridinium chlorochromate. Bull Korean Chem Soc 2001; 22: 325-326.
24. Nagayama K, Shimizu I, Yamamoto A. Direct hydrogenation of carboxylic acids to corresponding aldehydes catalyzed by palladium complexes. Bull Chem Soc Jpn 2001; 74:

1803-1815.

25. Shannon SK, Barany G. Colorimetric monitoring of solid-phase aldehydes using 2,4-dinitrophenylhydrazine. J Comb Chem 2004; 6: 165-170.
26. Osman Z. Thermal and conductivity studies of chitosan acetate-based polymer electrolytes. Ionics 2005; 11: 397-401.
27. Paulino AT, Simionato JI, Garcia JC, Nozaki G. Characterization of chitosan and chitin produced from silkworm crysalides. Carbohydr Polym 2006; 64: 98-103.
28. Kweon HY, Um IC, Park YH. Structural and thermal characteristics of *Antheraea pernyi* silk fibroin/chitosan blend film. Polymer 2001; 42: 6651-6656.
29. Park JW, Im SS. Phase behavior and morphology in blends of poly(L-lactic acid) and poly(butylene succinate). J Appl Polym Sci 2002; 86: 647-655.
30. Suzuki Y, Gage P, Brown DD. The genes for silk fibroin in *Bombyx mori*. J Mol Biol 1972; 70: 637-649.
31. Lehr CM, Bouwstra JA, Tukker JJ, Junginger HE. Intestinal transit of bioadhesive microspheres in an in situ loop in the rat-A comparative study with copolymers and blends based on poly(acrylic acid). J Contr Release 1990; 13: 50-62.
32. Kakoulides EP, Smart JD, Tsibouklis J. Azocrosslinked poly(acrylic acid) for colonic delivery and adhesion specificity: in vitro degradation and preliminary ex vivo bioadhesion studies. J Contr Release 1998; 54: 95-109.

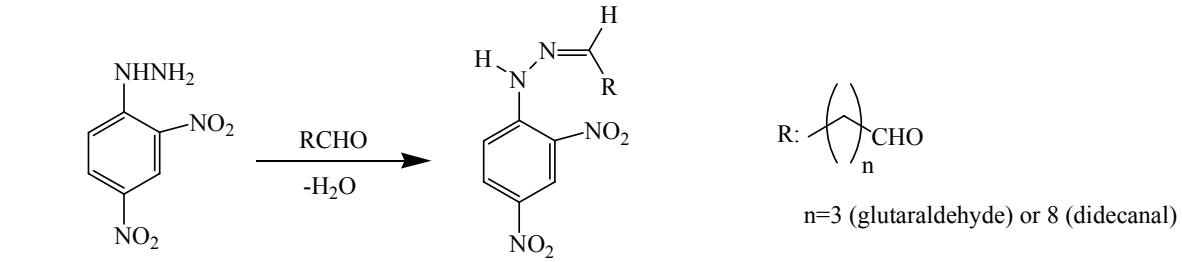

Scheme 2-1 Synthetic scheme of 2,4-dinitrophenyl hydrazone formation caused by a reaction between 2,4-dinitrophenyl hydrazine (2,4-DNPH) and aldehydes.

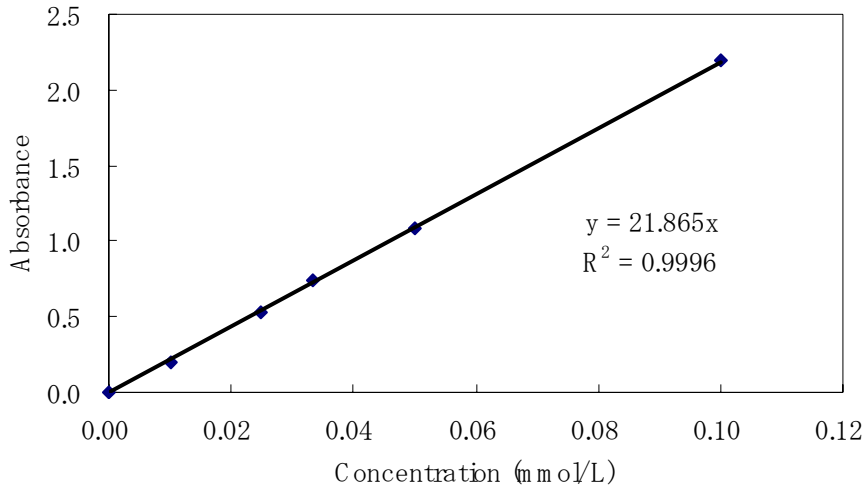

Figure 2-1 Standard curve for 2,4-dinitrophenylhydrazone of heptanal at 361nm.

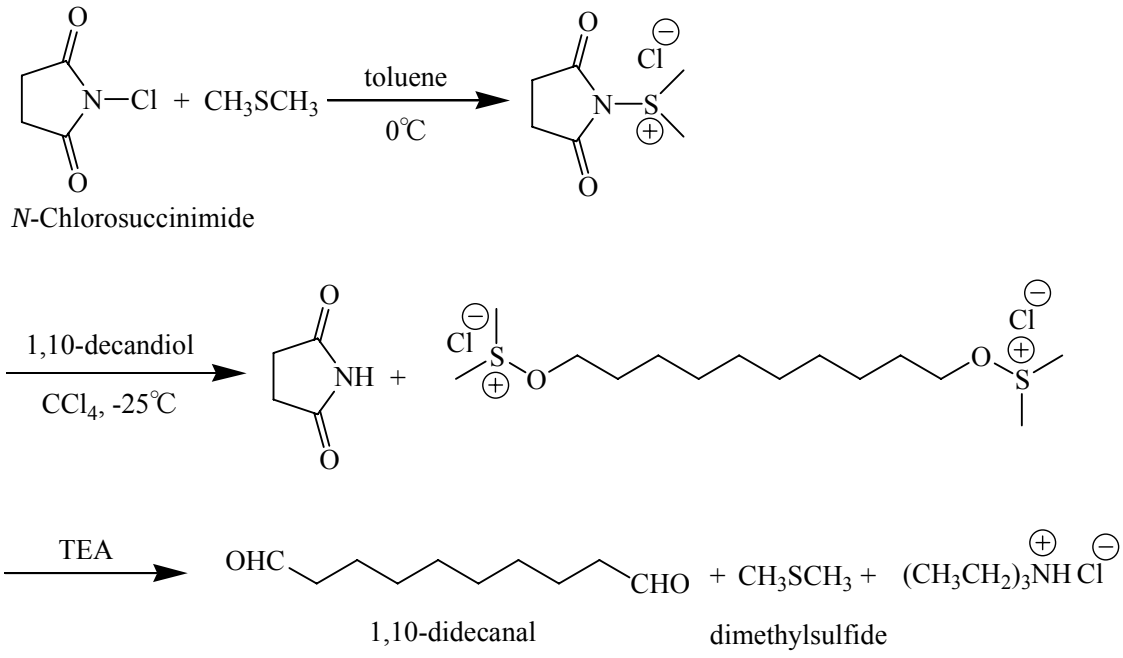

Scheme2-2 Synthetic scheme of 1,10-didecanal by oxidation of 1,10-decandiol to the corresponding dialdehyde (Modified Corey method).

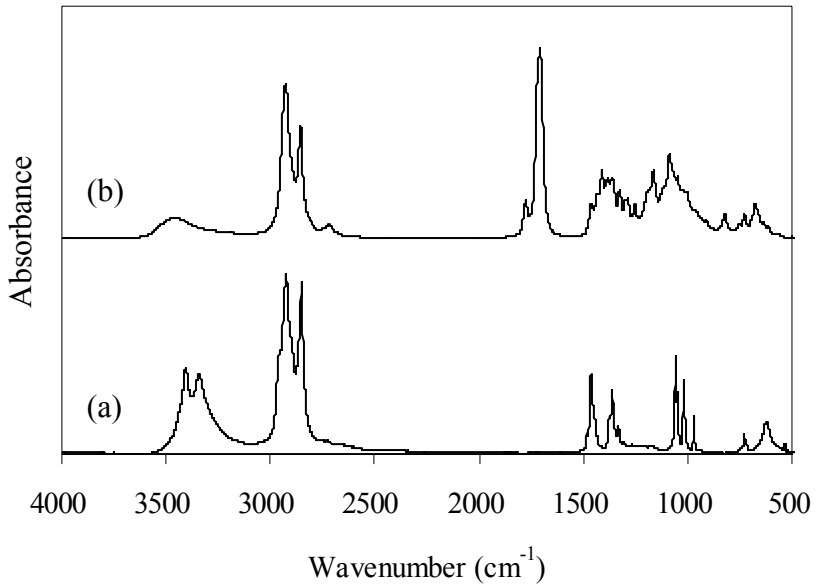

Figure 2-2 FTIR spectra of (a): 1,10-decandiol (starting material) and (b): 1,10-didecanal. The spectra were obtained as a KBr pellet.

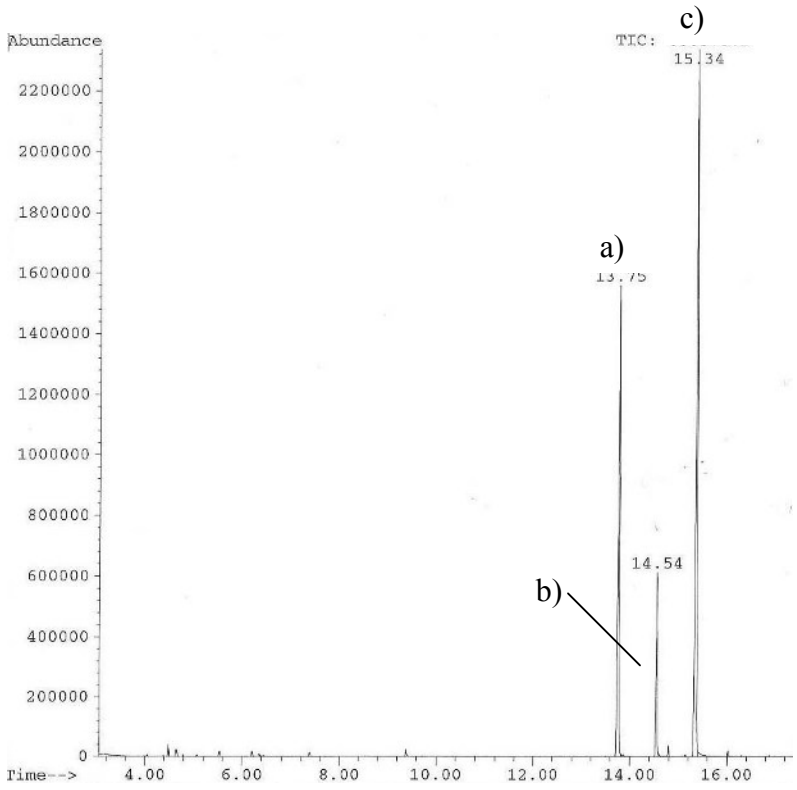

Figure 2-3 Gas chromatogram of didecanal mixture after the oxidation reaction. (a): didecanal, (b): mono-aldehyde, (c): decanediol

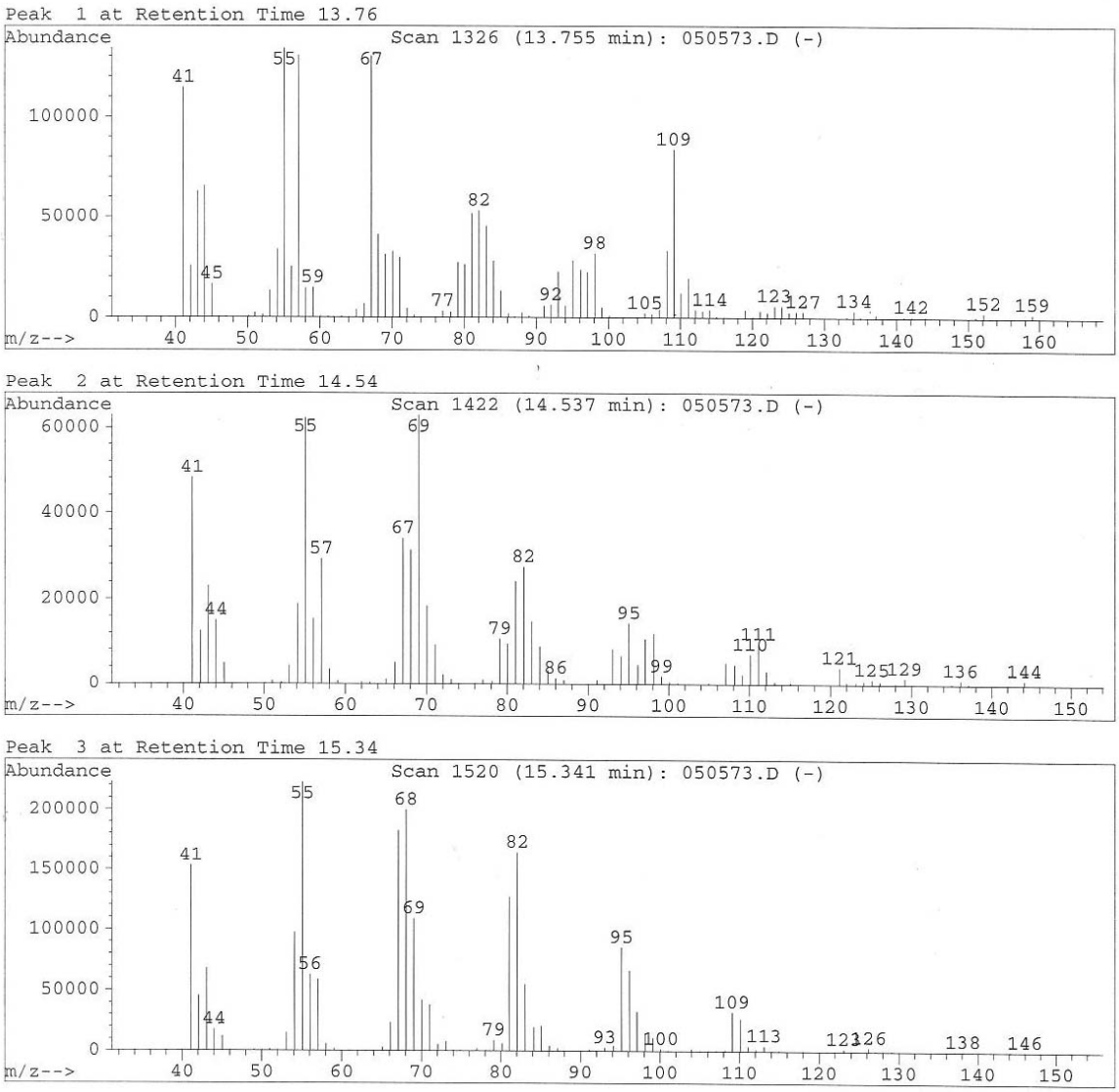

Figure 2-4 MS spectra of didecanal mixture after the oxidation reaction. (a): didecanal, (b): mono-aldehyde, (c): decanediol

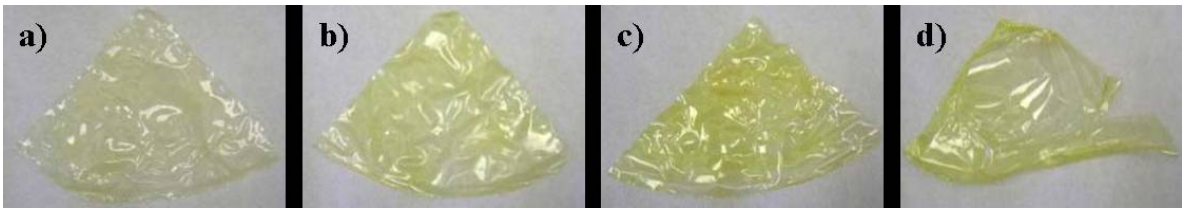

Figure 2-5 Digital images of 0.05M didecanal and 2,4-DNPH treated CS/SF blend films.(a): CS, (b): CS/SF=2/1, (c): CS/SF=1/1, (d): CS/SF=1/2. The yellow color indicates the presence of free aldehyde groups.

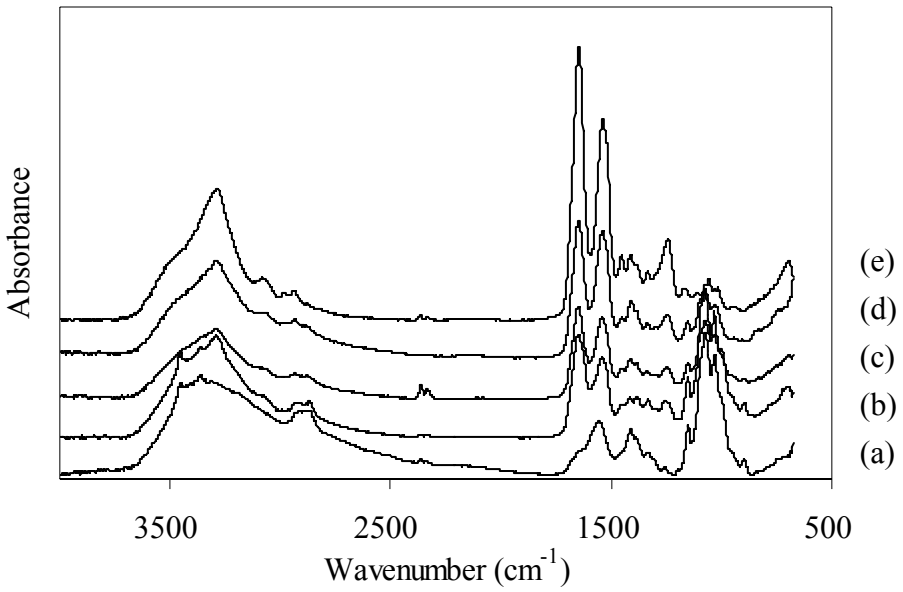

Figure 2-6 FTIR-ATR spectra of CS/SF blend films. (a): CS, (b): CS/SF=2/1, (c): CS/SF=1/1, (d): CS/SF=1/2, (e): SF. The spectra were obtained by the film sample on a Ge crystal.

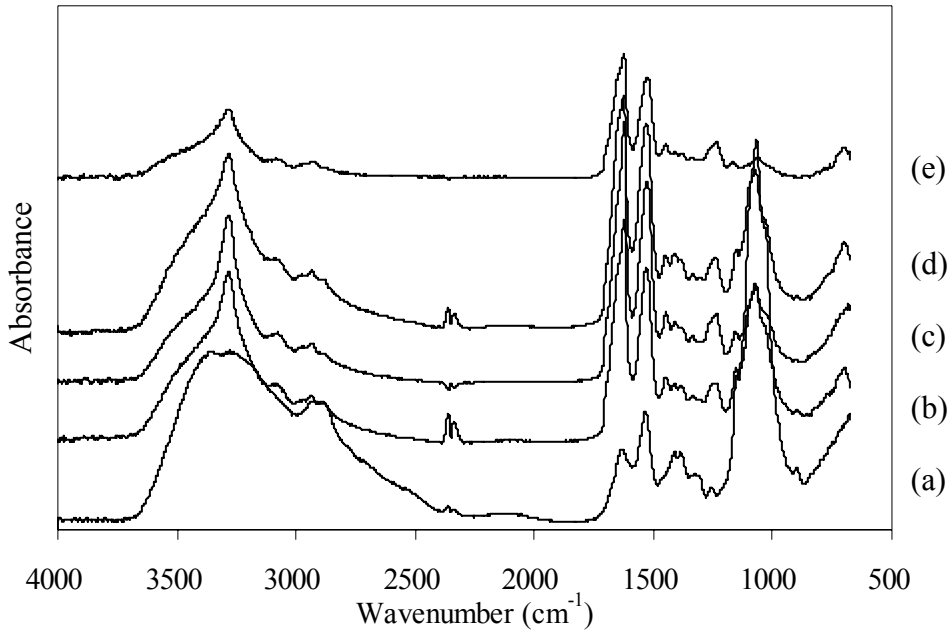

Figure 2-7 FTIR-ATR spectra of 2,4-DNPH treated CS/SF blend films. (a): CS, (b): CS/SF=2/1, (c): CS/SF=1/1, (d): CS/SF=1/2, (e): SF. The spectra were obtained by the film sample on a Ge crystal.

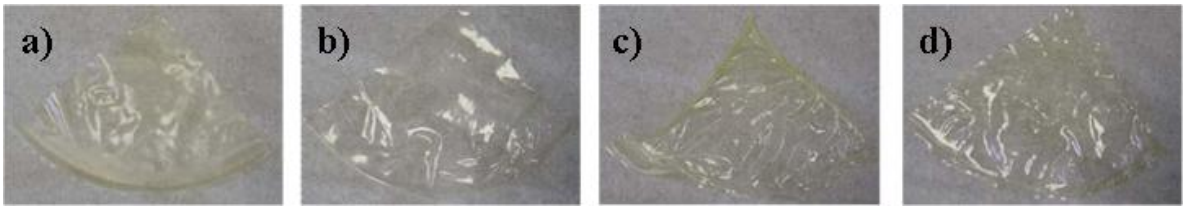

Figure 2-8 Digital images of 2,4-DNPH treated CS/SF blend films.(a): CS, (b): CS/SF=2/1, (c): CS/SF=1/1, (d): CS/SF=1/2. The yellow color indicates the presence of free aldehyde groups.

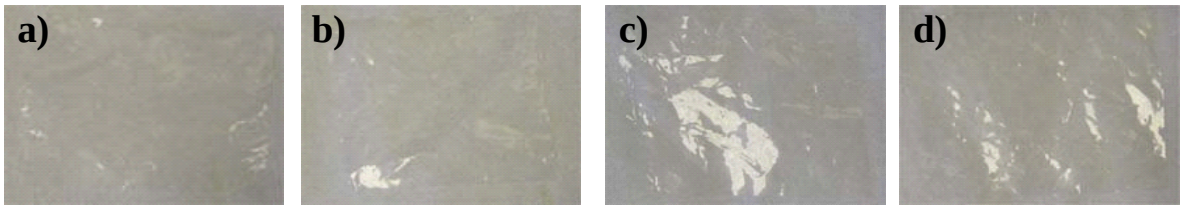

Figure 2-9 Digital images of 2,4-DNPH and GA treated low density polyethylene (LDPE) film.(a): control (without GA), (b):0.01M GA, (c): 0.05M GA, (d): 25% GA. Little yellow color was detectable after 2,4-DNPH treatment, which indicates the absence of free aldehyde groups.

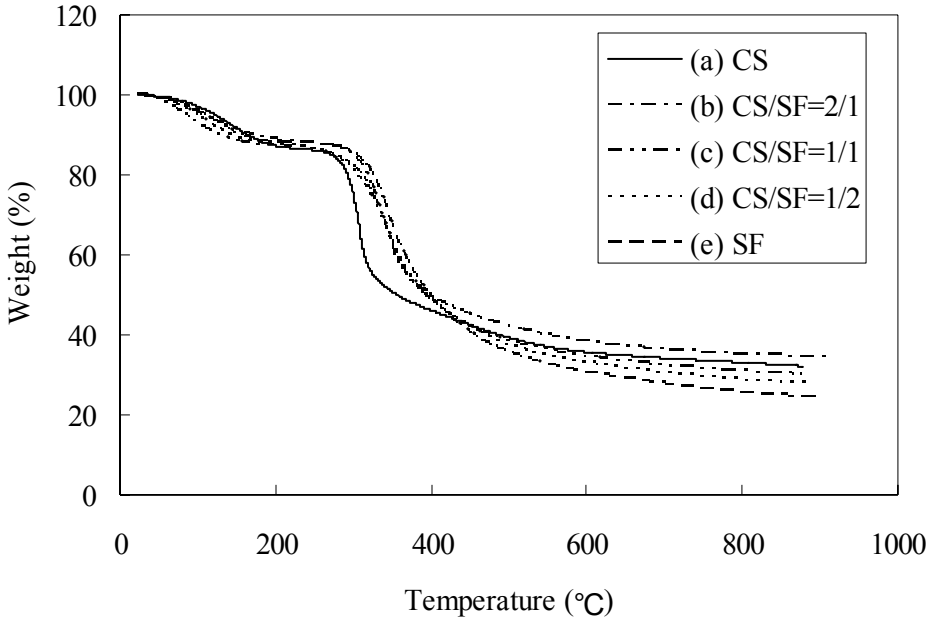

Figure 2-10 TGA thermograms of CS/SF blend films. (a): CS, (b): CS/SF=2/1, (c): CS/SF=1/1, (d): CS/SF=1/2, (e): SF. A scan rate of 50ºC/min was used.

Table 2-1 TGA data of chitosan, silk fibroin and their complex films.

	Onset Temp.	Temp. at max. rate	Max. rate	Residue at 340 ºC	Residue at 550 ºC
	(ºC)	(ºC)	(%/min)	(%)	(%)
CS	292	308	63.6	52.2	37.0
CS/SF 2/1	307	343	30.4	68.0	39.9
CS/SF 1/1	303	347	24.5	68.1	36.2
CS/SF 1/2	292	347	21.1	67.8	34.8
SF	312	344	30.7	73.2	32.7

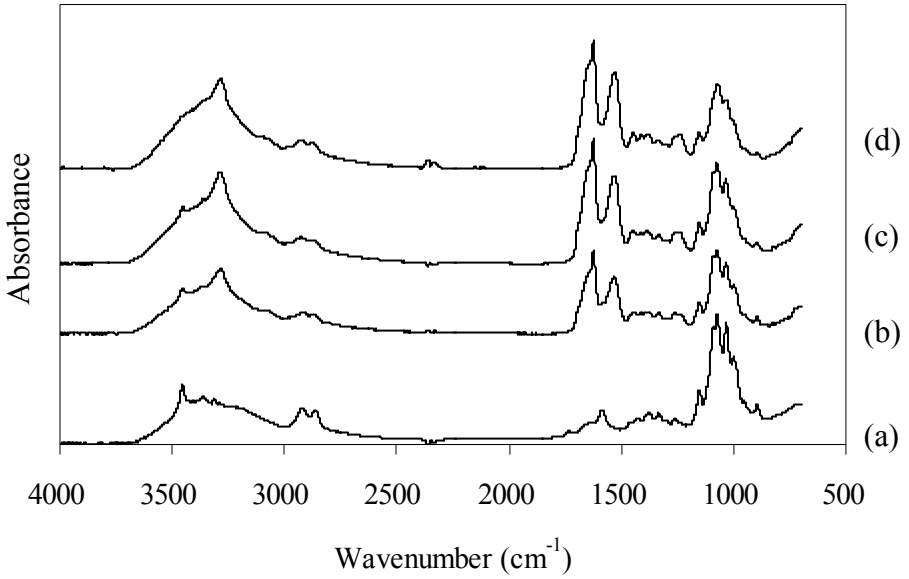

Figure 2-11 FTIR-ATR spectra of 0.01M GA treated CS/SF blend films. (a): CS, (b)CS/SF=2/1, (c): CS/SF=1/1, (d): CS/SF=1/2. The spectra were obtained by the film sample on a Ge crystal.

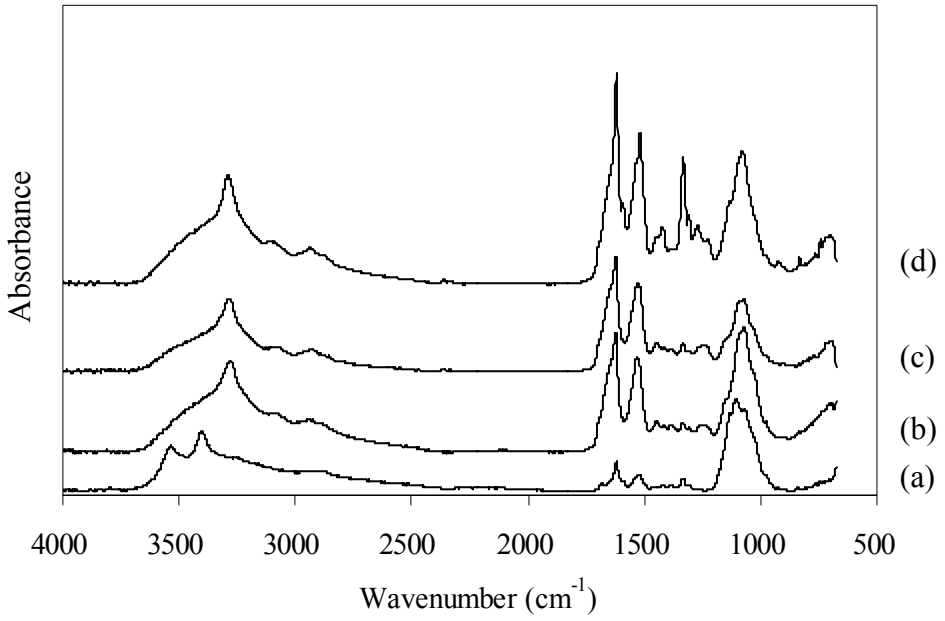

Figure 2-12 FTIR-ATR spectra of 0.01M GA and 2,4-DNPH treated CS/SF blend films. (a): CS, (b)CS/SF=2/1, (c): CS/SF=1/1, (d): CS/SF=1/2. The spectra were obtained by the film sample on a Ge crystal.

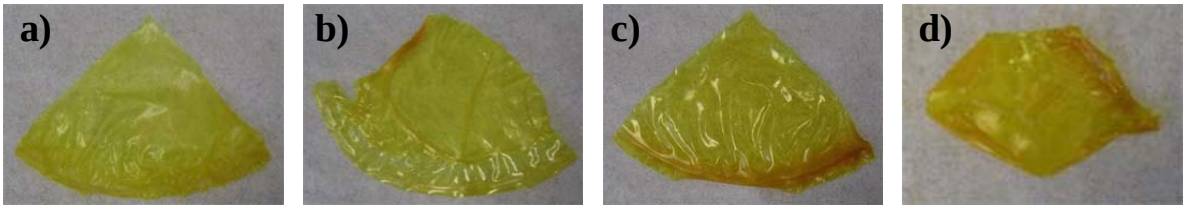

Figure 2-13 Digital images of 0.01M GA and 2,4-DNPH treated CS/SF blend films. (a):CS, (b): CS/SF=2/1, (c): CS/SF=1/1, (d): CS/SF=1/2. The yellow color indicates the presence of free aldehyde groups.

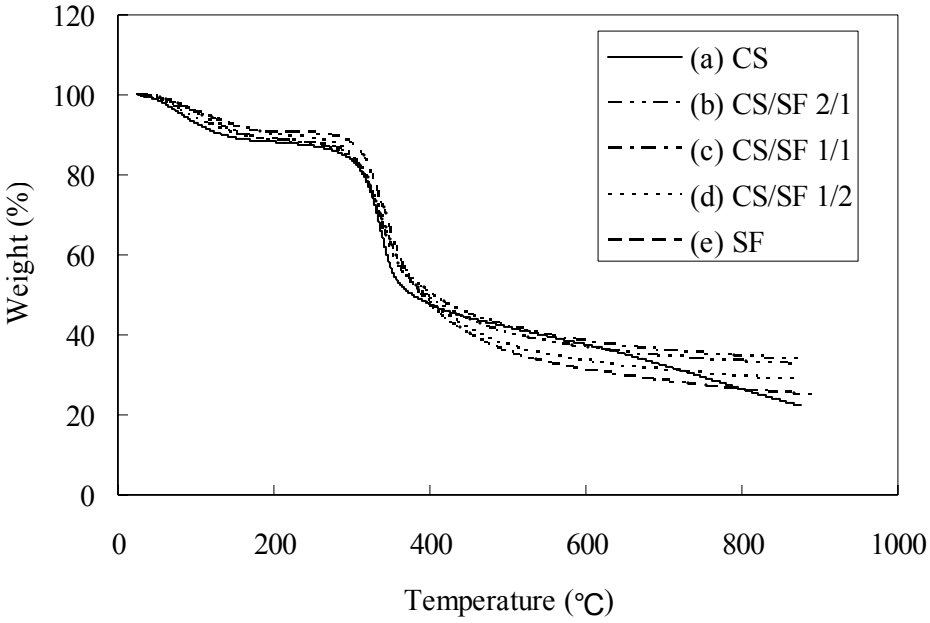

Figure 2-14 TGA thermograms of 0.01M GA treated CS/SF blend films. (a): CS, (b): CS/SF=2/1, (c): CS/SF=1/1, (d): CS/SF=1/2, (e): SF. A scan rate of 50ºC/min was used.

Table2-2 TGA data of 0.01M glutaraldehyde treated chitosan, silk fibroin and their blend films.

	Onset Temp.	Temp. at max. rate	Max. rate	Residue at 340 ºC	Residue at 550 ºC
	(ºC)	(ºC)	(%/min)	(%)	(%)
CS	312	338	42.1	63.7	39.8
CS/SF 2/1	306	334	30.0	66.3	38.2
CS/SF 1/1	301	331	27.7	67.3	40.0
CS/SF 1/2	305	341	31.6	68.2	35.0
SF	310	347	32.1	71.5	33.0

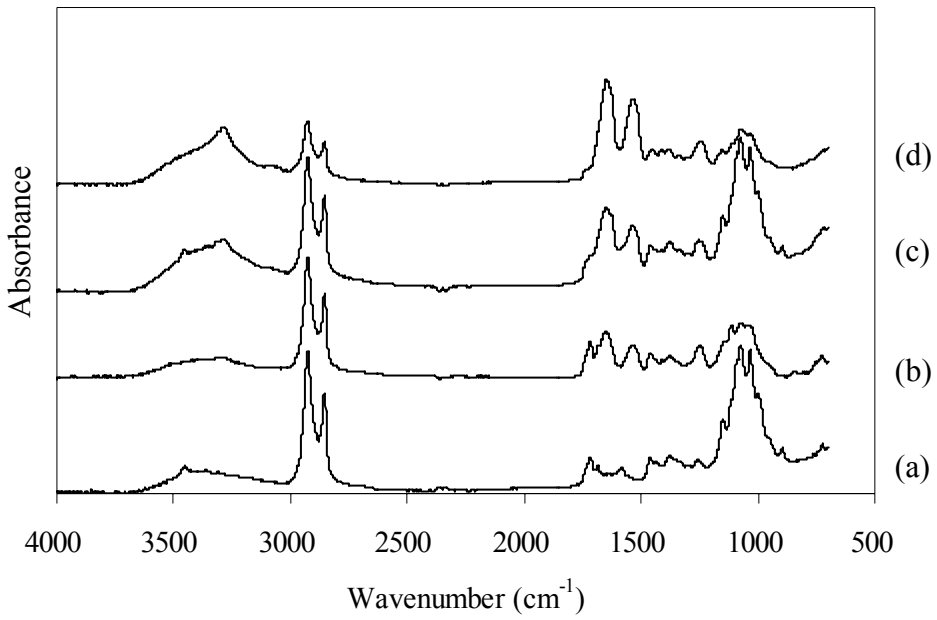

Figure 2-15 FTIR-ATR spectra of 0.05M didecanal treated CS/SF blend films.(a): CS, (b)CS/SF=2/1, (c): CS/SF=1/1, (d): CS/SF=1/2. The spectra were obtained by the film sample on a Ge crystal.

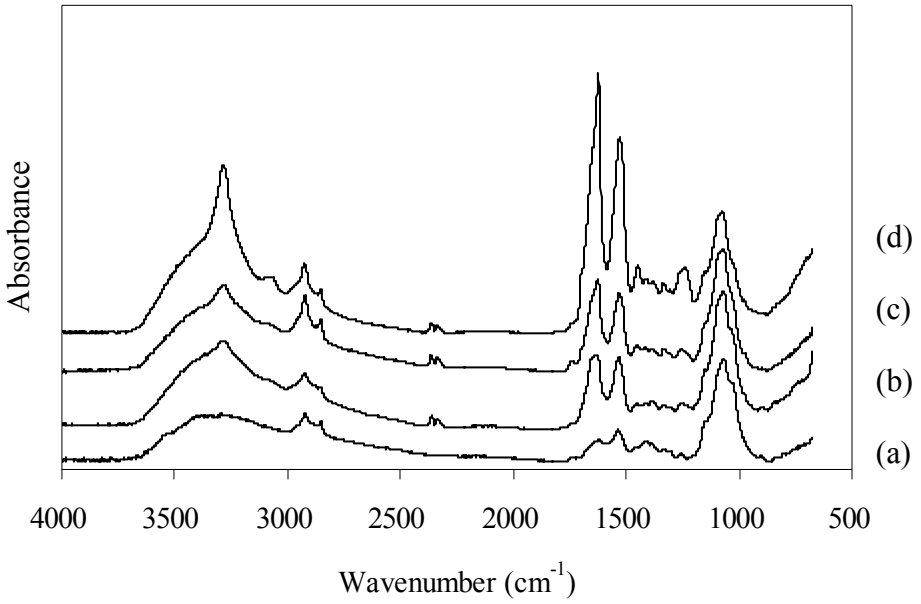

Figure 2-16 FTIR-ATR spectra of 0.05M didecanal and 2,4=DNPH treated CS/SF blend films. (a): CS, (b)CS/SF=2/1, (c): CS/SF=1/1, (d): CS/SF=1/2. The spectra were obtained by the film sample on a Ge crystal.

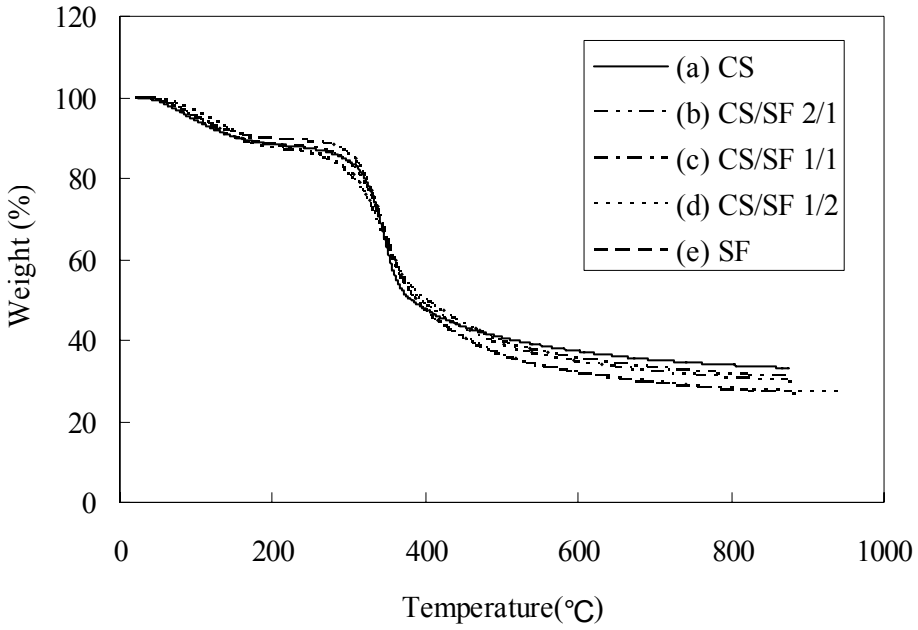

Figure 2-17 TGA thermograms of 0.05M didecanal treated CS/SF blend films. (a): CS, (b): CS/SF=2/1, (c): CS/SF=1/1, (d): CS/SF=1/2, (e): SF. A scan rate of 50ºC/min was used.

Table 2-3 TGA data of 0.05M didecanal treated chitosan, silk fibroin and their blend films.

	Onset Temp.	Temp. at max. rate	Max. rate	Residue at 340 ºC	Residue at 550 ºC
	(ºC)	(ºC)	(%/min)	(%)	(%)
CS	317	347	37.4	69.9	38.8
CS/SF 2/1	306	350	25.4	68.1	36.3
CS/SF 1/1	310	347	28.0	69.7	37.1
CS/SF 1/2	302	348	24.5	68.2	33.7
SF	308	345	29.5	70.7	33.5

Table 2-4 Graphical dipction of time to dessolution of CS/SF films in 96% formic acid.

Samples **	Pure CS and SF	CS/SF blend films	0.01M GA CS and CS/SF films	0.05M GA CS and CS/SF films	0.05M didecanal CS and CS/SF films
Room temperature	< 10 min	< 1 day	Remained > 5days	Remained > 5days	< 2 hours
Applied heat *	N/A	N/A	< 2 days	> 2 days	N/A

* Heat by temerature-controlled stirrer

** n=5

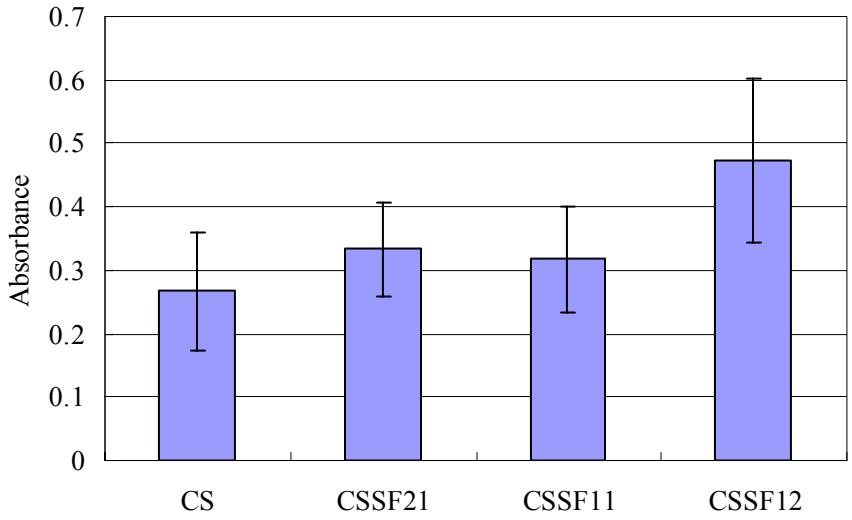

*Replication was n=5.

Figure 2-18 The absorbance at 361nm of hydrazone of 0.01M GA treated CS/SF blend films dissolved in 2mL of 96% formic acid after 6 hours without applying heat. Some fragmented portions remained for all films.

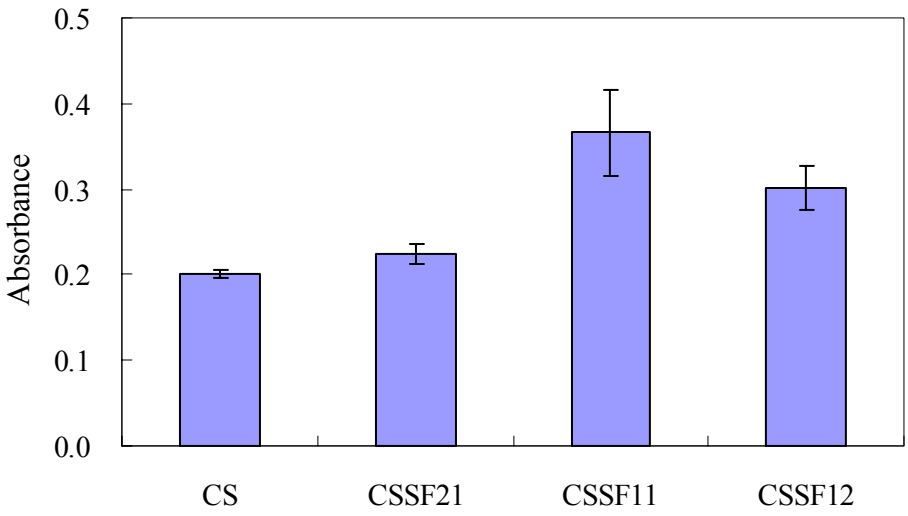

*Replication was n=5.

Figure 2-19 The absorbance at 361nm of hydrazone of 0.01M GA treated CS/SF blend films directly measured by UV-visible spectroscopy.

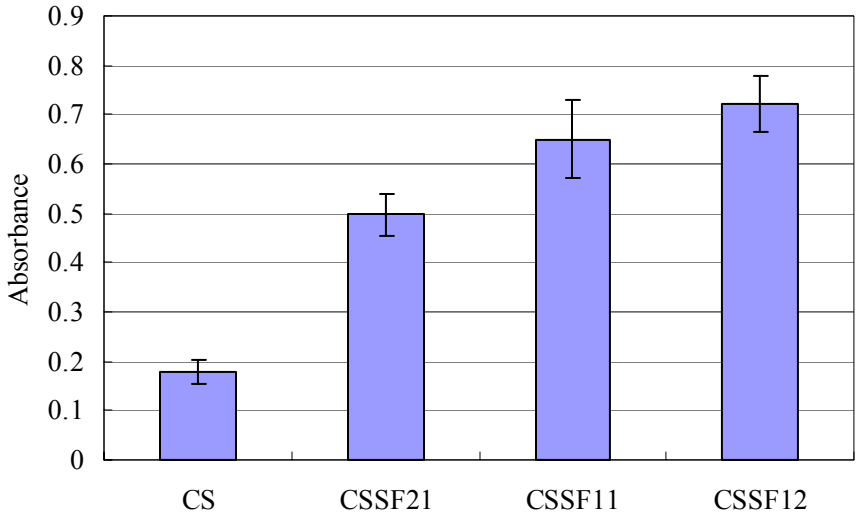

*Replication was n=5.

Figure 2-20 The absorbance at 361nm of hydrazone of 0.05M didecanal treated CS/SF blend films dissolved in 2mL of 96% formic acid after 6 hours without applying heat. All films were completely dissolved.

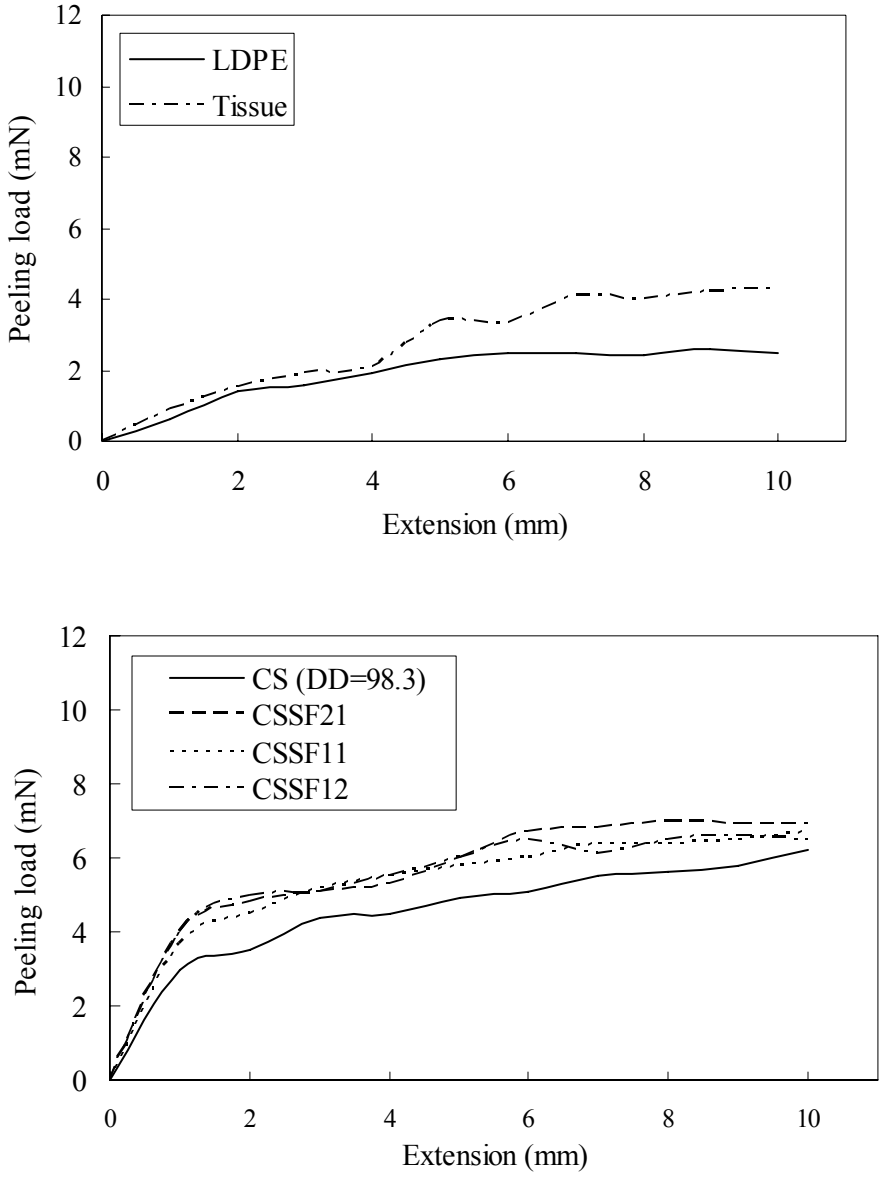

Figure 2-21 The mean load-extension curve of peeling test conducted by peeling two slices of porcine tissue holding various films; Control films, and CS/SF blend films. Load cell: 5N cell, gauge length: 10mm, and peeling rate: 6.0mm/min. Each experiment was repeated at least 5 times.

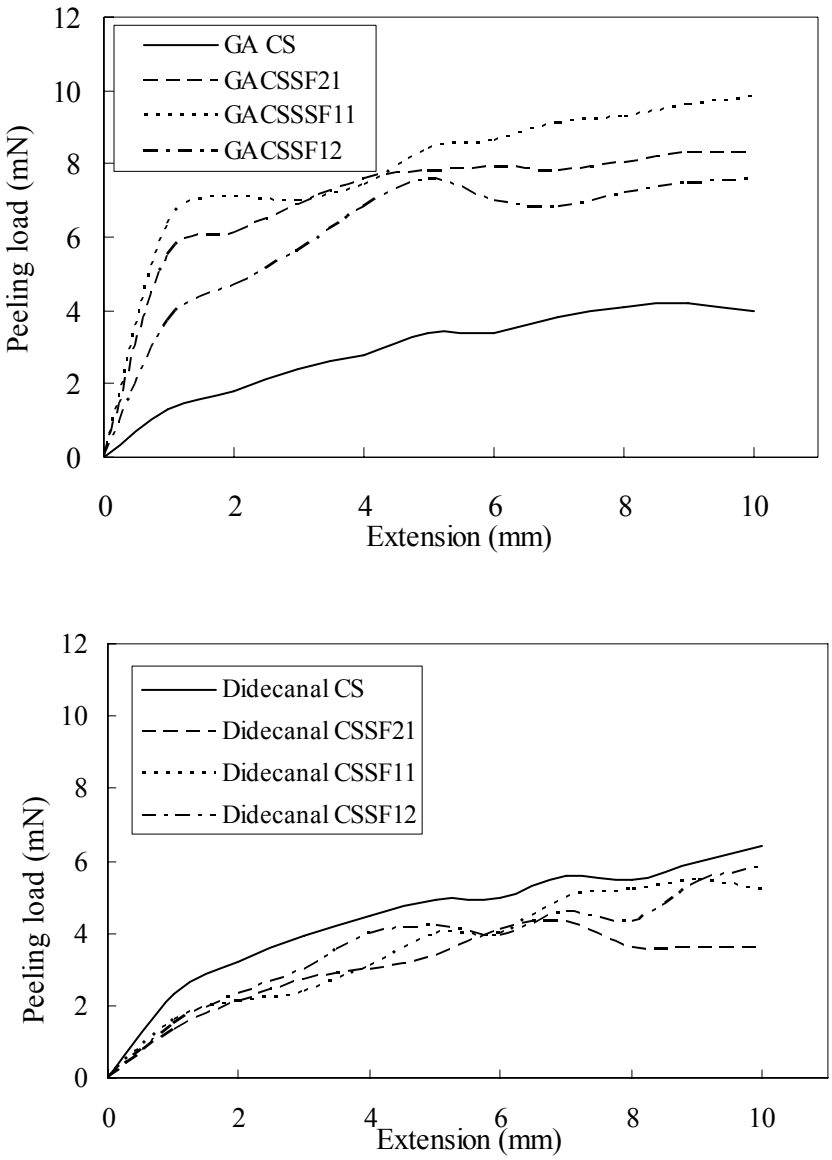

Figure 2-22 The mean load-extension curve of peeling test conducted by peeling two slices of porcine tissue holding various films; GA treated CS/SF blend films (above), Didecanal treated CS/SF blend films (below). Load cell: 5N cell, gauge length: 10mm, and peeling rate: 6.0mm/min. Each experiment was repeated at least 5 times.

(a)

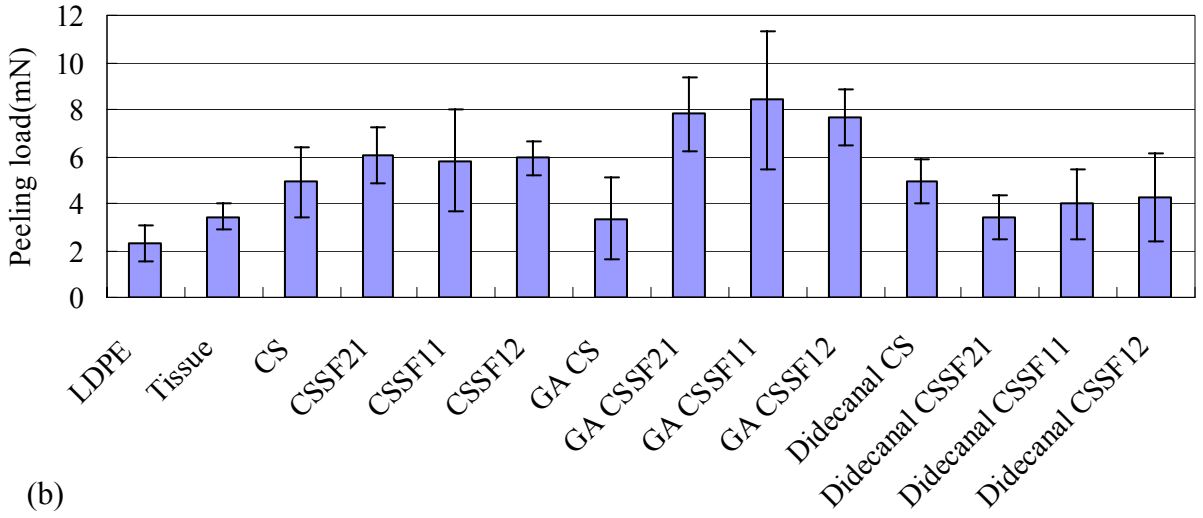

(b)

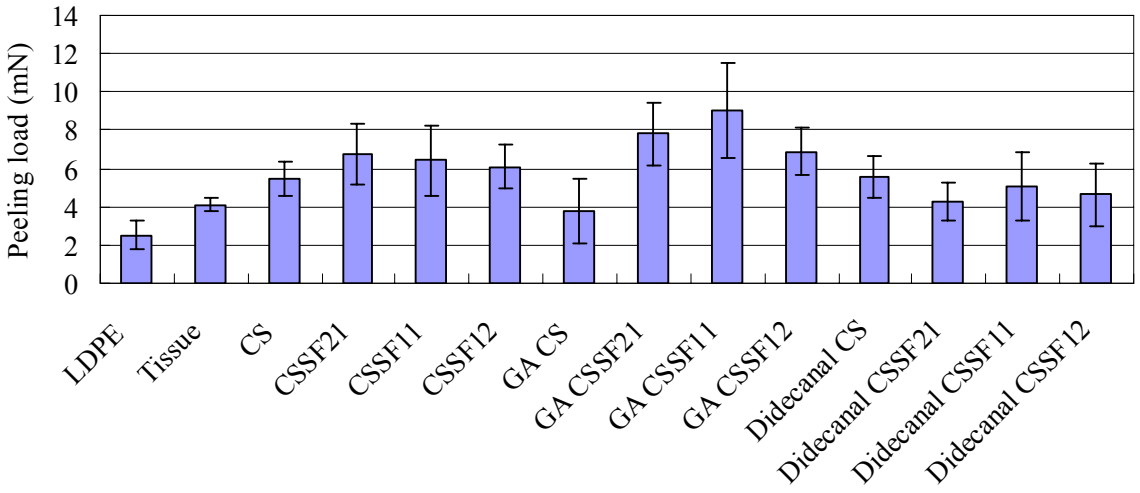

Figure 2-23 The load required at (a): 5mm and (b): 7mm to peel two slices of porcine tissue holding various films. Load cell: 5N cell, gauge length: 10mm, and peeling rate: 6.0mm/min. Each experiment was repeated at least 5 times.

CHAPTER 3

3. The Synthesis and Characterization of Novel Chitosan/Poly(aspartic acid) Polyelectrolyte Complex Layered Films with Improved Hemostatic Properties

Abstract

Novel chitosan and polyaspartic acid bilayer (CS/PAspNa) and trilayer (CS/AspNa/CS) films have been fabricated as a scaffold and hemostatic agent for tissue engineering. Chitosan (CS) is a cationic polymer, known to have a hemostatic property as well as biocompatibility and an antimicrobial effect. On the other hand, polyaspartic acid (PAsp) is a synthetic anionic polymer produced by a thermal polymerization. Combining these two substances could form a polyelectrolyte complex, which potentially can be an artificial substitute for the extracellular matrix (ECM).

In this study, the layered films exhibited physical properties better than the individual polymers. The layered film exhibited a smooth surface, whereas the CS film had a very rough surface. Several degradation studies demonstrated that the improved properties can be useful for long-term use in biological conditions. The three layered film successfully maintained a sustained-release of a model drug in acidic condition at pH 5. The bioadhesion test revealed that layered films exhibited nearly twice the peeling load of the control, although the CS film showed the highest value, probably due to the surface roughness. The blood coagulation test demonstrated that layered films could promote red blood cell aggregation significantly faster than chitosan films. The layered films fabricated in this study are proposed as new hemostatic agents.

3.1 Introduction

Recent advances in tissue engineering have been directed towards solving problems of patients who have suffered tissue/organ loss or skeletal defects [1,2]. Many natural, synthetic and hybrid matrices have been developed to cover wound sites to replace lost tissue functions and support cell growth. For example, aliphatic polyesters, of poly(lactic acid) and poly(glycolic acid) are versatile biomaterials, due to their biodegradability and biocompatibility [1-7]. Certain polyurethanes is are reported as substrates having biocompatibility and the mechanical and physical properties necessary for a blood-contacting material [8-10].

The synthetic matrices have many advantages because their molecular designs, and mechanical or physical properties can be controlled, and they can be manufactured on any scale. However, the usage of synthetic scaffolds is still limited because of poor cell attachment/growth, adsorption of untargeted proteins, and induction of thrombogenesis on the surface. Furthermore, some synthetic polymers, including polyesters, are difficult to modify due to the lack of sufficiently reactive functional groups [11]. On the other hand, natural substrates, such as adhesive proteins, have been used extensively, because of excellent biocompatibility and bioactivity. However, they have batch-to-batch variations, and there are difficulties with establishing large scale processes. Many attempts to establish novel biomedical applications have been undertaken by modification or combination of natural polymers, including proteins (e.g. collagen [12,13], silk fibroin [14]), polysaccharides (e.g. cellulose [15], hyaluronan [16], alginate [17,18], chitin, and chitosan [19]).

Polyamino acids and polypeptides are also attractive materials for drug delivery systems and tissue engineering [20,21]. Among them, polyaspartic acid (PAsp) is useful because it is hydrophilic, soluble in water and degrades quickly under biological conditions [22]. PAsp is readily polymerized by heat, going through the polysuccinimide (PSI) intermediate (Scheme 3-1) [5,23-29]. Mostly, polyamino acids have been prepared by *N*-carboxyamino acid anhydride (NCA) polymerization [30]. Compared to this method, the polycondensation of aspartic acid is easier to prepare at low cost, and without any toxic reagent, metal catalysts or solvents. Furthermore, PAsp can be easily modified in the presence of primary or secondary amino groups due to the high reactivity of PSI. This characteristic contributes to the production of various kinds of chemically functionalized PAsp derivatives [5,23,31,32]. Because of the high hydrophilicity, PAsp is difficult to process by itself for commercial applications, such as for forming fibers, films, and sponges. Combining PAsp with conventional polymers such as poly(L-lactide) and poly(ethylene oxide) [11,33,34] gives bioactive moieties as well as biodegradability and mechanical strength, and such properties are promising for various biomedical applications.

As described in the previous chapter, chitosan is a biodegradable polysaccharide, which is usually the copolymer of *N*-acetylated and *N*-deacetylated glucosamines. The structural characteristics of chitosan are similar to glycosaminoglycans (GAGs) that exist on the surface of cells and in the extracellular matrices (ECM) in nature. In addition, chitosan has potential utility for wound dressing and hemostasis applications, due to the biocompatible and hemostatic characteristics. Therefore, chitosan is one of the promising biomaterials because it mimicks natural ECM. However, chitosan fibers and films are

generally known to have poor mechanical strength, particularly when wet [35]. Combining other biodegradable polymers with chitosan would produce more ideal scaffolds for tissue engineering.

Chitosan is positively charged, whereas PAsp is negatively charged, thus they can form a polyelectrolyte complex. Similar complexes widely exist as ECM in nature. Recently, the importance of the three-dimensional structural morphology of ECM as well as the surface chemistry and topography, which determines how cells respond to the scaffold, has been recognized. Polyelectrolyte multilayer (PEM) [36,37] assembly is a step-by-step technique that builds up biomimetic biomaterials and controls the surface chemical/mechanical properties. Various combinations of polymers have been selected and studied for this purpose [36-39].

The layer-by-layer assembly of chitosan and PAsp potentially provides a substrate for antibacterial action and blood coagulation (hemostasis), as well as a good scaffold for cell growth and differentiation. Such a polyelectrolyte complex also has an ability to incorporate drugs for targeted delivery. Currently, no report has been published describing a chitosan/PAsp complex. This complex is worth developing as a novel hemostatic agent.

In this study, a layered-by-layer Chitosan/PAsp/Chitosan film is fabricated by solution casting. Chemical and thermal characterization includes Fourier transformed infrared spectroscopy (FTIR), thermogravimetric analysis (TGA), and differential scanning calorimetry (DSC). The physical properties of the film are also analyzed by a swelling test, degradation test, and tensile test and compared to the single chitosan film. The morphology of the layered film is examined by SEM and stereomicroscopy. Finally, the enzymatic

degradation test, model drug release test, and simple blood coagulation test provide the preliminary biological assessment of the film as a hemostatic agent.

3.2 Experimental

3.2.1 Materials

Chitosan was acquired from Natural Biopolymer, Inc. (Raymond, WA). All other chemicals used in this study were purchased from Fisher Scientific or Aldrich Chemicals and used without further purification.

3.2.2 Chitosan solution preparation

CS solution of 1 % (w/w) was prepared by following the method of 2.2.3.

3.2.3 Polysuccinimide (PSI) synthesis

The precursor of sodium poly(aspartate) (PAspNa), polysuccinimide (PSI), was synthesized by following the method by Neri et al [23] (Scheme 3-1). Fine L-aspartic acid powder (10g, 0.075 mol) was mixed with 5.0g of 85% H_3PO_4 solution in a 500mL flask. The mixture was heated for 2.5 h under reduced pressure in an oil bath at 180 ºC. The foam-like mass was dissolved in 100mL of DMF, and the solution was poured into 500mL of water. The precipitate was filtered and rinsed with water until it was neutral. The product was dried in an oven at 100 ºC for 24 h (Yield: 6.83g, 97%). The viscosity average molecular weight (M_v) was determined by the method of Vlásak et al [24]. Viscosity was measured in a size 75 Ubbelohde viscometer (Cannon Instrument Co., PA) with a solvent of

0.1 M LiCl/DMF at 25 ºC. The intrinsic viscosity was determined by the Mark-Houwink equation, where $K=1.32\times10^{-2}$, a=0.76 [24]. M_v was calculated to be 77,000.

3.2.4 Sodium poly(aspartate) (PAspNa) synthesis

The recovered PSI (0.3g, 0.003mol/unit) was dispersed in deionized water and 2N NaOH was added to adjust the pH to 9-11 [5]. The hydrolysis of the PSI to PAspNa occurred in 3 h. The solution was then neutralized with 1M HCl and precipitated into methanol. The white crystalline PAspNa was filtered and dried under vacuum (Yield: 0.495g, 118%). The excess yield was thought to be due to the presence of moisture, as the polymer is highly hydrophilic. The reaction scheme is shown in Figure 3-1.

3.2.5 PAspNa solution preparation

The dried PAspNa powder was dissolved into deionized water by stirring, to prepare 1 wt% sodium poly(aspartate) solution (PAspNa). The FTIR spectrum indicates the highly degree of hydrolysis, as described in section 3.3.4.

3.2.6 CS/PAspNa/CS three layered film fabrication

The solution of CS (10g) was cast into 100 mm diameter petri dishes and dried at room temperature. Then, the solution of PAspNa (10g) was poured onto the CS film. The second CS film was placed on the CS/PAspNa film/solution and left to dry at room temperature. The resulting CS/PAspNa/CS was to be called the 3 layered film, whereas CS

film (DD=98.3) and CS/PAspNa film were to be called the 1 layer film and 2 layered film, respectively.

3.2.7 Fourier Transform Infrared (FTIR) and FT-Attenuated Total Reflectance (FTIR-ATR) Spectroscopy

Synthesized PSI and PAspNa were analyzed using a KBr pellet. Each layered film was placed on a Ge crystal and the data were collected. All spectra were obtained using the Thermo Nicolet 510P FT-IR Spectrometer with OMNIC software. The scans were performed with an average of 32 repeated scans at 4 cm^{-1} scan resolution.

3.2.8 Nuclear Magnetic Resonance (NMR) Spectroscopy

NMR spectra were obtained on a Varian Mercury 300 NMR spectrometer operating at 300 MHz for the ^{1}H nucleus. Chemical shifts for ^{1}H NMR spectra were reported in δ (ppm), with positive values indicating downfield shifts from the reference, tetramethylsilane (TMS). Deuterated solvents reference the residual proton peaks to the chemical shift of samples. The solvent used in this study was as follows: DMSO-d_6, 2.50, quintet; and D_2O, 4.80. Significant ^{1}H NMR data are tabulated in a later section in the following order: chemical shift, multiplicity (s=singlet, d=doublet, t=triplet, q=quartet, and m=multiplet), and number of protons.

3.2.9 UV-Visible Spectroscopy

All UV/visible absorption measurements were performed and the spectra were analyzed by using a Varian Cary 3E spectrophotometer with Cary 300 software.

3.2.10 Thermogravimetric analysis (TGA)

Thermal degradation measurements were performed and the thermograms were obtained using a Perkin Elmer TGA Pyris 1^{TM}. CS, PSI, and PAspNa powder of ca. 2-4mg, were mounted onto a Pt pan sample holder. All samples were heated under N_2 purging, until the absorbed solvent and water were almost completely evaporated. Each analysis was run from 25 to 900ºC, at the rate of 30ºC/min. The thermograms indicate the weight loss of the sample obtained as a function of time.

3.2.11 Differential Scanning Calorimetry (DSC)

Thermal analysis was conducted and thermograms were obtained using a Perkin Elmer Diamond DSC with a Perkin Elmer intercooler 2P. CS, PSI, and PASpNa powder of ca. 2mg were encapsuled in an aluminum pan. The thermograms were scanned from 25 ºC to 250 ºC, at the rate of 40 ºC/min, under N_2 purging.

3.2.12 Polarized Light Microscopy

The synthesized polymer, PAspNa, was examined using a Nikon Labophot2-POL equipped with COOLPIX digital camera. The polymer was placed on a glass plate and

covered with a glass cover. The polymer morphology was examined using 40x lenses under polarized light.

3.2.13 Scanning Electron Microscopy (SEM)

Each layered film was fixed to an aluminum stage for examination by a Hitachi S3200 scanning electron microscope. The films were sputter-coated with gold by plasma in order to minimize electron charging on the surface and to obtain fine images. Their surface and cross-section morphology were examined.

3.2.14 Atomic Force Microscopy (AFM)

Topography of each layered film fixed with a double-sided tape on a stage was examined by a Dimension 3000 atomic force microscope equipped with Nanoscope IIIa scanning probe microscope controller (Digital Instruments, Santa Barbara, CA) at ambient condition. Topographical and three-dimensional images were acquired in dynamic mode using silicon microcantilever probes. The images were captured in 10 x 10 or 20 x 20 μm scale at a scan rate of 1.0 Hz, and the surface roughness (R_q), where the root mean square of the deviations from the center *x*-*y* plane, was also calculated by the software.

3.2.15 Tensile tests

Tensile testing was conducted using a tensionmeter, Instron (Model 5544P9181 with a 100N load cell). The layered films were cut into 0.5cm x 3.0cm in size and the ends of the film were clamped at a gauge length of 1cm and the tensile test was

immediately conducted at a rate of 4.0 mm/min. The load to the tissue for peeling is plotted as a function of extension. The load to the film to break was plotted as a function of extension of clamps, then the data was converted to the corresponding tensile stress-tensile strain curve. The values of energy, tensile stress, and tensile strain at break were measured, respectively. At least six replicates were obtained for each sample. The resulting profiles were analyzed by BlueHill software.

3.2.16 Swelling tests

Each dried layered film was cut into squares 1x1 cm in size and immersed in 10 mL of phosphate-buffered saline (PBS, pH 7.4) at 37ºC for 24 h. The swollen films were weighed and dried under vacuum, and the dried films were weighed again. The swelling ratio was calculated as:

$$q = (W_s - W_d) / W_d$$

where W_s is the weight of the swollen film and W_d is the weight of the dried film.
The experiments were done in six replicates.

3.2.17 Degradation tests in Phosphate Buffered Saline (PBS)

Each dried layered film was cut into squares 1x1 cm in size and immersed in 10 mL of phosphate-buffered saline (PBS, at 37ºC) for the predetermined period (0-28 days). The films were taken out of the solution and then dried, and the weight of the dried films was measured by a balance at an appropriate time interval. The medium was changed daily to a

fresh one, and the dried film after measurement, was put back into the vial. The weight loss of the film was recorded and plotted. CS film with DD=83.5% was used as a control, and all experiments were done in six replicates.

3.2.18 Enzymatic degradation tests

Each dried layered film was cut into squares 1x1 cm in size and immersed in 10 mL of deionized water containing enzymes, either lysozyme (from chicken egg white, EC 3.2.1.17, at a concentration of 1mg/mL) or papain (from papaya latex, crude, EC 3.4.22.2 at concentration of 10mg/mL) at 37 ºC for a predetermined period (0-14 days). The films were taken out of the solution then dried, and the weight of the dried films was measured by a balance at an appropriate time interval. The medium was changed every two days to a fresh one and the dried film after measurement was put back into the vial. The weight loss of the film was recorded and plotted. CS film with DD=83.5% was used as a control and all experiments were done in six replicates.

3.2.19 Model drug release tests

Aqueous solution of Basic Blue 22 (Astrazon, 2g/L) was prepared and 5mL of the solution was incorporated during layered film fabrication. All model drug incorporated films were cut to be the same weight and immersed in phosphate-buffered saline (PBS) with different pH (5.0, 6.5, and 7.4) and the same ionic strength by addition of NaCl. The samples were kept at 37ºC for a predetermined period (0-96 h). The films were removed from the solution and the absorbance at 630nm of the solution was measured using

UV-visible spectrophotometer. The drug release ratio was plotted as a function of time. All experiments were done in triplicates.

3.2.20 Bioadhesion/peeling tests

Porcine intestines were used as the biological testing substrate. The tissue samples were obtained from the Nahunta Pork Center, Nahunta, NC. They were immediately excised after slaughter and stored at –5 ºC in isotonic buffered saline at pH 7.4 (2.38 g of Na_2HPO_4, 0.19g of KH_2PO_4, and 8.00g of NaCl in 1000 mL deionized water). The intestine tissue was carefully washed the next day, the loose surface membranes were removed, and the tissue was cut into pieces 1cm x 3cm in size. Each layered film was cut into 1cm x 1cm squares, and each one was sandwiched between the two tissue samples and covered by two glass plates. A 50g weight was placed on the 1cm x 1cm bonding area under the glass for 10 min. Both ends of the tissue samples were clamped at a gauge length of 1cm, and the peeling test was immediately conducted at the rate of 6 mm/min (Instron Model 5544 with a 5N load cell). The load to the tissue for peeling was plotted as a function of extension of clamps. Polyethylene film, tissue without film, and chitosan were used as controls. At least six replicates were obtained for each sample.

3.2.21 Blood coagulation tests

Venous blood from a donor pig was obtained by a venipuncture in the laboratory of Dr. Nancy Monteiro-Riviere, at Clinical Science, College of Veterinary Medicine, NC State University. The blood was collected into a 50mL plastic syringe containing 3.5 wt% of

sodium citrate as an anticoagulant. A total of 1mL of blood was transferred to each glass tube (10 x 75mm) and it was preincubated for 5 min in a water bath at 37ºC. CS (DD=83.5) control, CS (DD=98.3) 1 layer film, 2 layered film, and 3 layered film were cut into 1 x 1cm in size. Half of the films were soaked in phosphate buffered saline (PBS, pH 7.4) for 30min to be wet, and the other half of the films were dried before the test. Each film specimen was put into the blood, and the tubes were placed and incubated at 37ºC until the blood was separated into two phases, supernatant and red blood cell aggregation. The tube was checked every 30 sec until the blood sedimentation was completed at almost a 1:1 ratio of two phases. The time of blood sedimentation was recorded for each sample. Four replicates at least were conducted.

After 1.5 h, all tests were stopped and films were taken out from the blood pool. The blood clot formed on each film was captured by a digital camera. The morphology of red blood cells was examined by Nikon Labophot2-POL equipped with COOLPIX digital camera. A drop from the phase containing red blood cells was placed on a glass plate and covered with a glass cover. The 10x and 40x lenses were used.

3.3 Results and Discussions

3.3.1 Synthesis of PSI

Figure 3-1 (b) shows the FTIR spectrum of the aspartic acid polymer, PSI. The imide peak of PSI synthesized from L-Asp was assigned to the C=O stretch at 1713 and 1630 cm^{-1}, as reported by Doll et al [28]. The absorption around 1800 cm^{-1} and 1735 $cm^{-1}$was assigned to the C=O antisym stretch in anhydrides of the polymer chain. The

^{1}H-NMR spectrum of PSI in DMSO-d_6 is shown in Figure 3-2. The characteristic methine proton of succinimide at δ=5.2 ppm was observed [5,22]. The peaks between 2.5 and 3.4 ppm were assigned to methylene protons of succinimide [5,22].

3.3.2 Synthesis of PAspNa

Figure 3-1 (c) provides the FTIR spectrum of the aspartic acid polymer, PAspNa. The spectrum of PAspNa converted from PSI by alkaline treatment exhibited characteristic absoption bands 3300 cm^{-1} for N-H stretch, 1650 cm^{-1} for C=O stretch in secondary amides (Amide I bond), 1610 and 1400 cm^{-1} for COO^- sym and antisym stretches, and 1550 cm^{-1} for N-H deformation in secondary amide (Amide II band), respectively [40].

The ^{1}H-NMR spectrum of PAspNa in D_2O is shown in Figure 3-3. The broad α/β-amide methine protons at δ=4.4 and 4.6 ppm were observed [41,42]. According to Matsuyama et al [42], the upfield peak was determined as β-aspartyl residues. The broad peak at 2.7 ppm was assigned to methylene protons. These results indicate that the starting monomer was highly polymerized to the corresponding polymer, PSI, and, following alkaline hydrolysis, converted to PAspNa.

3.3.3 Thermal studies of PSI and PAspNa

TGA thermograms of CS, PSI, and PAspNa powder are shown in Figure 3-4 and 3-5, and the corresponding data summary under nitrogen or air purge are listed in Table 3-1 and 3-2, respectively. Three decomposition steps could be observed for CS powder. The first weight loss occurred at around 100 ºC, which was apparently attributed to water

evaporation. The second decomposition step, the main decomposition of the polymer backbone, appeared in the range of 320-350 ºC, due to the degradation of the polysaccharide chains and deacetylated units of CS [43]. The third step was assigned to be the loss of residues during the final oxidizing process under air flow, as shown in Figure 3-5.

As for PSI, it was synthesized by a thermal condensation reaction in the presence of phosphoric acid as a catalyst. Four decomposition steps were observed. The first step, around 100 ºC, must be the loss of water, and the second one, in the range of 150-200 ºC, was attributed to the dehydration in the presence of H_3PO_4 catalyst [27]. The main decomposition step was observed in the range of 440-460 ºC, which indicated that PSI was more thermally stable than the other two polymers. Co-monomers polymerized with PSI can give thermoplastic polymers, poly(imide-amide)s, which exhibit decomposition temperatures lower than that of PSI [25]. The last step was assigned to be the loss of residues during the final oxidizing process under air flow, as shown in the figure.

PSI can be easily hydrolyzed in an alkali medium for conversion into PAspNa [27]. Three decomposition steps were involved for PAspNa degradation. The first step around 100 ºC must be the loss of water. The second one, in the range of 300-500, ºC seemed to involve two distinct processes, probably because the polymer has both α- and β- form in the chain when hydrolyzed [22,25,27,28]. Furthermore, PAspNa residue could still be observed even after the oxidation process. This result indicates that the residue contained some inorganic compounds, such as Na_2CO_3. According to a calculation, ca. 38% of ash

remains if the all polymer residue is converted to Na_2CO_3. Since the residue of PAspNa at 800 ºC was 31%, as shown in Table 3-2, this result corresponds to the prediction.

DSC thermograms of CS, PSI, and PAspNa powder are shown in Figure 3-6. Chitosan powder (a) exhibited a broad peak at 135 ºC, which is considered to be a glass transition, as reported in the article by Kweon et al [44]. On the other hand, Bae et al reported that chitosan films, with or without crosslinking, have a broad exothermic peak around 100 ºC [45]. PSI is known to be degraded without glass transition or melting [22]. The thermograph (b) demonstrated the same feature as reported, except for a major peak around 155 ºC. It is attributed to phosphoric acid residue, because the boiling temperature of phosphoric acid is 158 ºC. PAspNa thermograph (c) exhibited a very minor slope change at 145 ºC, which might be a glass transition. It also had an endothermic peak at 212 ºC, which was assumed to be the melting point.

The PAspNa powder was then analyzed by a polarizing microscope in order to confirm the presence of crystallinity in the polymer. As shown in Figure 3-7 (a) and (b), the images obtained using two polarizing filters revealed that some portion of polymer had an anisotropic crystal structure. This result also supported the fact that PAspNa was possibly a semi-crystalline polymer. For further investigation of PAspNa characteristics, dynamic mechanical analysis (DMA) technique will be more useful to understand the minor transition seen in the thermogram.

3.3.4 Characterization of CS/PAspNa/CS layered films

The ATR-FTIR spectra of first to the third layers of CS/PAsp/CS are shown in Figure 3-8. With respect to the first and third layer of chitosan (a) and (c), their characteristic absorption band looked almost the same. The absorption at 1555 and 1075 cm^{-1} was assigned to the R-NH_3^+ deformation and C-N stretch in primary amines. Furthermore, peaks at 1152, 1074, and 1024 cm^{-1} were assigned to the C-O stretch, C-O-C antisym stretch in ether bonds, and C-O stretch in C-OH in glucopyranose, respectively. On the other hand, the second layer of PAspNa deposited on the chitosan layer exhibited the characteristic peaks of carboxylic salts and secondary amides, instead of the peaks of *N*-glucosamine. The peaks at 1704 and 1408 cm^{-1} were assigned as C=O stretch and COO^- sym stretch in carboxylic acid salts of PAspNa. In addition, the peaks corresponding to C=O stretch and N-H deformation (amide II band) in secondary amides appeared at 1638 and 1550 cm^{-1}, respectively. Furthermore, the peaks due to the sugar rings decreased dramatically in the PAspNa layer because the PAspNa layer was covered by the first layer of CS. These results indicate that each layer could be assembled on the Petri dish layer-by-layer, without any mixing.

TGA thermograms of 1, 2, and 3 layered films are shown in Figure 3-9 and the corresponding data summary under nitrogen purge is listed in Table 3-3, respectively. Three decomposition steps were observed for all films. After water or solvent evaporation in the range of 100-200ºC, the main decomposition occurred, indicating the backbone cleavage of polymer chains. The temperature at the maximum rate for 1 layer film was lower than for other layered films, and the degradation maximum rate of CS film was much

higher than that of layered films. These results indicated that it was attributed to the formation of ionic bonds between the two kinds of polyelectrolytes, CS and PAsp. The third decomposition gradually occurred for all films, and the amount of residue at 550 ºC exhibited almost the same level for each sample.

3.3.5 Morphology of layered films

The surface and cross-sectional SEM images of chitosan and layered films are shown in Figure 3-10. The surface image of the pure chitosan film (a) showed a rough surface. The roughness is very evident at high magnification (b), although the degree of roughness could not be measured by SEM. On the other hand, 2 and 3 layered film exhibited smooth and uniform surfaces, as shown in Figure 3-10 (c), (e), and (f). However, some had cracks running in the same direction in a small area of the 2 layered film (d), although most of the surface was smooth. This indicated that some physical force was partially applied between the two components at the interface when the polyelectrolyte was formed. There was no such phenomenon observed at the surface of the 3 layered film, but it could happen at the interface inside the film.

The cross-sectional images of films are shown in Figure 3-11. The pure chitosan pure film (a) did not have a boundary, whereas distinct boundaries of 2 and 3 layers could be observed in layered films ((b)-(e)). These results indicate that layer-by-layer assembly of chitosan and PAspNa was maintained during the drying process.

Dynamic mode topographical and three-dimensional AFM images of CS film in a scan range of 10 x 10, and 20 x 20 μm are shown in Figure 3-12 and 3-13. Concave and

convex structures with an average size of 3.5μm were observed all over the scan area at both scales. This feature was expected from the SEM observation. The surface roughness R_q was 46.5 and 58.2 nm, respectively. In contrast, the surface of the 2 layered film was very smooth even in at 10 x 10 μm, as seen in Figure 3-14. There was a groove across the area, which is considered as some kind of artifact in the film. The surface roughness was 5.8 nm, almost 10% of the CS surface. On the other hand, the surface of 3 layered film was also smooth, however, lots of spikes in 0.5 μm size were distributed all over the area as seen in Figure 3-15 and 3-16. Nevertheless, those spikes did not affect the surface roughness parameter much, and the roughness was 5.3 and 8.1 nm, which was also about 10-15% of the roughness of a CS film. Furthermore, the background of the 3 layered film indicates the presence of fibril structure in the chitosan layer. This feature was also observed in the CS 1 layer film, however, the 3 layered had more developed structure. The flatness of the layered film surface is probably attributed to the increasing of surface energy while two phases were in contact and their drying process.

The identity of the spikes in the 3 layered film was not determined. However, it is obvious that the film becomes very smooth when they are formed from the polyelectrolyte complex. The observation was consistent with the expectation considered from the SEM results. The surface roughness is assumed to be one of the factors that can affect the bioadhesiveness or cell attachment.

3.3.6 Mechanical property of layered films

The variance of initial modulus, tensile stress at break, and tensile strain at break of dry layered films are listed in Table 3-4. As expected, the 1 layer film of CS exhibited the typical tough plastic behavior, with a yield point in the stress-strain curve. This class of polymers usually has a lower initial modulus than brittle plastics and a plastic flow region for stress in the range of 20 to 50MPa [46]. Tough polymers also break at about 50% elongation [46]. The CS film exhibited 1.78GPa initial modulus, 67.5MPa tensile strength, and 53% elongation at break, which correspond to the properties of a tough polymer. On the other hand, the 2 layered film showed a somewhat lower initial modulus of 1.53GPa. The film was ruptured without a yield point. The energy required to break was much lower than that of CS film, and the stress and strain at break were 30.6MPa and 6%, respectively. These results indicate that the properties of the film were greatly changed by forming a polyelectrolyte complex. At this point, the toughness of the layered film was very low. However, 3 layered film exhibited 3.48GPa of high initial modulus and no yield point, which is a feature of a brittle plastic. Typical stress in this class of polymers is about 60MPa [46], whereas that of 3 layered film was 102.9MPa. The strain at break was 14%, which is higher than that of typical brittle plastic, but much lower than that of the tough plastic. These results indicate that the 3 layered film has a very high modulus as a brittle plastic, by forming a polyelectrolyte complex, yet it slightly exhibits the property of tough polymers because of the two outer layers of chitosan.

3.3.7 Swelling property of layered films

The effect of pH on the swelling of the layered films was examined in PBS at different pH levels at 37 ºC. Figure 3-17 shows the swelling ratio of the films soaked in PBS with pH 5.0. The control CS film (DD=83.5) and the 1 layer CS film (DD=98.3) were dissolved after 24 hours. On the other hand, 2 and 3 layered films retained their shape and exhibited the swelling ratios of 6.6 and 0.8, respectively. The 2 layered film was swollen more than 8-fold, as was the 3 layered film, probably due to less polyelectrolyte complex formation.

The swelling ratio in PBS with pH 7.4 is shown in Figure 3-18. The highly deacetylated CS film was much more swollen (swelling ratio: 22.1) than other types of film (swelling ratio: 2.5-4.0), including the reference CS film, with DD=83.5. The 1 layer CS film (DD=98.3) exhibited 5-9 times the swelling ratio of the rest of the films. This may be due to the fact the highly deacetylated CS film was somewhat protonated and solvated by water, whereas other films excluded water molecules, due to the ionic interaction between the polyelectrolytes in layered films or hydrogen bonding attributed to N-acetyl content in the reference CS film.

The swelling ratio in PBS with pH 9.0 is shown in Figure 3-19. The swelling ratio of all films was relatively low (0.5-1.5) compared to the swelling ratio in other pH conditions. The value was changed, possibly depending on the amount of available amino group content that could interact with water.

3.3.8 Degradation tests in Phosphate Buffered Saline (PBS)

Film weight changes of CS and layered films immersed in PBS (pH 7.4, 37 ºC) were illustrated in Figure 3-20. A great decrease in weight of all films was observed at the very beginning of the period. The degree of decrease in weight became lower in the following sequence: 1 layer CS film (DD=98.3), 2 layered film, 3 layered film, and control CS film (DD=83.5). The CS 1 layer film was quickly swollen and became pulp-like fragments. Therefore, 1 layer film was only 56% of its original weight after a 24 hour immersion. The film weight decreased continuously toward the end of the period, and the final weight was 16%. The film no longer retained its original shape but shattered to small pieces, as seen in Figure 3-21.

On the other hand, 2 layered film and 3 layered film retained their shape throughout the experiment, as shown in Figure 3-21. A sharp weight loss was observed for both layered films for the first 24 h, then the weight was almost constant after that. The final weight of 2 and 3 layered films were 54 and 72% of the original, respectively. These results indicate the ionic interaction between polyelectrolytes somewhat prevent degradation of layered films, and the overall structure of 3 layered film was stronger than that of 2 layered film.

The control CS film lost only 20% of original weight throughout the period. This is because partial N-acetyl residue forms intermolecular hydrogen bonds, just like chitin does, which makes the film hard to degrade. The film's shape was retained even after 28 days (Figure 3-21).

3.3.9 Enzymatic degradation tests

Film weight changes of CS and layered films immersed in lysozyme solution (1mg/mL, 37 ºC) are illustrated in Figure 3-22. As expected, the control CS film (DD=83.5) was completely degraded by lysozyme within 15 h, whereas 1 layer CS film (DD=98.3) retained 74% the original weight after 14 days. The 3 layered film was degraded to the same level as the 1 layer of CS, whereas the 2 layered film was more degraded and retained 57% of its original weight. Only in the case of layered films, the media became turbid as soon as the enzyme solution was poured into the vial.

Stereomicroscope images of films are shown in Figure 3-23. All films, except for control, retained their shape, even though some weight loss occurred during the degradation process. Lysozyme is a well known enzyme that binds a polysaccharide segment of six sugar rings and cleaves the molecular chain by hydrolysis of the acetal link [47]. For instance, lysozyme is active to gram-negative bacteria, which has polysaccharides with the N-acetylglucosamine residue on the cell wall. For chitosan, fully deacetylated oligomers and highly deacetylated chitosan are little degraded by lysozyme [47,48] because N-acetylglucosamine moieties are needed for binding with lysozyme [49]. The control CS film was more acetylated (DD=83.5) than the 1 layer CS film (DD=98.3), thus the result corresponds to the trend already reported. Therefore, the result supports the fact that lysozyme is active to N-acetylglucosamine residue, not to N-glucosamine.

Film weight changes of CS and layered films immersed in crude papain solution (yellowish powder, 10mg/mL, at 37 ºC) are illustrated in Figure 3-24. The control CS film was completely degraded by lysozyme within 24 h, whereas 1 layer CS film remained and actually increased in weight by 5% after 14 days. The weight increase is probably due to the binding of crude papain residues on the film. The 3 layered film also inhibited degradation and retained its original weight, whereas the 2 layered film was more degraded and retained 87% of its original weight. Only in the case of layered films, the media became turbid as soon as the enzyme solution was added, as did the lysozyme solution.

Overall, lysozyme was more effective in the degradation of CS and layered films. Stereomicroscope images of films are shown in Figure 3-25. All films, except for the control, retained their shape even though some weight loss occurred during the degradation process. The films became brown, probably due to the deposition of crude papain residues. In general, papain is known to cleave peptide bonds of basic amino acids, such as leucine or glycine, and also to hydrolyze esters and amides. Papain is also a non-specific enzyme that is active to chitosan depolymerization [50], as well as cellulose, pectinase, pepsine, and wheatgerm lipase [51]. Accoding to the results, the papain activity varied depending on the degree of deacetylation, which was observed in the case of lysozyme. Therefore, it is suggested that papain recognizes N-acetylglucosamine residue as well as lysozyme.

3.3.10 Model drug release tests

The effects of pH on the release of model drug (Basic Blue 22, a cationic dye) from CS and layered films are shown in Figures 3-26 to 3-28. At pH 5.0,as shown in Figure

3-26, the 1 layer CS film was quickly swollen and started to break into pulp-like fragments. Therefore, a bursting diffusion of the dye occurred, and the release ratio kept shifting to around 82%. The 2 layered film was found to be swollen greatly at this pH (Section 3.3.7), thus a similar trend was observed for the film with the release ratio of around 88%. Generally, the swelling behavior and film uniformity greatly influence the drug release trend [52,53]. On the other hand, the drug release from the 3 layered film was much less (~ 53%) at the beginning of the test and stayed around 60% for 24 h, and finally increased to 84%. The release from the 3 layered film at pH 5.0 was the slowest among all conditions due to the low swelling ratio. These results indicate that the outer layer of chitosan was sufficiently ionized to form a polyelectrolyte complex with PAspNa, without dissolution. At this pH, the dye and CS are cationic and repel each other, whereas PAsp is partially protonated and neutral. Nevertheless, a sufficient polyelectrolyte complex and interaction between the cationic dye and PAsp are likely formed, which prevents quick release of dye from the film.

Figure 3-27 shows the results at pH 6.5. The 1 layer CS film was quickly swollen and it diffused the dye right after immersion. This pH probably was low enough to make the film swell, but not enough to produce a significant level of the ammonium ions in chitosan (The pK_a of CS is about 6.0.) in order to form a polyelectrolyte complex. The 2 and 3 layered films also released 65 % of dye within 2 hours and maintained release up to 85% and 86%, respectively. Even though the PAspNa in the 2 layered film has an anion that can interact with the cationic dye, the PAspNa component is susceptible to water.

Therefore, the dye was quickly washed out, together with PAspNa, when the 2 layered film was soaked in the medium.

At pH 7.4 shown in Figure 3-28, all films released around 80-88% of the dye at the end of the period. However, the overall diffusion rate of 1 layer was smaller than that of 2 and 3 layered films. It indicates that it took more time for the layered films to be swollen. It will be possible to control the drug release rate, depending on the outer CS thickness, degree of deacetylation, and degree of ion complex formation, as well as the pH of media. Moreover, the effect of film architecture is also important for drug release behavior [39]. More studies of the film morphology (porous/ non-porous, uniformity) and film assembly will be needed.

3.3.11 Bioadhesive/peeling tests

Intestinal tissue is often used for bioadhesion tests, due to the stronger adhesiveness among mucosal tissues. The mean load-extension curve of each layered film is described in Figure 3-29. The peeling load was monitored while the film sample (1 x 1 cm) was extended. As a general trend, the 1 layer CS (DD=98.3) exhibited a higher peeling load than that of 2 and 3 layered films. The mean load at 5 and 7mm extension, relatively at the start of plateau region, were depicted to compare the peeling load among controls and samples in Figure 3-29.

Figure 3-30 (a) shows the load required at 5mm extension to peel two slices of porcine tissue holding CS and layered films. Two controls, the low density polyethylene (LDPE) and porcine tissue without films, exhibited low peeling load values compared to

the 1 layer CS (DD=98.3) and layered films because they can only form physical bonds between amino acid residues, and CS functional groups. The layered films tended to show lower load values than that of CS film. Amaral et al reported that highly deacetylated chitosan membrane with DD=96% improved the cell adhesion and fibronection adsorption on the surface more than those of membranes with lower DD [54].

The l layer CS film exhibited the highest peeling load with the strongest bioadhesion among all test conditions, which supports this report. The total peeling load for the 1 layer CS film was 2.5 times that of the control LDPE film. However, the 3 layered film, also sandwiched with the same chitosan layers, showed a lower bioadhesiveness than 1 layer CS. This could be because of the low surface roughness of the 3 layered film, which also influences the adhesiveness. The 2 layered film surface was also smooth, according to the SEM result, which is also the reason for the lower peeling load. Nevertheless, the layered films exhibited about 1.7-fold peeling strength of the control. For further investigation of the surface morphology, Atomic Force Microscopy (AFM) revealed differences in surface roughness among the films. The 1 layered film had almost 10 times the surface roughness of the 2 and 3 layered films, as described in the earlier section.

Figure 3-30 (b) shows the load at 7mm required to peel two slices of porcine tissue holding CS and layered films. A similar trend was observed for the 1 layer, and layered films, which exhibited increases of 2.3- and 1.9-fold in peeling strength over that of the control LDPE film, respectively. It indicates that the force being applied to films during the peeling, tends to reach the plateau at the end of extension, as described in Figure 3-29.

3.3.12 Blood coagulation tests

The blood coagulation test was conducted by measuring the time of red blood cell sedimentation or "erythrocyte sedimentation rate", in anti-coagulated blood. A standardized method called erythrocyte sedimentation rate (ESR) has been widely used for one of the diagnosis of various diseases [55]. The Westergren method is frequently used, which requires a specific glass tube (2.5 x 300 mm) to let the blood is settle for an hour. In this study, conventional glass tubes (7.5 x 100 mm) were used whether the blood sedimentation is observed or not, by addition of fabricated chitosan and layered films into the tube.

The effects of various films on the blood sedimentation time when the supernatant and erythrocyte agglutination were separated as equal phases at 1:1, are summarized in Table 3-5. The anticoagulant blood did not separate during the testing. Two CS films (DD=83.5 and DD=98.3) did not completely agglutinated the blood cells within 1.5 h, whereas the layered films exhibited the clear blood sedimentation with both dry and wet films. In fact, the difference in DD values had no observable effect on the sedimentation time. The 2 layered film exhibited the fastest blood sedimentation rate at 26 min with dried film, and 33 min with wet film. On the other hand, 3 layered film showed the second fastest blood sedimentation rate at 31 min with dry, and 44 min with wet film. The wet film state slowed the diffusion of the blood components, while the dry state allowed immediate contact of the blood. The blood sedimentation of 2 layered film was 5-10 min faster than that of 3 layered film.

Chitosan is known to improve the blood coagulation time, as introduced in Chapter 1. Surprisingly, both chitosan films used in this study did not show the rapid red blood cell

agglutination, even though the blood separation was slightly observed, as shown in Figure 3-30 (above). Interestingly, both 2 and 3 layered films exhibited rapid blood sedimentation rates. The effect of the layered films on formation of blood clots was obvious. The blood cell phase of 2 and 3 layered films became viscous, compared to the chitosan ones and the control blood sample that was only citrated. Large clots were formed on the layered films after 1.5 h immersion, whereas two CS films had only small clots present (Figure 3-30, below). It is well known that chitosan generally activates platelets during hemostasis. However, the blood used in this study contained sodium citrate which can chelate calcium ions that are involved with the platelet activation. These results indicate that blood coagulation via platelet pathway of chitosan might be blocked due to the chelation. Furthermore, the 2 and 3 layered films promoted the red blood cell aggregation in the absence of enough calcium ions, which indicates the layered films can activate erythrocytes. At this point, the detail mechanism how the layered films interact with erythrocytes, either chemically or physically, is not clear. The role of erythrocytes when the blood contacts to materials has been less considered, because the concentration of red blood cell is usually much less near vessel wall than in the middle of the vessel [56], thus the involvement of erythrocytes is considered to be minor factor for the blood coagulation. However, the results obtained suggest that the layered films trigger the red blood sedimentation and form blood clots via different blood coagulation pathway from the general pathway.

After the blood sedimentation test, a drop was taken from the agglutination phase and the cell morphology was examined by a stereomicroscope as shown in Figure 3-31 and 3-32. At lower magnification (x10), erythrocytes were evenly distributed in the blood

without film (Figure 3-31(a)), whereas they were partly aggregated in all other films. However, at higher magnification (x40), erythrocytes of two CS films (DD=83.5 and 98.3) were partly aggregated but less dense than those of 2 and 3 layered films. More studies will be needed to determine which film can form a larger blood aggregation effectively. Nevertheless, the layered films were proven to be effective materials that promote the red blood cell aggregation and thus are promising materials as new hemostasis agents.

3.4 Conclusions and Suggestions for Future Work

Novel CS/PAspNa bilayer and CS/AspNa/CS trilayer films have been fabricated by layer-by-layer deposition. Several characterization techniques confirmed the synthesis of one of the polyelectrolytes, PAspNa, by thermal condensation polymerization, and subsequent hydrolysis. In order to assess the thermal/physical properties of polymers and layered films, other techniques, such as dynamic mechanical analysis (DMA), and transmission electron microscopy (TEM), will be useful to obtain more detailed information of polymer microstructures.

The mechanical properties of 3 layered film were much improved by forming a polyelectrolyte complex. CS was a tough polymer, whereas the layered film was a more brittle plastic with higher initial modulus and less stain at break. The complex also affected the swelling properties of the film, as the layered film gave much lower swelling ratios, even under acidic conditions.

The 1 layer CS film was not enzymatically degraded, due to the high deacetylation, as other studies have already reported. CS with DD=83.5% was completely degraded,

whereas the 1 layer film with DD=98.3 was not. The layered film was also resistant to enzymatic degradation, as well as physiological degradation, due to the polyelectrolyte complex.

The model drug release test revealed that 3 layered film demonstrated the sustained-release of drug at pH 5.0. The acidic condition probably produces enough ions to help retain the drug (dye) between the layers. However, more acidic conditions are unavailable, since both CS and layered film were dissolved below pH 4. Further improvements in the layered films will be useful to control the drug release, by changing film architecture, such as film thickness, uniformity, porosity, and surface roughness.

Bioadhesion tests demonstrated that the 1 layer CS and layered films improved the bonding strength of porcine tissue 2.5-fold. The 1 layer film exhibited the best bioadhesion among the samples, perhaps due to its roughness.

Blood coagulation tests revealed that 2 and 3 layered films effectively form red blood cell aggregates, whereas chitosan films were not as effective, based on macroscopic and microscopic observations. These layered films can be proposed as new hemostatic agents, even though the detailed hemostasis mechanism must be clarified in future studies. Other conventional blood coagulation tests, such as whole blood clotting time and plasma factor time, will also be useful methods in order to understand the blood coagulation pathway associatedwith the layered films.

It is well known that cell adhesive peptide sequences, such as Arg-Gly-Asp, play an important role in various cell cycles, including cell adhesion. Further improvement in

bioadhesion can be expected by chemical modification of the cell-binding motif on the layered film. Such an attempt will be addressed in future work.

3.5 References

1. Barrera D.A, Zylstra E, Lansbury P.T, and Langer R. Sysnthesis and RGD peptide modification of a new biodegradable copolymer: poly(lactic acid-*co*-lysin). J. Am. Chem. Soc. 1993; 115, 11010-11011.
2. Hu Y, Winn SR, Krajbich I, Hollinger JO. Porous polymer scaffolds surface-modified with arginine-glycine-aspartic acid enhance bone cell attachment and differentiation *in vitro*. J Biomed Mater Res. 2003; 64A, 583-590.
3. Moon S.I, Lee C.W, Miyamoto M, and Kimura Y. Melt polycondensation of L-lactic acid with Sn(II) catalysts activated by various proton acids: a direct manufacturing route to high molecular weight poly(L-lactic acid). J. Polym. Sci. Part A. 2000; 38, 1673-1679.
4. Moon S.I, Lee C.W., Miyamoto M, and Kimura Y. Melt/solid polycondensation of L-lactic acid: an alternative route to poly(L-lactic acid) with high molecular weight. Polymer. 2001; 42, 5059-5062.
5. Shinoda H, Asou Y, Suetsugu A, and Tanaka K. Synthesis and characterization of amphiphilic biodegradable copolymer, poly(aspartic acid-co-lactic acid). Macromol. Biosci. 2003; 3, 34-43.
6. Lan P, Jia L. Thermal properties of copoly(L-lactic acid/glycolic acid) by direct melt polycondensation. J Macromol Sci PartA: Pure Appl Chem 2006; 43: 1887-1894.
7. Pietro L, Silva DRM Alberto-Rincon MC, Duek EAR. The influence of triethylcitrate on the biological properties of poly(L-lactic-co-glycolic acid) membranes. J Mater Sci: Mater Med 2006; 17: 849-857.
8. Hsu SH, and Chen WC. Improved cell adhesion by plasma-induced grafting of L-lactide onto polyurethane surface. Biomaterials. 2000; 21, 359-367.
9. Lin H.B, Garcia-Echeverria C, Asakura S, Sun W, Mosher D.F, and Cooper S.L. Endothelial cell adhesion on polyurethanes containing covalently attached RGD-peptides. Biomaterials. 1992; 13, 905-914.
10. Takahashi A, Kita R, and Kaibara M. Effects of thermal annealing of segmentated-polyurethane on surface properties, structure and antithrombogenecity. J Mater Med. 2002; 13, 259-264.
11. Karal-Yilmaz O, Kayaman-Apohan N, Misirli Z, Baysal K, Baysal BM. Synthesis and characterization of poly(L-lactic acid-co-ethylene oxide-co-aspartic acid) and its interaction with cells. J Mater Sci: Mater Med 2006; 17: 213-227.

12. Wang XH, Li DP, Wang WJ, Feng QL, Cui FZ, Xu YX, Song XH, and Werf M. Crosslinked collagen/chitosan matrix for artificial livers. Biomaterials. 2003; 24, 3213-3220.
13. Wang X, Yan Y, and Zhang R. A comparison of chitosan and collagen sponges as hemostatic dressings. J Bioact Compat Polym. 2006; 21, 39-53.
14. Hirano S, Nakahira T, Nakagawa M, and Kim SK. The preparation and applications of functional fibres from crab shell chitin. J Biotech. 1999; 70-373-377.
15. Ishihara K, Takayama R, Nakabayashi N, Fukumoto K, and Aoki J. Improvement of blood compatibility on cellulose dialysis membrane. Biomaterials. 1992; 13, 235-239.
16. Yamane S, Iwasaki N, Majima T, Funakoshi T, Masuko T, Harada K, Minami A, Monde K, and Nishimura S. Feasibility of chitosan-based hyaluronic acid hybrid biomaterial for a novel scaffold in cartilage tissue engineering. Biomaterials. 2005; 26, 611-619.
17. Knill CJ, Kennedy JF, Mistry J, Smart G, Groocock MR, and Williams HJ. Alginate fibres modified with unhydrolyzed and hydrolyzed chitosans for wound dressings. Carbohydr Polym. 2004; 55, 65-76.
18. Remuñán-López C, and Bodmeier R. Mechanical, water uptake and permeability properties of crosslinked chitosan glutamate and alginate films. J Control Release. 1997; 44, 215-225.
19. Mori T, Okumura M, Matsuura M, Ueno K, Tokura S, Okamoto Y, Minami S, and Fujinaga T. Effects of chitin and its derivatives on the proliferation and cytokine production of fibroblasts *in vitro*. Biomaterials. 1997; 18, 947-951.
20. Deming TJ. Methodologies for preparation of synthetic block copolypeptides: materials with future promise in drug delivery. Adv Drug Deliv Rev 2002; 54: 1145-1155.
21. Löwik DWPM, Ayres L, Smeenk JM, Hest JCMV. Synthesis of bio-inspired hybrid polymers using peptide and protein engineering. Adv Polym Sci 2006; 202: 19-52.
22. Thombre SM, Sarwae BD. Synthesis and biodegradability of polyaspartic acid: A critical review. J Macromol Sci, Part A: Pure Appl Chem 2005; 42: 1299-1315.
23. Neri P, Antoni G, Benvenuti F, Cocola F, Gazzei G. Synthesis of α,β-poly[(2-hydroxyethyl)-DL-aspartamide], a new plasma expander. J Med Chem 1973; 16: 893-897.
24. Vlasák J, Rypáček F, Drobník J, Saudek V. Properties and reactivity of polysuccinimide. J Polym Sci: Polym Symposium 1979; 66: 59-64.

25. Tomida M, Nakato T, Kuramochi M, Shibata M, Matsunami S, Kakuchi T. Novel method of synthesizing poly(succinimide) and its copolymeric derivatives by acid-catalyzed polycondensation of L-aspartic acid. Polymer 1996; 37: 4435-4437.
26. Tomida M, Yabe M, Arakawa Y. Preparation conditions and properties of biodegradable hydrogels prepared by γ-irradiation of poly(aspartic acid)s synthesized by thermal polycondensation. Polymer 1997; 38: 2791-2795.
27. Nakato T, Kusuno A, Kakuchi T. Synthesis of poly(succinimide) by bulk polycondensation of L-aspartic acid with an acid catalyst. J Polym Sci: Part A: Polym Chem 2000; 38: 117-122.
28. Doll KM, Shogren RL, Holser RA, Willett JL, Swift G. Polymerization of L-aspartic acid to polysuccinimide and copoly(succinimide-aspartate) in supercritical carbon dioxide. Letter Org Chem 2005; 2: 687-689.
29. Zhao Y, Su H, Fang L, Tan T. Superabsorbent hydrogels from poly(aspartic acid) with salt-, temperature- and pH-responsiveness properties. Polymer 2005; 46: 5368-5376.
30. Deming TJ. Polypeptide and polypeptide hybrid copolymer synthesis via NCA polymerization. Adv Polym Sci 2006; 202: 1-18.
31. Suwa M, Hashidzume A, Morishima Y. Self-association behavior of hydrophobically modified poly(aspartic acid) in water studied by fluorescence and dynamic light scattering techniques. Macromol 2000; 33: 7884-7892.
32. Lee HY, Jee YW, Seo SM, Kwak BK, Khang G, Cho SH. Diethylenetriaminepentaacetic acid-gadolinium (DTPA-Gd)-conjugated polysuccinimide derivatives as magnetic resonance imaging contrast agents. Bioconjugate Chem 2006; 17: 700-706.
33. Shinoda H, Asou Y, Kashima T, Kato T, Tseng Y, Yagi T. Amphiphilic biodegradable copolymer, poly(aspartic acid-co-lactide): acceleration of degradation rate and improvement of thermal stability for poly(lactic acid), poly(butylene succinate) and poly(ε-caprolactone). Polym Degradation Stability 2003; 80: 241-250.
34. Arimura H, Ohya Y, Ouchi T. The formation of biodegradable polymeric micelles from newly synthesized poly(aspartic acid)-*block*-polylactide AB-type diblock copolymers. Macromol Rapid Commun 2004; 25: 743-747.
35. Knaul JZ, Hudson SM, Creber KAM. Crosslinking of chitosan fibers with dialdehydes: Proposal of a new reaction mechanism. J Polym Sci: Part B: Polym Phys 1999; 37: 1079-1094.

36. Etienne O, Schneider A, Taddei C, Richert L, Schaaf P, Voegel JC, Egles C, Picart C. Degradability of polysaccharides multilayer films in the oral environment: an in vitro and vivo study. Biomacromol 2005; 6: 726-733.
37. Schneider A, Francius G, Obeid R, Schwinté P, Hemmerlé J, Frisch B, Schaaf P, Voegel JC, Senger B, Picart C. Polyelectrolyte multilayers with a tunable Young's modulus: Influence of film stiffness on cell adhesion. Langmuir 2006; 22: 1193-1200.
38. Kujawa P, Moraille P, Sanchez J, Badia A, Winnik FM. Effect of molecular weight on the exponential growth and morphology of hyaluronan/chitosan multilayers: A surface plasmon resonance spectroscopy and atomic force microscopy investigation. J Am Chem Soc 2005; 127: 9224-9234.
39. Berg MC, Zhai L, Cohen RE, Rubner MF. Controlled drug release from porous polyelectrolyte multilayers. Biomacromol 2006; 7: 357-364.
40. Vegotsky A, Harada K, Fox SW. The characterization of polyaspartic acid and some related compounds. J Am Chem Soc 1958; 80: 3361-3366.
41. Joentgen W, Müller N, Mitschker A, Schmidt H. Biopolymers. Part 7. Polyamides and Complex Proteinaceous Materials Chapter 7 Polyaspartic acids pp175-
42. Matsuyama M, Kokufuta E, Kusumi T, Harada K. On the poly(β-DL- aspartic acid). Macromolecules 1980; 13: 196-198.
43. Paulino AT, Simionato JI, Garcia JC, Nozaki J. Characterization of chitosan and chitin produced from silkworm crysalides. Carbohydr polym 2006; 64: 98-103.
44. Kweon HY, Um IC, Park YH. Structural and thermal characteristics of *Antheraea pernyi* silk fibroin/chitosan blend film. Polymer 2001; 42: 6651-6656.
45. Bae HS, Hudson SM. The cooperative binding behavior of sodium dodecyl sulfate to crosslinked chitosan films. J Polym Sci PartA, Polym Chem 1997; 35: 3755-3765.
46. Sperling LH. Introduction to physical polymer science, third edition. Wiley-InterScience, New York, 2001; pp. 482-483.
47. Varum KM, Anthonsen MW, Nordtveit RJ, Grasdalen H, Smidsrod O. Quantitative determination of molecular composition and sequence in chitosans by high-field N.M.R.-spectroscopy-Relations to solubility, and degradability by lysozyme. Chitin derivatives in life science 1992; 77-85.
48. Ren D, Yi H, Wang W, Ma X. The enzymatic degradation and swelling properties of chitosan matrices with different degrees of *N*-acetylation. Carbohyd Res 2005; 340: 2403-2410.

49. Wan Y, Yu A, Wu H, Wang Z, Wen D. Porous-conductive chitosan scaffolds for tissue engineering II. *in vitro* and *in vivo* degradation. J Mater Sci: Mater Med 2005; 16: 1017-1028.
50. Muzzarelli RAA, Terbojevich M, Muzzarelli C, Francescangeli O. Chitosans depolymerized with the aid of papain and stabilized as glycosylamines. Carbohydr Polym 2002; 50: 69-78.
51. Vishu Kumar AB, Varadaraj MC, Goeda LR, Tharanathan RN.Characterization of chito-oligosaccharides prepared by chitosanolysis with the aid of papain and pronase, and their bacterial action against *Bacillus cereus* and *Escherichia coli*. Biochem J 2005; 391: 167-175.
52. Rujiravanit R, Kruaykitanon S, Jamieson AM, Tokura S. Preparation of crosslinked chitosan/silk fibroin blend films for drug delivery system. Macromol Biosci 2003; 3: 604-611.
53. Dhanikula AB, Panchagnula R. Development and characterization of biodegradable chitosan films for local delivery of paclitaxel. AAPS J 2004; 6: 1-11.
54. Amaral IF, Lamghari M, Sousa SR, Sampaio P, Barbosa MA. Rat bone marrow stromal cell osteogenic differentiation and fibronectin adsorption on chitosan membranes: The effect of the degree of acetylation. J Biomed Mater Res 2005; 75A: 387-397.
55. Sengupta S, Lohse CM, Cheville JC, Leibovich BC, Thompson RH, Webstar WS, Frank I, Zincke H, Blute ML, Kwon ED. The preoperative erythrocyte sedimentation rate is an independent prognostic factor in renal cell carcinoma. Cancer 2006; 106: 304-312.
56. Goel MS, Diamond SL. Encyclopedia of Biomaterials and Biomedical Engineering, Vol. 1; Marcel Dekker, Inc., 2004; pp. 144-154.

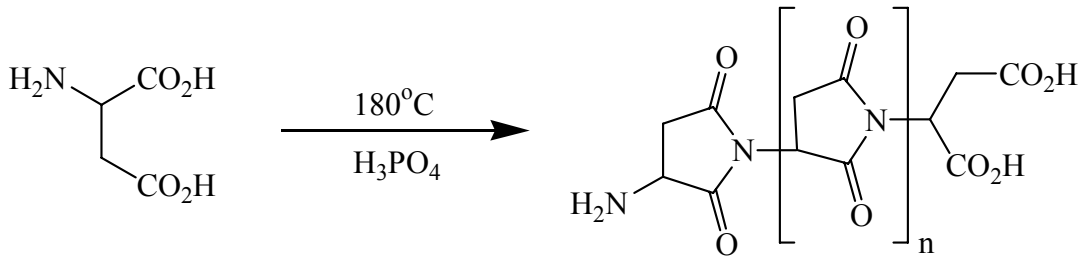

L-aspartic acid

Anhydropoly(aspartic acid), PSI

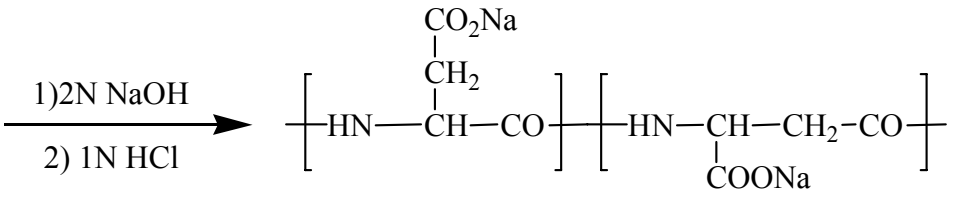

Sodium Poly(aspartate), PAspNa

Scheme 3-1 Thermal condensation polymerization of L-aspartic acid and hydrolysis to poly(aspartic acid).

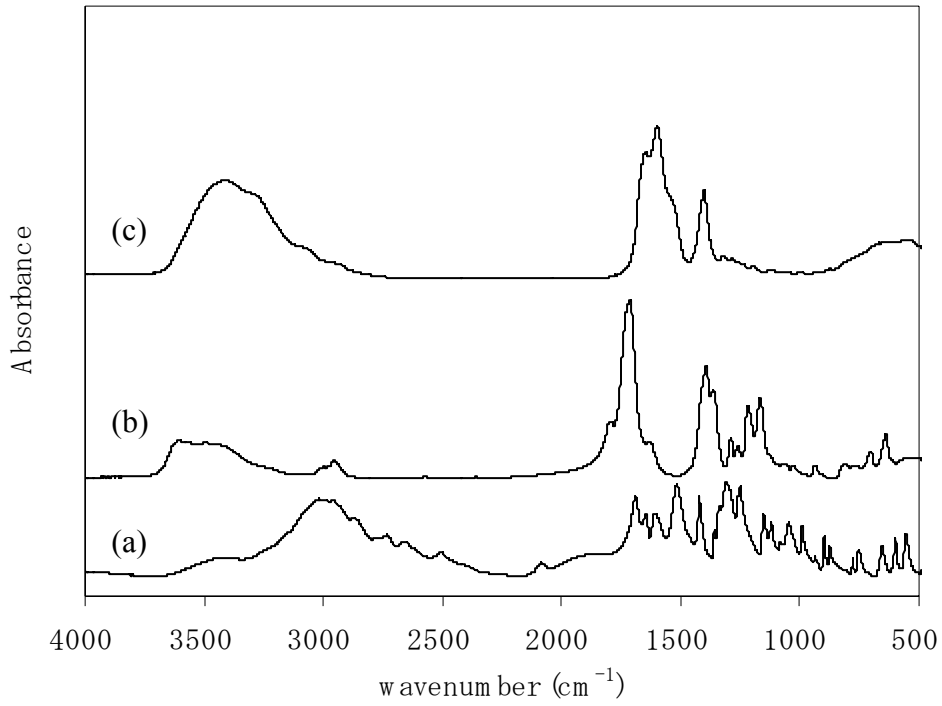

Figure 3-1 FTIR spectra of (a): L-aspartic acid(starting material), (b): PSI, and (c): PAspNa
The spectra were obtained using a KBr pellet.

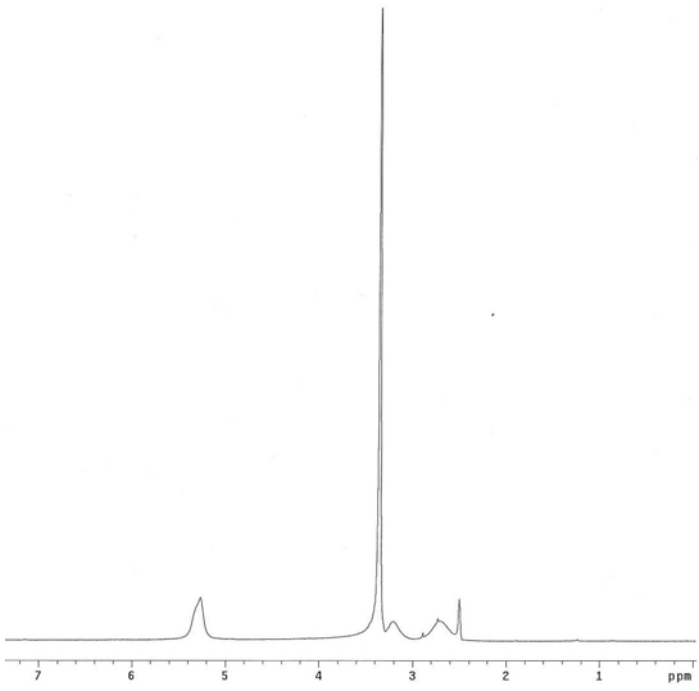

Figure 3-2 ^{1}H NMR spectra of PSI in DMSO-d_6 (300MHz).

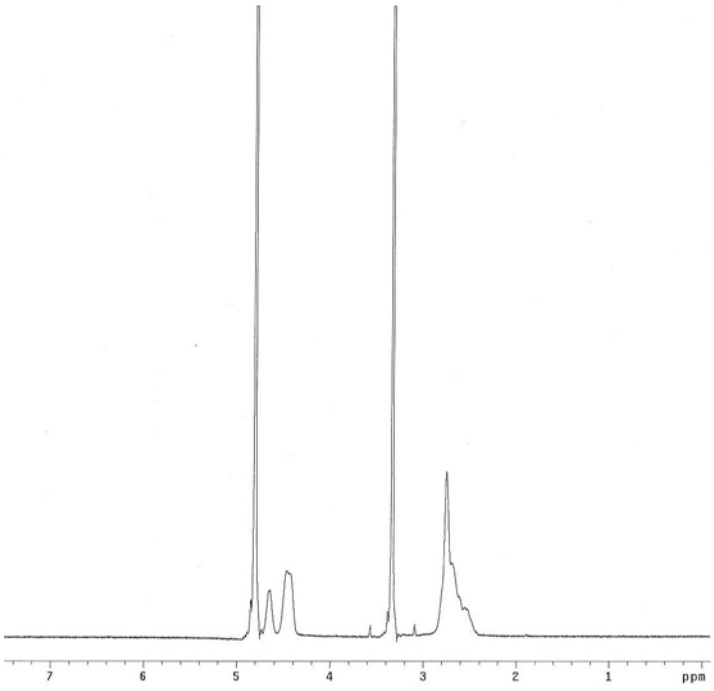

Figure 3-3 ^{1}H NMR spectra of PAspNa in D_2O (300MHz).

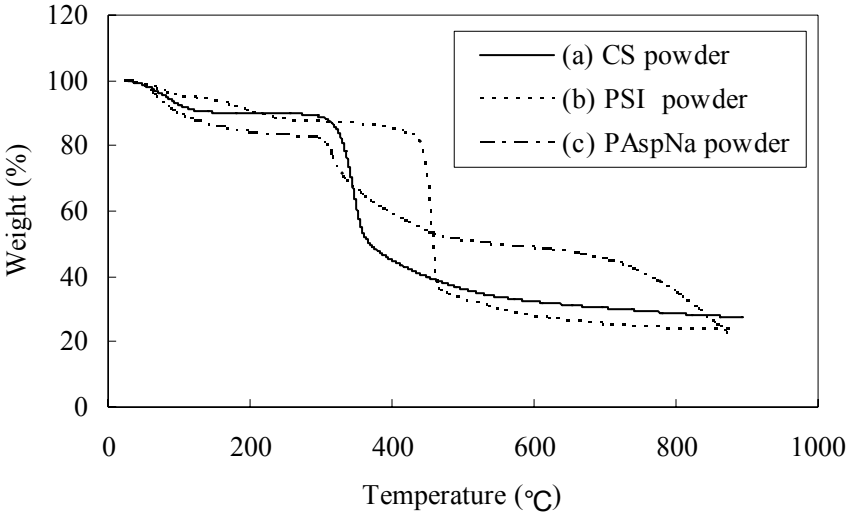

Figure 3-4 TGA thermograms of polymers under N_2 atmosphere. (a): CS, (b): PSI, and (c): PAspNa. A scan rate of 30 ºC/min was used.

Table 3-1 TGA data from various polymer powders (under N_2 atmosphere).

	Onset Temp.	Temp. at max. rate	Max. rate	Residue at 350 ºC	Residue at 550 ºC
	(ºC)	(ºC)	(%/min)	(%)	(%)
CS	325	346	36.3	61.1	33.8
PSI	444	456	91.7	86.7	30.1
PAspNa	303	316	15.0	66.7	49.7

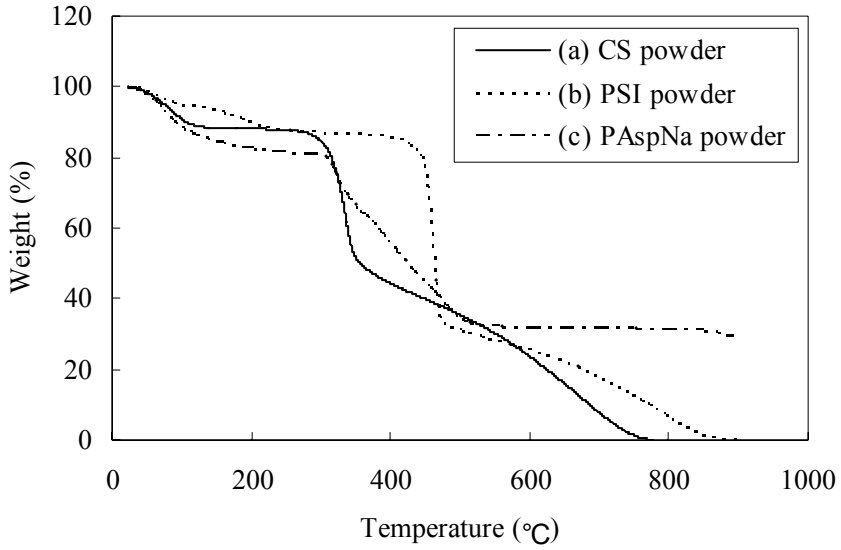

Figure 3-5 TGA thermograms of polymers under air flow. (a): CS, (b): PSI, and (c): PAspNa. A scan rate of 30 ºC/min was used.

Table 3-2 TGA data from various polymer powders (under air flow).

	Onset Temp.	Temp. at max. rate	Max. rate	Residue at 350 ºC	Residue at 800 ºC
	(ºC)	(ºC)	(%/min)	(%)	(%)
CS	314	335	35.2	51.7	0.0
PSI	446	461	80.0	86.5	6.5
PAspNa	307	321	13.1	66.3	31.2

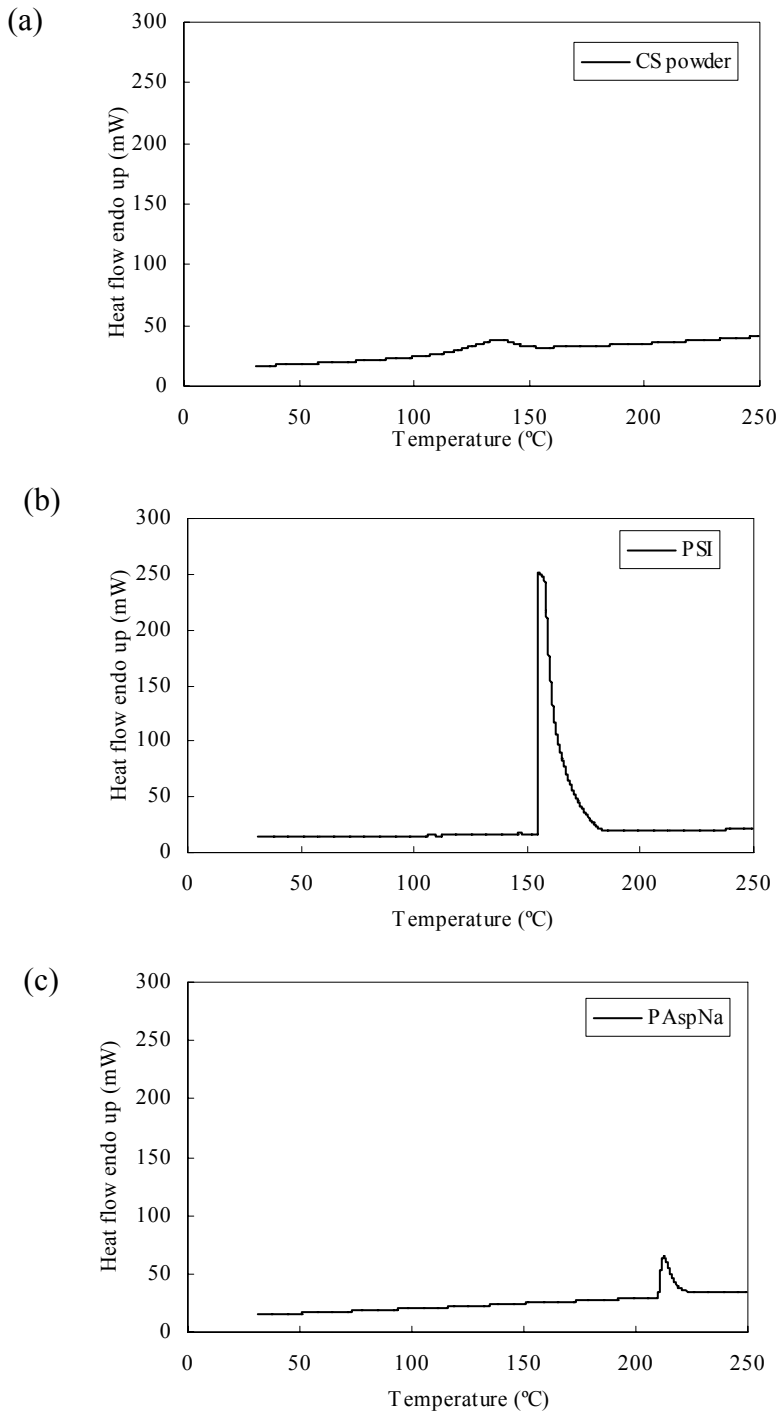

Figure 3-6 DSC thermograms of polymers under N_2 atmosphere. (a): CS, (b): PSI, and (c): PAspNa. A rate of 40 ℃/min was used.

(a)

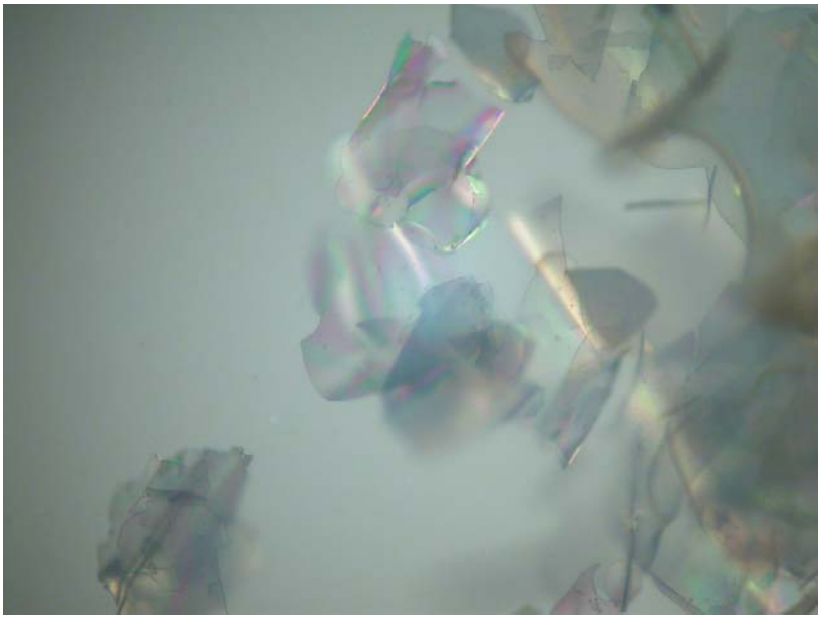

(b)

Figure 3-7 Digital images of PAspNa under the polarizing microscope (40x). (a): parallel position (b): perpendicular position

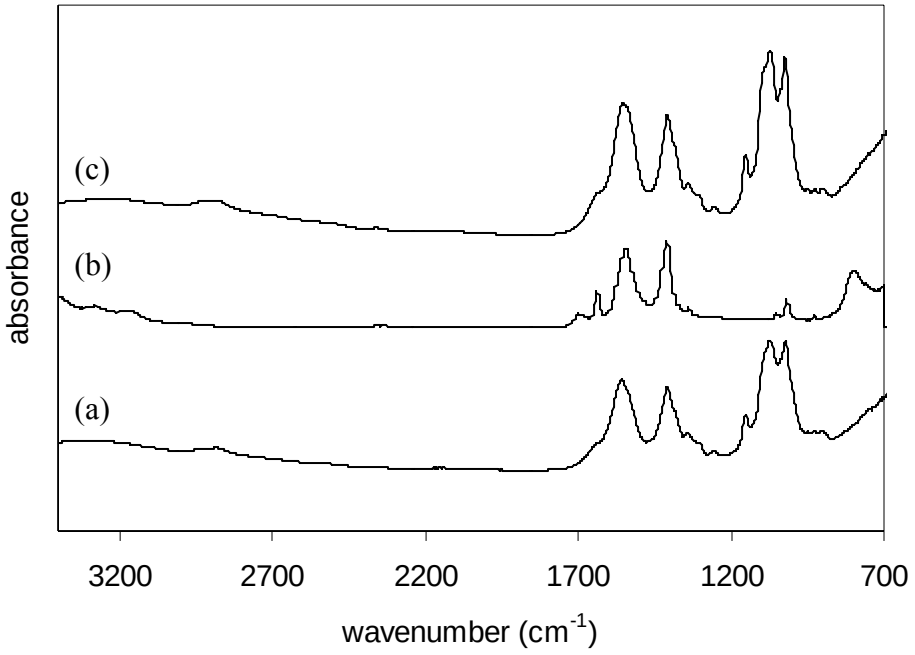

Figure 3-8 ATR-FTIR spectra of (a): 1 layer (CS) , (b): 2 layered (CS/PAspNa), and (c): 3 layered (CS/PAspNa/CS) films. The spectra were obtained using a Ge crystal.

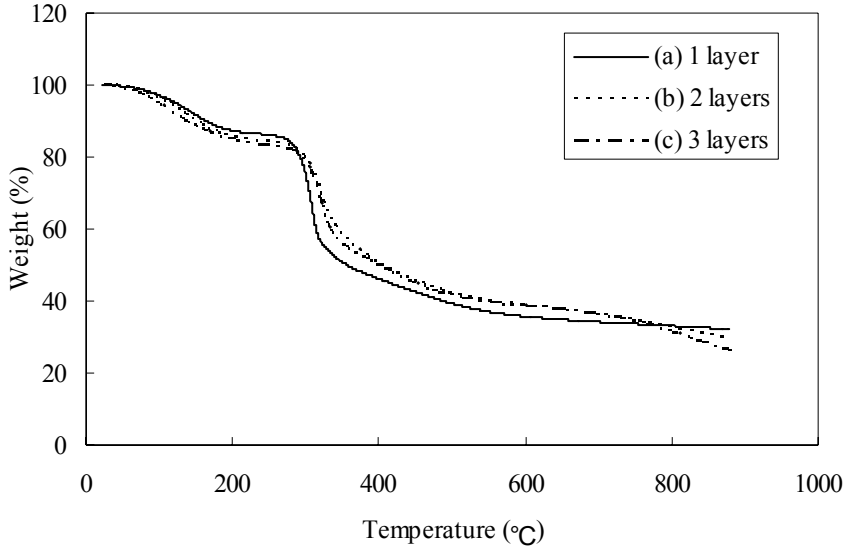

Figure 3-9 TGA thermograms of polymers under N_2 atmosphere. (a): 1 layer (CS), (b): 2 layered (CS/PAspNa), and (c): 3 layered (CS/PAspNa/CS) films. The rate of 50 ºC/min was used.

Table 3-3 TGA data from Chitosan and PAsp layered films.

	Onset Temp.	Temp. at max. rate	Max. rate	Residue at 315 ºC	Residue at 550 ºC
	(ºC)	(ºC)	(%/min)	(%)	(%)
1 layer (CS)	292	308	63.6	59.3	37.0
2 layers (CS/PAsp)	296	322	31.9	73.0	40.1
3 layers (CS/PAsp/CS)	300	320	35.9	71.3	39.6

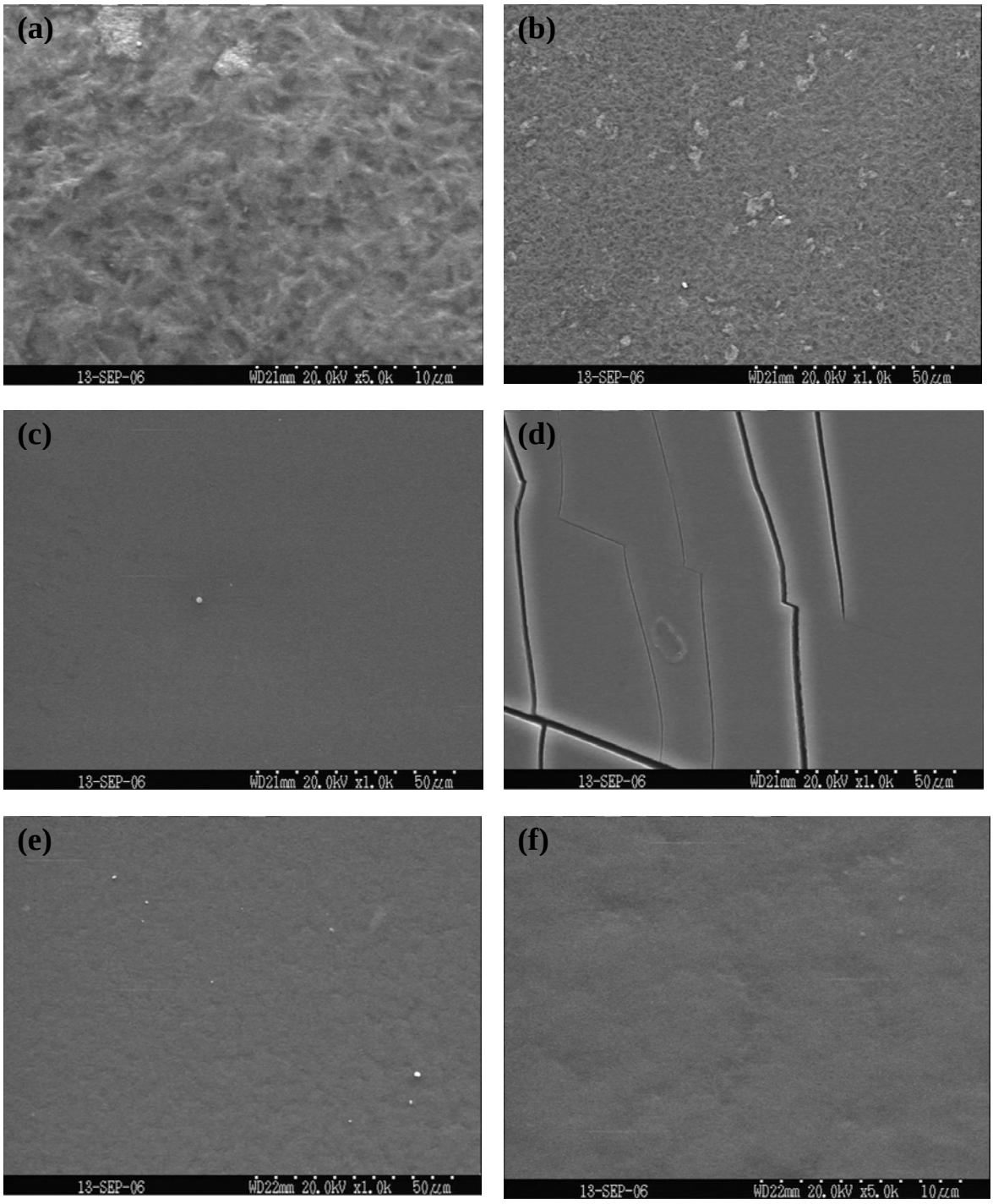

Figure 3-10 SEM images of the surface of layered films; (a),(b): CS, (c),(d): 2 layered film (PAspNa phase), (e),(f): 3 layered film.

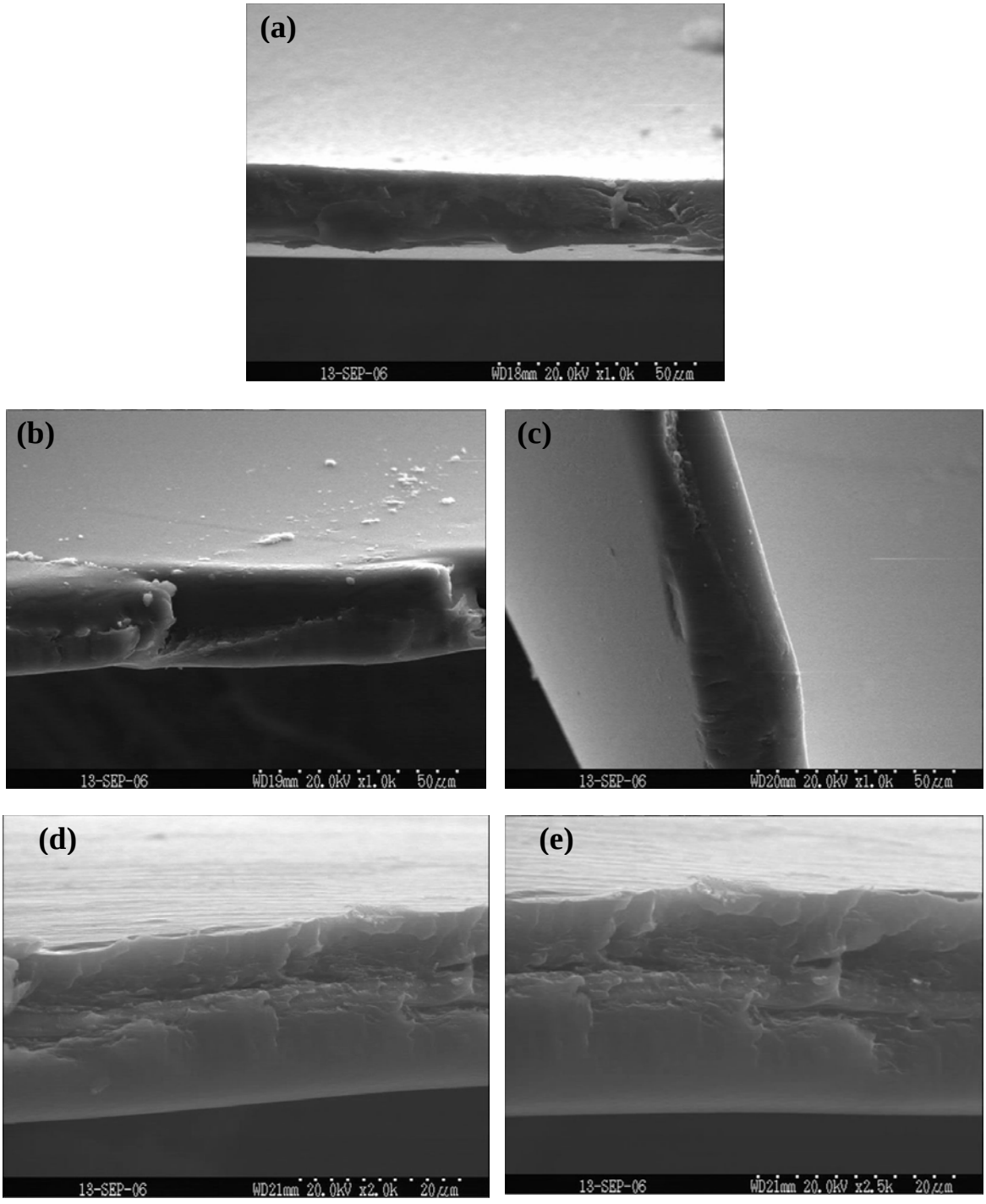

Figure 3-11 SEM images of the cross-section of layered films; (a): CS, (b),(c): 2 layered film (PAspNa phase), (d),(e): 3 layered film.

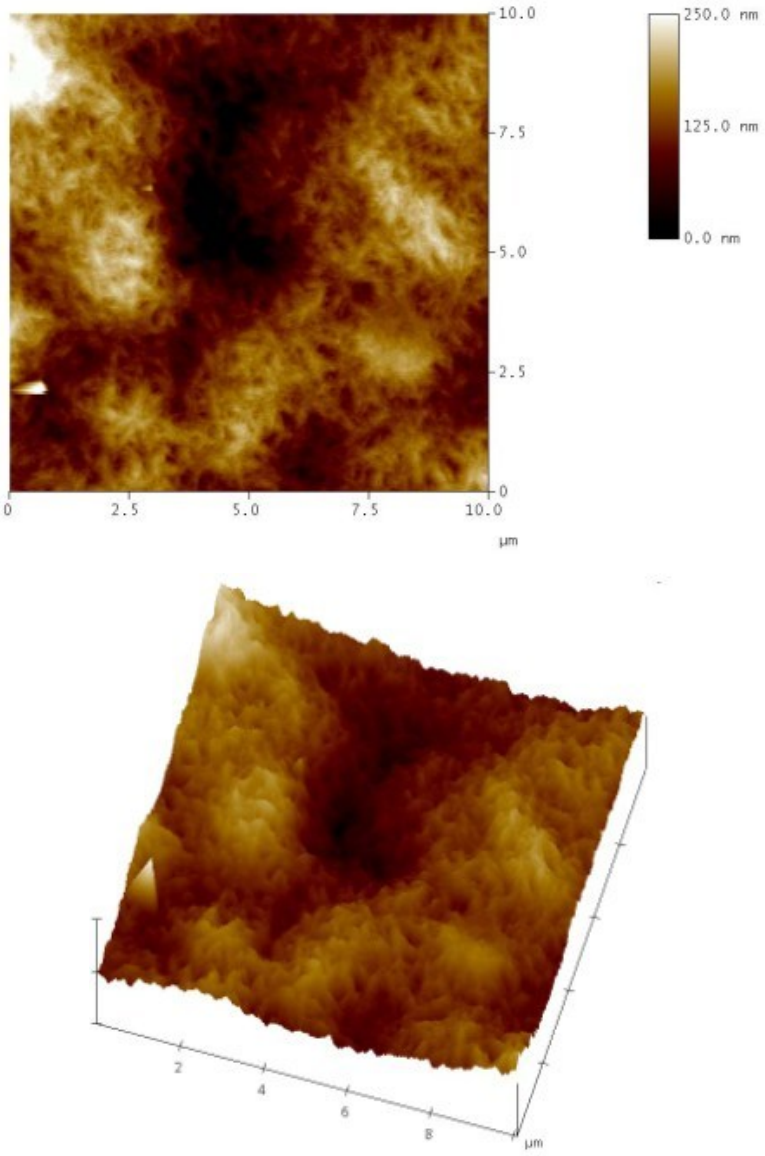

Figure 3-12 AFM images of CS film (10µm x 10µm); the topography (above), and three-dimensional height image (below). The images obtained in dynamic mode at a scan rate of 1.0Hz.

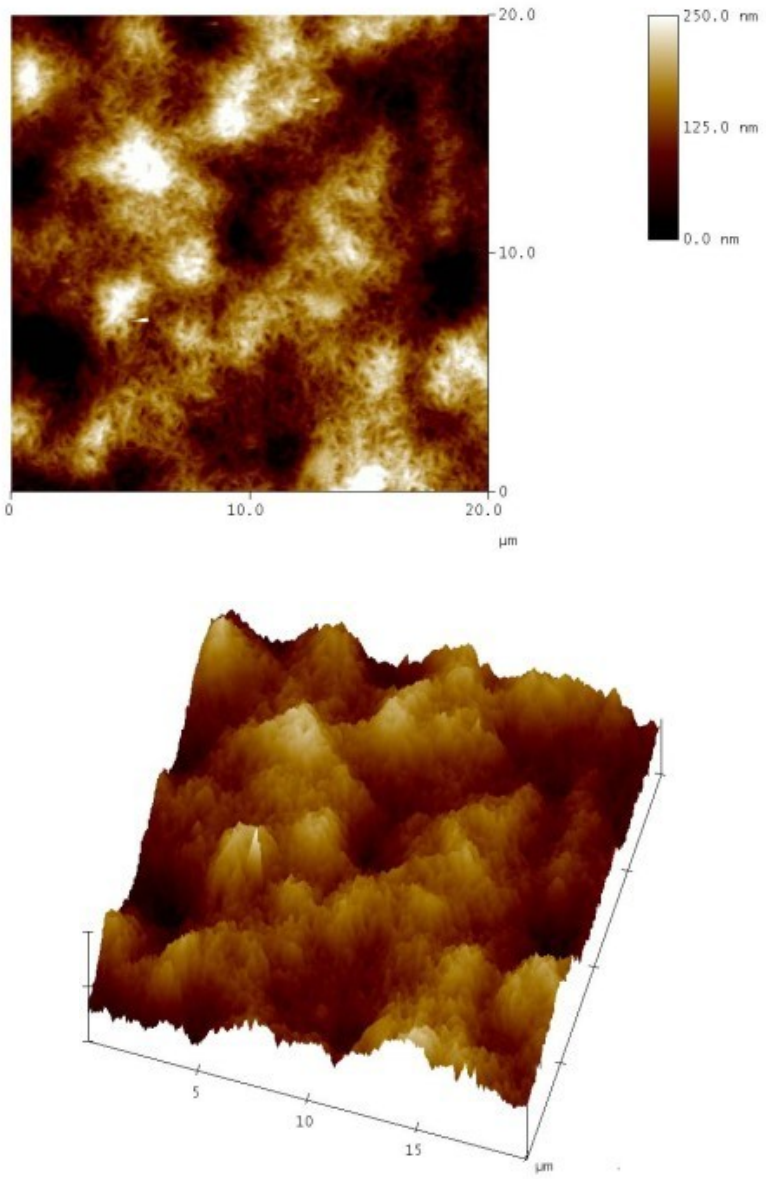

Figure 3-13 AFM images of CS film (20µm x 20µm); the topography (above), and three-dimensional height image (below). The images obtained in dynamic mode at a scan rate of 1.0Hz.

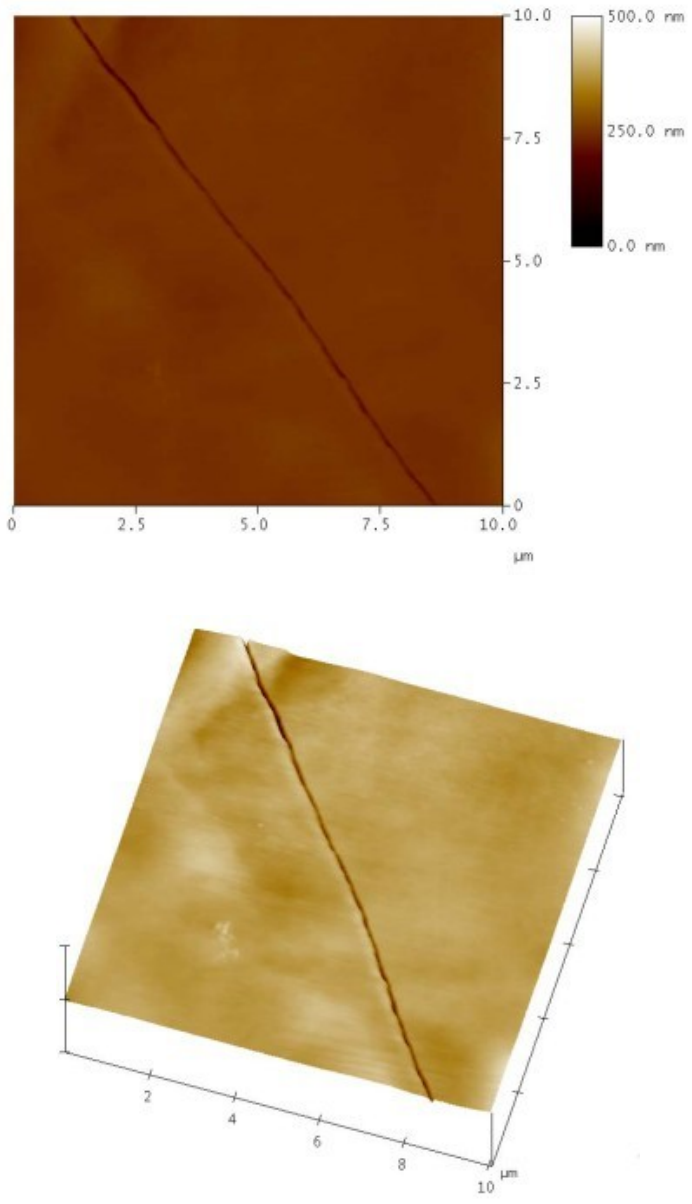

Figure 3-14 AFM images of 2 layered film (10µm x 10µm); the topography (above), and three-dimensional height image (below). The images obtained in dynamic mode at a scan rate of 1.0Hz.

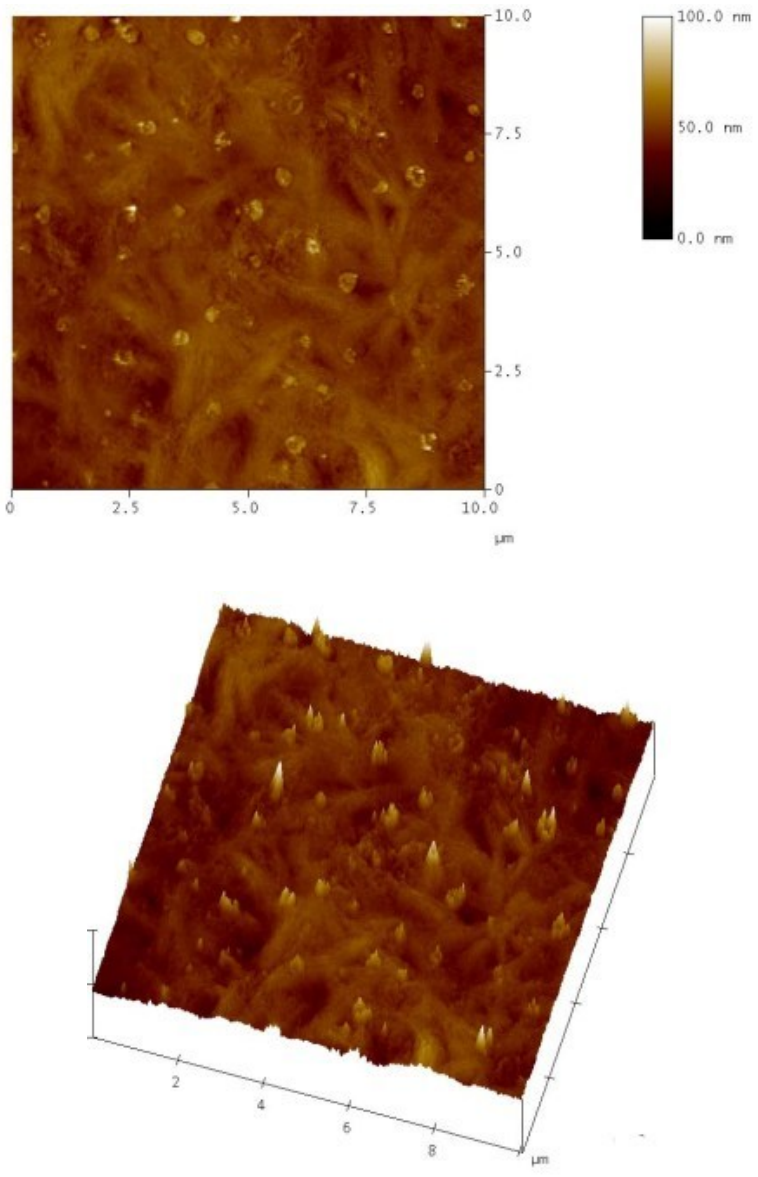

Figure 3-15 AFM images of 3 layered film (10µm x 10µm); the topography (above), and three-dimensional height image (below). The images obtained in dynamic mode at a scan rate of 1.0Hz.

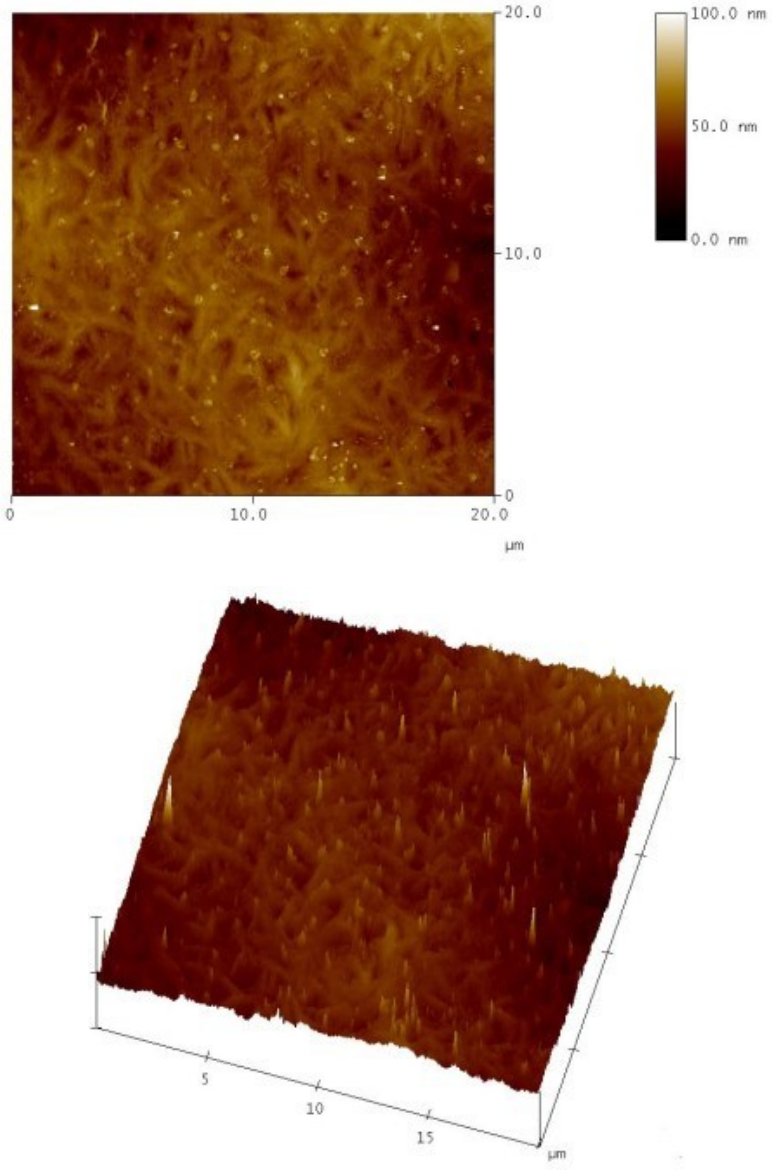

Figure 3-16 AFM images of 3 layered film (20µm x 20µm); the topography (above), and three-dimensional height image (below). The images obtained in dynamic mode at a scan rate of 1.0Hz.

Table 3-4 The variation of layered film mechanical properties* at 65% RH and 20ºC.

	Modulus (Gpa)	Tensile stress at break (Mpa)	Tensile strain at break (%)
1 layer	1.78±0.51	67.52±12.75	52.9±17.2
2 layers	1.53±0.41	30.57±8.91	5.7±0.9
3 layers	3.48±0.48	102.87±12.80	14.4±3.1

* Mean±SD. Gauge length was set at 10mm. At least six replicates were tested.

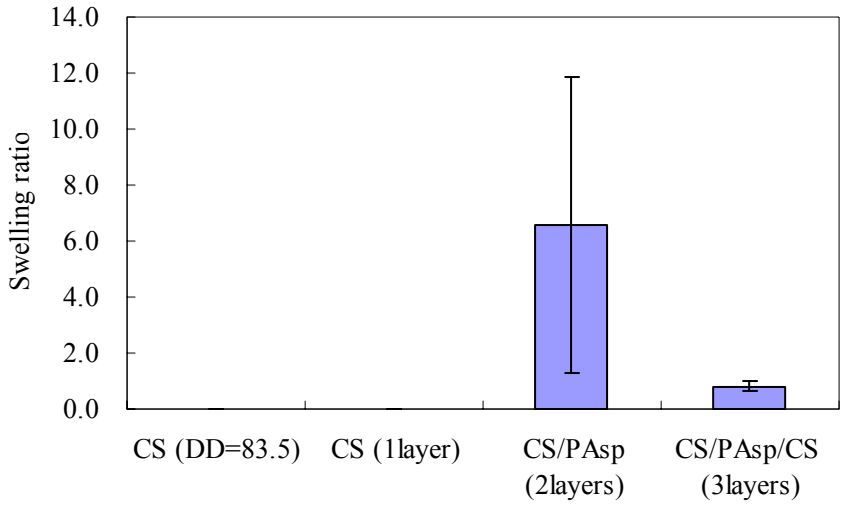

Figure 3-17 Swelling ratio of the CS and layered films immersed in PBS with pH 5.0 at 37 ºC for 24 hours (n=6). The CS with degree of deacetylation of 83.5% was used as a control.

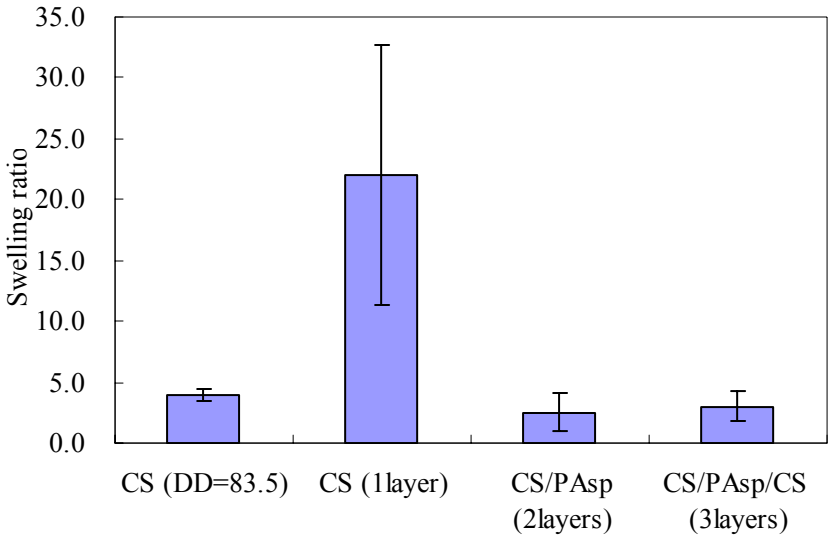

Figure 3-18 Swelling ratio of the CS and layered films immersed in PBS with pH 7.4 at 37 ºC for 24 hours (n=6). The CS with degree of deacetylation of 83.5% was used as a control.

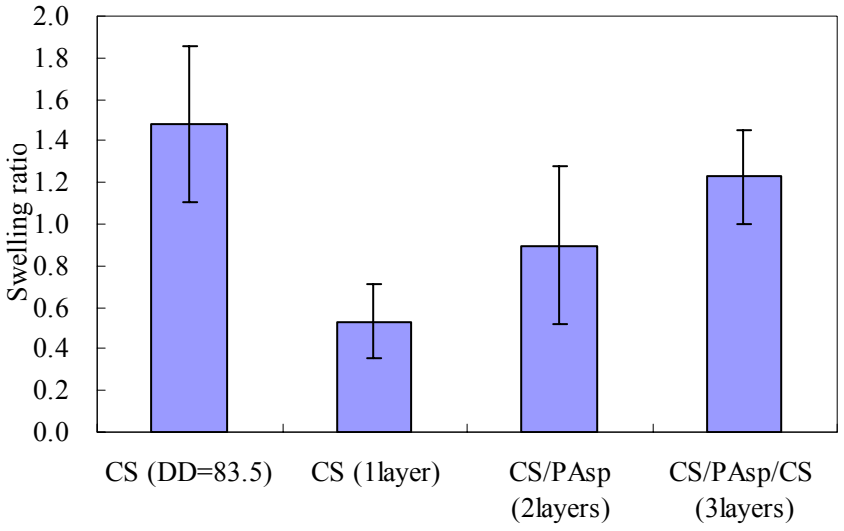

Figure 3-19 Swelling ratio of the CS and layered films immersed in PBS with pH 9.0 at 37 ºC for 24 hours (n=6). The CS with degree of deacetylation of 83.5% was used as a control.

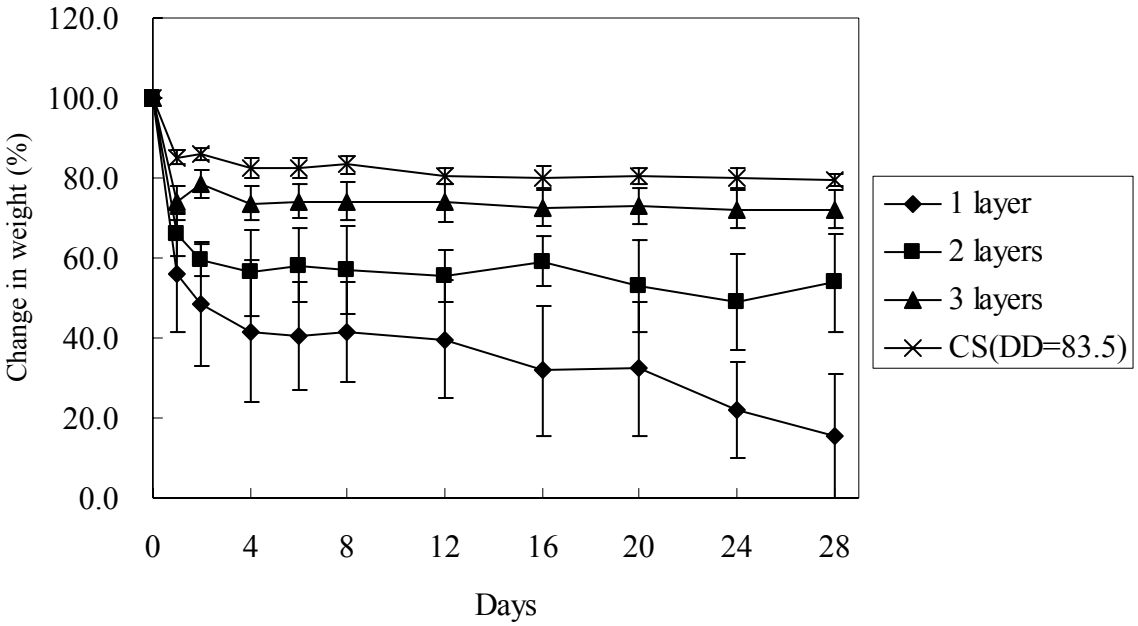

Figure 3-20 Film weight changes of CS and layered films immersed in PBS with pH 7.4 at 37 ºC (n=6). The CS with degree of deacetylation of 83.5% was used as a control.

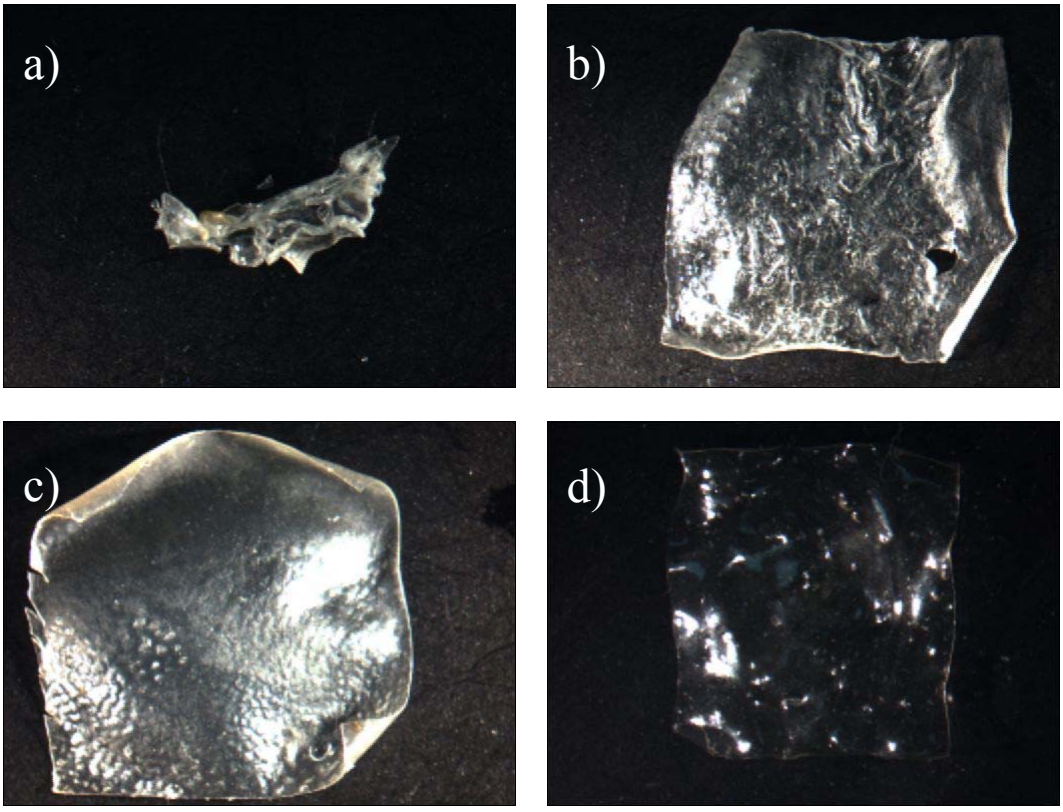

Figure 3-21 Stereomicroscope images (x1) of films after 28 days of degradation test in PBS (pH 7.4) at 37 ºC; (a): CS (1 layer), (b): 2 layered film, (c): 3 layered film, and (d): CS (DD=83.5). Only the 1 layer film turned into small pieces.

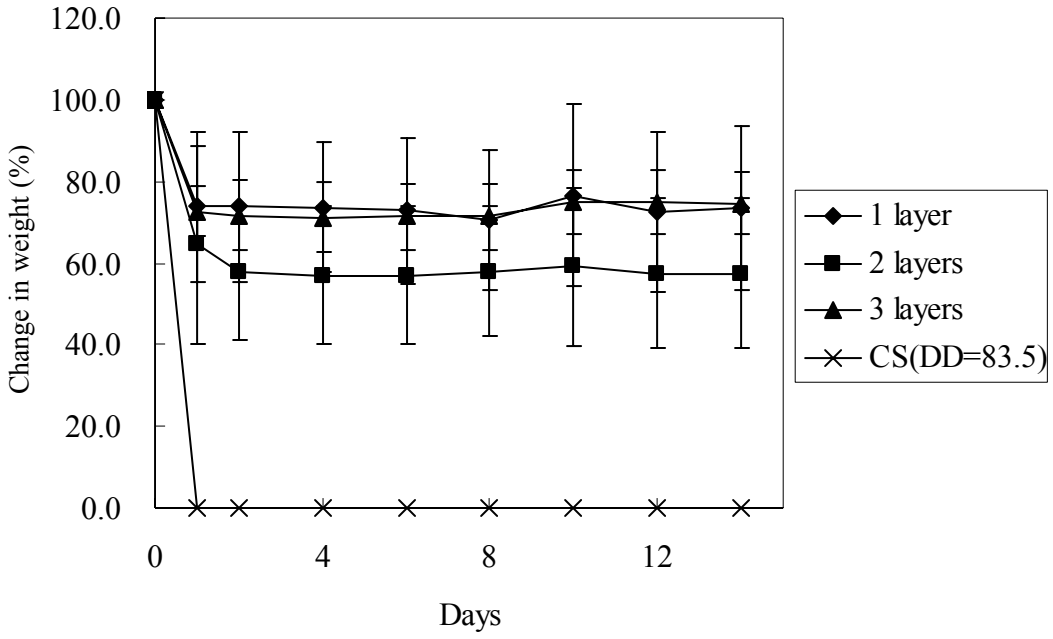

Figure 3-22 Film weight changes of CS and layered films immersed in lysozyme solution (1mg/mL) at 37 ºC (n=6). The CS with degree of deacetylation of 83.5% was used as a control.

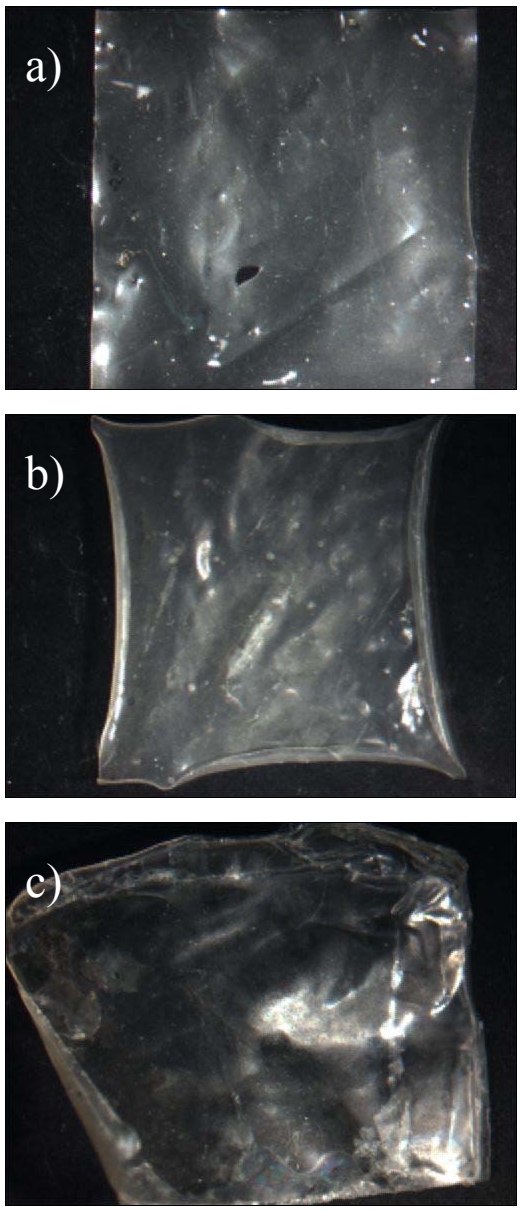

Figure 3-23 Stereomicroscope images (x1) of films after 14 days of degradation test in lysozyme solution (1mg/mL) at 37 ºC; (a): CS (1 layer), (b): 2 layered film, and (c): 3 layered film. The control CS film was completely degraded.

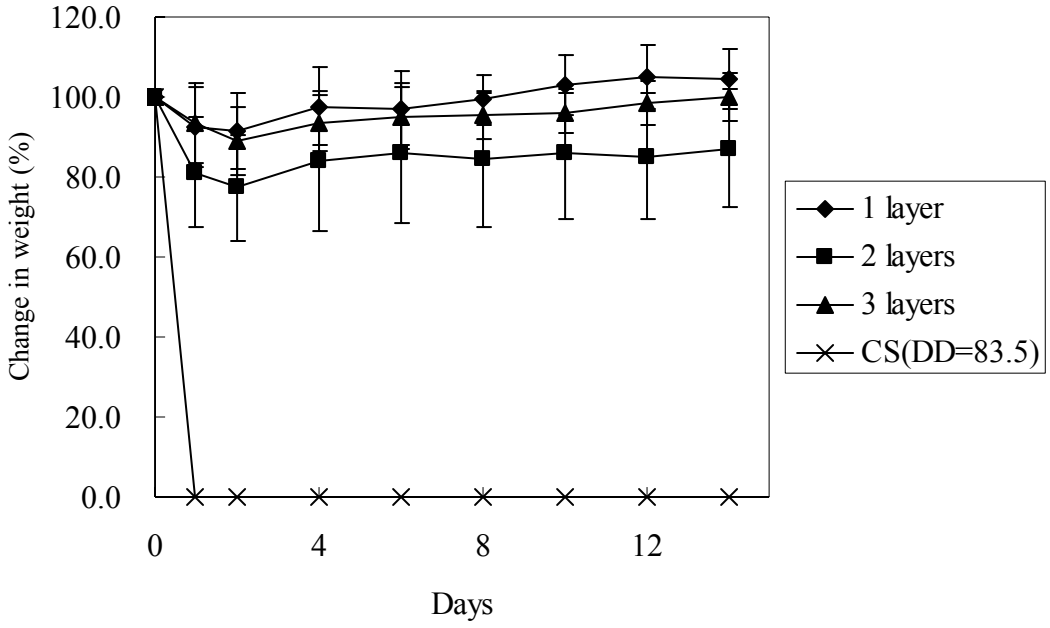

Figure 3-24 Film weight changes of CS and layered films immersed in crude papain solution (10mg/mL) at 37 ºC (n=6). The CS with degree of deacetylation of 83.5% was used as a control.

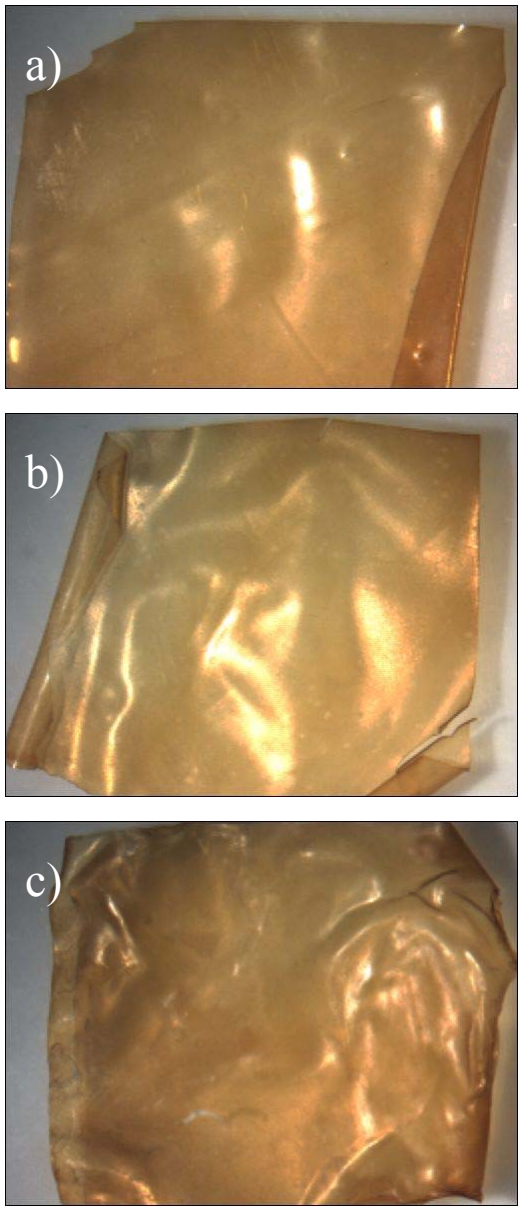

Figure 3-25 Stereomicroscope images (x1) of films after 14 days of degradation test in crude papain solution (10mg/mL) at 37 ºC; (a): CS (1 layer), (b): 2 layered film, and (c): 3 layered film. The control CS film was completely degraded.

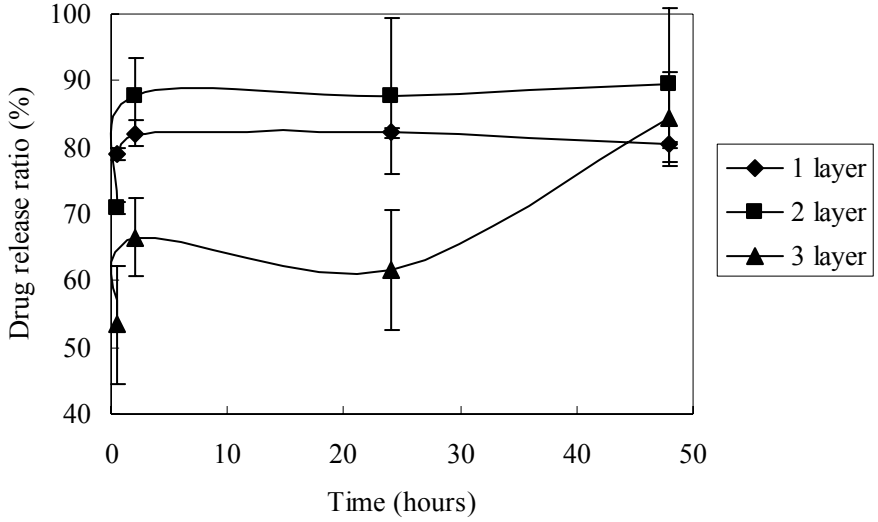

Figure 3-26 Release ratio of Blue22 incorporated to CS and layered films immersed in PBS (pH 5.0) at 37 ºC; (closed diamond): 1 layer, (closed square): 2 layered film, and (closed triangle): 3 layered film. The absorbance at 630nm was measured by UV-visible spectroscopy. All experiments were done with three replicates.

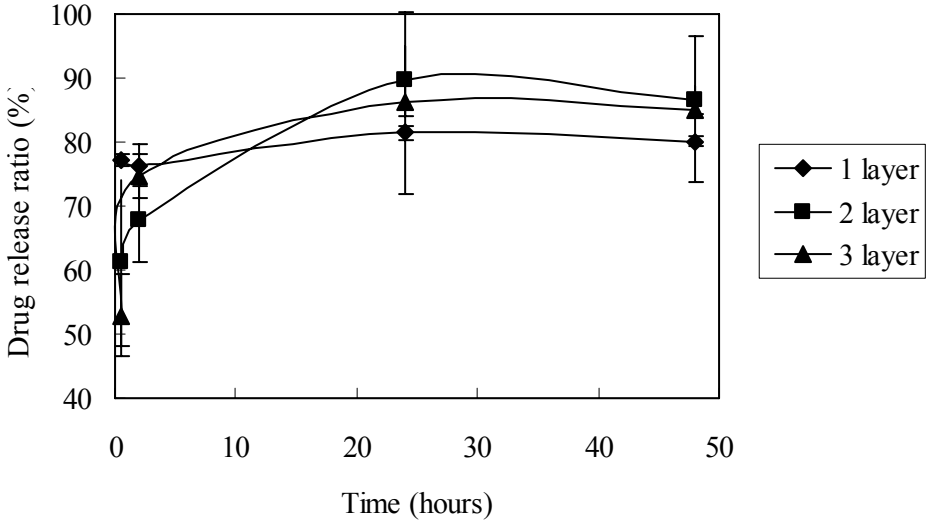

Figure 3-27 Release ratio of Blue22 incorporated to CS and layered films immersed in PBS (pH 6.5) at 37 ºC; (closed diamond): 1 layer, (closed square): 2 layered film, and (closed triangle): 3 layered film. The absorbance at 630nm was measured by UV-visible spectroscopy. All experiments were done with three replicates.

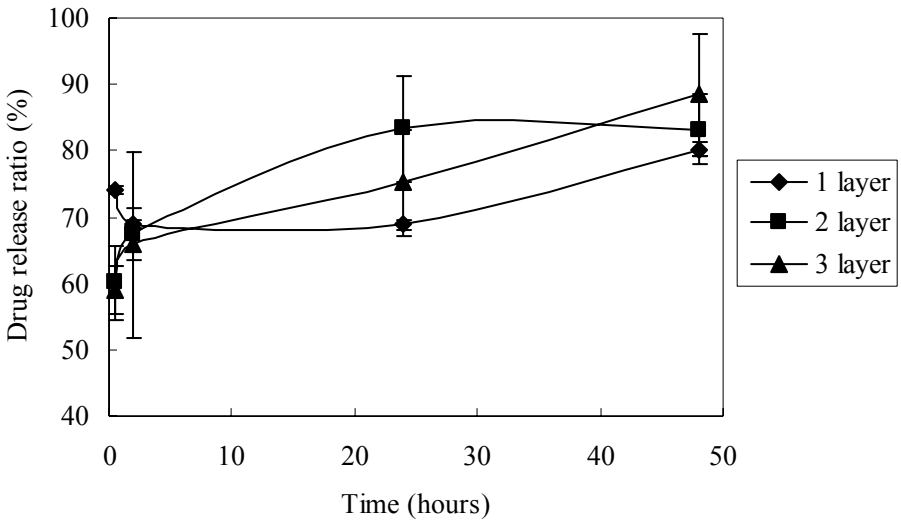

Figure 3-28 Release ratio of Blue22 incorporated to CS and layered films immersed in PBS (pH 7.4) at 37 ºC; (closed diamond): 1 layer, (closed square): 2 layered film, and (closed triangle): 3 layered film. The absorbance at 630nm was measured by UV-visible spectroscopy. All experiments were done three replicates.

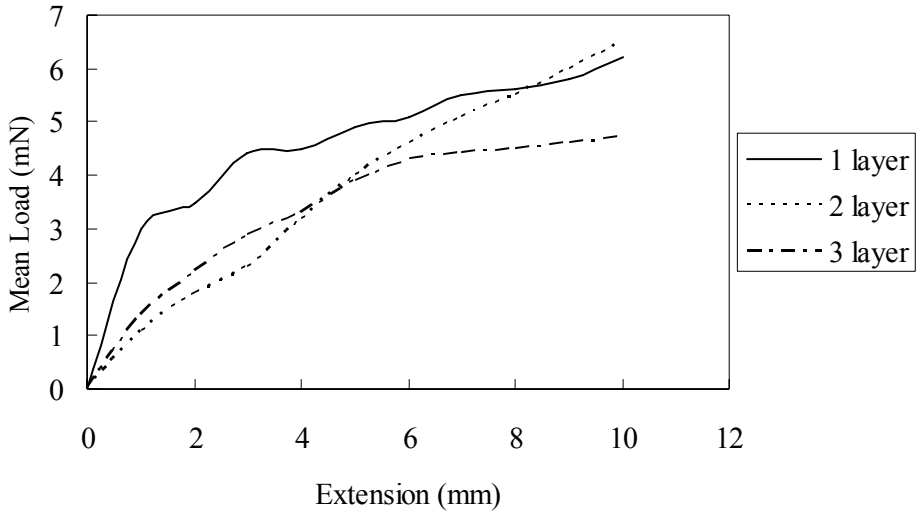

Figure 3-29 The mean load-extension curve of peeling test conducted by peeling two slices of porcine tissue holding various films. Load cell: 5N cell, gauge length: 10mm, and peeling rate: 6.0mm/min. Each experiment was repeated at least 5 times.

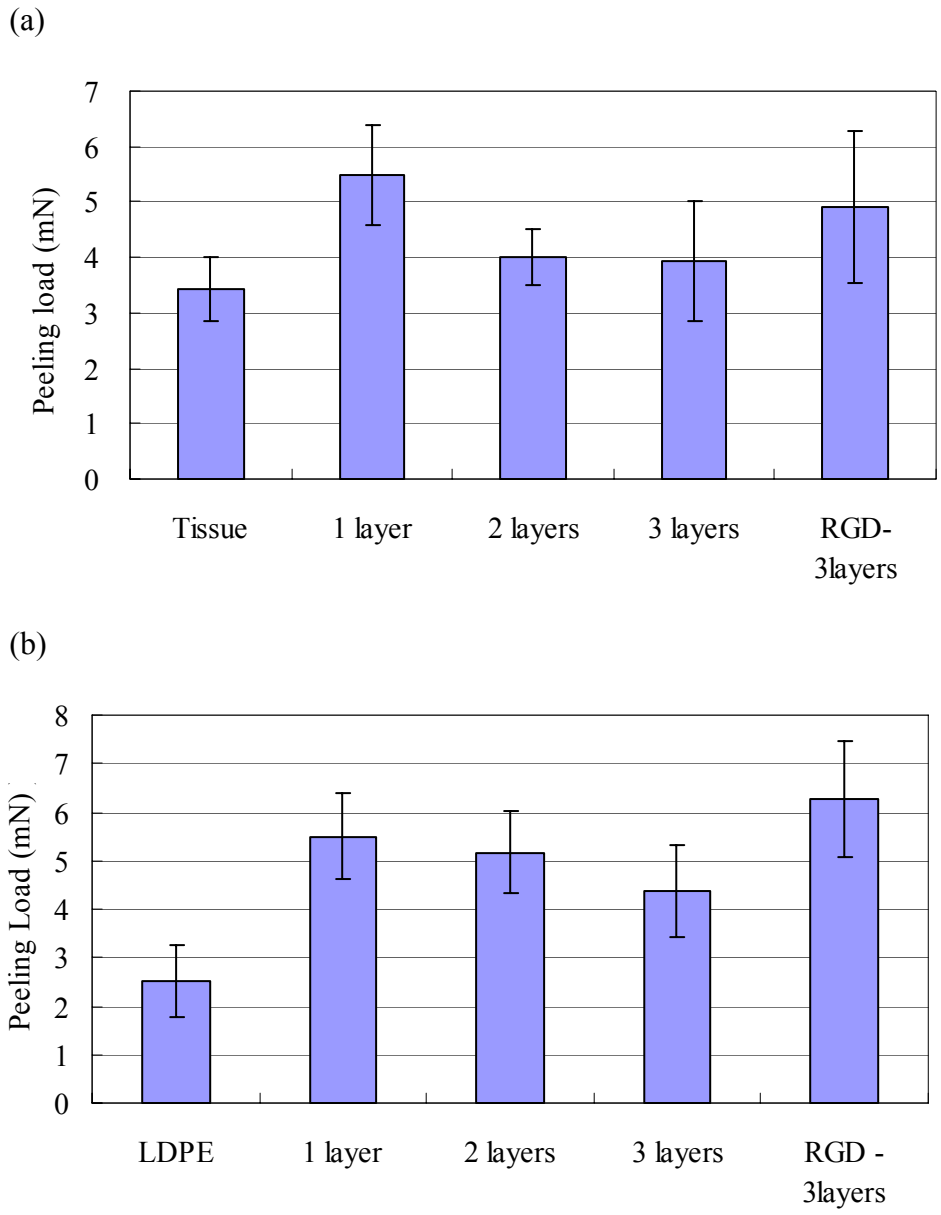

Figure 3-30 The load required at (a): 5mm and (b): 7mm to peel two slices of porcine tissue holding various films. Load cell: 5N cell, gauge length: 10mm, and peeling rate: 6.0mm/min. Each experiment was repeated at least 5 times.

Table 3-5 Blood sedimentation time* (min) of various films in 1mL of anti-coagulant blood.

	CS (DD=85.3)	CS (DD=98.3)	2 layers	3 layers	RGD-3layers
Dried film	> 90	> 90	25.6±5.9	30.6±7.0	50.5±13.5
Wet film	> 90	> 90	33.0±11.0	43.8±12.9	51.5±5.1

* Mean±SD. The blood containing films was incubated at 37 ºC for 90 min.

a) CS (DD=83.5)

b) CS (DD=98.3) 1 layer

c) 2 layered film

d) 3 layered film

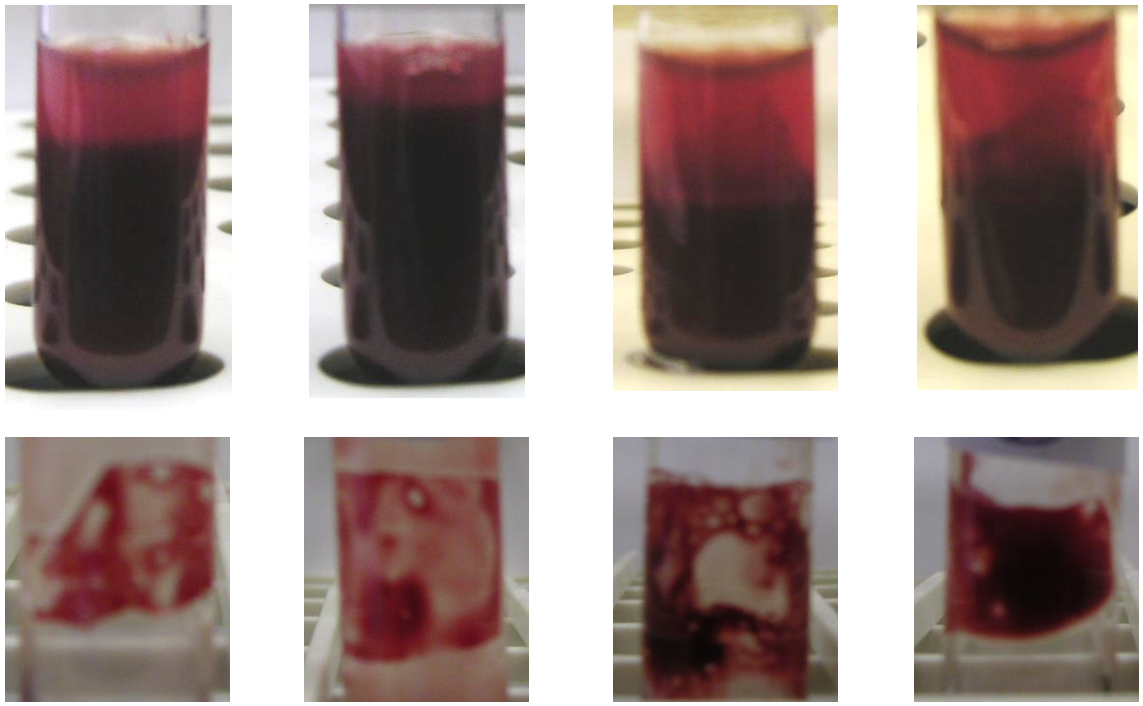

Figure 3-31 Blood sedimentation after immersing of various films1.5 hour at 37 ºC (above) and blood clot formed on films (below); (a): CS (DD=83.5), (b): CS (DD=98.3) 1 layer film, (c): 2 layered film, (d): 3 layered film. The blood containing 3.5 wt% of sodium citrate was used. Each experiment was repeated 5 times.

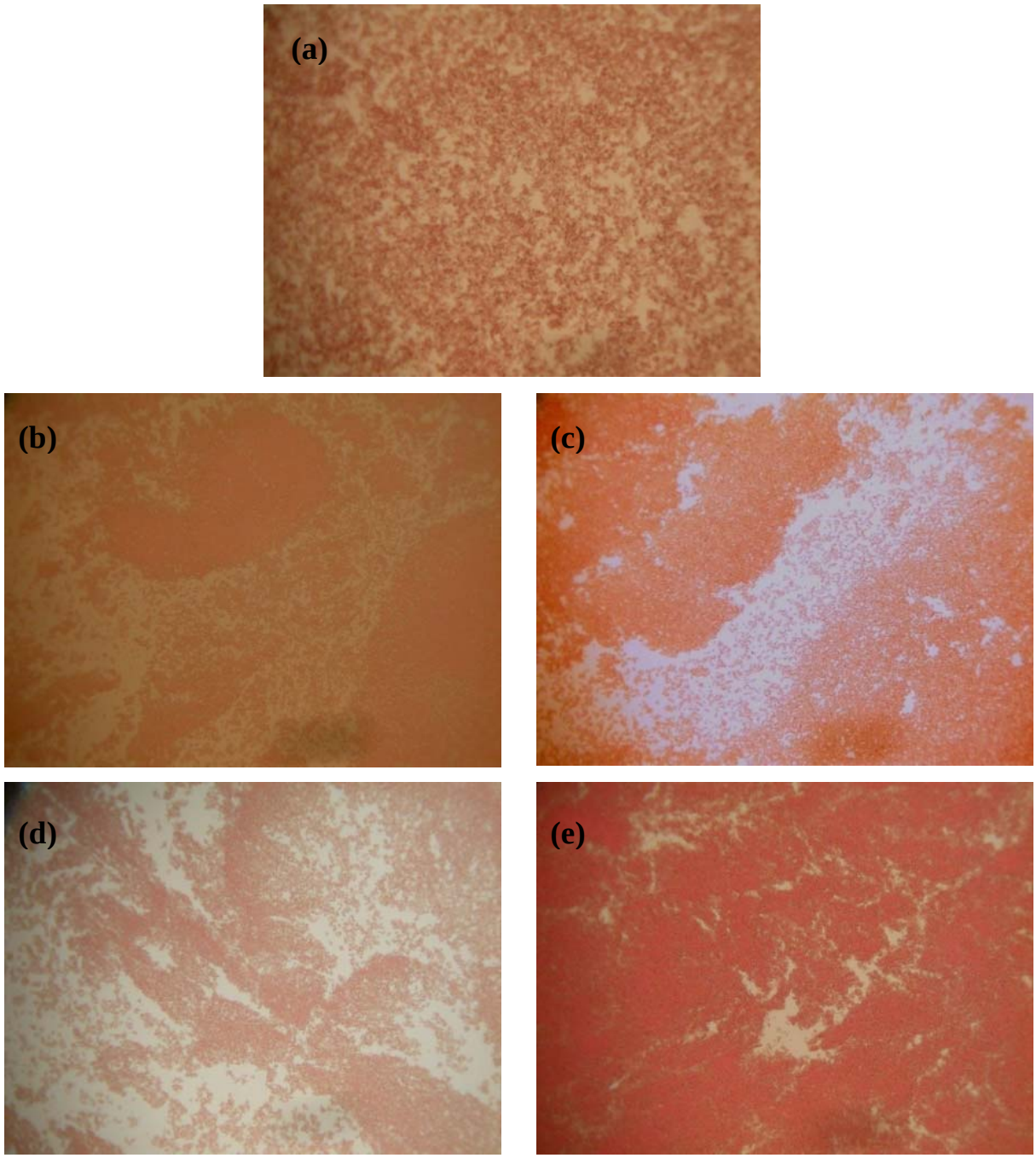

Figure 3-32 Stereomicroscope images (x10) of red blood cells after 1.5 hour-sedimentation; (a): Anticoagulated blood without film, (b): CS (DD=83.5), (c): CS (DD=98.3) 1 layer film, (d): 2 layered film, (e): 3 layered film.

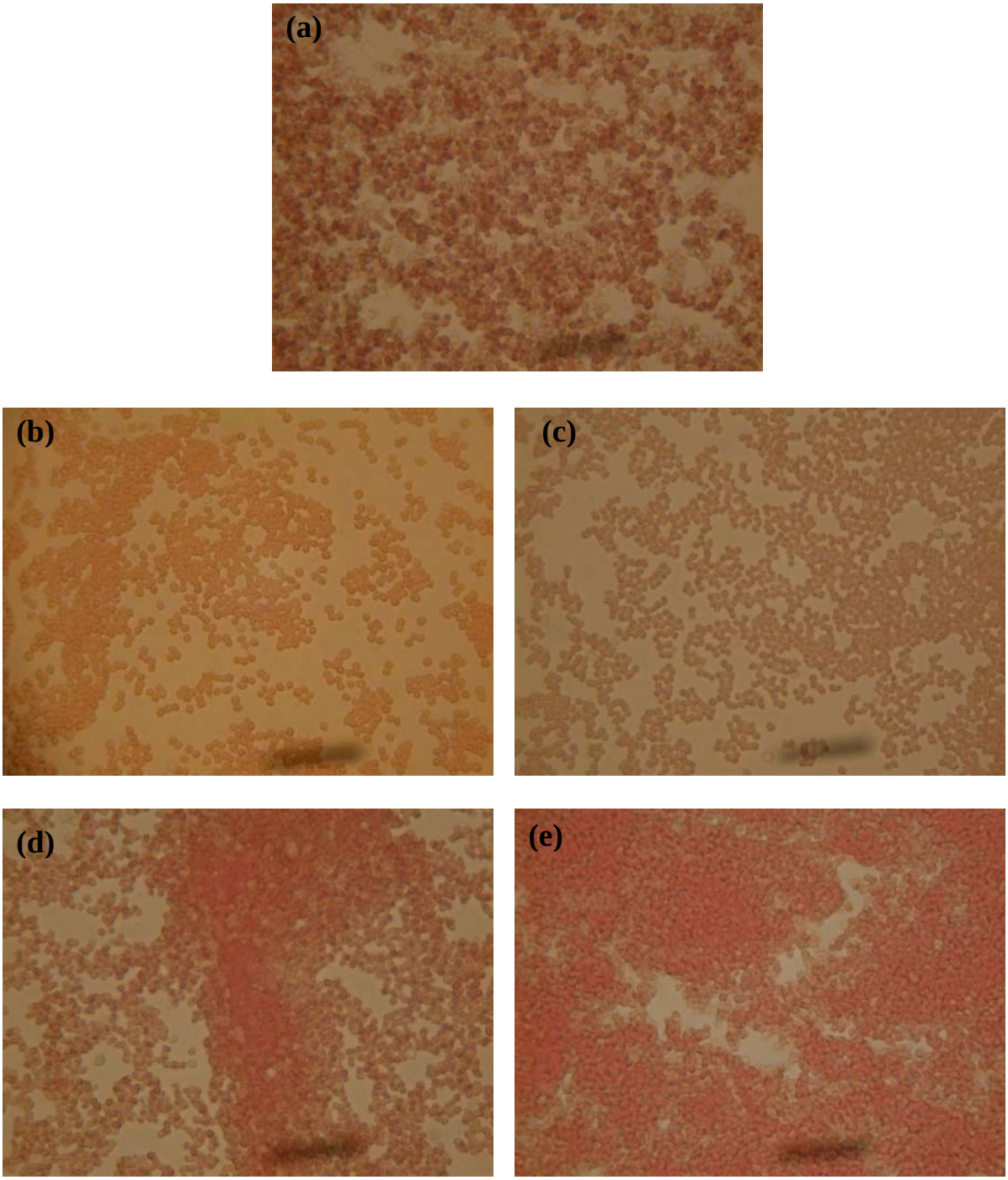

Figure 3-33 Stereomicroscope images (x40) of red blood cells after 1.5 hour-sedimentation; (a): Anticoagulated blood without film, (b): CS (DD=83.5), (c): CS (DD=98.3) 1 layer film, (d): 2 layered film, (e): 3 layered film.

CHAPTER 4

4. Synthesis and Characterization of RGD (Arg-Gly-Asp) Peptides and its Modification on Chitosan/Poly(aspartic acid) Layered Films

Abstract

The RGD peptide was synthesized by a conventional stepwise liquid synthesis method for the layered film modifications in order to improve the bioadhesiveness of the layered films described in the previous chapter. The amino group of the chitosan outer layers was reacted with GA for further reaction with the N-terminal of the RGD peptide. Each step of the peptide synthesis was spectroscopically characterized, and the final product of RGD, was obtained, though it contained some impurities. Techniques to improve the yield and purity of the RGD peptide are suggested. In addition, some RGD peptides were grafted as a pendant-group via GA, which also bonds to the chitosan amino group, and the presence of RGD moiety was confirmed by FTIR-ATR. The bioadhesion test demonstrated that the bioadhesiveness of the RGD-modified layered film was improved, possibly due to the RGD peptides.

4.1 Introduction

Cell adhesion is a primary cellular event employed to maintain the proper cell shape and cell functions by the interaction between cell and material surface. Generally, cell attachment to the extracellular matrix (ECM) plays an important role in cell behavior, which regulates gene expression followed by a series of signal transductions initiated by cell-cell/cell-material interactions.

Cell-substrate interactions are being rapidly clarified and the membrane associated receptors on the cell involved in cell attachment are being determined. These receptors recognize certain peptide sequences, such as RGDS (Arg-Gly-Asp-Ser) and RGDV (Arg-Gly-Asp-Val), found in adhesive proteins, such as fibronectin, vitronectin, collagen, and laminin of the ECM [1,2]. Numerous other adhesive peptide sequences have been identified and isolated, following the discovery of the RGD peptide motif [3]. It is believed that a peptide motif can provoke desired phenotypic responses in individual cell types, depending on the peptide sequence [3]. Cell adhesion on the material surface is improved by incorporation of RGD on the tissue scaffold, which is recognized by receptors called integrin [4-6].

Surface modification of biomaterials as well as novel scaffold developments has been extensively studied. Conventional synthetic polymers and their copolymers, such as polyurethane [2,7] poly(L-lactic acid) [3,8,9,10], and poly(vinyl alcohol) [1,11], and poly(ethylene glycol) [12-14], usually exhibit poor cell adhesion on their surfaces. Many attempts have been done in order to improve the cell adhesion and growth by coating or immobilizing the cell binding motif to the substrates, especially using peptides containing the RGD sequence [1-3, 5-14]. Most of the studies reported that RGD-incorporated scaffolds enhanced cell adhesion and spreading, mostly in a concentration-dependent manner.

As discussed in the previous chapter, chitosan is one of the promising biomaterials, due to its biocompatibility, and it can be a substitute for the ECM or be a scaffold for tissue engineering. The RGD-modified chitosan-based materials have already been reported by several researchers [15-19]. In many cases, the RGD peptide was covalently bonded to the

spacer, which is also bonded to the chitosan amino group [15,16,19]. The spacer enables making bonds with the peptide, due to the reactive group in the spacer molecule. The concentration of RGD grafting was adjusted moderately so that the peptide-to-peptide spacing makes for good cell spreading [20]. Since chitosan potentially has a hemostatic property, the improved adhesiveness to the tissue is also expected to induce quicker hemostasis.

In an earlier chapter, a novel chitosan/PAsp/chitosan layered film was fabricated as a new scaffold for tissue engineering. The layered film exhibited different physical and mechanical properties, which were sufficient enough to function as a scaffold. Grafting the RGD peptide to the chitosan backbone will provide further affinity to tissue/cells, when it is applied to a wound area.

In this chapter, the RGD peptide was synthesized by a conventional stepwise process in liquid synthesis method (Scheme 4-1). The basic concept of peptide synthesis is amide bond formation between the amine group-protected amino acids and the carboxyl group-protected amino acid by the coupling reaction. Each step of the peptide synthesis was traced spectroscopically. The obtained peptide and chitosan were crosslinked by glutaraldehyde as a spacer, and the RGD modified layered film was characterized. Finally, a bioadhesion test and simple blood coagulation test were conducted to obtain the preliminary biological data of the film as a bioadhesive/hemostatic agent.

4.2 Experimental

4.2.1 Materials

Chitosan was acquired from Natural Biopolymer, Inc. (Raymond, WA). All other chemicals used in this study were purchased from Fisher Scientific or Aldrich Chemicals and used directly, without further purification.

4.2.2 Chitosan solution preparation

CS solution of 1% (w/w) was prepared by following the method of 2.2.3.

4.2.3 PAspNa solution preparation

PAspNa solution of 1% (w/w) was prepared by following the method of 3.2.5.

4.2.4 CS/PAspNa/CS three layered film fabrication

Layered films were fabricated by following the method of 3.2.6.

4.2.5 Synthesis of RGD peptide

The RGD peptide was synthesized by a conventional stepwise liquid synthesis method. The series of reactions used in this study were as follows:

4.2.5.1 Asp(Obzl)$_2$

L-Aspartic acid (Asp; 3.325g, 0.025mol), p-toluenesulfonic acid monohydrate ($TsOH \cdot H_2O$; 11.4g, 0.06mol), 25mL of benzyl alcohol, and 50mL of benzene were put into a 250mL of 3-neck flask, then heated at 80 ºC under reflux. Generated water was removed by a

Dean-Stark trap. The reaction was tracked under UV short-wave by Thin Layer Chromatography (TLC). After 5 h, the solution was cooled and 80mL of diethyl ether and 80mL of hexanes were added, and the precipitate was filtered. This crude material was recrystallized in MeOH and diethyl ether. The white crystalline material was filtered and dried over night (Yield: 9.10g, 92.2%).

4.2.5.2 Boc-Gly

Glycine (Gly; 5.50g, 0.073mol) was dissolved in 150mL of dioxane, 75mL of water, and 75mL of 1M NaOH in an ice bath. Di-*tert*-butyl dicarbonate (Boc_2O; 10.2g, 0.074mol) was added and stirred at room temperature. TLC was performed (solvent; $CHCl_3$:MeOH:HOAc=95:5:3; Rf=0.45) and the presence of the desired product was visualized by ninhydrin reagent. The solution was concentrated and cooled in an ice bath. A 10% citric acid solution was added to adjust the pH to around 3, and then 30mL of ethyl acetate. The organic layer was washed with deionized water three times and dried with Na_2SO_4. The solvent was concentrated and a white powder was obtained from hexane (Yield: 10.75g, 83.7%).

4.2.5.3 $^{\alpha}$Z-Arg

L-Arginine (Arg; 8.75g, 0.05mol) and $NaHCO_3$ (10.9g, 0.10mol) were dissolved in 75mL of water and stirred at room temperature. A solution of 5.2mL of benzyl chloroformate (Z-Cl; 0.03mol) and 15mL of diethyl ether was added and stirred for 2 h. Then, $NaHCO_3$ (5.45g, 0.06mol) and 5.2mL of Z-Cl was added and stirred overnight. The crude was washed with cold water and recrystallized with hot water. The resulting white solid was washed with acetone and diethyl ether and dried under vacuum (Yield: 12.6g, 81.8%).

4.2.5.4 Boc-Gly-Asp(Obzl)$_2$

The N-and C-protected amino acids, Boc-Gly (1.76g, 10mmol) and Asp(Obzl)$_2$ (4.0g, 10mmol), were dissolved in 40mL of dichloromethane (CH_2Cl_2). While a water bath was cooled at 0 ºC, triethylamine (Et_3N; 1.68mL, 10.3mmol) and dicyclohexyl carbodiimide (DCC; 2.27g, 10.1mmol) were added and stirred for 2 h at 0 ºC, then 20 hours at room temperature. The mixture was concentrated and 100mL of ethyl acetate was added. Dicyclohexyl urea, a by-product, was filtered and the organic layer was washed with 10% citiric acid solution (30mL x 2), 4% $NaHCO_3$ solution (30mL x 2), and water (30mL x 2). The organic layer was dried with Na_2SO_4 and concentrated. A syrup was obtained, which was directly used for the deprotection reaction that followed.

4.2.5.5 Gly-Asp(Obzl)$_2$

The syrup of Boc-Gly-Asp(Obzl)$_2$ was dissolved to a total volume of 40mL with a trifluoroacetic acid (CF_3CO_2H) and CH_2Cl_2 mixture (1:1) and stirred for 1 h at 0 ºC. The solution was concentrated and a slightly yellowish powder of protected dipeptide was recovered after rinsing with diethyl ether-hexanes (Yield: 2.95g, 80.0%).

4.2.5.6 $^{\alpha}$Z-Arg-Gly-Asp(Obzl)$_2$

The N-and C-protected amino acids, $^{\alpha}$Z-Arg (1.54g, 5mmol) and Gly-Asp(Obzl)$_2$ (1.85g, 5mmol), were dissolved in a total of 40mL of CH_2Cl_2 and DMF. While a water bath was cooled at 0 ºC, *N*,*N*-diisopropylethylamine (DIEA; 1.88mL, 5.0mmol), dicyclohexyl carbodiimide (DCC; 1.13g, 10.1mmol), and 1-hydroxybenzotriazole(HOBt; 0.769g, 5mmol) were added and stirred for 2 h at 0 ºC, then it was stirred for additional 20 h at room temperature. The mixture was concentrated and 100mL of ethyl acetate was added. The

by-product of dicyclohexyl urea was filtered off and the organic layer was washed with 10% citiric acid solution (30mL x 2), 4% $NaHCO_3$ solution (30mL x 2), and water (30mL x 2). The organic layer was dried with Na_2SO_4 and concentrated. A yellowish solid was recovered after rinsing with diethyl ether-hexanes (Yield: 2.20g, 66.5%).

4.2.5.7 Arg-Gly-Asp

The protected RGD peptide (3.57g, 5.5mmol) was dissolved in 30mL of MeOH and 5mL of 0.1M HCl in a 100mL flask. A powder of palladium black, 5% (w/w) on activated carbon (0.18g, 5% (w/w) of the peptide) was added and stirred in the flask filled with hydrogen gas overnight. The hydrogenation reaction product was checked with TLC. The catalyst was filtered off, and the filtrate was concentrated and dried under vacuum overnight. The white solid of RGD peptide salt was obtained (Yield: 2.21g, 104.7%).

4.2.6 RGD-modified 3 layered film preparation

The 3 layered film was treated with 0.01M glutaraldehyde solution. The film was soaked with the solution for 10 sec and washed with deionized water for 10 min then air-dried subsequent to treatment with RGD solution (1mg/mL). The RGD-modified 3 layered film was stored in a desiccator for later use.

4.2.7 Fourier Transform Infrared (FTIR) and FT-Attenuated Total Reflectance (FTIR-ATR) Spectroscopy

Synthesized PSI and PAspNa were analyzed using KBr pellets. Each layered film was placed on a Ge crystal and the data were collected. All spectra were obtained using a Thermo Nicolet 510P FT-IR Spectrometer with OMNIC software. The scans were performed with an average of 32 repeated scans at 4 cm^{-1} scan resolution.

4.2.8 Nuclear Magnetic Resonance (NMR) Spectroscopy

NMR spectra were obtained on a Varian Mercury 300 NMR spectrometer operating at 300 MHz for the ^{1}H nucleus. Chemical shifts for ^{1}H NMR spectra were reported in δ (ppm), with positive values indicating downfield shifts of the reference, tetramethylsilane (TMS). Deuterated solvents reference the residual proton peaks to the chemical shift of the samples. The solvents used in this study were as follows: $CDCl_3$, 7.24, singlet; D_2O, 4.80; CD_3OD, 4.78, singlet. Significant ^{1}H NMR data are tabulated in a subsequent section in the following order: chemical shift, multiplicity (s=singlet, d=doublet, t=triplet, q=quartet, and m=multiplet), and number of protons.

4.2.9 Bioadhesion/peeling tests

Porcine large intestines were used as the biological testing substrate. The tissue samples were obtained from the Nahunta Pork Center, Nahunta, NC. They were immediately excised after slaughter and stored at –5 ºC in isotonic buffered saline at pH 7.4 (2.38 g of Na_2HPO_4, 0.19g of KH_2PO_4, and 8.0g of NaCl in 1000 mL deionized water). The intestine

tissue was carefully washed the next day, the loose surface membranes were removed, and the tissue was cut into pieces 1cm x 3cm in sections. RGD-treated 3 layered film was cut into 1cm x 1cm squares, and each one was sandwiched between the two tissue samples and covered by two glass plates. A 50g weight was placed on the 1cm x 1cm bonding area under the glass for 10 min. Both ends of the tissue samples were clamped at a gauge length of 1cm, and the peeling test was immediately conducted at the rate of 6 mm/min (Instron Model 5544 with a 5N load cell). The load to the tissue for peeling was plotted as a function of the extension of the clamps. Polyethylene film and tissue without film were used as controls. At least six replicates were obtained for each sample.

4.2.10 Blood coagulation tests

Venous blood from a pig donor was obtained by a venipuncture. The blood was collected into a 50mL plastic syringe containing 3.5% (w/w) of sodium citrate as an anticoagulant. A total of 1mL of blood was transferred to each glass tube (10 x 75mm) and it was preincubated for 5 min in a water bath at 37ºC. CS (DD=83.5) control, CS (DD=98.3) 1 layer film, 2 layered film, and 3 layered film were cut into 1 x 1cm in size. Half of the films were soaked in phosphate buffered saline (PBS, pH 7.4) for 30min to be wet, and other the half were dried before the test. Each film specimen was put into the blood, and the tubes were placed and incubated at 37ºC until the blood was separated into two phases, supernatant and red blood cell aggregation. The tube was checked every 30 sec until the blood sedimentation was completed at almost a 1:1 ratio of the two phases. The time of blood sedimentation was recorded for each sample. Five replicates at least were conducted.

After 1.5 h, all tests were stopped and films were taken out from the blood pool. The blood clot formed on each film was captured by a digital camera. The morphology of the red blood cells was examined with a Nikon Labophot2-POL microscope equipped with COOLPIX digital camera. A drop from the phase containing red blood cells was placed on a glass plate and covered with a glass cover. The 10x and 40x lenses were used.

4.3 Results and Discussions

4.3.1 Synthesis of RGD peptides

The RGD peptide was synthesized by a series of stepwise liquid synthesis steps. The derivatives and product were examined by FTIR and ^{1}H-NMR spectroscopy, whose spectra are shown in Figures 4-1 to 4-5. As the synthesis proceeded the spectrum became more complicated, especially the ^{1}H-NMR spectrum. Indeed, the ^{1}H-NMR spectrum of C-, and N-protected RGD peptide had many peaks, and some of them could not be assigned. Generally, peptide synthesis is prone to side-reactions, such as racemization, migration, and cyclyzation. This makes it difficult to produce peptides on an industrial scale, however, relatively small peptides/proteins, which are in great demand, are available on a small scale [21].

Careful selection of the reagent and reaction condition, in addition to the synthesis method, is crucial. The automated amino acid synthesizer is a better way to obtain pure peptides, while solid-state synthesis is another technique for peptide formation on a larger scale. In this synthesis work, the peptide bond formation between $^{\alpha}$Z-Arg and Gly-Asp(Obzl)$_2$ likely involves a side reaction, because substitution of the guanidine

functional group does not prevent the cyclization (formation of lactams) during activation [22]. Therefore, the final product, RGD, possibly also contained impurities, which are difficult to remove.

Here, listed below, is a summary of characteristic peaks for each step.

4.3.1.1 Asp(Obzl)$_2$

FTIR (KBr): *v*=1755 and 1735 (C=O stretch, ester), 1210 (C-O-C antisym stretch, ester), 1185 (C-O-C stretch, ester), 695 and 685cm^{-1} (two bands, CH out-of-plane deformation, monosubstituted benzene).

^{1}H-NMR (CD_3OD): δ=7.6 (d, 2H, tosyl group), 7.1 (s, 10H, benzene group), 7.0 (d, 2H, tosyl group), 5.1 and 5.0 (s, 4H, CH_2 in benzyl group), 4.2 (t, 1H, CH), 3.1 (s, 3H, NH_3), 3.0 (m, 2H, CH_2), 2.1ppm (s, 3H CH_3).

4.3.1.2 Boc-Gly

FTIR (KBr): *v*=3125 (broad, -OH stretch, carboxylic acid), 2980 and 2940 (CH antisym and sym stretch, aliphatic CH_3 and CH_2), 1750 (C=O stretch, ester), 1670 (C=O stretch, Amide I), 1540 (N-H deformation, Amide II), 1400 (CH_3 deformation, *tert*-butyl), 1255 (skeletal vibration, *tert*-butyl), 1200 (C-O-C antisym stretch, ester), 1165cm^{-1} (C-O-C stretch, ester).

^{1}H-NMR (CD_3OD): δ=3.6 (s, 1H, NH), 3.1 (s, 2H, CH_2), 1.4ppm (s, 6H, *tert*-butyl).

4.3.1.3 $^{\alpha}$Z-Arg

FTIR (KBr): *v*=1640 (C=O stretch, Amide I), 1555 (N-H deformation, Amide II), 1500 (benzene ring, ring stretch), 1265 (C-O-C antisym stretch, ester), 740 and 720 cm^{-1} (two bands, CH out-of-plane deformation, monosubstituted benzene).

^{1}H-NMR (DMSO-d_6): δ=9.4 (s, 1H, COOH), 7.3 (s, 5H, benzene group), 5.0 (s, 2H, CH_2 in benzyl group), 3.7 (q, 1H, CH), 3.0 (m, 2H, CH_2 next to NH), 1.7-1.4ppm (m, 4H, CH_2).

4.3.1.4 Gly-Asp(Obzl)$_2$

FTIR (KBr): *v*=1740 (C=O stretch, ester), 1690 (C=O stretch, carboxylic acid from trifluoroacetic acid), 1660 (C=O stretch, Amide I), 1550 (N-H deformation, Amide II), 1500 (benzene ring, ring stretch), 1200 (C-O-C antisym stretch, ester), 1175 (C-O-C stretch, ester), 720 and 700 cm^{-1} (two bands, CH out-of-plane deformation, monosubstituted benzene).

^{1}H-NMR (CD_3OD): δ=7.1 (s, 10H, benzene group), 5.0 (two peaks, s, 4H, CH_2 in benzyl group), 3.6 (t, 1H, CH), 3.2 (s, 2H, CH_2 in Gly), 2.8ppm (d, 2H, CH2 in Asp).

4.3.1.5 $^{\alpha}$Z-Arg-Gly-Asp(Obzl)$_2$

FTIR (KBr): *v*=2930 and 2850 (CH antisym and sym stretch, aliphatic CH_3 and CH_2), 1740 (C=O stretch, ester), 1660 (C=O stretch, Amide I), 1530 (N-H deformation, Amide II), 1500 (benzene ring, ring stretch), 1200 (C-O-C antisym stretch, ester), 720 and 700 cm^{-1} (two bands, CH out-of-plane deformation, monosubstituted benzene).

^{1}H-NMR (CD_3OD): δ=7.3 (m, 15H, benzene group), 5.1 (m, 6H, CH_2 in benzyl group), 4.0 (m, 1H, CH in Arg), 3.4 (m, 2H, CH_2 in Gly), 3.0 (m, 1H, CH in Asp), 1.8-0.9 ppm (broad multiple peaks of CH_2 in Arg).

4.3.1.6 Arg-Gly-Asp

FTIR (KBr): *v*=1700 (C=O stretch, carboxylic acid), 1670 (C=O stretch, Amide I), 1560 (shoulder, N-H deformation, Amide II), 1430 cm^{-1} (-OH bending, carboxylic acid).

^{1}H-NMR (D_2O): δ=3.9-3.6 (s, amine), 3.1 (t, 2H, CH_2 in Gly), 3.8 (d, 2H, CH_2 in Asp), 3.5 and 3.4 (t, 1H, CH in Gly and Asp), 1.8-1.5 ppm (broad multiple peaks of CH_2 in Arg).

4.3.2 Characterization of CS/PAspNa/CS layered films

Figure 4-7 shows a digital image of the 3 layered film treated with 0.01 glutaraldehyde (GA) and 2,4-DNPH. The film had a vivid yellow color, which indicated a chemical reaction occurred between dangling aldehydes of the 3 layered film and 2,4-DNPH. Since the film has a reactive aldehyde group on the surface, further chemical reaction can be done with the RGD peptides as a pendant molecule.

The FTIR-ATR spectrum of RGD-modified 3 layered film is shown in Figure 4-8. Overall, absorption bands of the film (b) look similar to the CS pure film (a), because the outer layers of the layered film were made of chitosan. However, the characteristic absorption at 1665 cm^{-1} was assigned to the C=O stretch in secondary amides, due to the modified RGD peptide. The absorption of N-H deformation, also corresponding to the secondary amides, was not observable, because the peak overlapped with the original CS spectrum. This result indicates that the RGD peptide was present on the 3 layered film, but as a small amount, because the characteristic peaks were relatively small.

4.3.3 Bioadhesive/peeling tests

Intestinal tissue is often used for bioadhesion tests, due to the stronger adhesiveness among mucosal tissues. The mean load-extension curve of each layered film is described in Figure 4-9. The peeling load was monitored while the film sample (1 x 1 cm) was peeled. As a general trend, the RGD-modified layered film had a higher bioadhesiveness than that of tissue control and unmodified 3 layered film throughout peeling. However, the 1 layer CS (DD=98.3) exhibited a higher peeling load than that of RGD-modified 3 layered films until 5mm extension. The peeling load for the RGD-3 layered film kept increasing as the extension continued. The mean load at 5 and 7mm extension, relatively a plateau region, were depicted, to compare the peeling load among controls and samples in Figure 4-9, as also done in Chapter 3.

Figure 4-10 (a) shows the load required at 5mm to peel two slices of porcine tissue holding 1 layer CS (DD=98.3), 2 and 3 layered films, and RGD-modified 3 layered film. In the previous chapter, layered films had a lower bioadhesiveness than the 1 layer CS. The RGD-modified 3 layered film improved the adhesive property by around 20% of the layered one, and about 1.5 times of the tissue control. The peeling strength of the RGD-3layered film was about the same as the 1 layer CS at this point, though it was more improved than the 1 layer CS at a subsequent extension.

Figure 4-10 (b) shows the load at 7mm required to peel two slices of porcine tissue holding CS, layered films, and RGD-modified 3 layered film. Surprisingly, the RGD-modified 3 layered film exhibited the highest peeling load among all samples, and it was 1.6-, 1.2-, 1.4-fold the peeling strength of the tissue control, 1 layer CS, and unmodified

3 layered film, respectively. As mentioned in Chapter3, CS film likely had a rough surface, and it probably causes the tissue to adhere to the surface easier. On the other hand, the layered films had a much smoother surface, which makes it more difficult for tissue to stick to the surface.

Interestingly, the RGD-modified 3 layered film gave better bioadhesion than the 1 layer CS. The non-modified 3 layered film which has a very smooth surface, did not have bioadhesion as good as the 1 layer CS due to the small surface roughness, already discussed in Chapter 3. However, its bioadhesion improved by RGD treatment. The RGD motif contributed to the tissue adhesiveness by its sequential adhesive property, and might give the surface roughness by the grafted peptides. A further investigation of the surface morphology, by Atomic Force Microscopy (AFM) will reveal how much surface roughness is changed before and after the RGD treatment. In addition, cell adhesion, proliferation, and viable examination *in vitro* will give a clearer evidence that the 3 layered film with RGD peptide motif is an effective bioadhesive biomaterial and a tissue scaffold.

4.3.4 Blood coagulation tests

The blood coagulation test was conducted by measuring the time of red blood cell sedimentation, also called as erythrocyte sedimentation rate, in anti-coagulated blood. A standardized method called erythrocyte sedimentation rate (ESR) has been widely used as a diagnosis of various diseases, as described in Chapter 3. The Westergren method is frequently used, which requires a specific glass tube (2.5 x 300 mm) to let the blood is settle for an hour. In this study, conventional glass tubes (7.5 x 100 mm) were used whether the

blood sedimentation is observed or not, by addition of fabricated chitosan and layered films into the tube, as described in Section 3.3.12.

The effect of various films on the blood sedimentation time when the supernatant and erythrocyte agglutination were separated as equal phases at 1:1, are summarized in Table 4-1. The anticoagulant blood did not separate during the testing. Two CS films (DD=83.5 and DD=98.3) did not completely agglutinate the blood cells within 1.5 h, whereas the 2 and 3 layered films exhibited clear blood sedimentation with both dry and wet films, as already discussed in Chapter 3. On the other hand, the RGD-modified 3 layered film exhibited blood sedimentation at 50 min for both dried and wet film, even though the sedimentation time was 15-25 min slower than those of 2 and 3 layered films. The blood sedimentation occurred for the RGD-modified 3 layered film as shown in Figure 4-11 (above). The RGD-modified 3 layered film became more hydrophobic than that of the unmodified 3 layered film because of the alkyl chain present on the film surface, thus the time of the blood clot formation was slightly retarded. Nevertheless, the effect of the clot formation on the film was similar to those of layered films. Even though the blood sedimentation time was slow for the RGD-modified 3 layered film, large blood clots were formed on the film surface, as well as other layered films after 1.5 h immersion. The effect of the layered films on of blood clot formation was obvious, whereas the CS (DD=98.3) 1 layer film had few clots on it (Figure 4-11, below).

A molecule containing a RGD sequence is known as a specific fibrinogen receptor antagonist [23]. A study demonstrated that platelet aggregation was inhibited when the RGD-containing peptide was treated with platelets [23]. In other words, the immobilized

RGD sequence is potentially recognized by platelet receptors and the platelet aggregation is induced. However, the blood used in this study contained sodium citrate which can chelate calcium ions that are involved with platelet activation. Blood clot formation was triggered because of the dangling RGD peptides, or simply the layered film characteristics. In order to clarify the effect of immobilized RGD peptide on blood clot formation, the film property and the quantitative dangling RGD need to be determined. As discussed in Chapter 3, the 2 and 3 layered films promoted red blood cell aggregation in the absence of enough calcium ions, which indicates the layered films can activate erythrocytes. At this point, the detail mechanism of how the layered films interact with erythrocytes, either chemically or physically, is not clear.

After the blood sedimentation, a drop was taken from the agglutination phase and the cell morphology was examined by a stereomicroscope as shown in Figures 4-12 and 4-13. At lower magnification (x10), erythrocytes were evenly distributed in the blood without film (Figure 3-27(a)), whereas they were partly aggregated in the RGD-modified film. At higher magnification (x40), this feature is more observable. The red blood cells are stacked on top of each other, unlike the citrated blood. Further study will be needed to elucidate the effect of dangling RGD peptides on blood coagulation. Nevertheless, the layered films and RGD-modified 3 layered film were proven to be effective materials that promote red blood cell aggregation and thus are promising materials as new hemostasis agents.

4.4 Conclusions and Suggestions for Future Work

The RGD peptide was synthesized by a conventional stepwise liquid synthesis method for modification of the 3 layered film. The amino group of chitosan's outer layers was reacted with GA for a further reaction with the N-terminal of the RGD peptide. Finally, the RGD pendant-3 layered film was obtained. Each step of the peptide synthesis was spectroscopically monitored, however, the final product had some impurities. Some side-reactions likely occurred during the coupling of $^{\alpha}$Z-Arg and Gly-Asp(Obzl)$_2$. Purification of this synthesized RGD is the primary problem for this peptide synthesis. Other techniques, such as solid-state synthesis or use of an amino acid synthesizer will be useful for small scale synthesis. Since the extent of RGD grafting is not always necessarily high, these methods can provide pure peptides which allows easier characterization.

The RGD modified layered film was characterized by FTIR, and the presence of peptide was confirmed. Since FTIR spectra are usually considered as a qualitative analysis, other quantitative techniques must be needed to determine the amount of grafted peptide. X-ray photoelectron spectroscopy (XPS) will reveal the surface chemical characteristics of the RGD-modified film by the elemental composition calculation [13,14,19]. Amino acid analysis (AAA) can provide the quantitative result, showing how much RGD peptide was bonded per unit area, by hydrolysis of the peptide to each amino acid [13,19]. These techniques will optimize the concentration of modified RGD peptides on the 3 layered film, because the degree of grafting can be adjusted, depending on the tissue or cell variation.

Bioadhesion tests demonstrated that RGD-modified 3 layered film exhibited the highest peeling load among the samples at the extension of 7mm. Peeling strength of

RGD-modified film was almost 1.6, 1.2, and 1.4-fold of control tissue, 1 layer CS, and unmodified 3 layered film, respectively. This result suggests that the RGD-modified film could improve the tissue affinity, which is one of the important parameters of bioadhesives/biomaterial.

Blood coagulation tests revealed that the RGD-modified 3 layered film effectively form red blood cell aggregates as well as 2 and 3 layered films, even though the blood sedimentation rate slightly retarded. The feature was not observable in chitosan films, thus the significant red blood cell aggregation ability was proven by both macroscopic and microscopic observations. Other conventional blood coagulation tests, such as whole blood clotting time and plasma factor time, will also be useful methods in order to clarify the roll of RGD sequence to trigger platelet aggregation. The concentration of modified RGD peptides needs to be quantitatively determined in future study. In conclusion, these layered films can be proposed as new hemostatic agents, as well as novel scaffolds for cell culturing, even though the detail hemostasis mechanism must be clarified in future studies.

4.5 References

1. Nakajima K, Hirano Y, Iida T, Nakajima A. Adsorption of plasma proteins on Arg-Gly-Asp-Ser peptide-immobilized poly(vinyl alcohol) and ethylene-acrylic acid copolymer films. Polym J 1990; 22: 985-990.
2. Lin HB, García-Echeverría C, Asakura S, Sun W, Mosher DF, Cooper SL. Endothelial cell adhesion on polyurethanes coating covalently attached RGD-peptides. Biomaterials 1992; 13: 905-914.
3. Quirk RA, Chan WC, Davies MC, Tendler SJB, Shakesheff KM. Poly(L-lysine)-GRGDS as a biomimetic surface modifier for poly(lactic acid). Biomaterials 2001; 22: 865-872.
4. Clark EA, Brugge JS. Integrins and signal transduction pathways: The road taken. Science 1995; 268: 233-239.
5. Lechner AM, Assfalg-MAchleidt I, Zahler S, Stoeckelhuber M, Machleidt W, Jochum M, Nägler DK. RGD-dependent binding of procathepsin X to integrin $\alpha_v\beta_3$ mediates cell-adhesive properties. J Biol Chem 2006; 281: 39588-39597.
6. Chada D, Mather T, Nollert MU. The synergy site of fibronectin is required for strong interaction with the platelet integrin $\alpha IIb\beta_3$. Annal Biomed Engineer 2006; 34: 1542-1552.
7. Lin HB, Sun W, Mosher DF, García-Echeverría C, Schaufelberger K, Lelkes PI, Cooper SL. Synthesis, surface, and cell-adhesion properties of polyurethanes containing covalently grafted RGD-peptides. J Biomed Mater Res 1994; 28: 329-342.
8. Barrera D.A, Zylstra E, Lansbury P.T, and Langer R. Sysnthesis and RGD peptide modification of a new biodegradable copolymer: poly(lactic acid-*co*-lysin). J. Am. Chem. Soc. 1993; 115, 11010-11011.
9. Hu Y, Winn SR, Krajbich I, Hollinger JO. Porous polymer scaffolds surface-modified with arginine-glycine-aspartic acid enhance bone cell attachment and differentiation *in vitro*. J Biomed Mater Res. 2003; 64A, 583-590.
10. Cook AD, Hrkach JS, Gao NN, Johnson IM, PAjvani UB, Cannizzaro SM, Langer R. Characterization and development of RGD-peptide-modified poly(lactic acid-*co*-lysine) as an interactive, resorbable biomaterial. J Biomed Mater Res 1997; 35: 513-523.
11. Sugawara T, Matsuda T. Photochemical surface derivatization of a peptide containing Arg-Gly-Asp (RGD). J Biomed Mater Res 1995; 29: 1047-1052.
12. Burdick JA, Anseth KS. Photoencapsulation of osteoblasts in injectable RGD-modified

PEG hydrogels for bone tissue engineering. Biomaterials 2002; 23: 4315-4323.
13. Deng C, Tian H, Zhang P, Sun J, Chen X, Jing X. Synthesis and characterization of RGD peptide grafted poly(ethylene glycol)-*b*-poly(L-lactide)-*b*-poly(L-glutamic acid) triblock copolymer. Biomacromol 2006; 7: 590-596.
14. Knerr R, Weiser B, Drotleff S, Steinem C, Göpferich A. Measuring cell adhesion on RGD-modified, self-assembled PEG monolayers using the quartz crystal microbalance technique. Macromol Biosci 2006; 6: 827-838.
15. Chung TW, Lu YF, Wang SS, Lin YS, and Chu SH. Growth of human endothelial cells on photochemically grafted Gly-Arg-Gly-Asp (GRGD) chitosans. Biomaterials 2002; 23: 4803-4809.
16. Chung TW, Lu YF, Wang HY, Chen WP, Wang SS, Lin YS, and Chu SH. Growth of human endothelial cells on different concentration of Gly-Arg-Gly-Asp (GRGD) grafted chitosan surface. Artif Organ 2003; 27: 155-161.
17. Park JH, Kwon S, Nam JO, Park RW, Chung H, Seo SB, Kim IS, Kwon IC, Jeong SY. Self-assemble nanoparticles based on glycol chitosan bearing 5β-cholanic acid for RGD peptide delivery. J Control Release 2004; 95: 579-588.
18. Ho MH, Wang DM, Hsieh HJ, Liu HC, Hsien TY, Lai JY, and Hou LT. Preparation and characterization of RGD-immobilized chitosan scaffolds. Biomaterials. 2005; 26, 3197-3206.
19. Li J, Yun H, Gong Y, Zhao N, Zhang X. Investigation of MC3T3-E1 cell behavior on the surface of GRGDS-coupled chitosan. Biomacromol 2006; 7: 1112-1123.
20. Massia SP, Hubbell JA. An RGD spacing of 440 nm is sufficient for Integrin $\alpha_v\beta_3$-mediated fibroblast spreading and 140 nm for focal contact and stress fiber formation. J Cell Biol 1991; 114: 1089-1100.
21. Bodanszky M. Principles of peptide synthesis: 2nd edition. Springer Laboratory, 1993; pp: 1-8.
22. Zervas L, Otani TT, Winitz M, Greemsterin JP. Studies on Arginine peptides. II. Synthesis of L-arginyl-L-arginine and other N-terminal dipeptides. J Am Chem Soc 1958; 81: 2878-2884.
23. Sheu JR, Lin CH, Chung JL, Teng CM, Huang TF. Triflavin, an Arg-Gly-Asp containing snake venom peptide, inhibits aggregation of human platelets induced by human hepatoma cell line. Thrombosis Res 1992; 66: 679-691.

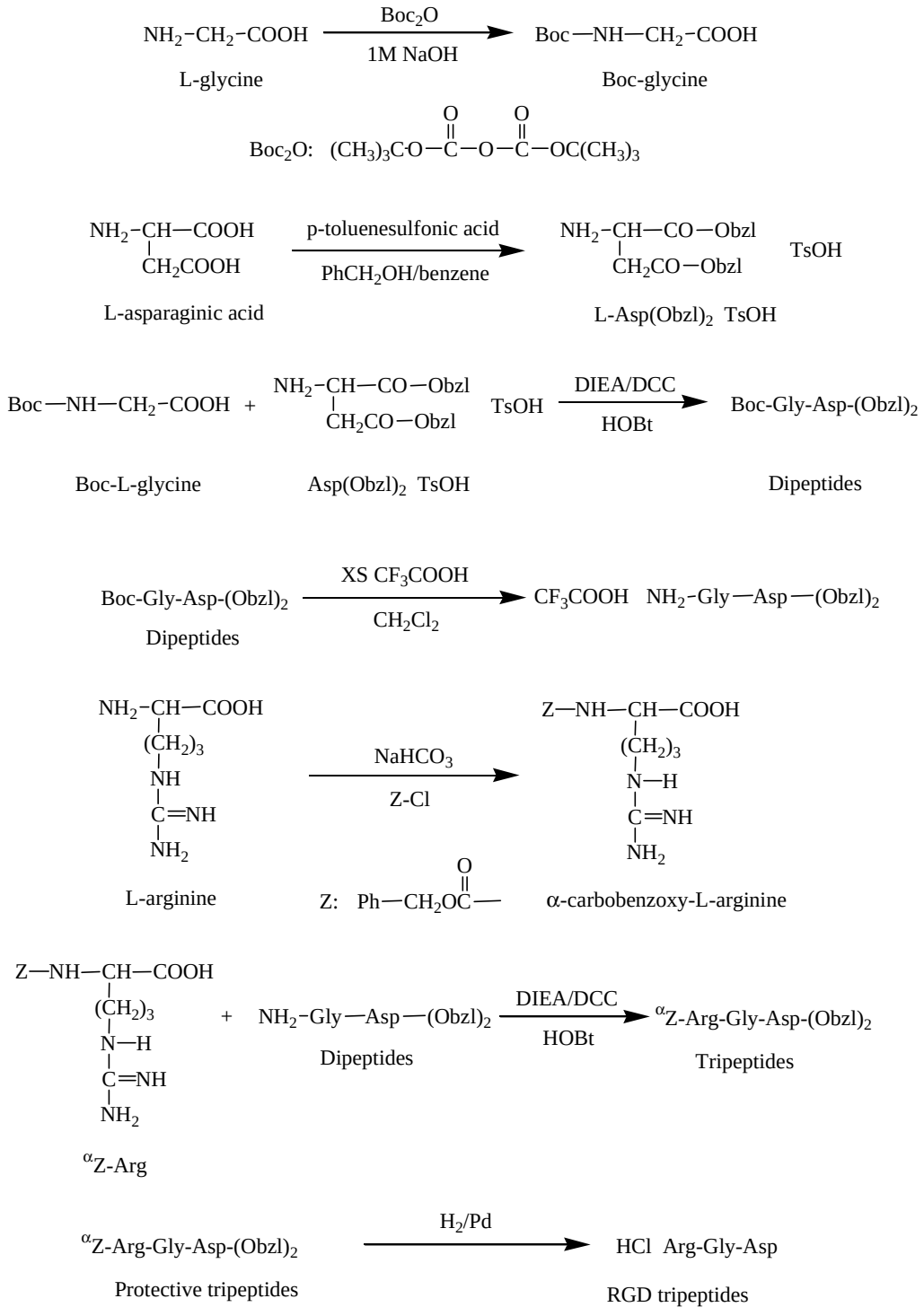

Scheme 4-1 Synthetic scheme of stepwise RGD peptide synthesis.

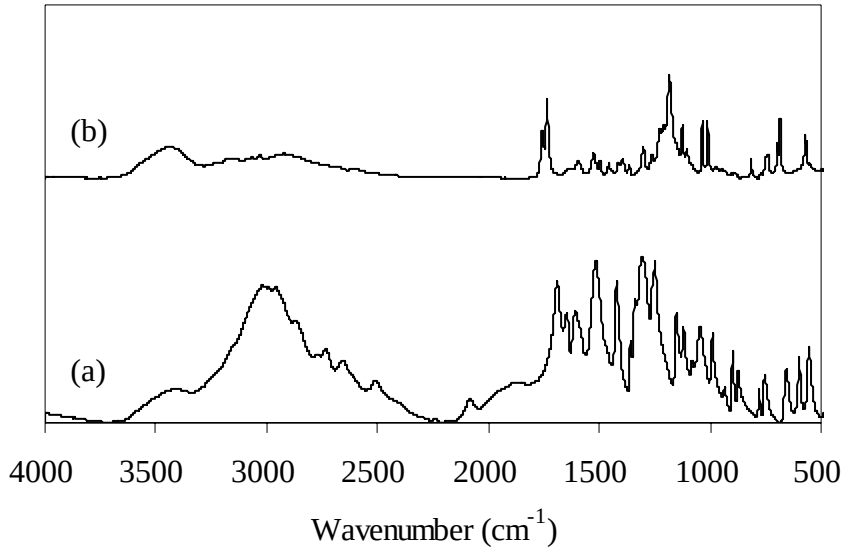

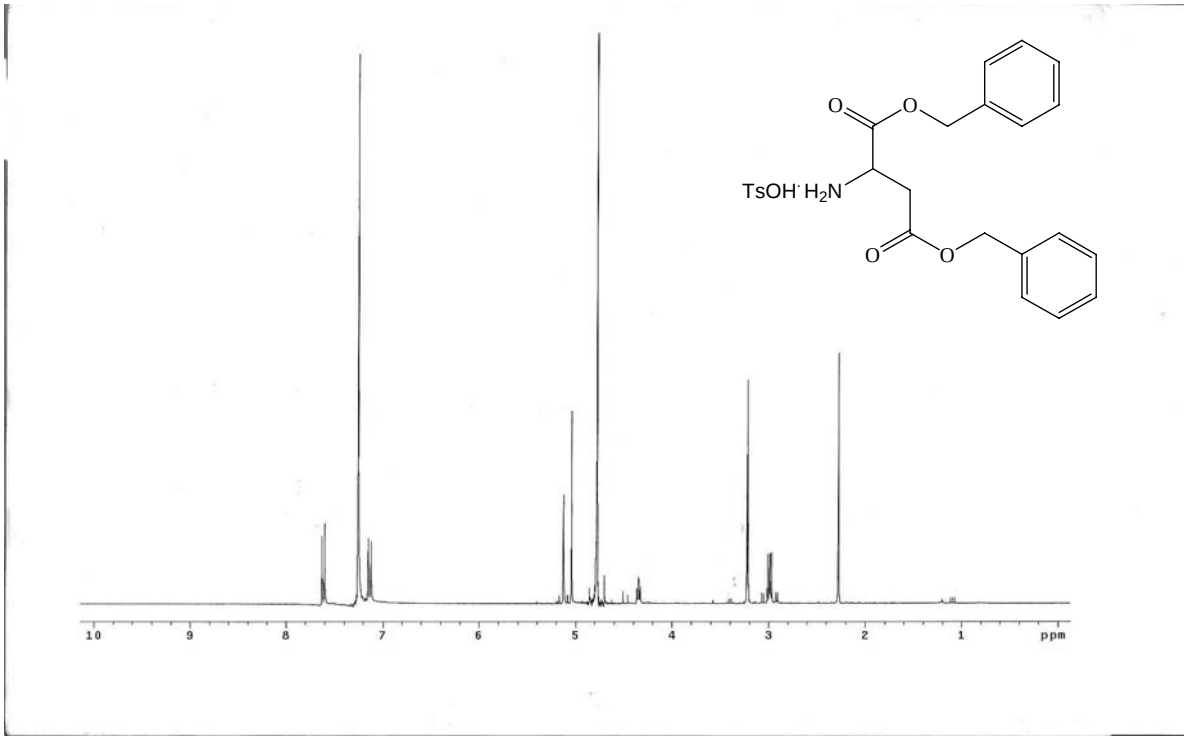

Figure 4-1 (above) FTIR spectra of (a): L-aspartic acid(starting material), (b): $Asp(Obzl)_2$.
The spectra were obtained using a KBr pellet.
(below) ^1H NMR spectra of $Asp(Obzl)_2$ in CD_3OD (300MHz).

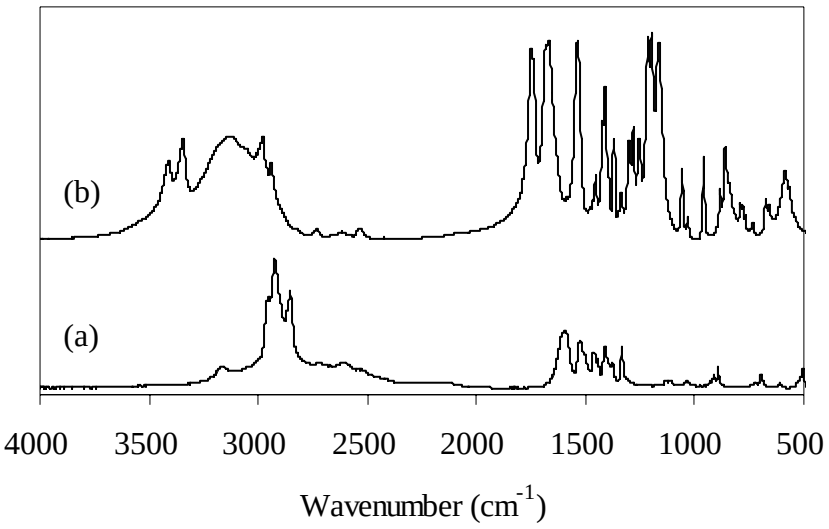

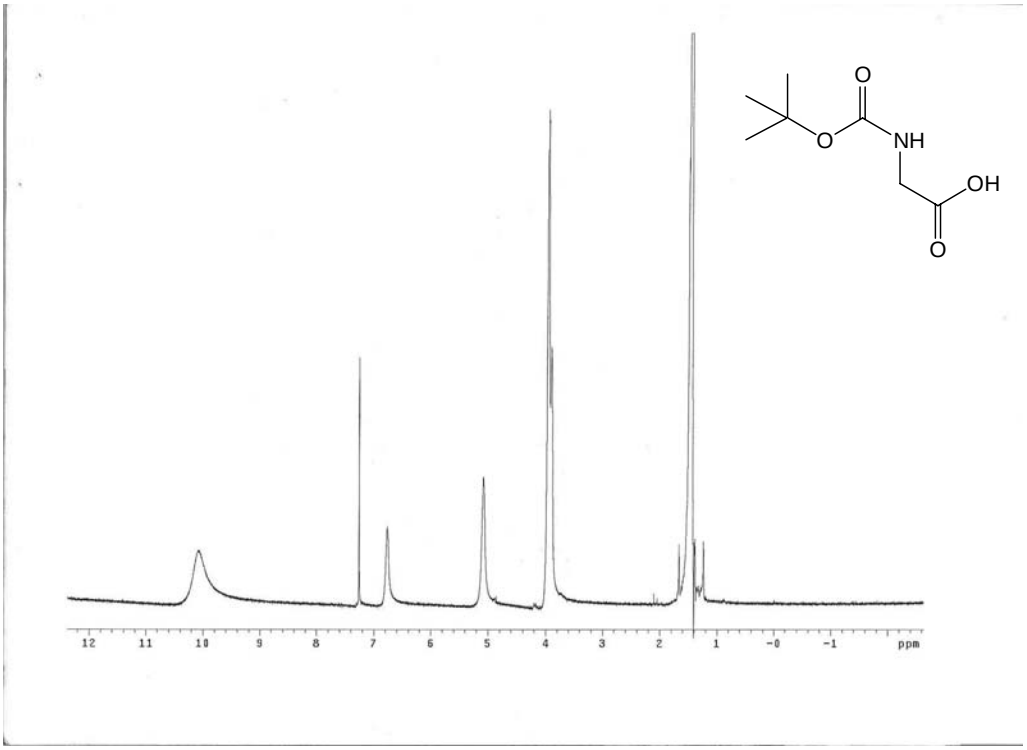

Figure 4-2 (above) FTIR spectra of (a): Gly (starting material), (b): Boc-Gly. The spectra were obtained using a KBr pellet.
(below) ^{1}H NMR spectra of Boc-Gly in $CDCl_3$ (300MHz).

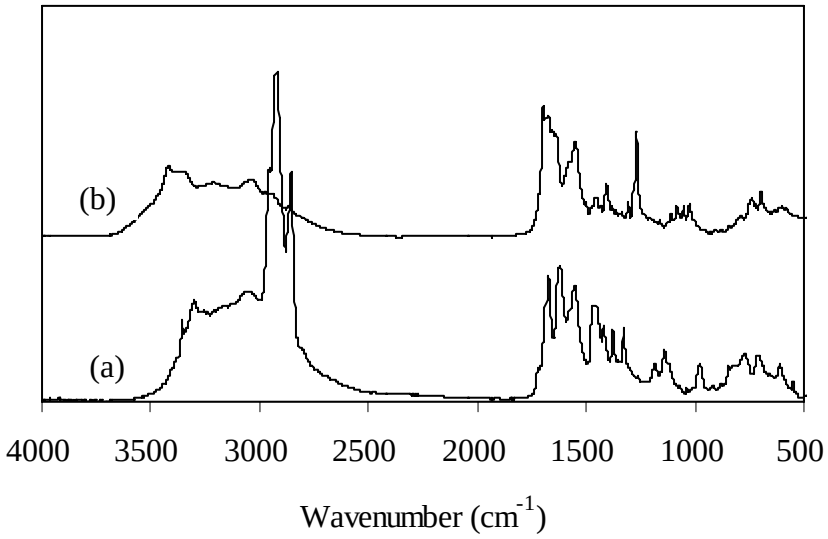

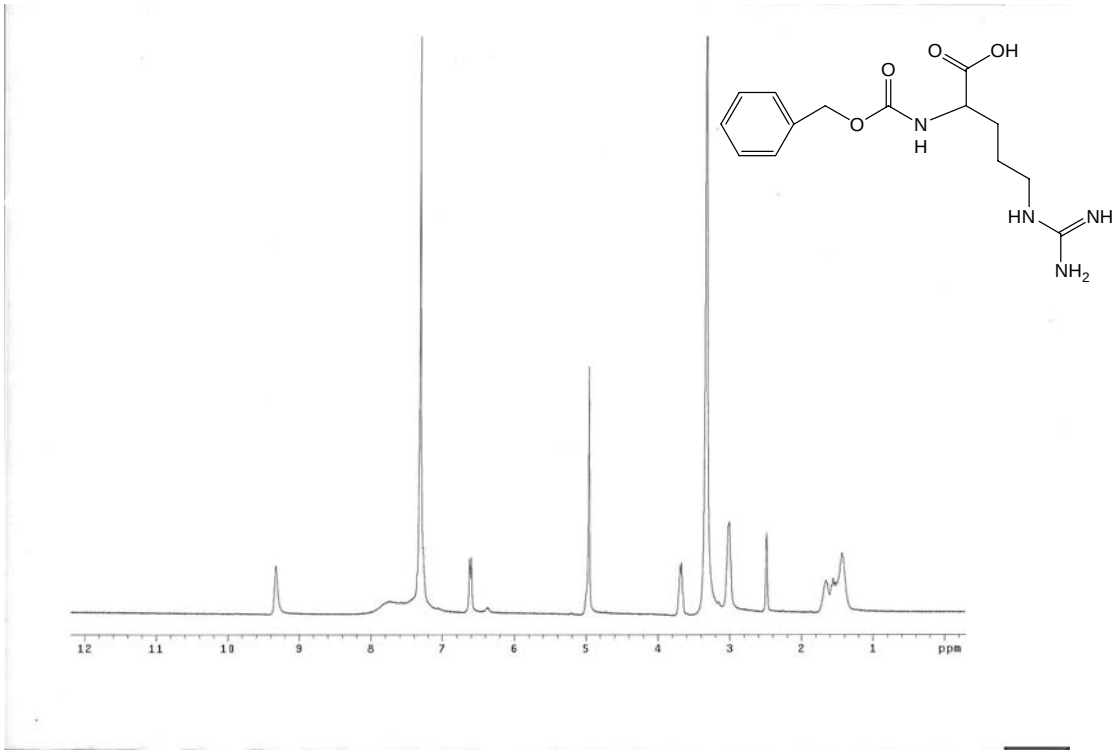

Figure 4-3 (above) FTIR spectra of (a): L-Arg (starting material), (b): $^{\alpha}$Z-Arg. The spectra were obtained using a KBr pellet.

(below) ^{1}H NMR spectra of Z-Arg in DMSO-d_6 (300MHz).

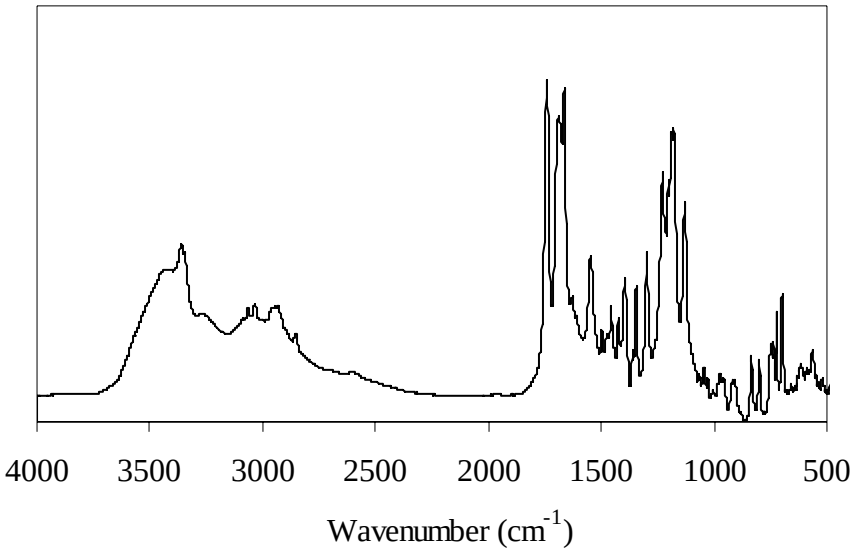

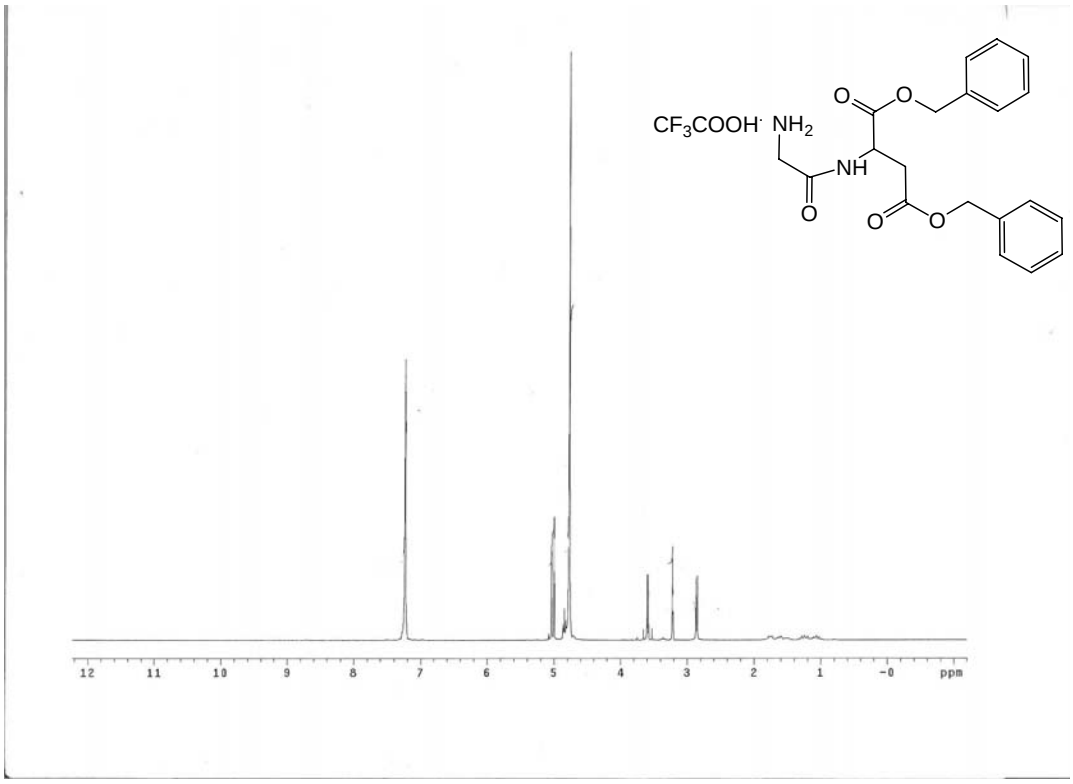

Figure 4-4 (above) FTIR spectra of Gly-Asp(Obzl)$_2$. The spectra were obtained using a KBr pellet.

(below) ^{1}H NMR spectra of Gly-Asp(Obzl)$_2$ in CD_3OD (300MHz).

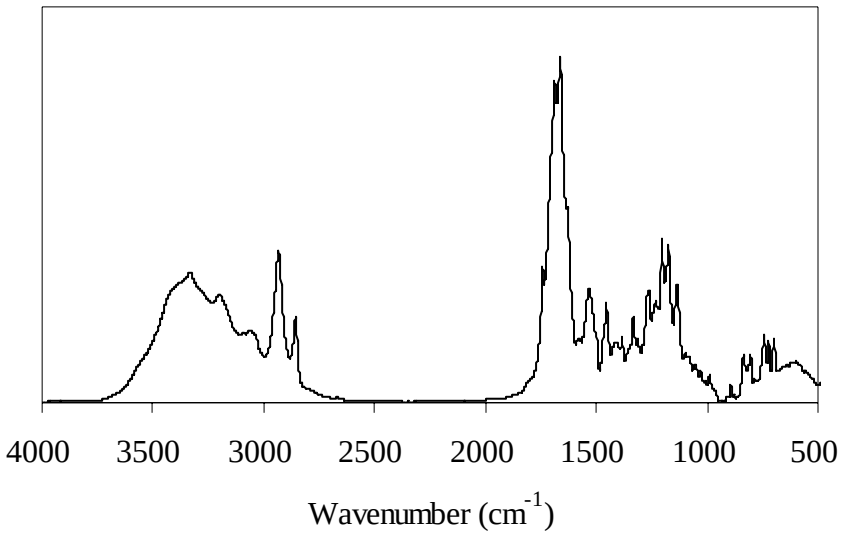

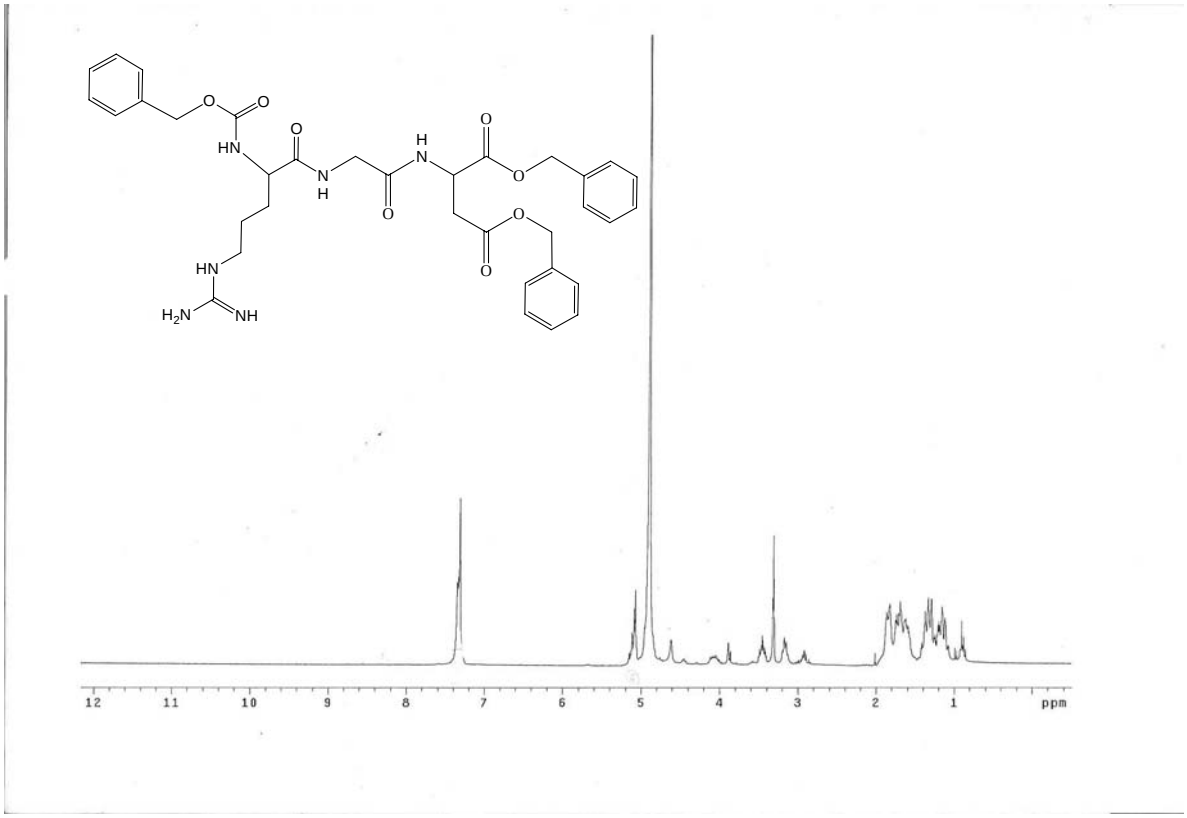

Figure 4-5 (above) FTIR spectra of Z-Arg-Gly-Asp(Obzl)$_2$. The spectra were obtained using a KBr pellet.

(below) ^{1}H NMR spectra of Z-Arg-Gly-Asp(Obzl)$_2$ in CD_3OD (300MHz).

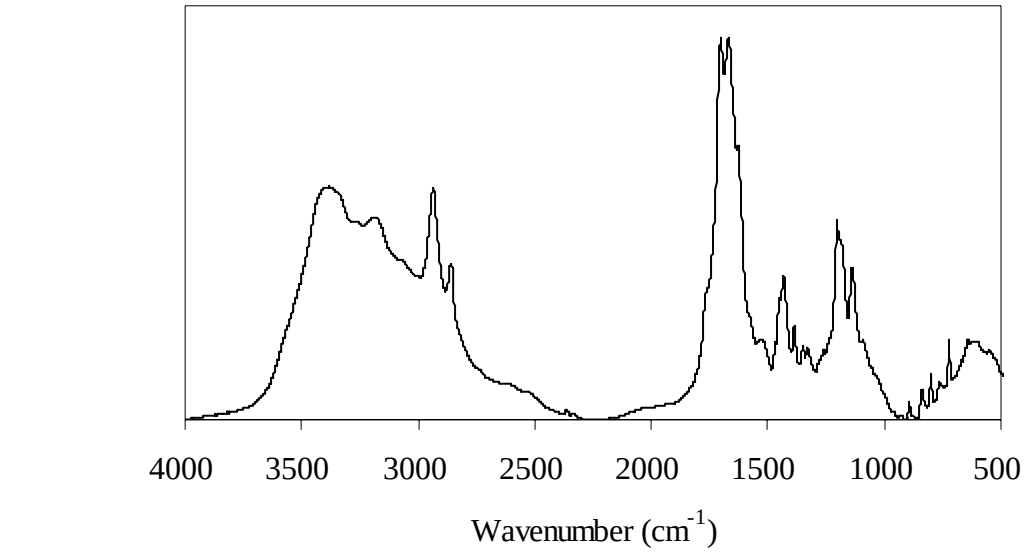

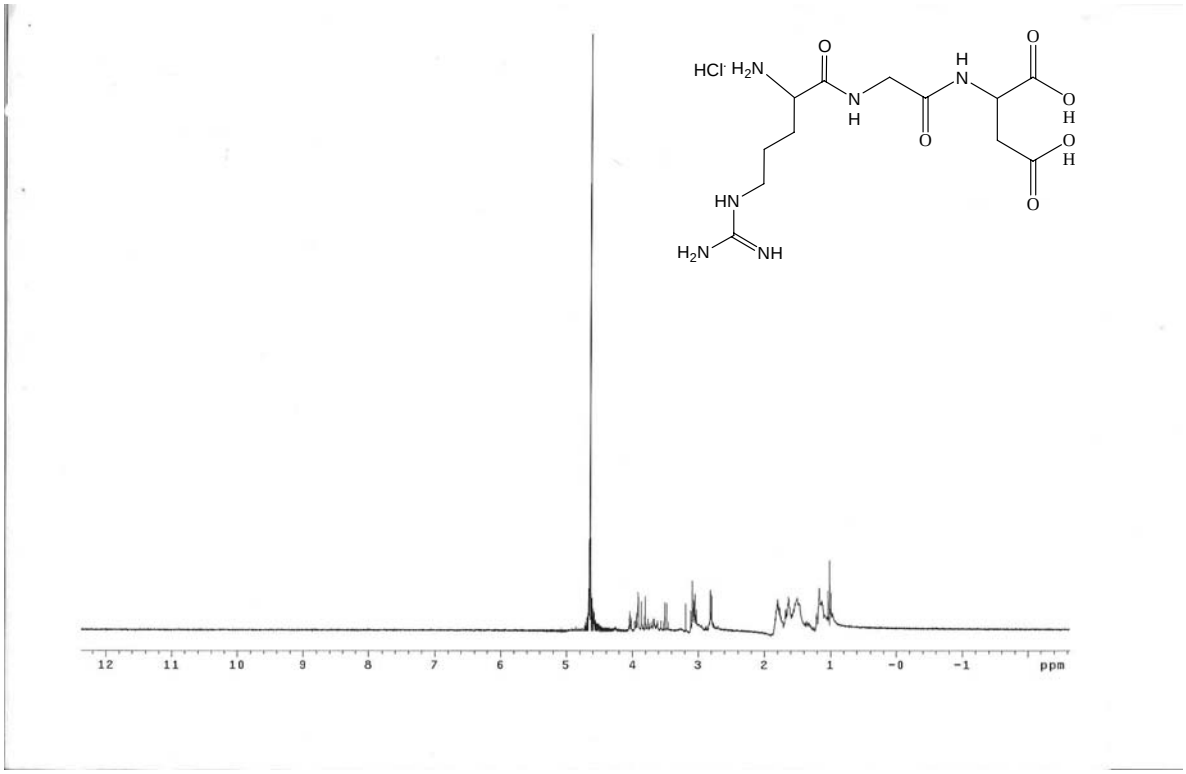

Figure 4-6 (above) FTIR spectra of Arg-Gly-Asp. The spectra were obtained using a KBr pellet.

(below) ^{1}H NMR spectra of Arg-Gly-Asp in D_2O (300MHz).

Figure 4-7 A digital image of 2,4-DNPH treated the 3 layered film after treatment with 0.01M glutaraldehyde (GA). The yellow color indicates the presence of free aldehyde groups. The free aldehyde group reacts with RGD peptide in the subsequent reaction.

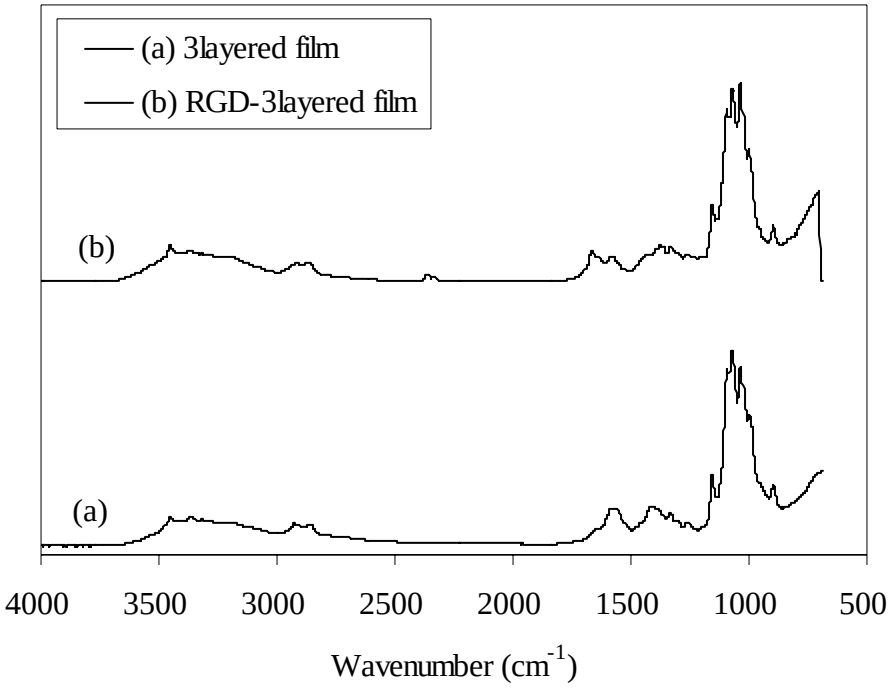

Figure 4-8 ATR-FTIR spectra of (a): 3 layered film , (b): RGD-modified 3 layered film. The spectra were obtained using Ge crystal.

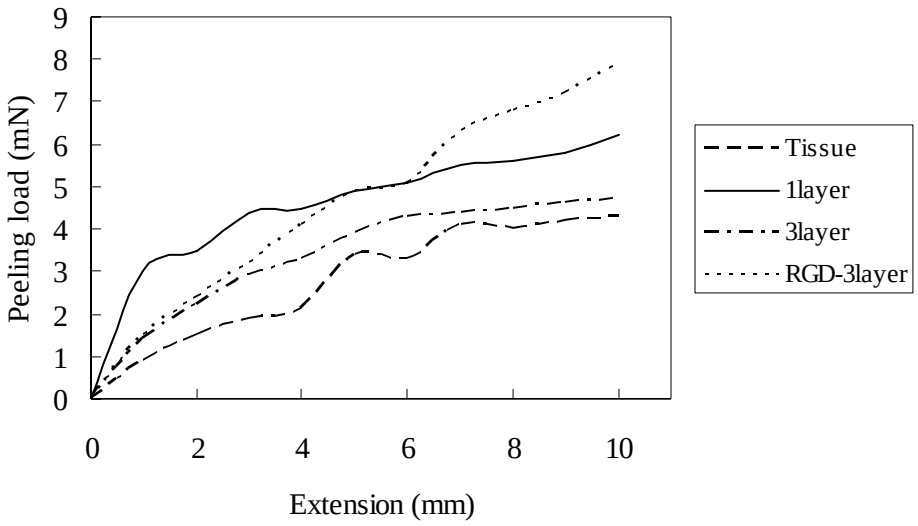

Figure 4-9 The mean load-extension curve of peeling test conducted by peeling two slices of porcine tissue holding various films. Load cell: 5N cell, gauge length: 10mm, and peeling rate: 6.0mm/min. Each experiment was repeated at least 5 times.

(a)

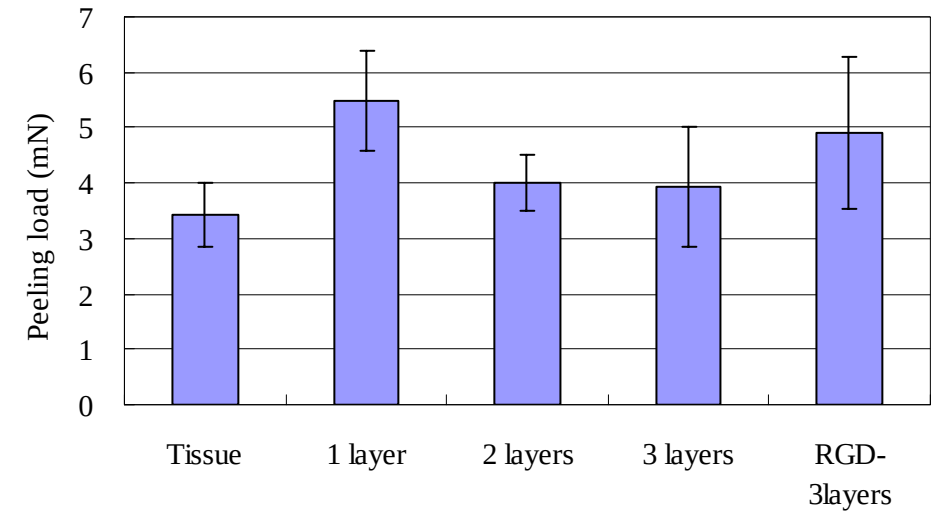

(b)

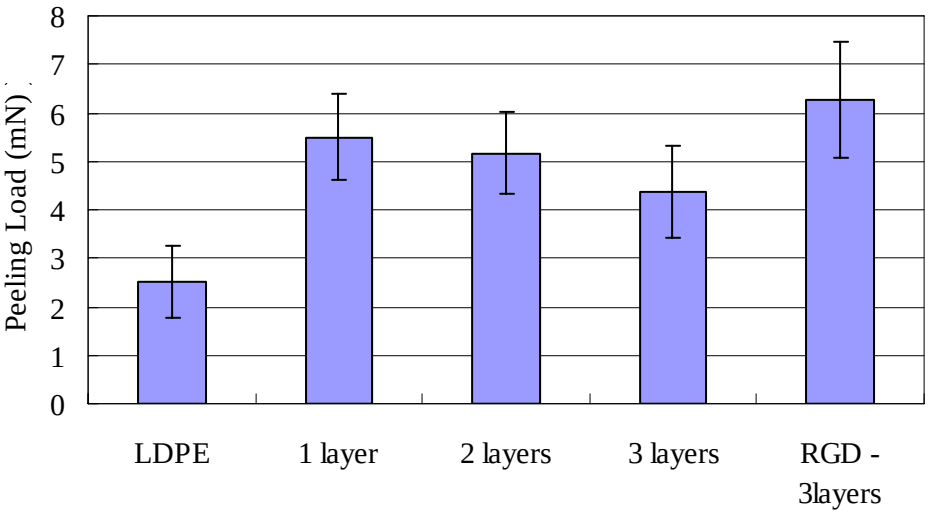

Figure 4-10 The load required at (a): 5mm and (b): 7mm to peel two slices of porcine tissue holding various films. Load cell: 5N cell, gauge length: 10mm, and peeling rate: 6.0mm/min. Each experiment repeated at least 5 times.

Table 4-1 Blood sedimentation time* (min) of various films in 1mL of anti-coagulant blood.

	CS (DD=85.3)	CS (DD=98.3)	2 layers	3 layers	RGD-3layers
Dried film	> 90	> 90	25.6±5.9	30.6±7.0	50.5±13.5
Wet film	> 90	> 90	33.0±11.0	43.8±12.9	51.5±5.1

* Mean±SD. The blood containing films was incubated at 37 ºC for 90 min.

a) CS (DD=98.3) 1 layer

b) 2 layered film

c) 3 layered film

d) RGD- 3 layered film

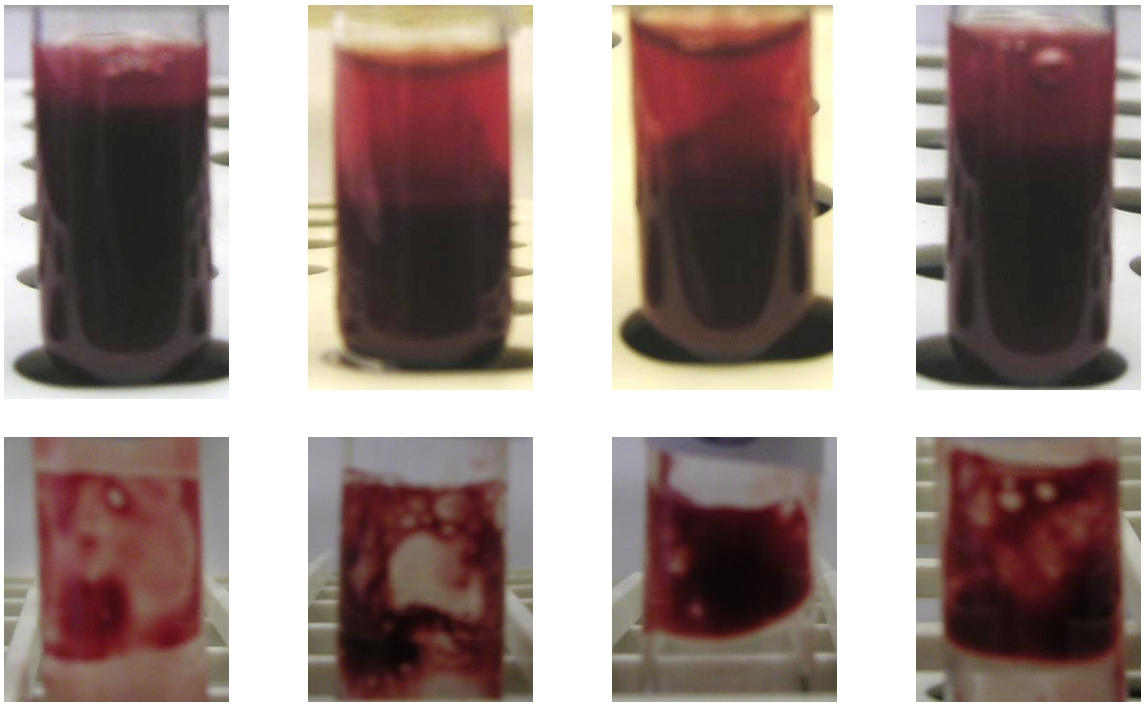

Figure 4-11 Blood sedimentation after immersing of various films1.5 hour at 37 ºC (above) and blood clot formed on films (below); (a): CS (DD=98.3) 1 layer film, (b): 2 layered film, (c): 3 layered film, (d): RGD-3 layered film. The blood containing 3.5 wt% of sodium citrate was used. Each experiment was repeated 5 times.

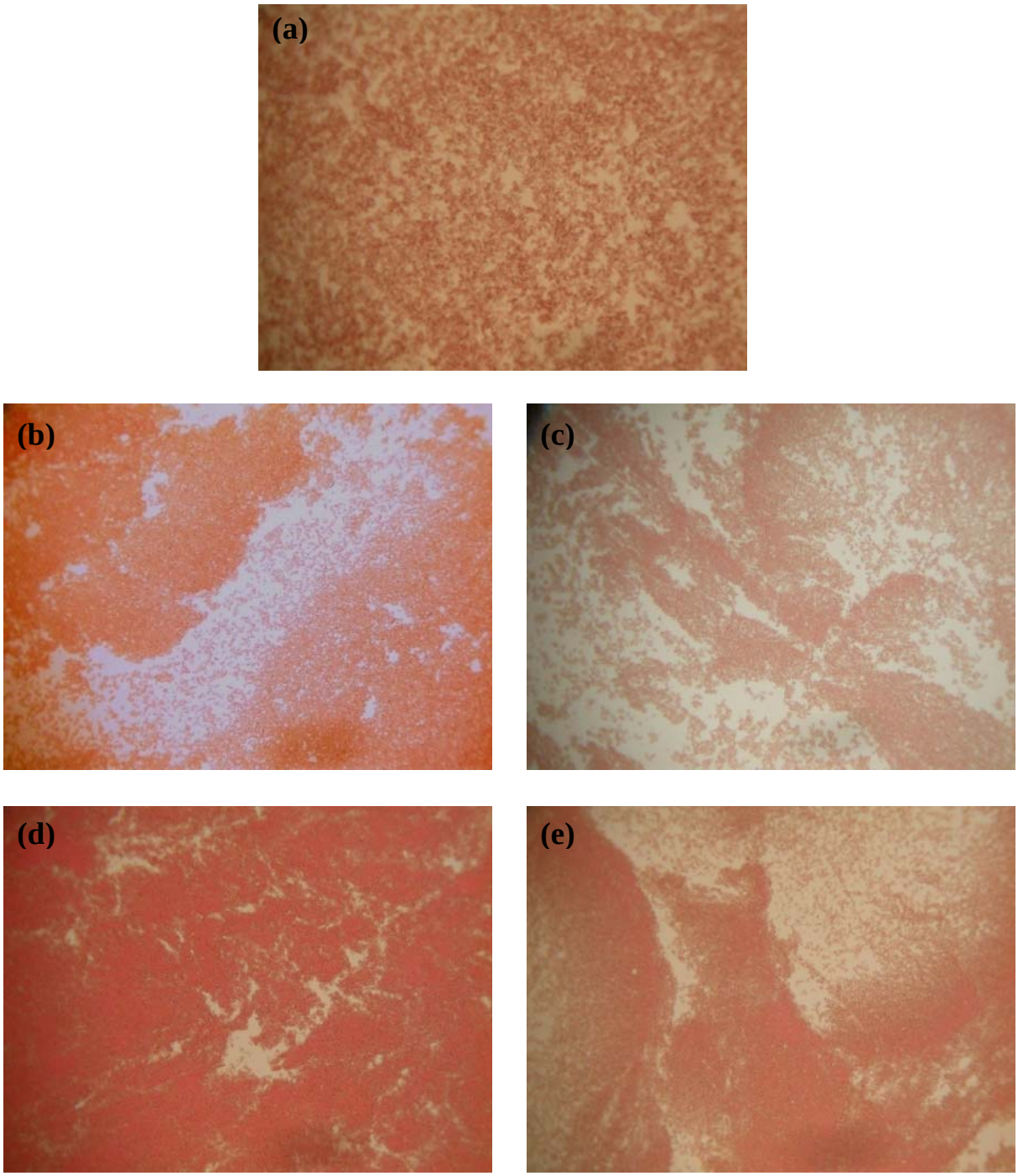

Figure 4-12 Stereomicroscope images (x10) of red blood cells after 1.5 hour-sedimentation; (a): Anticoagulated blood without film, (b): CS (DD=98.3) 1 layer film, (c): 2 layered film, (d): 3 layered film, (e): RGD-3 layered film.

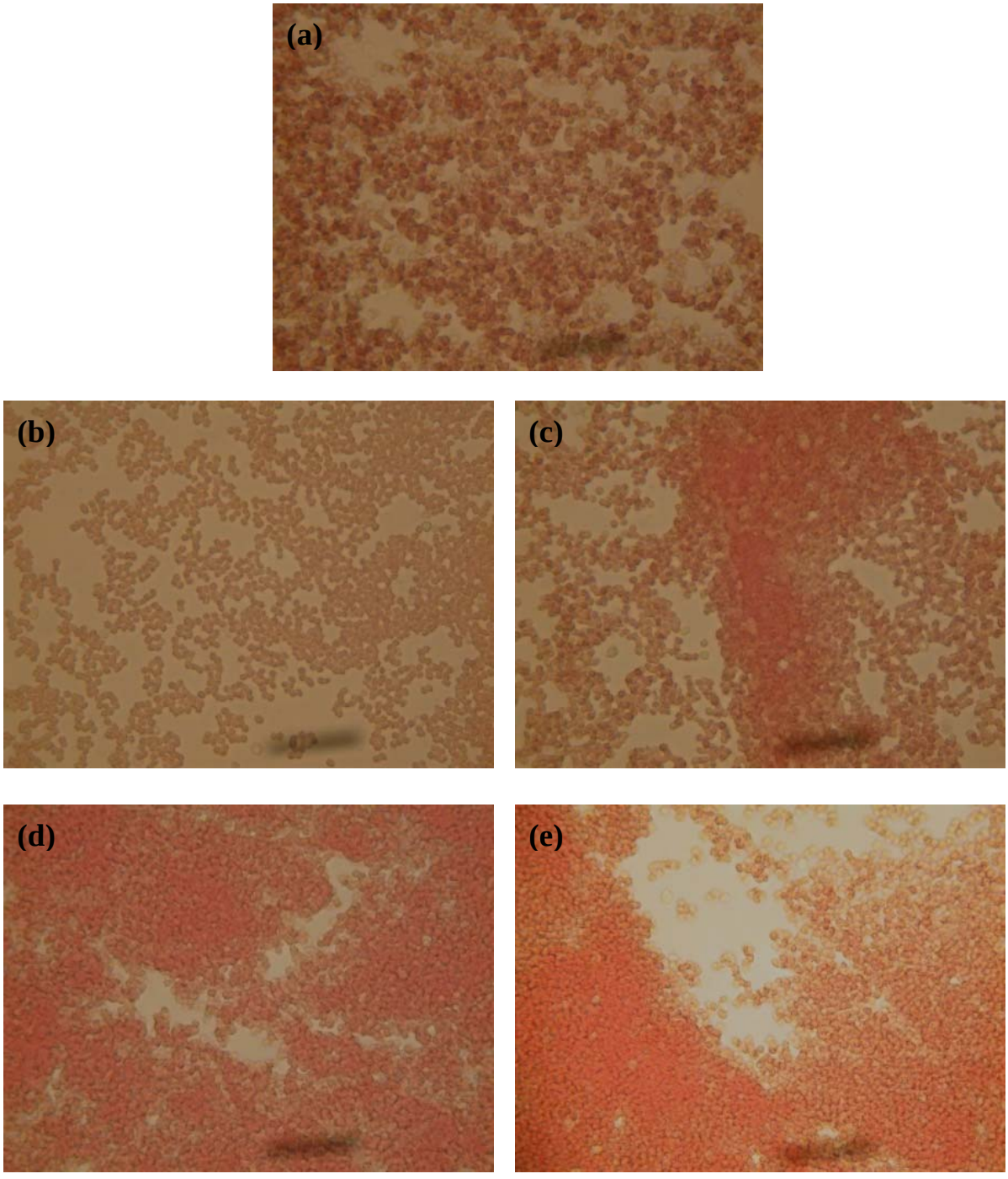

Figure 4-13 Stereomicroscope images (x40) of red blood cells after 1.5 hour-sedimentation; (a): Anticoagulated blood without film, (b): CS (DD=98.3) 1 layer film, (c): 2 layered film, (d): 3 layered film, (e): RGD-3 layered film.